Fisheries and Oceans Canada | Pêches et Océans Canada
Ecosystems and Oceans Science | Sciences des écosystèmes et des océans

Canadian Science Advisory Secretariat (CSAS)

Research Document 2026/001

National Capital Region

Assessment of Port Ocean Prediction System Developed Under Canada's Oceans Protection Plan: Vancouver Harbour

Michael Dunphy[1], Maxim Krassovski[1], Stephanne Taylor[2], Hauke Blanken[1], Rachel Horwitz[2], Simon St-Onge Drouin[3], Adam Drozdowski[2]

[1] Fisheries and Oceans Canada
Institute of Ocean Sciences
9860 West Saanich Road
Sidney, British Columbia V8L 4B2

[2] Fisheries and Oceans Canada
Bedford Institute of Oceanography
1 Challenger Drive
Dartmouth, Nova Scotia B2Y 4A2

[3] Fisheries and Oceans Canada
Maurice Lamontagne Institute
850 route de la Mer
Mont-Joli, Québec G5H 3Z4

February 2026

Canada

Foreword

This series documents the scientific basis for the evaluation of aquatic resources and ecosystems in Canada. As such, it addresses the issues of the day in the time frames required and the documents it contains are not intended as definitive statements on the subjects addressed but rather as progress reports on ongoing investigations.

Published by:

Fisheries and Oceans Canada
Canadian Science Advisory Secretariat
200 Kent Street
Ottawa ON K1A 0E6

http://www.dfo-mpo.gc.ca/csas-sccs/
DFO.CSAS-SCAS.MPO@dfo-mpo.gc.ca

ISSN 1919-5044
ISBN 978-0-660-79952-0 Cat. No. Fs70-5/2026-001E-PDF

Correct citation for this publication:

Dunphy, M., Krassovski, M., Taylor, S., Blanken, H., Horwitz, R., St-Onge Drouin, S., and Drozdowski, A. 2026. Assessment of Port Ocean Prediction System Developed Under Canada's Oceans Protection Plan: Vancouver Harbour. DFO Can. Sci. Advis. Sec. Res. Doc. 2026/001. xi + 128 p.

Aussi disponible en français :

Dunphy, M., Krassovski, M., Taylor, S., Blanken, H., Horwitz, R., St-Onge Drouin, S. et Drozdowski, A. 2026. Évaluation du système de prévisions océaniques portuaires élaboré dans le cadre du Plan de protection des océans du Canada - port de Vancouver. Secr. can. des avis sci. du MPO. Doc. de rech. 2026/001. xi + 134 p.

TABLE OF CONTENTS

LIST OF TABLES

LIST OF FIGURES

ABSTRACT

Canada's Oceans Protection Plan (OPP) was launched in 2016 to support initiatives aimed at protecting our marine environment from anthropogenic pressures. To this end, the Improving Drift Prediction and Nearshore Modelling sub-initiative of OPP developed six high-resolution port-scale hydrodynamic models, to improve safe navigation, and provide operational emergency response to events such as marine oil spills. The models were downscaled from the Coastal Ice-Ocean Prediction Systems East and West (CIOPS-E, CIOPS-W). Atmospheric forcing was provided by the High-Resolution Deterministic Prediction System (HRDPS). Model performance is assessed against available observational data and contrasted with the parent model using a multi-year hindcast. Evaluations of 48-hour forecasts are performed during a two-month period.

This document reports on the performance assessment for the Vancouver Harbour model (VH20) and the northern part of the South Salish Sea model (SSS150). The VH20 domain covers English Bay to Port Moody Arm and is nested within SSS150 that covers Burrard Inlet and the southern part of Salish Sea and the Fraser River to Mission and to Pitt Lake.

Results show that the high-resolution models provide either similar or better performance than the larger-scale models in the areas where they overlap and have adequate performance in the areas not covered by the larger-scale models. At most water level stations, tidal water level error is 5-6 cm CRMSE and non-tidal water level error is 4-5 cm, giving a total water level error of about 7 cm CRMSE, with one exception at 9 cm CRMSE.

At Second Narrows, mean outflow of order 14 cm/s is captured by both models and total CRMSE for the alongshore current ranges from 16.3-27.0 cm/s. Surface water temperature near English Bay is biased cold by about 0.7 °C and modelled to 1 °C CRMSE. Temperature and salinity profiles in Howe Sound and English Bay outperform the Salish Sea model at 500 m nominal resolution (SS500; part of CIOPS-W) and this level of performance is maintained in the rest of Burrard Inlet.

Drift evaluation indicates that VH20 marginally outperforms SSS150 although large uncertainties limit the ability to constrain the performance. The forecast evaluation showed that non-tidal water level error increased gradually with forecast lead time as expected.

All model runs completed without stability issues including periods of extreme weather events and real-time instrument failure.

1. INTRODUCTION

Under the Improving Drift Prediction and Nearshore Modelling (DPNM) sub-initiative of Canada's Oceans Protection Plan (OPP), high-resolution models were developed for six Canadian ports and their approaches to enhance the Government of Canada's ocean modelling capabilities in support of environmental protection and marine safety applications (e.g., drift prediction for oil spills) and safety for navigation via a hydrographic e-navigation application. The six ports (three on the east coast and three on the west coast) were selected as at-risk for environmental incidents owing to their high tanker traffic and complex navigational needs. Models have been developed for the west coast ports of Kitimat, Lower Fraser River and Vancouver Harbour, and for the east coast ports of Saint John, the Strait of Canso, and the St. Lawrence estuary.

The models have been developed with both hindcast and forecast capabilities. For each port, a multi-year hindcast is presented with model validation against observations of water levels, velocities, temperature and salinity, as well as a drift experiment conducted using available drifters. Forecast performance is assessed over a two-month period.

The purpose of this document is to review the performance of the model for the Vancouver port model. The design is common to all port models and is presented in Section 2, while Section 3 describes the specifics of the Vancouver port model. The evaluation parameters used to evaluate all models are detailed in Section 4, and Sections 5 and 6 respectively analyze the long hindcast evaluation results and the forecasts evaluation results for the Vancouver port model. The performance of the Vancouver port model is summarized in Section 7, and the main key findings are listed in Section 8.

2. PORT MODEL DESIGN

The port models ("port ocean prediction systems," or POPS) follow a common structure designed to constrain system complexity. We use the same ocean general circulation model and code version, downscaling strategy, preprocessing tools, surface forcing product, and automation suite for all six POPS. The model grids, configuration/tuning, open boundary forcing, and freshwater input sources differ between POPS configurations.

2.1. MODEL SELECTION

The precursor to much of the OPP port modelling effort was conducted using the Finite Volume Community Ocean Model (FVCOM) (Chen et al. 2003) under the World Class Tanker Safety System (WCTSS) program, yielding prototype models for ports of Canso, Kitimat, and Vancouver Harbour. Even earlier, there have been modelling efforts based on Backhaus (Backhaus 1983; 1985) yielding models for the St. Lawrence estuary (Saucier and Chassé 2000) and the Gulf of St. Lawrence (Saucier 2003). These were then followed by implementation of an equivalent NEMO model by Environment and Climate Change Canada (ECCC), the Regional Marine Prediction System (RMPS) GSL. The RMPS was operational from 2011 to 2021, though none of these earlier models were considered for use in OPP. The WCTSS FVCOM prototypes used unstructured model meshes to resolve the coastal regions to within tens of metres or less, with resolution gradually decreasing to kilometres to match the parent model grid on the open boundary.

FVCOM has no history of operational deployment in Canada, while NEMO 3.6 (Nucleus of European Modelling of the Ocean) is used operationally by the Canadian Operational Network for Coupled Environmental PredicTion Systems (CONCEPTS). In the early part of OPP, a

comparison exercise between FVCOM 4.1 and NEMO 3.6 (Nudds et al. 2020) informed the decision-making process to select which codebase to use for the POPS models. Both codebases were used to construct models of the Bay of Fundy and the Port of Saint John (Paquin et al. 2020), which was chosen due to the large tides and complex circulation. NEMO 3.6's most significant deficiency in this context is the lack of wetting and drying, so if NEMO 3.6 could provide satisfactory results in the Bay of Fundy, then it would likely be suitable for use in the other regions. The two models were evaluated on how well they matched observations, as well as on computational efficiency, stability, and robustness. Both models were found to be skillful at reproducing observed data: neither model was significantly superior, and the choice of model to use going forward rested more heavily on the other factors.

Ultimately the decision was taken to proceed with NEMO 3.6, despite its structured grid, a somewhat coarser nearshore resolution, and higher demand for computational resources, to facilitate operationalization and align with modelling efforts at ECCC. Additional advantages of NEMO include active development that delivers regular code updates and bug fixes, an international NEMO Consortium group where members steer code development, and a well-established international operational modelling community.

Thus the ocean model used for all port ocean prediction systems is the CONCEPTS code: a fork of NEMO 3.6 (Madec 2016) that has been customized to meet the operational needs of CONCEPTS, for example (Dupont et al. 2015).

2.2. DOWNSCALING STRATEGY

The port models are downscaled solutions driven by larger-scale coastal ocean models currently operational at ECCC: the Coastal Ice-Ocean Prediction Systems East and West (CIOPS-E, CIOPS-W; Paquin et al. 2021a, Paquin et al. 2021b) which have 2-2.5 km resolution, and Salish Sea 500 (~500 m resolution; hereafter SS500) which is part of the CIOPS-W system. Output from these models forms the boundary conditions for our higher-resolution, smaller-area models. We use two levels of nesting to achieve a resolution fine enough to reach port scale. The nesting is one-way (coarse to fine), so no information is fed back to the larger scale models, allowing the models to run sequentially but otherwise independently of each other. This one-way nesting strategy also enables systematic errors to be corrected at the open boundaries.

We do not employ a dynamic ice model. Instead, we use a NEMO feature called "ice if", which uses input ice fields and the local freezing point to assess where ice cover exists, and in those locations it restores the sea surface temperature to the local freezing point and sets heat fluxes to -4 Wm^{-2} (Madec 2016).

We do not employ data assimilation or spectral nudging; all model runs are free runs.

River discharge data is used where available to supply the most realistic freshwater input to the model, and climatology is used when this is not available. Gauge data is also used in some cases to construct water level boundary conditions.

2.3. SIMULATION SEQUENCING

The port models operate in three configurations: hindcast, pseudo-analysis and forecast. Hindcasts are the most straightforward, using larger-scale model forcing and quality-controlled gauge data to drive the models. The model begins in the past from a cold-start (temperature and salinity interpolated as initial conditions, water at rest) or a hot-start (temperature, salinity, velocity, and sea-surface height interpolated as initial conditions) and reaches a spun-up state after a period of adjustment to the forcing. The model output is considered usable once spun up, and the model can run nearly up to the present in this configuration, provided that forcing data is

available. Pseudo-analysis runs are daily runs that keep the model state caught up to near-real-time, and do not include a direct data-assimilation component. Rather, the state is indirectly driven by data via boundary and surface forcing terms. These runs are used to initialize the first forecast of each day and may use different input than hindcasts depending on what data is available in real-time.

The pseudo-analysis and forecast schedule is chosen to match the schedule of the parent models that we use for forcing. Shortly after 00Z each day, a 24 hour pseudo-analysis simulation runs to catch up the model state to 00Z. This process uses restart files (so no spin up needed) and, where possible, uses gauge data drawn from a near-real-time data feed which receives limited quality control. Following the pseudo-analysis, the POPS generates four forecasts per day, each 48 hours long, which start from 00Z, 06Z, 12Z and 18Z. The daily 00Z forecast starts using the restart file from the daily pseudo-analysis and runs for 48 hours, saving a restart file six hours into the simulation. The 06Z forecast starts from this restart file, also saving a restart file six hours in, and similarly for the 12Z and 18Z forecasts. A schematic of this setup is shown in Figure 1. We focus only on the 00Z forecasts in this evaluation.

While the 00Z forecast simulation is nominally started at 00Z each day, in practice, the initialization of the simulation is delayed as it can not begin until all inputs are available from the larger scale models and the pseudo-analysis completes. At time of writing, this delay is approximately 5 hours, such that upon completion, each forecast simulation has about 43 hours of output that is in the future.

2.4. SURFACE FORCING

Surface forcing is derived from the High-Resolution Deterministic Prediction System (HRDPS) (Milbrandt et al. 2016) that runs operationally at ECCC and provides atmospheric weather forecasts four times per day at 2.5 km resolution. This is the highest-resolution operational atmospheric product available and is chosen to be consistent with the forcing used in CIOPS-E/W. In hindcast and pseudo-analysis mode, we use a time-blended form of the HRDPS forecasts, where hours 06–17 from successive forecasts are combined using weighted averaging to form temporally continuous fields with the same blending schedule as CIOPS-E/W. Additional details are given in the technical documentation for CIOPS-W version 1.5 (Paquin et al. 2022). Time blending is not used for forecasts.

The surface forcing is applied to the NEMO model using the CORE algorithms (Large and Yeager 2004) with modifications by ECCC to (a) read input data from the in-house RPN file format and (b) use the lowest diagnostic level of the atmospheric model rather than the conventional 2 m and 10 m data. Precipitation and sea-level pressure variations are also applied to the surface of the model.

2.5. AUTOMATION SUITE

The hindcast, pseudo-analysis and forecast simulations are all managed using ECCC's Maestro sequencing software. We have constructed a Maestro suite that is based on ECCC's CIOPS-E/W suites, where we use some of ECCC's functionality for the atmospheric forcing preparation and the mechanics of running the NEMO model, including managing restart files and outputs. We augment this baseline with functionality to prepare boundary forcing, extract data from the real-time data feed, generate the runoff forcing and prepare ice-concentration input files for the "ice-if" feature. Fallback strategies for missing data and persistence strategies for forecasts using gauge data are also implemented here.

2.6. ROBUSTNESS AND LIMITATIONS

For an operational model to be useful, it must be robust and not prone to failure. We have not assessed the models exhaustively in this regard; such testing is an ongoing process. However, some aspects have been explored:

- Where gauge data is needed as a model input, fallback mechanisms are implemented to mitigate missing or bad gauge data. Typically, this means we prepare a climatology for each gauge to stand in when the gauge data is unavailable. With these prepared ahead of time and with appropriate tooling to automate the switchover, the models can run despite missing gauge data and experience a graceful degradation through forcing with lower-quality data rather than a failure. Measuring the severity of the degradation under data-loss scenarios is reserved for future work.
- A long hindcast is conducted for model performance assessment. This long simulation demonstrates that the model is stable subject to a multi-year sample of weather/forcing conditions. In some cases, the hindcast period samples some extreme events, which helps bolster the case for model stability.
- Daily demonstration simulations (pseudo-analysis and four forecasts) have run for order one year on the General Purpose Science Cluster (GPSC) on a best-effort basis, to show that the automation suite can run the models routinely and reveal edge cases that can be fixed to improve robustness further. The purpose of running these pre-operational, best-effort simulations is to demonstrate the functionality/stability of the NEMO-based numerical model and the driving automation suite and identify issues that would impact operational deployment. The dominant source of issues experienced that impede on-schedule daily forecasts are (a) GPSC compute system downtime, both planned and unplanned, and (b) lack of availability of the forcing data from the larger-scale models that are nominally mirrored on schedule from ECCC's systems. These issues are deemed an expected consequence of using a research cluster and would be mitigated using an operational cluster.

The models will have some limitations:

- Intrinsic variability is expected in each model, and this has not been characterized.
- The lack of wetting and drying capability in NEMO 3.6 requires artificial bathymetry deepening in intertidal regions.

3. VANCOUVER HARBOUR

This section describes the Vancouver Harbour 20 m resolution port ocean prediction system.

3.1. REGIONAL OCEANOGRAPHY

The area of focus is Burrard Inlet, a fjord in the lower mainland of BC situated between the Northshore mountains and Burrard Peninsula on the north and south, respectively. The fjord begins at the span from Point Atkinson to Point Grey and progresses eastward through the First Narrows constriction to reach Vancouver Harbour. From there it continues east through the Second Narrows constriction and then forks to the east as the Port Moody Arm and to the north as Indian Arm. The depth is relatively shallow throughout except for Indian Arm, which reaches 220 m. Sills are found at First and Second Narrows and at the entrance to Indian Arm.

Circulation in Burrard Inlet is primarily estuarine, with fresher water flowing down the inlet near the surface and saltier water flowing in at depth from the Strait of Georgia. The bulk of the

freshwater input comes from the Capilano and Seymour rivers and Lynn Creek in Vancouver Harbour, and from the Indian River and the Buntzen power plant in Indian Arm, with the rest coming from small tributaries and direct precipitation. Strong tidal flow at First and Second Narrows induces significant turbulent mixing. Indian Arm is known to occasionally experience freshwater renewals (de Young and Pond 1988).

Howe Sound is outside Burrard Inlet to the northwest, and to the south is the mouth of the Fraser River. The Fraser River is the largest source of freshwater discharge into the Strait of Georgia and produces a significant plume of often-turbid water. Working west to east, a north and south arm of the Fraser fork at New Westminster, where roughly 80% of the discharge leaves through the south arm. The river again forks at Douglas Island, and the Pitt River fork reaches north to Pitt Lake, a large tidal lake.

3.2. DOMAIN AND CONFIGURATION

The downscaling model setup for the Vancouver Harbour model includes an outer and inner grid as shown in Figure 2. The outer grid is South Salish Sea 150 (hereafter SSS150) and has an approximate resolution of (dx, dy) = (129, 98) m, and has three open boundaries: along the west reaching from the west side of Howe Sound to the north end of Galiano Island, along the south reaching from the same north end of Galiano Island to Point Roberts, and at the east on the Fraser River at Mission. The inner grid is Vancouver Harbour 20 (hereafter VH20) which has an approximate resolution of (dx, dy) = (26, 19) m, and begins with a western open boundary at the mouth of English Bay and covers all of Vancouver Harbour, and ends with a northern open boundary at the mouth of Indian Arm. These two grids are refinements of the CIOPS-W grid, a refinement of the tri-polar global grid (Madec and Imbard 1996) and thus share the same local grid rotation. First Narrows is resolved with about 7 (SSS150) and about 35 (VH20) grid cells, and Second Narrows resolved with about 3 (SSS150) and about 12 (VH20) grid cells.

The bathymetry is assembled from the Canadian Hydrographic Service (CHS) data shifted to the Canadian Geodetic Vertical Datum of 1928 (CGVD28) (Mitchell O'Flaherty-Sproul, pers. comm.) and patched where available with the most recent bathymetry survey data available as of May 2020. The high-water coastline (CHS, pers. comm.) was used as part of the bathymetry dataset (with local high-water values shifted to CGVD28) and to calculate the land mask. We impose a minimum depth of 4 m to ensure model stability at low tide as NEMO 3.6 does not have a wetting and drying formulation, which has the impact of artificially deepening inter-tidal areas. The vertical grid uses z-levels with partial cells and a variable volume formulation (Levier et al. 2007), such that the grid spacing conforms to the sea-surface elevation as it rises and falls. The nominal vertical grid spacing is inherited from the Salish Sea model at 500 m nominal resolution (SS500), a component of the CIOPS-W v2.0.0 system (Paquin et al. 2021b) and ranges from 1 m near the surface to 27 m at depth.

Table 1 lists the grid parameters and key NEMO settings for each grid.

To contrast the resolution of the models, we plot in Figure 3 through Figure 5 the surface layer speed for three levels of zoom. At Figure 3 we see that CIOPS-W and SS500 both do not resolve the majority of Burrard Inlet nor the tidal jet leaving First Narrows, while SSS150 includes both. Figure 4 shows SSS150 and VH20 over the common areas, where we see tidal jets that are much more defined in the high-resolution model. Figure 5 shows a zoom of Figure 4.

Lastly, we note that the resolution of these grids is considerably higher than that of the surface forcing (2.5km). This relatively coarse surface forcing product is unlikely to resolve the differences between over land and over water at the scale of the harbour, in particular for the

wind forcing. We expect the POPS to benefit from higher resolution atmospheric products as they become available.

3.3. INITIALIZATION

The SSS150 hindcast begins 2016-12-23, and we designate the first nine days of simulation a spin-up period and thus consider SSS150 output from 2017-01-01 onward for evaluation. The VH20 model's initial conditions are interpolated from SSS150 on 2016-12-24, one day into SSS150's spin-up. Similarly, we evaluate VH20 output from 2017-01-01 onward.

The primary source of initial conditions for SSS150 is the forcing model SS500, where temperature, salinity, sea-surface height and velocities from a SS500 hindcast are interpolated to the SSS150 domain. Where needed, we employ a horizontal flooding-type extrapolation near coastlines and a vertical extrapolation near the bottom to ensure the initialization of all grid points.

The SS500 model resolves only part of Burrard Inlet: the domain ends outside of First Narrows. To initialize the area east of First Narrows, we use temperature and salinity interpolated spatially and temporally from an updated climatology (Foreman et al. 2008), we extrapolate sea-surface height from the SS500 limit in English Bay through the head of Indian Arm and ramp velocity to zero across First Narrows. Similarly, the SS500 model does not resolve the Fraser River upstream of the Port Mann bridge. Here we extrapolate the SS500 conditions from near the Port Mann bridge (near-uniform temperature and near-zero salinity) to the Pitt River, Pitt Lake and the main arm up to Mission. The extrapolation of freshwater into Pitt Lake is considered reasonable as the lake is known to be fresh. However, the extrapolation of temperature into Pitt Lake sets a nearly uniform value throughout the lake – this is not likely realistic. While we expect the temperature to spin up towards a more realistic condition as the hindcast proceeds, we lack observational data within Pitt Lake to confirm. Pitt Lake's role in the model is to allow a portion of the tidal energy that reaches the fork at Douglas Island to propagate in a dynamically consistent manner and consequently avoid the need for an open boundary condition on the Pitt River below the lake.

While these sea-surface height and velocity extrapolations are crude estimates of the initial conditions in these areas, they are spatially continuous and adequate to hot-start the SSS150 hindcast and wash out after a few tidal cycles of simulation.

3.4. OPEN BOUNDARY FORCING

The SSS150 west and south open boundaries are forced using snapshot output from SS500 and updated hourly. The baroclinic velocity and tracer boundary conditions directly use the hourly snapshot data with the flow relaxation boundary condition (Martinsen and Engedahl 1987). The barotropic open boundary condition type is Flather (Flather 1976), where we use the non-tidal component from SS500 and augment it with 15 tidal constituents listed in Table 1. To find the non-tidal component of SS500, we analyze the SS500 tides over five one-year periods (2017 through 2021) and use the average of the five analysis periods to synthesize the barotropic tidal signal and subtract it from SS500 when generating boundary forcing. Nodal corrections are applied at every hour.

The first eight constituents listed in Table 1 are derived from a single-year tidal analysis of SS500. We start with the analysis to force tides at the SSS150 boundary and conduct a one-year simulation. Analysis of the one-year simulation reveals the amplitude and phase mismatches at stations within the domain, and we adjust the boundary forcing to reduce systematic mismatches. The remaining seven minor tidal constituents are estimated at the model boundaries through inference. The inference is approximate, and we again use a one-

year simulation to find the mismatches and adjust the boundaries accordingly. This process successfully reduces water level errors as shown in section 5. The availability of the FES2022 tidal database in late 2022 poses an opportunity to revisit the tidal forcing in a future revision.

The SSS150 east open boundary at Mission uses a sea-surface height boundary condition forced by water level data from the Mission gauge (08MF024) with a no-gradient condition for the barotropic velocity and zero for the baroclinic velocity. Mission is situated upstream of the salt wedge limit, and thus the salinity is set to zero, and the temperature specified using the climatology of (Allen and Wolfe 2013). The boundary update frequency is every 30 minutes.

Constraining only the water level at the Mission boundary means that the model's internal physics implicitly determines the discharge. The dominant control here is the bottom friction along the Fraser River and requires tuning to match the water level at the stations downstream of Mission and to match the discharge. A tuning effort was employed to derive a spatially varying bottom friction field that minimizes these errors.

Analysis of simulations conducted during the development process revealed that the forcing models, CIOPS-W and SS500, have a sea-surface height bias of order 12 cm with respect to the CGVD28 vertical datum in the southern Salish Sea area. Meanwhile, the Mission gauge data for forcing the east boundary is on the CGVD28 datum. To avoid imposing an order 12 cm systematic error in the hydraulic slope along the Lower Fraser River, the Mission boundary should be raised, or the west and south boundaries should be lowered. Here we choose the latter and apply an offset of -12 cm to the non-tidal sea-surface height from SS500 at the west and south open boundaries. This offset of -12 cm is an estimate of the difference between CGVD28 and the geoid model EGM-DIR-R4 used by CIOPS-W/SS500 and revising this estimate is reserved for future work.

The VH20 boundary conditions are supplied from snapshot data saved from SSS150 at 15-minute frequency. The barotropic mode uses a Flather-type condition and the baroclinic velocity and tracers use the flow relaxation scheme. The rationale for 15-minute frequency is to mitigate tidal peak shaving that otherwise occurs with hourly forcing. No tidal adjustments or offsets are applied at this model connection, so there is no discontinuity at this boundary.

All open boundary forcing is linearly interpolated in time between the updates by NEMO during the simulation to avoid imparting discontinuities at the open boundaries.

3.4.1. Non-stationary tidal model

Hindcast and pseudo-analysis simulations cover past periods such that the near-real-time gauge data from the Mission station is available and we use the data directly for the sea-surface height condition at Mission for SSS150. We require a prediction/fallback to substitute the data for forecasts and periods where the Mission data is unavailable or not usable. The water level at Mission is mixed tidal-fluvial: The tides are non-stationary owing to a substantial seasonal variation in the river discharge. To build a prediction model for this non-stationary tide, we use the NS_TIDE analysis package (Matte et al. 2013). The non-stationary model for Mission water level is constructed using the package in an analysis mode, then it is leveraged to synthesize water level estimates in a prediction mode, roughly analogous to T_TIDE (Pawlowicz at al. 2002) usage. For analysis, the tool takes as input a timeseries from the gauge of interest, a downstream diurnal tidal range and a timeseries for one or more predictors, and it uses a fitting procedure to arrive at a model and optimal lag for each predictor. The prediction phase uses as input the model, downstream diurnal tidal range, and predictor timeseries with lags to calculate the water level at the gauge of interest. Here the gauge of interest is Mission, we chose the Steveston water level gauge to provide the diurnal tidal range and the non-tidal water level as a predictor, and the Hope gauge to provide the discharge and water level as additional predictors.

We ran the model using data from 2014, and the model is able to reproduce the Mission water level gauge with RMSE of 0.21 m over a historical period. This error level is deemed adequate for the purpose, although we may revisit this model for future revisions of SSS150.

While this model is suitable as a prediction/fallback for the Mission gauge, and the diurnal tidal range input is deterministic, it depends on two near-real-time gauges as predictors. These also need a prediction/fallback for forecasting and data unavailability. Table 2 lists these predictors, their lags, the fallback used for each, and the ramping timescale that we use to ramp from last valid data to the fallback. This ramping timescale is intended to avoid discontinuous switches between data and the fallback.

These data sources also require quality control to mitigate the impact of bad data because the near-real-time data feeds do not receive manual quality control. We use an automated threshold-based invalidation to reject erroneous data and fill it using the fallbacks. The provision of fallbacks enables the model to continue running when data feeds are unavailable at the expense of a modest degradation in simulation quality along the Fraser River.

3.5. FRESHWATER INPUT

While the Fraser River is the most significant freshwater source in the SSS150 domain, several other rivers also discharge into the area. Table 3 lists the nine that are configured, where five are available as near-real-time data feeds, and the remaining four are available as a monthly climatology. We have computed a monthly climatology for each of the five near-real-time sources to use as fallbacks should any of the real-time data feeds be unavailable. Threshold-based quality control is implemented to reject bad data and fill it with the fallback climatology data on a 5-day ramping time scale. These discharge sources are input into the model as daily averages and updated once per day. The water temperature for all freshwater sources follows a climatology (Allen and Wolfe 2013).

Forecast runoff for these inputs is estimated by persisting the runoff anomaly (difference from climatology) at the time of the latest good data for the forecast period. A consequence of this approach is that we may occasionally under or overestimate the discharge. For example, if the latest gauge runoff data stops just before a large runoff event, our method will persist the low runoff value for the forecast duration, and this may introduce a positive near-surface salinity bias near the mouth of the river during the forecast period. Similarly, if the gauge data ends at the peak of a large runoff event, that value will be persisted over the forecast as the runoff drops off and may result in a negative near-surface salinity bias. However, because the daily pseudo-analysis runs with the latest real gauge data, we do not accumulate these errors due to the persistence strategy. A hydrological model that derives discharge from atmospheric forecasts could improve upon this situation.

3.6. ICE MODEL

Burrard Inlet and Howe Sound are not known for forming sea ice. However, the Fraser River can form river ice for short periods, such as during winter cold snaps. We lack measurements of such river ice that could be used to validate an ice model, and as such we opt to configure NEMO's ice-if feature with an empty ice climatology instead of a dynamic ice model.

3.7. MODELLING SYSTEM STABILITY

The model hot starts as described above and simulates the five-year hindcast period and a set of 55 forecasts without experiencing simulation failure. While this is not definitive, this amounts to evidence that the numerical model is stable subject to the forcing conditions experienced during this evaluation period. Notably, this includes several unusual events:

- In November 2021, the lower mainland of BC experienced severe flooding due to an atmospheric river system that contributed a substantial amount of precipitation in a short period and high winds that stranded a barge on the beach near English Bay. The Fraser River discharge levels were elevated for several days, much beyond the norm for the Fall. Although the peak discharge was comparable to or less than the yearly freshet, the rapid rise and drop were unusual. The SSS150 and VH20 models remained stable through the entire period of high winds and unusual discharge.
- In December 2021, the lower mainland of BC experienced a cold snap severe enough to form river ice in the lower Fraser River. Media reports include land-fast river ice near Maple Ridge and loose chunks of ice downstream near the Patullo bridge and New Westminster. While the lack of a dynamical ice model did not allow for the simulation of this ice, the ice-if substitute kept the river temperature above freezing, and the model remained stable.
- The December 2021 cold snap also took the Mission water level gauge out of service for several weeks. During this time, the fallbacks for missing gauge data were activated, and the model ran without failure.

The automation system ("port_models Maestro suite") which sequences the daily pseudo-analysis and forecasts runs was operated on the General Purpose Science Cluster (GPSC) by the port modelling group for one year (2021-05 to 2022-04) for both the SSS150 and VH20 grids (i.e., the Vancouver Harbour POPS system). In 2022-03, CHS assumed this responsibility and has operated the system for more than one year.

Systematic stress testing, including but not limited to applying exaggerated forcing to probe the stability limits, has not been conducted at the time of writing and is reserved for future work.

4. EVALUATION METRICS

The model performance is assessed through the analysis of a multi-year hindcast and a shorter set of forecasts, where the dates considered are constrained by available surface and boundary forcing from larger scale models. The hindcast evaluation uses a wide set of observations to analyze the model's representation of ocean conditions, including tidal analysis and model drift that would be difficult to assess on a short model run. Meanwhile, the forecast evaluation focuses on measuring the degradation of model skill as a function of forecast lead time for a smaller set of observations available during the forecast period.

Quality controlled data sources were preferred where possible. We performed additional quality control to some data as needed, including visual inspection, thresholding and automatic de-spiking to eliminate suspect data.

4.1. HINDCAST

Hindcast performance is assessed through comparison with available observational data. For each observation, we extract the corresponding virtual observation from the model. The error is defined as

$$\text{ERROR} = \mathcal{X}_m - \mathcal{X}_o ,$$

where $\mathcal{X}_o$ and $\mathcal{X}_m$ are the observed and modelled values such that a positive/negative value indicates a model over/underestimate. For currents, $\mathcal{X}_o$ and $\mathcal{X}_m$ are taken as complex numbers with the real part representing the eastward and imaginary the northward components of velocity.

We use several scores, the bias, the centered root mean square error (hereafter CRMSE) and the root mean square error (hereafter RMSE),

$$\text{bias} = \frac{1}{N}\sum \text{ERROR} = \frac{1}{N}\sum \mathcal{X}_m - \frac{1}{N}\sum \mathcal{X}_o = \overline{\mathcal{X}_m} - \overline{\mathcal{X}_o},$$

$$\text{CRMSE} = \sqrt{\frac{1}{N}\sum (ERROR\text{-}bias)^2},$$

$$\text{RMSE} = \sqrt{\frac{1}{N}\sum ERROR^2} = \sqrt{bias^2 + CRMSE^2},$$

and these measures retain the units of $\mathcal{X}$.

We also use the unitless gamma squared score,

$$\gamma^2 = \frac{CRMSE^2}{\sum(x_o - \overline{x_o})^2},$$

which is the ratio of error variance to observed variance, such that zero indicates perfect agreement between model and observation variance, and unity indicates error variance is as large as the signal variance. A value of unity or larger indicates no skill.

For scalar quantities, we use the unitless sample Pearson correlation coefficient score,

$$\text{PEARSONR} = \frac{\sum (x_m - \overline{x_m})(x_o - \overline{x_o})}{\sqrt{\sum (x_m - \overline{x_m})^2 \sum (x_o - \overline{x_o})^2}},$$

where zero indicates no correlation and unity indicates perfect correlation. For vector quantities (currents) we have the vector correlation coefficient (Kundu 1976; Röhrs and Christensen 2015),

$$\text{VECTORR} = \frac{\sum (x_m - \overline{x_m})^* (x_o - \overline{x_o})}{\sqrt{\sum (x_m - \overline{x_m})^2 \sum (x_o - \overline{x_o})^2}},$$

where the asterisk represents complex conjugation, which is also implied for squaring of complex numbers. This quantity is a complex number, where the magnitude measures the overall correlation and the angle is a measure of the average angle of the modelled current with respect to the observation. Here we compute the angle as positive clockwise to be consistent with the convention of representing the velocity direction as positive clockwise from North. Lastly, the vector correlation angle is only considered meaningful when the correlation magnitude is large (Kundu 1976).

4.1.1. Water level

Water level observations from the Canadian Hydrographic Service (CHS) are transformed from CHS Chart Datum to Canadian Geodetic Vertical Datum of 1928 (CGVD28) by subtracting a station-specific offset. CHS provides these offsets are based on measurements from a GNSS (Global Navigation Satellite System) occupation at each station. Pacific US stations are shifted from the US datum to CGVD28 via NOAA's VDatum and NRCan Vertical Datum Transformations online tools. Atlantic US stations were gathered with a mean low-low water datum and converted to CGVD28 using conversion surfaces provided by CHS. Water level observations from the Water Survey of Canada (WSC) are shifted to CGVD28 using offsets provided by WSC.

Tidal analysis is performed using T_TIDE on one-year segments at an hourly sampling interval. Where data is available at a higher frequency, it is interpolated/subsampled to hourly frequency.

Observations missing more than 10% of the data points are not detided. The tidal analysis enables the decomposition of the total water level into tidal and non-tidal parts as

$$H_{total} = H_{tidal} + H_{nontidal}.$$

The annual (SA) and semi-annual (SSA) constituents are excluded from the tidal analysis; these constituents are subsumed into the non-tidal component. For the present purpose this is adequate as the same process is applied to both model and observations, and the extent to which the models do not reproduce SA or SSA is captured in the non-tidal error scores. Constituents with signal-to-noise ratios below 2 are also subsumed into the non-tidal part. Water level bias is included in the non-tidal component. Scores are reported for the total, tidal and non-tidal components. Owing to a negligible cross-correlation between tidal and non-tidal water levels, to a good approximation, we have

$$\mathrm{CRMSE}^2_{total\ wl} \cong \mathrm{CRMSE}^2_{tidal\ wl} + \mathrm{CRMSE}^2_{nontidal\ wl},$$

which shows how these two errors contribute to the total. Amplitude and phase errors are reported for the significant constituents, as is the tidal error.

$$\text{TIDAL ERROR} = \left[\frac{1}{2}({h_o}^2 + {h_m}^2) - h_o h_m \cos(\phi_o - \phi_m)\right]^{\frac{1}{2}},$$

where h_o and ϕ_o are the observed (subscript *o*) amplitude and Greenwich phase lag for a given tidal constituent, while h_m and ϕ_m are the modeled (subscript *m*) amplitude and phase (Cummins and Oey 1997).

4.1.1.1. Storm surge evaluation

To evaluate the port models' performance during storms, a handful of stormy periods are selected for each port. The cyclone database of (Zhang et al. 2019), which provides global storm tracks from 1958 to 2021(Figure 6 shows a zoom of North America), guides the selection. The database was queried for storms passing within a few hundred kilometres of each port model domain, and it provides a comprehensive list of storm events during the hindcast period. However, this list is quite extensive for some ports (particularly Canso and Saint John), so longer lists are narrowed down by considering minimum central pressure, examining water level gauges, and local media reports of storm impacts. The evaluation follows the residual water level hindcast evaluation in terms of performance scores and plots but is limited to the storm periods.

Storm surge detiding is done using a 40-day window around the storm's peak, i.e., 20 days before to 20 days after. This differs from the typical water level analysis, which is done in yearly spans and as such can include more constituents. However, using a shorter window does a better job removing the tides during each storm, particularly in areas with non-stationary tides.

We note that storm surges may interact non-linearly with tides to impact water levels, but we do not investigate this phenomenon here.

4.1.2. Water velocity

Velocity data is available from ADCPs and some current metres in one of four configurations: mounted on a mooring, buoy mounted (i.e., floating), in a float towed by a ship, or horizontally mounted on a shore structure (HADCP). Only horizontal (east-west / north-south, u/v) velocities are considered here. The horizontal velocity's u/v and speed/direction decompositions are both considered, and directions are calculated as positive clockwise from north.

Model data is extracted to match the observed data's time span and spatial location. Time series longer than 29 days and with less than 10% of data points missing are detided using

T_TIDE; hourly data is used for detiding, and where more frequent data is available, it is first down sampled. As with water level, the SA and SSA constituents are excluded from fitting, a Rayleigh value of 2 is used, and the observations and model data are processed the same way.

Currents are noisier, tend to have more missing data, are less stationary, and are impacted by more non-linear processes than water level observations, and these factors make the detiding process less robust. Owing to nonlinear processes such as bottom friction, some tidal (kinetic) energy will spread into adjacent frequencies, so fitting to tidal harmonics does not capture all variability induced by the tides, and some near-tidal variability remains in the residual velocities. We do not apply low-pass or band-stop filters to the residual to reduce the noise. While doing so would provide a more completely de-tided residual time series, some of the total signal would be unaccounted for by either the tidal or non-tidal evaluation. Given these caveats, the tidal component may be more accurately described as "the component of the currents that T_TIDE is able to fit." Currents are evaluated using similar metrics to water level, using complex formulations. Tidal constituents are evaluated using the ellipse error (Cummins and Thupaki 2018)

$$D_u = \left[\frac{1}{2}(A_o^2 + B_o^2 + A_m^2 + B_m^2) - \cos(g_o - g_m)\cos(\theta_o - \theta_m)(A_o A_m + B_o B_m) - \sin(g_o - g_m)\sin(\theta_o - \theta_m)\,(A_o B_m + A_m B_o)\right]^{1/2},$$

where A and B are semi-major and semi-minor axes, respectively, the subscripts *o* and *m* correspond to observed and modelled, g is phase, and θ is angle of inclination. For the non-tidal and total time series, complex formulations of the metrics listed at the beginning of the section are used, including bias, CRMSE, γ^2, and vector correlation.

We note that for single-location instruments, in particular moored current meters and moored and horizontally mounted ADCPs, we expect the scoring to be sensitive to the details of the model run under evaluation. Small errors in bathymetry can adjust the location of deterministic features (eddies, jets, meanders, etc.) and this can lead to large errors in the scoring. Meanwhile, chaotic internal variability can also affect the location of such features. An ensemble of model runs could help mitigate the latter but is beyond the scope of the current effort.

4.1.2.1. Horizontal ADCPs

HADCP data is decomposed into along- and cross-channel components, and evaluation is done primarily with mid-beam data to avoid edge effects. When a long enough time series is available, a tidal analysis is done as with moored instruments. Time series of the first week of data are plotted, regardless of how long the total time series is, to show the daily variability in the signal and how well the model captures it. Scatter plots are used to show the distribution of speed and direction of the total velocity, and the semi-major axis for the tidal ellipses are compared when feasible.

4.1.2.2. Current meters and moored ADCPs

Current meters report velocity at a single depth, so those velocities are evaluated at instrument-specific depths. For ADCPs on moorings or buoys, a standard set of depths at which to evaluate the velocities is selected on a per-port basis, taking into account local bathymetry and data availability; for brevity, statistics may be reported only at some depths for each instrument considered. These levels are defined relative to either a nominal surface (i.e., one with no sea-surface height variation) or the time varying sea surface. For regions with ADCPs in relatively deep water without a large tidal range, using the nominal surface is sufficient. For shallow regions and/or those with large tidal ranges, the evaluation is done relative to the time-varying

sea surface, using the observed total water depth to process the observations and modelled sea surface to process the modelled currents.

The observations are preprocessed to remove any spurious data points: values larger than 10 m/s are discarded and the data points are resampled if needed to be evenly spaced.

Tidal analysis is done on all timeseries of at least 29 days at depths with less than 10% of the data missing. Tidal ellipses are plotted for the largest tidal constituents, including depth profiles of tidal ellipses for the largest constituents. Time series and histograms are plotted for both the non-tidal and total velocities. Analysis of total velocities only is done for shorter time series or time series with missing data. We note that if data is missing at consistent phases of the tide, then the analyzed results may be aliased, and so time series with substantive regular gaps are not analyzed or presented.

4.1.2.3. ADCP transects

ADCP transects are too short for tidal analysis, so only the total velocities are considered. An along-transect / cross-transect decomposition is used, with a constant angle used for decomposition for the entire transect; this is sufficient as the transects are typically short and straight. Along-transect plots of velocities at depth are used for evaluation. Scatter plots of bias vs CRMSE are also plotted, with the statistics calculated at each physical point and integrated over the transect.

4.1.3. Water properties

Conductivity-Temperature-Depth (CTD) profiles are grouped into manually defined subregions based on the geography of each port domain. This enables an aggregate assessment over areas, including bias and CRMSE as a function of depth for each area. Model results are taken from the nearest point to the data location and nearest to the observation time. Vertical profiles are interpolated to the model z-levels to bring all data to consistent depths.

Sea surface temperature buoy and moored CTD measurements are evaluated using the bias, CRMSE, γ^2 and Pearson's *r* scores over the evaluation period. Model values are linearly interpolated to observation locations in the horizontal and vertical dimensions. The observed and modelled time series are interpolated to the largest common data interval.

Ferry thermosalinographs are vessel-mounted temperature and conductivity sensors. They provide a measure of near-surface water temperature and salinity by collecting data through one of the vessel's seawater circuits. Model results for comparison with these data are taken from the point nearest to the observed locations both horizontally and vertically and then linearly interpolated to the observation times. Hovmöller plots of observations, model results and differences, plus basic statistics, are used to assess the model performances relating to near-surface water.

4.1.4. Drift

The models' performance in drift trajectory prediction is assessed by comparing the observed tracks of ocean surface drifters with analogous trajectories modelled using the surface currents output by the port models, in combination with wind forcing from the National HRDPS atmospheric forecast. This comparison is done using the drift evaluation tool developed as part of the DPNM sub-initiative, in the OpenDrift configuration (Soontiens and Holden 2024).

Windage on the surface drifters is applied by computing the wind drag coefficient based on the drifters' drag area ratio (Niiler et al. 1995; Daniel et al. 2002; Röhrs et al. 2012; Hourston 2021; Blanken et al. 2021). This coefficient parameterizes the effect of direct wind drag on the parts of

the drifter exposed above the water surface and varies with drifter geometry. To account for wave-induced Stokes' drift, an additional 1% of the wind speed is added (Sutherland et al. 2020), and this sum is applied as the windage in the trajectory prediction.

This method of applying windage assumes that currents over the draft of the drifter are known exactly, as are winds directly at the ocean surface. However, in reality, neither of these assumptions is true, since:

1. The representation of surface currents in NEMO is limited by stability restrictions on near-surface vertical resolution and model uncertainty in general; and
2. Wind speed from the HRDPS model is also subject to model uncertainty and given at 10 m where winds are usually ~30% larger than at 1 m but could be as much as five times larger depending on wind speed and atmospheric stability (Smith 1988).

The representation of Stokes' drift as 1% of the wind speed represents a further assumption, as this value was derived by comparing tracks from various types of surface drifters to currents from the Regional Ice-Ocean Prediction System (RIOPS) ocean model and Canadian Arctic Prediction System (CAPS) atmospheric model (Sutherland et al. 2020). As noted in the discussion section of (Sutherland et al. 2020) and references therein, this value can vary widely depending on the combination of ocean and atmospheric forcing, which implies that model uncertainty contributes significantly to the appropriate value here. The authors also note that explicitly including Stokes drift based on a wave prediction system is preferable over parameterization based on wind velocity.

The windage term used here could be optimized by deriving it for each ocean/atmospheric model combination using the procedure in (Sutherland et al. 2020). However, this is beyond the scope of this report: the focus is on improvements to the current forcing for drift simulations without evaluating the suitability of wind predictions in the port model domains for drift prediction or commenting on the potential utility of a port-scale wave prediction system. The windage parameterization used here is merely intended to provide a consistent, deterministic linkage between modelled currents, winds, and the motion of various drifter types. As considerable uncertainty is associated with this windage term, evaluation of surface currents against observations from ADCPs and current meters is deemed the primary determinant of model suitability for drift prediction, rather than analysis of observed and modelled drifter tracks.

Periods where drifters were active in the model domain are identified, and modelled trajectories are started every hour along the drift tracks. The benefits of starting drift tracks in this manner are to reduce the sensitivity to initial conditions and increase the number of tracks available. However, it means that some drift tracks are not independent and thus the errors may be correlated. Modelled trajectories were computed for a user-specified period of 24 hours or more, where possible. However, in some regions, the majority of the observed drifter tracks were less than 24 hours long, and here a shorter modelled trajectory length was chosen.

Observed drifter tracks were truncated to areas covered by the 'wet' cells of the port model domains to avoid launching virtual drifters in 'dry' parts of the domain where observed drifters are near the shoreline, which may not be precisely resolved. In addition, to facilitate interpolation of starting locations for virtual drifters, observed trajectories were split where time gaps between positional records exceeded two hours. In the remaining portions, positional records were interpolated to a consistent time interval ranging from five minutes to one hour.

For each model – observation pair of trajectories, two statistics are computed to assess the model performance. First is the separation distance, D, which is given by,

$$D(t) = |\dot{x_o}(t) - \dot{x_m}(t)|$$

Here $\dot{x_o}$ and $\dot{x_m}$ are the positions of the observed and modelled drifter, and || denotes the magnitude of the vector difference, i.e., the distance, between them.

Second is the instantaneous skill score, S, following (Molcard et al. 2009), which is given by

$$S(t) = \max\left(0, 1 - \frac{D(t)}{d_o(t)}\right)$$

Here $d_o(t)$ is the displacement of the observed drifter from the starting point of the pair. The rationale for the normalization by $d_o(t)$ is to increase the skill assigned to a trajectory prediction as the trajectory length increases, even if the separation distance remains constant. A separation distance of, for example, 500 m represents a less grievous error in a trajectory that is 10 km long than in one that is 500 m long. A value of S=1 indicates a perfect prediction.

4.2. FORECAST

The forecast evaluation involves running a set of forecasts (here 48 hours long, each starting at 00Z) and evaluating the performance over the independent forecasts as a function of lead time. Forecast evaluation was performed for a set of order 60 consecutive forecasts by comparing the model values with tide gauge, sea surface temperature and horizontal ADCP records. The set of forecasts were taken from winter 2021/22 for logistical reasons. Forecast performance was evaluated as the discrepancy (bias and CRMSE) with observed values as a function of forecast lead time. The error growth curves represent the discrepancy averaged over the set of evaluated forecasts, and we include 95% confidence intervals computed with a bootstrap method.

To detide the forecast and the corresponding hindcast water level series we subtract the tidal signal precalculated based on the hindcast covering the forecast evaluation period. The tidal signal is obtained with a T_TIDE fit with a Rayleigh number as low as 0.1 (overfitting) to ensure maximal energy removal at tidal frequencies. Such strong suppression of tidal energy was implemented to clear the error growth curves of any tidal residual, which otherwise would dominate the curve.

5. HINDCAST EVALUATION RESULTS

The focus here is to assess the performance of the SSS150 and VH20 models, and comparisons with results from the larger-scale CIOPS-W and SS500 models are included where possible. Results from these larger-scale models are available as hourly snapshots for sea level, barotropic currents, surface and bottom currents and surface and bottom tracers, and available as daily averages for 3D currents and tracers.

The hindcast evaluation period spans five years, from 2017-01-01 through 2022-01-01. The SSS150 and VH20 results are saved as snapshots at hourly snapshot frequency to enable comparisons that employ tidal analysis. Figure 7, Figure 8 and Figure 9 show the locations of the observation data used to assess the model performance.

We limit the assessment to the northwestern subset of SSS150 covering a patch of the Salish Sea near the entrance of Howe Sound and English Bay, Howe Sound and Burrard Inlet. The rest of the domain covering the Lower Fraser and Pitt Rivers are assessed in similar document focused on the South Fraser 30 m port ocean prediction system (Dunphy et al. In press) to avoid duplication here.

5.1. WATER LEVEL

We evaluate the water level performance using the water level stations listed in Table 4, where we have water level data for our hindcast period for the first eight stations, and constituents computed from historical records of at least 365 days in length for three additional stations. The stations are ordered from outside of Burrard Inlet and progress to the east and then north and shown in Figure 8.

5.1.1. Mean sea surface height

The five-year mean water level (2017-2021 inclusive) is shown in Figure 10 and Figure 11 for the SSS150 and VH20 grids, respectively. In the SSS150 grid we see the hydraulic slope along the lower Fraser dominates the range. Meanwhile in VH20 we see depressions in mean water level at first and second narrows.

5.1.2. Tidal water level

Tidal constituents are evaluated at each station in Table 4 for 15 tidal constituents in Table 5 through Table 19. We compute the observed amplitude and phase via T_TIDE from 2020 water level data for the first eight stations and include the uncertainties provided by T_TIDE. Values for the last three stations are from historical data from the Canadian Hydrographic Service (CHS). The model amplitude and phases are computed from the simulation year 2020 and presented as amplitude, phase and tidal errors relative to the observed values. Values appearing as 0.000 or 0.0 result from including only three or one decimal places in our analysis and should not be considered precisely zero, but that they round to zero.

The CIOPS-W results are included for completeness although the focus is on the representation of tides in the SSS150 and VH20 models. Here we aim to show that the constituents are well represented and at a comparable or better level than SS500 at common stations. The tidal error is the most revealing score and will receive the most attention, while the amplitude and phase errors are included to show how each contributes to the tidal error.

The first eight constituents presented (M2, S2, N2, K1, O1, Q1, K2 and P1) are included in the forcing of the larger-scale models CIOPS-W and SS500 and the fits to these are coherent across all four models. The remaining seven constituents (L2, 2N2, NU2, J1, NO1, OO1, SO1) are not part of the CIOPS-W and SS500 open boundary forcing but may be introduced through another mechanism in those models (including, but not limited to, non-linear generation within the domain where such a pathway exists). We include them in the tables because some appear significantly out of phase with the fits from observations which leads to non-negligible tidal errors, and to demonstrate that including them in the forcing of the higher resolution models is a systematic improvement. Note that the NO1 results are included as reported by T_TIDE, although this constituent is forced as M1 (Schureman 1958, p 41). M1 and NO1 are deemed interchangeable for the present purpose because we are analyzing one-year records, further details are available in (Woodworth 2019).

Starting at Table 5 with M2, the largest constituent in the area, we see the forcing model SS500 performs well, leaving little room for improvement at higher resolution. The SSS150 marginally improves on this, removing a few mm of tidal error at most stations. VH20 performs similarly to SSS150 except at Port Moody, where we find a phase error of 2.56 degrees. At N2, skill is comparable between SS500 and SSS150 with slightly better amplitude but slightly degraded phases for SSS150, such that there is little change in tidal error. At S2, we have a slight improvement in amplitude and phase that yields a small improvement in tidal error. In O1, we have a minor degradation in the amplitude of about 2 mm but an improvement of about 1.5 deg in the phase leading to about a 0.5 cm improvement in tidal error. At K1, skill is comparable

between SS500 and SSS150 and VH20. At K2, the error in SSS150 and VH20 is about half of that in SS500 due to a phase adjustment. At P1 and Q1, the skill is again comparable between the three highest-resolution models.

Meanwhile, the additional seven constituents show a different story. These constituents are generally small, ranging from about 2 to about 5 cm in amplitude in the area. For L2, J1, NO1, OO1, NU2 and 2N2, we find these constituents under-represented in amplitude and with large phase errors in CIOPS-W and SS500. Meanwhile, in SSS150 and VH20, we find better amplitude and phase representation with significantly smaller tidal errors. Finally, SO1 is anomalous because it is over-represented in amplitude in CIOPS-W and SS500 but with a large phase error, such that SSS150 and VH20 again achieve smaller tidal errors.

Each of the seven additional constituents significantly improves tidal error for the larger-scale models, contributing to the overall reduction in water level CRMSE reported earlier. However, the tables show that amplitude and phase errors remain that exceed the observed uncertainties for some of these additional constituents in the higher-resolution models. These errors may be reducible through further tidal tuning efforts.

5.1.3. Non-tidal water level

Figure 12 through Figure 19 show the non-tidal water level comparisons between each model. For the outermost stations we see that all four models perform similarly. For the inner stations, we see SSS150 and VH20 also perform similarly, which is expected.

5.1.4. Overall scores

Here we assemble tables that compare the performance of each model for each station for the year 2020, where missing entries in the table are due to stations not residing in the model domain or due to missing or unusable data. The water level for CIOPS-W and SS500 is reduced by 12 cm for this analysis such that our analysis runs on the same GCVD28 datum.

Table 20 shows the tidal water level scores for year 2020 for three scores. Here there are significant differences in scores between models. The CRMSE is order 20 cm in CIOPS-W, is halved to order 9.5 cm in SS500, and almost halved again to order 5.5 cm in SSS150 and VH20. The scores are similar between stations, indicating that the tides are represented with similar quality throughout Howe Sound and Burrard Inlet. The improvement of SS500 with respect to CIOPS-W is beyond the current scope and is discussed in (Paquin et al. 2021b). The improvement from SS500 to SSS150 is ascribed to the tide tuning applied to the main eight constituents derived from SS500, and to the inference and tuning procedure employed to develop the forcing for the additional seven constituents.

Table 21 shows the non-tidal water level scores for year 2020 for three scores. Here we see little variation between the models with CRMSE scores ranging from 4 to 5 cm, except for Indian Arm Head which has CRMSE of 7 cm. This similarity between models is expected because much of the non-tidal water level is inherited from the larger-scale models and because the same surface forcing applied to each model. Locally generated non-tidal water level signals (e.g., seiches) may be contributing to this error but are not investigated here.

Table 22 summarises the total water level scores for 2020 for four score types. Aside from one anomalous station (Darrell Bay) with a significant bias of 17.9 cm, the bias ranges from 2.1 to 10.6 cm. The CRMSE score shows a significant improvement as we increase resolution. The CIOPS-W CRMSE is order 20 cm, for SS500, it is order 10 cm, and for the high-resolution SSS150 and VH20 models, it is order 7 cm. This improvement is also reflected in the γ^2 score that scales quadratically with CRMSE and the Pearson score.

To showcase the stability of the scores from Table 20 through Table 22 across years we include a summarising plot in Figure 20, where each row depicts a different model, the left panels show total water level bias vs CRMSE, the right panels show tidal CRMSE vs non-tidal CRMSE, each colour depicts a different station, and each marker depicts a different year.

In terms of bias, we see some year-to-year variability of order 10 cm depending on station, which may be explained by interannual variability in the data that is not captured by the model or may be an artifact of incomplete data. In total CRMSE we see the shift to lower errors for the higher-resolution models and see 1-3 cm of variability year to year. Meanwhile at tidal CRMSE we see the reduction in error as we go down the column and see stable scores for each model with order 1-3 cm variation year to year. The non-tidal CRMSE is also stable with about 2 cm of variability year to year.

Finally, we show the water level spectrum for Sandy Cove in 2018 and for Vancouver Harbour in 2019 in Figure 21 and Figure 22, respectively. Water level is well represented at both stations, and in the Sandy Cove plot we can see the improved tidal representation in the higher-resolution models SSS150 and VH20, while at Vancouver Harbour we confirm both models perform similarly in water level.

5.1.5. Storm surge water level

Storm surge evaluation is conducted over eight storms selected from the storm database and are listed in Table 23. The results are similar between stations, so we showcase just five stations in Figure 23 through Figure 27. At Darrell Bay we see the largest bias offset, and similar performance between the three models that cover the area, while Sandy Cove also shows comparable performance between all four models. At Vancouver Harbour and Port Moody we again see similar performance between the two active models here SSS150 and VH20. Lastly at Indian Arm Head we only have data for five of the eight storms and comparing these panels with Port Moody we see similar performance although the larger bias at Indian Arm is evident.

The corresponding scores averaged over storms and shown in Table 24 also indicate that the storm surge performance is similar between models. The similarity between models is expected as discussed above: the surge water level is largely inherited through the model hierarchy and the same surface forcing is applied to each model. Note that the CRMSE scores are smaller than those reported in Table 21 (order 3 cm vs 4-5 cm) and this is ascribed to the “over fitting” strategy used to detide water level over shorter periods centred about each storm.

5.2. WATER VELOCITY

We evaluate water velocity using three instrument types in this subsection.

5.2.1. Horizontal ADCPs

Near surface current measurements at Second Narrows are available via a horizontal acoustic doppler current profiler (HADCP) operated by Port Metro Vancouver. The device is mounted to the Second Narrows train bridge footing at a depth of 7.34 m below mean sea level and directed toward true-north. The instrument is configured to measure velocity in 65 bins at 2 m resolution, the first of which begins 4.1 m from the transducer. Bins 6 through 60, corresponding to the 110 m span from 14.1 to 124.1 m from the transducer, are averaged before broadcasting over the Automatic Identification System (AIS) for reception by vessels. This data stream is recorded using an AIS receiver, courtesy of Ocean Networks Canada (ONC). The data available spans 2017-11-21 through 2022-02-01 although there are several gaps in the data. We analyze this data over five periods chosen to avoid large gaps (ranging from 131 to 322 days in length) which are listed in Table 25. Also available are a set of constituents that are used for prediction

of currents at Second Narrows that were provided by CHS (Marlene Jeffries, pers. comm.). These constituents were constructed using an earlier dataset (2011-06-21 to 2012-06-20) and we note some differences in data preparation (averaging was over the 80 m span from 20-100 m) and in post-processing (constituents scaled up by 7% such that the average predicted speeds match the average observed speeds).

Figure 28 shows the instrument location and a scatter plot for the longest period ("year2020b") which reveals that the flow is nearly rectilinear (upper left scatterplot) with >99% of the variance explained by the principal axis of variance. As such we will focus on this component, which corresponds to the alongshore current where positive is roughly eastward toward Port Moody. The corresponding scatterplots for SSS150, VH20 and currents synthesized from the constituent file are also shown in Figure 28.

Figure 29 shows a six-day sample comparing data, models and constituents-based current. The top panel shows total alongshore velocity and we see that SSS150 typically matches or under-represents the peaks in the velocity extrema, VH20 matches or over-represents these peaks, and the constituents-based current also matches or over-represents the peaks but over-represents to a stronger degree than VH20 when it does. The middle panel shows the residual current, which reveals negative values (outflow) most of the time for both models and observations, and similarities in the residual current variation of the models with the observations. Finally, the bottom panel shows total velocity error where the SSS150 error curves are dominated by the underestimates, the constituents-based current dominated by overestimates and the VH20 model errors are largely in between those extremes.

To quantify this performance, Table 26 shows the scores for the total alongshore flow and it's tidal and non-tidal components, for the two models and the synthesis from constituents. For the total flow, the bias is less than 7 mm/s for SSS150 and is marginally higher at 1.5-3.1 cm/s in VH20, where for reference the observed mean outflow is 12.9-14.4 cm/s. Thus, the data show that we are capturing the estuarine outflow of roughly 14 cm/s as this is fairly consistent across periods analyzed, although it is underestimated by the highest resolution model. The synthesis from constituents shows a negative bias of 4.2-7.5 cm/s which corresponds to an overestimate of the near surface outflow (provided as 19.8 cm/s in the constituents file), and we note that the constituents dataset is based on the earlier 2011/06-2012/06 period wherein the near surface outflow may have been stronger.

Meanwhile, total velocity CRMSE is 21.3-25.7 cm/s in the SSS150 model, 16.3-27 cm/s in VH20, and 20.5-31.6 cm/s for the constituents synthesis if we consider it to represent the full currents. The first period (year2018a) shows VH20 with a large CRMSE, but the other four periods show a significantly smaller CRMSE, indicating that VH20 is more skillful at capturing the total variability (consistent with Figure 29 bottom panel). This performance is reflected in the γ^2 and Pearson scores for the later four periods. The reason for the poor performance for the year2018a period is unclear.

The non-tidal velocity shows comparable scores between SSS150 and VH20. The skill here is modest, with γ^2 ranging from 0.26-0.86 across periods, indicating that we are capturing some of the non-tidal variability and thus outperforming a constituents-only prediction (which would score as $\gamma^2=1$).

Lastly, for the tidal velocity, with the exception of the year2018a period, VH20 outperforms SSS150, which outperforms the constituent-based prediction. Here the γ^2 scores are around 0.01 for VH20 indicating that we are capturing the tidal signal well.

Table 27shows the tidal analysis for eight main constituents over the same five periods. Here we see a significant amount of variability in the amplitude of the constituents between periods.

At M2, 15 cm/s difference between the strongest and weakest periods, amounting to about 11% variability. Similarly, at N2 and S2 we have 20-25% variability in the amplitudes. At time of writing the source of variability is unclear. Interannual variability or non-stationarity in tides is known to occur in other settings (tidal rivers, internal tides, etc.) and that may be the case here, although data problems may also be responsible.

Despite the lack of clarity on the variability in the observed tidal constituent values, the model comparison therewith remains useful. Restricting attention to the second through fifth period, at M2 we see a consistent under-representation of the amplitude by about 20 cm/s in SSS150 that changes to an over-representation of about 5 cm/s in VH20, but with similar phase errors for each, and this is reflected in the tidal error as a reduction by about 2.5×. This pattern follows at N2, S2, O1, K1, P1 and Q1 – under-representations in SSS150 amplitudes are significantly improved upon in VH20 with similar phases which yields reductions in tidal error of order 1.5-3×. Lastly at K2 the differences between models do not improve the tidal error.

5.2.2. Current meters

No current meter records are available.

5.2.3. Moored ADCPs

ADCP measurements are available at two locations in Burrard Inlet (see Figure 7) and we select one deployment from each: BUW02 (2017-01-01 to 2017-06-14) and BIIP (2019-04-04 to 2020-04-03). Table 28, Table 29 and Table 30 show the total, non-tidal and tidal scores, respectively, and we will look at each station in turn.

For station BUW02, Figure 30 and Figure 31 show the residual currents at mid-depth (21.9 m) and near bottom (40.4 m), respectively. At mid-depth, the model east component (u) shows a small positive mean, while the observations show a negative mean (westward). For both components, the models do not capture as much variability as found in the observations and the histogram shows a peak centered about small velocities. At 40.4 m the observed mean in the east component is smaller and better reflected in the model. Variability levels, as shown in the histograms, are better in VH20 than SSS150.

Figure 32 shows the vertical profile of mean currents speed and direction (first column), and the vector correlation magnitude and angle for total, tidal and non-tidal currents (second to fourth columns). The mean currents do not match well, with the observed mean flow being westward from 20 m down to about 35 m, where it rotates counterclockwise going from 35 to 40 m depth. The models, meanwhile, both show a mean flow eastward, and this discrepancy is reflected in the bias scores with large offsets of order 20 cm/s.

The vector correlation performance ranges between 0.6 and 0.75 and is similar for the total and tidal velocities, owing to a large contribution of the tidal component to the total. In vector correlation magnitude, SSS150 outperforms VH20 from 20-35 m depth and then VH20 outperforms SSS150 below that. Meanwhile the vector correlation angle drops from around 20 degrees to 5-10 degrees going from SSS150 to VH20. Lastly the non-tidal component is poorly reproduced in vector correlation magnitude with values spanning about 0.05 to 0.25. As the vector correlation angle is only meaningful at large correlations, we do not find the vector correlation angle plot compelling. The score tables include samples of these vector correlation curves at four selected depths for the total and non-tidal, and also include RMSE and γ^2 scores as corroboration. For total we have γ^2 of order 0.5-0.7 indicating modest agreement, and for non-tidal the γ^2 scores are about 1-1.5 indicating poor agreement. The modest agreement of the total is also reflected in γ^2 of 0.4-0.68 in the tidal component.

Figure 33 and Figure 34 show rotary spectra for the 21.9 and 40.4 m depth levels, respectively. At 21.9 m, SSS150 performs similarly to VH20 at lower frequencies, and both models under-represent signals faster than about 6 cycles per day with SSS150 doing so to a larger degree than VH20. At 40.4 m, SSS150 is significantly weaker than VH20 at all frequencies. At both levels, there is a flattening of the spectra at higher frequencies, and this may be due to an elevated level of non-linear tides in the area. No strong inertial peak is found at either level, and this indicates that Burrard Inlet does not host significant inertial oscillations.

Figure 35 through Figure 40 show the tidal ellipses as a function of depth for six main constituents (M2, S2, N2, K1, O1, and Q1) that were resolved based on the record length. Here we find that neither model captures the ellipses completely, but there is a general improvement in VH20 relative to SSS150. For each constituent we see that the VH20 inclination better matches the observations, and a systematic reduction in ellipse size with depth in SSS150 that is less pronounced or not seen in VH20. Thus, we conclude that VH20 is better at representing the tidal currents at BUW02.

For station BIIP, Figure 41 and Figure 42 show the residual currents at 15.95 m and 36.95 m, respectively. At the upper-level station, performance is similar between the two models with variability levels reasonably captured by each model. At the lower level, SSS150 presents weaker variability than VH20.

Figure 43 and Figure 44 show rotary spectra for the 15.95 and 36.95 m depth levels, respectively. At the upper level, we see better performance in VH20 than SSS150 at almost all frequencies, and in particular the tidal frequencies. At the lower level, SSS150 is significantly underrepresenting all frequencies.

Figure 45 shows the mean currents and vector correlation profiles. The mean current is captured reasonably well in both models, with VH20 performing better near the bottom of the record. The total current correlation is high for both models (0.6 near surface, rising to roughly 0.85 at depth), with VH20 exhibiting a smaller angle. The tidal velocity is excellent with vector correlation in about 0.94-0.98 with VH20 on the higher end of that range for most of the depth. The non-tidal currents, however, are poorly represented with a correlation between about 0.09 and 0.38, although VH20 is consistently ahead of SSS150. The score tables reflect this assessment. Total γ^2 ranges from 0.42-0.72, non-tidal γ^2 is order 1. For the tidal component, for the upper three depth levels chosen, we see γ^2 improves from 0.07-0.16 to 0.03-0.06 as we go from SSS150 to VH20 and improves from 0.65 to 0.12 for the deepest level.

Figure 46 through Figure 53 shows the tidal ellipses for eight main constituents. Here we see improvements in ellipse representation as we go from SSS150 to VH20. A consistent feature across these plots is a reduction in ellipse size in SSS150 near the bottom that is not present in VH20. Broadly the improvement in ellipses matches the improvement in γ^2 observed in the score tables.

The discrepancy in performance at depth between the two models may be explained by differences in resolution that would favour VH20, differences in bottom friction, or other factors and investigating this is reserved for future work.

5.2.4. ADCP transects

During OPP surveys of Burrard Inlet, 289 velocity transects were collected using a vessel mounted ADCP instrument. Five examples are shown in Figure 54 through Figure 58 ordered from west to east along with the corresponding model velocities, with normal-to-transect velocity shown on the left and along-transect velocity shown on the right. The agreement between the models and the measurements varies significantly between transects and within areas of each

transect. The first transect in English Bay shows a near surface (5-10 m) normal jet near First Narrows end in both models that is not seen in the observation panel. This transect is 41 minutes long and the hourly snapshot frequency from the model may be responsible for the poor comparison. Meanwhile the comparison at the transect across first narrows (Figure 55) compares favourably in both normal and along-transect velocity where VH20 captures more of the detail.

The fourth transect west of Second Narrows shows a stark difference between SSS150 and VH20 in terms of representing the normal jet in the centre. Here the jet is roughly 150 m wide (roughly matching the width of the shipping channel), which contrasts with the SSS150 model resolution of about 96 m in the along-transect direction, leaving SSS150 with only 1-2 grid cells to resolve the current, which it struggles to do. Meanwhile VH20 has about 19 m resolution and is able to marginally resolve the jet, although it appears broadened (smoothed) compared to the measurements. Despite the poor resolution of SSS150 in resolving the shape of this jet, it does capture the transport by virtue of having good tidal performance, and we interpret the result at SSS150 as a well-smoothed version of the jet that has smaller velocity values. This reconciles with the HADCP analysis of 5.2.1 above that showed weaker currents and constituents in SSS150 vs VH20. This comparison points toward a need for resolution higher than 20 m to properly resolve Second Narrows.

Figure 59 shows a target diagram with one marker per transect indicating the bias and CRMSE, and Figure 60 compares a measure of kinetic energy between the model results and observed velocities. In both plots we do not see a clear improvement with model resolution across all transects. Unconstrained variability may be playing an outsized role in degrading the comparisons here. It is plausible that further model adjustments (tuning, resolution) would yield better representation here. Further investigation into the ADCP transect dataset is warranted.

5.3. WATER PROPERTIES

5.3.1. Sea surface temperature

The outer domain contains one weather buoy installed as part of the OPP program in 2019 near the entrance to English Bay (see Figure 8). Figure 61 shows the model comparison for the sea-surface temperature recorded from late 2019 through the end of 2021. All three models capture the broad seasonal cycle and SS500 and SSS150 track each other closely. CIOPS-W is biased cold in the summer while SS500 and SSS150 are biased cold in the winter. The corresponding scores in Table 31 show that the bias is roughly -0.6 °C, and that variability is better captured as smaller CRMSE in the higher resolution models (approx. 1 °C). SSS150 and SS500 use the same surface forcing and freshwater discharge temperature so similar performance here is expected.

5.3.2. Moored CTDs

Burrard Inlet contains one moored CTD instrument (see Figure 8) which was installed in 2019 as a joint effort between Ocean Networks Canada and Tsleil-Waututh first nation. The installation depth is 37 m, and two deployment records are available with comparisons shown in Figure 62 and Figure 63 and with the corresponding scores listed in Table 32.

For temperature, SSS150 and VH20 track each other closely and capture a seasonal cycle. Winter temperature is best represented, and summer temperature is biased warm with warming events over-represented. This is consistent between the two deployment records and also confirmed by similar scores in the score table with warm biases of about +0.3 and +0.16 °C for

the two records. The CRMSE score ranges from 0.29-0.34 °C and is marginally improved in the VH20 model.

For salinity, the models do not track each other as closely; SSS150 has a fresh bias and over-represents freshening events while VH20 shows a small salty bias. The patterns are qualitatively consistent between the two deployment records. The score table indicates a bias of -0.36 to -0.20 PSU for SSS150 and +0.08 to +0.27 for VH20, while CRMSE scores are comparable across models, ranging from 0.29 to 0.38 PSU.

5.3.3. CTD profiles

We evaluate temperature and salinity measured by CTD casts over six sub-regions shown in Figure 9 where the number of profiles per region is listed in Table 33. The amount of data here is limited so we analyze over the full five-year period 2017-2021. The per-region summarizing plots show mean bias as a function of depth in solid curve and the shaded area indicates ± the CRMSE (one standard deviation of the error). Note that the vertical axis on the plots is log-scale in pressure.

Beginning with Howe Sound region, which includes some of the Strait of Georgia near the entrance to Howe Sound, we summarize the comparisons in Figure 64. In temperature, CIOPS-W has a bias of about -0.8 °C near the surface and a +1.2 °C bias below that around the 8-12 m depth, which drops to less than +0.25 °C near the bottom. Meanwhile SS500 and SSS150 track each other closely with a consistent bias of about +0.3 °C except near the surface where SSS125 is showing a negligible bias. In near-surface salinity, CIOPS-W is biased salty by about +3 PSU while SS500 and SSS150 are biased fresh by about -4 PSU, with SSS150 marginally outperforming SS500. At depth, CIOPS-W is biased salty by roughly +0.5PSU while SSS500 and SSS150 show a negligible bias.

English Bay (Figure 65) shows similar patterns as the Howe Sound region. CIOPS-W is biased cold (-0.75 °C) and salty (+1.5 PSU) near the surface, at 8-10 m depth it becomes biased warm (+1.5 °C) and fresh (-2.5 PSU), and at depth the biases warm and salty but small. Meanwhile SS500 is biased warm (+0.5 °C) and quite fresh (-7 PSU) at the surface and these biases drop off with depth. SSS150 performs better here, with bias starting at about -0.25 °C at the surface and rising to +0.25 °C at depth and improving from about -4 PSU at surface to negligible at depth. Lastly, VH20 tracks SSS150 quite closely in this region.

In the Vancouver Harbour region, shown in Figure 66, SSS150 and VH20 perform similarly in temperature, showing negligible bias at the surface and rising to +0.25 °C at depth. In salinity, both SSS150 is biased fresh at the surface (-2 PSU) and negligibly at depth, which outperforms VH20 that is biased fresh at the surface (-3.5 PSU) and biased salty at depth (+0.5 PSU).

Figure 67 summarizes the Vancouver Harbour East region. For temperature we find a bias of about +1 °C at the surface for both models and nearly negligible bias at depth, and for salinity find that SSS150 is consistently biased fresh (approx. -0.5 to -1 PSU) while again outperforms VH20 which is biased fresh at the surface (approx. -3 PSU) and salty at depth (+1 PSU).

The Port Moody region shown in Figure 68 has few profiles, but we find almost no temperature bias in SSS150 and biases ranging from roughly +0.25 to +1.2 °C in VH20. Meanwhile in salinity SSS150 is biased fresh between -0.25 and -1 PSU, while VH20 is biased fresh by -0.75 to -2.5 PSU as a function of depth.

Lastly in Figure 69 we examine the Indian Arm region where only SSS150 is active, and we have bias within +/- 0.5 °C as a function of depth, and a fresh salinity bias within -1 to -0.5 PSU.

5.3.4. Ferries

No instrumented ferries available.

5.4. DRIFT

We conducted a drift evaluation experiment with 28 drifters, 2 SCT-type and 26 OSKER-type (for details about drifter types see Hourston 2021) that were released in Vancouver Harbour during OPP surveys. Figure 70 shows the drift tracks within the VH20 domain. The drift tracks are short and that limits the time scale of the drift skill assessment. The performance of SSS150 and VH20 is summarized by the Molcard score in Figure 71 and the separation distance score in Figure 72, where the scores sampled at each hour are tabulated in Table 34.

Both models score similarly in terms of Molcard and there is evidence of improvement in the VH20 model after about 3 hours although the standard deviation dwarfs the difference between the models. This marginal score improvement is also reflected in the separation distance score, where the VH20 model's separation distance grows slower than SSS150 and the standard deviation bands are narrowed. In short there is weak evidence here that VH20 outperforms SSS150 on drift performance.

In addition to the caveats discussed in section 4.4, we note that the number of drifters here is small and the standard deviation bands are large. Together these aspects expose a large amount of uncertainty in these results, which should be regarded as a first look at the drift performance. Further work is needed to constrain the skill of the combined SSS150/VH20+HRDPS+OpenDrift system in conducting drift predictions.

6. FORECAST EVALUATION RESULTS

The forecast evaluation period is 2021-12-03 through 2022-01-26, where we conduct a 48h forecast from 00Z daily for a total of 55 forecasts. Bias and CRMSE curves are shown where the shaded areas indicate the 95% bootstrap confidence intervals. We note that this period does not cover the late spring freshet period.

6.1. NON-TIDAL WATER LEVEL

Forecast evaluation for seven water level stations is shown in Figure 73 through Figure 79. Darrell Bay station is excluded from this evaluation due to poor data quality during the forecast evaluation period. For all stations, there is no significant change in bias as a function of lead hour, while there is an increase in CRMSE as a function of lead hour that is marginally statistically significant. This increase is order 1 cm CRMSE over the 48 hours of forecast and qualitatively consistent with the expectation that forecasts gradually degrade with lead time. The performance of all four models is similar in this regard, and this is expected because (a) the smaller scale models largely inherit non-tidal water level from the larger-scale models via the open boundary forcing, and (b) we use the same atmospheric pressure forcing at the surface for all four models which imparts the same inverse barometer effect.

6.2. HORIZONTAL ADCP

Figure 80 shows the forecast evaluation for the HADCP instrument at Second Narrows where we consider only the total alongshore velocity (no detiding). The bias panel shows a statistically significant non-monotonic signal for both SSS150 and VH20 that is smaller in the latter. The period looks to be diurnal, and as such we ascribe it to tidal error in diurnal constituent(s). The reduced size of this signal in the VH20 model supports ascribing to tidal error as we have seen improved tidal performance in VH20 in the earlier hindcast evaluation. Meanwhile on the

CRMSE panel we also see a diurnal signal in the SSS150 curve that is not present in the VH20 curve, again indicating better performance at higher resolution, and both curves do not show a statistically significant trend in error growth with lead hour.

6.3. SEA SURFACE TEMPERATURE

Sea-surface temperature forecast evaluation is shown in Figure 81 for the English Bay buoy. From the upper right panel there is an offset between CIOPS-W (which has a small positive bias) and SS500 and SSS150 (which have a larger negative bias). These overall biases are consistent with the hindcast evaluation shown in Figure 61. However, the focus here is on the forecast performance, and in all three models we do not see a statistically significant warming or cooling trend as a function of lead hour. There is a small diurnal signal in the higher resolution models, which is marginally less pronounced in the VH20 model compared to the SSS150 model, but in both cases is not statistically significant. Meanwhile in the lower left panel we do not see an increase in CRMSE as a function of lead hour for any of the models.

7. SUMMARY

High-resolution NEMO-based ocean models have been constructed covering the southern Salish Sea region, Burrard Inlet, Lower Fraser River and Pitt Lake at 150 m resolution and for Vancouver Harbour at 20 m resolution. The models are configured to run with an automation suite that facilitates daily pseudo-analysis runs and a set of four 48-hour forecasts that update every 6 hours, driven by output from larger-scale models SS500 and HRDPS that run at ECCC.

Model performance was assessed using a five-year hindcast and a set of 55 forecasts. For tidal water level, the SSS150 and VH20 models achieve CRMSE of 5-6 cm in the Howe Sound and Burrard Inlet area, which compares favourably with the larger-scale models that achieve CRMSE of approx. 9.5 and 20 cm for SS500 and CIOPS-W, respectively. This improvement is ascribed to the tuning of eight tidal constituents that are common with the parent forcing model, and to the inclusion of seven additional minor constituents.

For non-tidal water level, all four models under assessment achieve typical CRMSE of 4-5 cm, with one exception at 7 cm, where the exact numbers are sensitive to detiding parameter choices. This similarity in non-tidal performance across models is largely due to inheriting non-tidal water level through the nesting hierarchy, and due to the use of the same surface forcing product. Locally generated non-tidal signals that are not inherited, such as seiches, were not investigated here.

Water level bias varies between 2 and 18 cm depending on station although these biases can be mitigated in post-processing. Total water level CRMSE is 6-7 cm with one exception of 9 cm, and we ascribe this error to roughly equal contributions from the errors associated with the tidal and non-tidal components.

The SSS150 model is shown to be of adequate resolution to resolve the main geometry of the area and propagate water level signals throughout. The inner VH20 grid inherits this water level skill and does not contribute further improvements in water level performance.

Meanwhile, the SSS150 model is marginally capable of representing the currents at the observed locations within Vancouver Harbour. Currents are underestimated relative to measurements from the Second Narrows HADCP and tidal ellipses at two ADCP stations are under-represented at depth. The VH20 model improves substantially here: the HADCP measurement is less under-represented, and the tidal current ellipses are better represented at depth. Improvements are also seen at some ADCP transect measurements, in particular near

Second Narrows, although this points to a need for resolution even higher than 20 m to fully resolve the Second Narrows currents.

Sea-surface temperature is assessed at one location near the entrance to English Bay and we find cold biases in the high-resolution model in the winter, which may be inherited from the parent model SS500. Overall bias is about -0.7 °C and CRMSE is roughly 1 °C.

One moored CTD instrument in Vancouver Harbour at 37 m depth shows that the seasonal cycle in temperature is captured with a warm bias in the summer of +0.16 to+0.3 °C for both SSS150 and VH20, while CRMSE is around 0.3 °C for both models. Meanwhile salinity is biased fresh by -0.2 to -0.36 PSU in SSS150 and biased salty by +0.08 to +0.27 PSU in VH20 with CRMSE of about 0.34 PSU.

The assessment against CTD profiles indicates that performance is better in the SSS150 and VH20 models in the regions that overlap with the larger-scale SS500 and CIOPS-W models. Within Vancouver Harbour and as far as Port Moody, SSS150 performs as well or better than VH20, indicating that there is room for improvement in VH20 through further tuning efforts.

Drift assessment conducted within the VH20 model domain shows weak evidence that the VH20 model outperforms SSS150, although the small number of drifters used, and a number of other concerns limits the ability to constrain drift performance.

Forecast assessment for water level shows no trend in bias and shows a small trend in CRMSE as a function of lead hour that is marginally statistically significant at a level of approximately 1 cm CRMSE over the 48-hour forecast period. No statistically significant trend in bias or CRMSE is detected for the forecast velocities at the Second Narrows HADCP, nor for the sea-surface temperature measurement at the entrance to English Bay.

8. KEY FINDINGS

- The high-resolution models resolve areas that are not covered by any current operational NEMO-based model: Burrard Inlet beyond First Narrows, the Lower Fraser River from Douglas Island up to Mission and the Pitt River and Pitt Lake at 150 m resolution, and Vancouver Harbour from English Bay to Port Moody Arm at 20 m.
- The SSS150/VH20 models have simulated a five-year historical period (2017-2021) without simulation failure, which included a record setting flooding event in November 2021.
- The automated fallbacks for Mission water level data successfully recovered from a gauge failure in late 2021.
- Tidal water level CRMSE is 5-6 cm in the Howe Sound and Burrard Inlet area, which is roughly half of that in the parent SS500 model.
- Non-tidal water level performance is comparable at the high-resolution models and the coarser forcing models in areas resolved in both and is ascribed primarily to being inheriting these signals from the larger-scale models.
- Currents are marginally resolved in the SSS150 model and significantly better resolved in the VH20 model as measured at Second Narrows and two ADCP stations. Higher resolution than 20 m may be needed to fully resolve the jets that form in the narrows.
- Sea surface temperature bias is about -0.7 °C cold at the entrance to English Bay with CRMSE of 1 cm.

- Seasonal cycles of temperature and salinity are captured by the high-resolution models at one moored CTD instrument at 37 m depth in Burrard Inlet with absolute biases less than 0.3 °C / 0.27 PSU and with CRMSE of 0.3 °C / 0.34 PSU.
- CTD profiles reveal that the high-resolution models match or outperform the larger-scale models where they overlap in Howe Sound and English Bay, and this level of performance is maintained or exceeded in the rest of Burrard Inlet.
- Drift evaluation indicates that VH20 marginally outperforms SSS150 in terms of drift skill, although large uncertainties limit the ability to constrain the performance.
- Forecast assessment reveals a marginally statistically significant increase in CRMSE for non-tidal water level as a function of lead hour.
- Forecast assessment finds no statistically significant increase in CRMSE for horizontal velocities or sea-surface temperature, each measured at one location.

9. ACKNOWLEDGEMENTS

We thank ECCC colleagues Jean-Philippe Paquin, Greg Smith, Fred Dupont, and Oleksandr (Sasha) Huziy for advice and ideas in developing and evaluating the models, Pascal Matte for his advice in constructing the NS TIDE model, and Sarah MacDermid and Ji Lei for lending their maestro expertise. We thank Mitchell O'Flaherty-Sproul for help with bathymetric data. We thank Marlene Jeffries, Pete Wills and colleagues at CHS for provisioning tide, bathymetric and survey data. Thanks to Nancy Soontiens and Jennifer Holden for the drift prediction tool and help running it. Thanks also to Roy Hourston for facilitating drift measurements and collecting survey data. We further thank Jesse Montgomery at Metro Vancouver for Capilano River discharge data, Patrick Lilley at Kerr Wood Leidal for North Vancouver river discharge data, Ocean Networks Canada for recording the Second Narrows HADCP AIS data stream, and the waterproperties.ca team for their careful data curation. Thanks are also extended to Charles Hannah, Jon Chamberlain, Denis Lefaivre and Youyu Lu for advice and guidance. Lastly, we thank Denis Lefaivre, Joël Chassé, Nancy Soontiens, Yvonnick Le Clainche, Ji Lei, Justine McMillan, Isabelle Gaboury and Phil MacAulay for feedback during writing.

10. REFERENCES CITED

Allen, S.E., and M.A. Wolfe. 2013. “Hindcast of the Timing of the Spring Phytoplankton Bloom in the Strait of Georgia, 1968–2010.” *Progress in Oceanography* 115 (August):6–13. https://doi.org/10.1016/j.pocean.2013.05.026.

Backhaus, Jan O. 1983. “A Semi-Implicit Scheme for the Shallow Water Equations for Application to Shelf Sea Modelling.” *Continental Shelf Research* 2 (4): 243–54. https://doi.org/10.1016/0278-4343(82)90020-6.

———. 1985. “A Three-Dimensional Model for the Simulation of Shelf Sea Dynamics.” *Deutsche Hydrographische Zeitschrift* 38 (4): 165–87. https://doi.org/10.1007/BF02328975.

Blanken, Hauke, Caterina Valeo, Charles Hannah, Usman T. Khan, and Tamás Juhász. 2021. “A Fuzzy-Based Framework for Assessing Uncertainty in Drift Prediction Using Observed Currents and Winds.” *Frontiers in Marine Science* 8 (November):618094. https://doi.org/10.3389/fmars.2021.618094.

Chen, Changsheng, Hedong Liu, and Robert C. Beardsley. 2003. “An Unstructured Grid, Finite-Volume, Three-Dimensional, Primitive Equations Ocean Model: Application to Coastal Ocean and Estuaries.” *Journal of Atmospheric and Oceanic Technology* 20 (1): 159–86. https://doi.org/10.1175/1520-0426(2003)020<0159:AUGFVT>2.0.CO;2.

Cummins, Patrick F., and Lie-Yauw Oey. 1997. “Simulation of Barotropic and Baroclinic Tides off Northern British Columbia.” *Journal of Physical Oceanography* 27 (5): 762–81. https://doi.org/10.1175/1520-0485(1997)027<0762:SOBABT>2.0.CO;2.

Cummins, Patrick F., and Pramod Thupaki. 2018. “A Note on Evaluating Model Tidal Currents against Observations.” *Continental Shelf Research* 152 (January):35–37. https://doi.org/10.1016/j.csr.2017.10.007.

Daniel, Pierre, Gwénaële Jan, Fanch Cabioc’h, Yves Landau, and Erwann Loiseau. 2002. “Drift Modeling of Cargo Containers.” *Spill Science & Technology Bulletin* 7 (5–6): 279–88. https://doi.org/10.1016/S1353-2561(02)00075-0.

Dunphy, M., Krassovski, M., Taylor, S., Blanken, H., Horwitz, R., St-Onge Drouin, S., and Drozdowski, A. In press. Assessment of Port Ocean Prediction System Developed Under Canada’s Oceans Protection Plan: Fraser River. DFO Can. Sci. Advis. Sec. Res. Doc.

Dupont, Frédéric, Simon Higginson, Romain Bourdallé-Badie, Youyu Lu, François Roy, Gregory C. Smith, Jean-François Lemieux, Gilles Garric, and Fraser Davidson. 2015. “A High-Resolution Ocean and Sea-Ice Modelling System for the Arctic and North Atlantic Oceans.” *Geoscientific Model Development* 8 (5): 1577–94. https://doi.org/10.5194/gmd-8-1577-2015.

Flather, R.A. 1976. “A Tidal Model of the Northwest European Continental Shelf” 6 (10): 141–64. https://doi.org/10.1080/07055900.1987.9649262

Foreman, M. G. G., W. R. Crawford, J. Y. Cherniawsky, and J. Galbraith. 2008. “Dynamic Ocean Topography for the Northeast Pacific and Its Continental Margins.” *Geophysical Research Letters* 35 (22): L22606. https://doi.org/10.1029/2008GL035152.

Hourston, Roy A.S. 2021. *Surface Ocean Circulation Tracking Drifter Data from the Northeastern Pacific and Western Arctic Oceans, 2014-2020*. Sidney, B.C.: Fisheries and Oceans Canada = Pêches et Océans Canada.

Kundu, Pijush K. 1976. “Ekman Veering Observed near the Ocean Bottom.” *Journal of Physical Oceanography* 6 (2): 238–42. https://doi.org/10.1175/1520-0485(1976)006<0238:EVONTO>2.0.CO;2.

Large, WIlliam George, and Stephen G. Yeager. 2004. “Diurnal to Decadal Global Forcing for Ocean and Sea-Ice Models: The Data Sets and Flux Climatologies.” NCAR Technical Note NCAR/TN-460+STR. Boulder, CO: Climate and Global Dynamics Division: National Center for Atmospheric Research.

Levier, Bruno, Anne-Marie Tréguier, Gurvan Madec, and Valérie Garnier. 2007. “Free Surface and Variable Volume in the Nemo Code.” MERSEA IP report WP09-CNRS-STR-03-1A.

Madec, Gurvan. 2016. *NEMO Ocean Engine*. Note Du Pole de Modelisation de l’Institut Pierre-Simon Laplace 27. NEMO European Consortium.

Madec, Gurvan, and Maurice Imbard. 1996. “A Global Ocean Mesh to Overcome the North Pole Singularity.” *Climate Dynamics* 12 (6): 381–88. https://doi.org/10.1007/BF00211684.

Martinsen, Eivind A., and Harald Engedahl. 1987. “Implementation and Testing of a Lateral Boundary Scheme as an Open Boundary Condition in a Barotropic Ocean Model.” *Coastal Engineering* 11 (5–6): 603–27. https://doi.org/10.1016/0378-3839(87)90028-7.

Matte, Pascal, David A. Jay, and Edward D. Zaron. 2013. “Adaptation of Classical Tidal Harmonic Analysis to Nonstationary Tides, with Application to River Tides.” *Journal of Atmospheric and Oceanic Technology* 30 (3): 569–89. https://doi.org/10.1175/JTECH-D-12-00016.1.

Milbrandt, Jason A., Stéphane Bélair, Manon Faucher, Marcel Vallée, Marco L. Carrera, and Anna Glazer. 2016. “The Pan-Canadian High Resolution (2.5 Km) Deterministic Prediction System.” *Weather and Forecasting* 31 (6): 1791–1816. https://doi.org/10.1175/WAF-D-16-0035.1.

Molcard, A., P.M. Poulain, P. Forget, A. Griffa, Y. Barbin, J. Gaggelli, J.C. De Maistre, and M. Rixen. 2009. “Comparison between VHF Radar Observations and Data from Drifter Clusters in the Gulf of La Spezia (Mediterranean Sea).” *Journal of Marine Systems* 78 (November):S79–89. https://doi.org/10.1016/j.jmarsys.2009.01.012.

Morrison, J., M. G. G. Foreman, and D. Masson. 2012. “A Method for Estimating Monthly Freshwater Discharge Affecting British Columbia Coastal Waters.” *Atmosphere-Ocean* 50 (1): 1–8. https://doi.org/10.1080/07055900.2011.637667.

Niiler, Pearn P., Andrew S. Sybrandy, Kenong Bi, Pierre M. Poulain, and David Bitterman. 1995. “Measurements of the Water-Following Capability of Holey-Sock and TRISTAR Drifters.” *Deep Sea Research Part I: Oceanographic Research Papers* 42 (11–12): 1951–64. https://doi.org/10.1016/0967-0637(95)00076-3.

Nudds, Shannon, Youyu Lu, Simon Higginson, Susan P. Haigh, Jean-Philippe Paquin, Mitchell O’Flaherty-Sproul, Stephanne Taylor, et al. 2020. “Evaluation of Structured and Unstructured Models for Application in Operational Ocean Forecasting in Nearshore Waters.” *Journal of Marine Science and Engineering* 8 (7): 484. https://doi.org/10.3390/jmse8070484.

Paquin, Jean-Philippe, Youyu Lu, Stephanne Taylor, Hauke Blanken, Guillaume Marcotte, Xianmin Hu, Li Zhai, et al. 2020. “High-Resolution Modelling of a Coastal Harbour in the Presence of Strong Tides and Significant River Runoff.” *Ocean Dynamics* 70 (3): 365–85. https://doi.org/10.1007/s10236-019-01334-7.

Paquin, Jean-Philippe, François Roy, Gregory C. Smith, Frédéric Dupont, Yukie Hata, Oleksandr Huizy, Yosvany Martinez, Hauke Blanken, Jennifer Holden, and Nancy Soontiens. 2021a. “Coastal Ice Ocean Prediction System for the East Coast of Canada (CIOPS-E) Update from Version 1.5.0 to 2.0.0.” Canadian Centre for Meteorological and Environmental Prediction. https://collaboration.cmc.ec.gc.ca/cmc/cmoi/product_guide/docs/tech_notes/technote_ciops-east-200_e.pdf.

Paquin, Jean-Philippe, Gregory C. Smith, Frédéric Dupont, Sarah MacDermid, Yukie Hata, Oleksandr Huizy, Ji Lei, et al. 2021b. “Coastal Ice Ocean Prediction System for the West Coast of Canada (CIOPS-W) Update from Version 1.5.0 to 2.0.0.” Canadian Centre for Meteorological and Environmental Prediction. https://collaboration.cmc.ec.gc.ca/cmc/cmoi/product_guide/docs/tech_notes/technote_ciops-west-200_e.pdf.

Paquin, Jean-Phillipe, Gregory C. Smith, Francois Roy, Frederic Dupont, Sarah MacDermid, Ji Lei, Youyu Lu, Stephanne Taylor, Hauke Blanken, and Li Zhai. 2022. “Coastal Ice Ocean Prediction System for the West Coast of Canada (CIOPS-W): System Description for Versions 1.0.0 and 1.5.0.” Canadian Centre for Meteorological and Environmental Prediction. https://collaboration.cmc.ec.gc.ca/cmc/cmoi/product_guide/docs/tech_notes/technote_ciops-west-100_e.pdf.

Pawlowicz, Rich, Bob Beardsley, and Steve Lentz. 2002. “Classical Tidal Harmonic Analysis Including Error Estimates in MATLAB Using T_TIDE.” *Computers & Geosciences* 28 (8): 929–37. https://doi.org/10.1016/S0098-3004(02)00013-4.

Röhrs, Johannes, and Kai H. Christensen. 2015. “Drift in the Uppermost Part of the Ocean.” *Geophysical Research Letters* 42 (23). https://doi.org/10.1002/2015GL066733.

Röhrs, Johannes, Kai Håkon Christensen, Lars Robert Hole, Göran Broström, Magnus Drivdal, and Svein Sundby. 2012. “Observation-Based Evaluation of Surface Wave Effects on Currents and Trajectory Forecasts.” *Ocean Dynamics* 62 (10–12): 1519–33. https://doi.org/10.1007/s10236-012-0576-y.

Saucier, François J. 2003. “Modeling the Formation and Circulation Processes of Water Masses and Sea Ice in the Gulf of St. Lawrence, Canada.” *Journal of Geophysical Research* 108 (C8): 3269. https://doi.org/10.1029/2000JC000686.

Saucier, François J., and Joël Chassé. 2000. “Tidal Circulation and Buoyancy Effects in the St. Lawrence Estuary.” *Atmosphere-Ocean* 38 (4): 505–56. https://doi.org/10.1080/07055900.2000.9649658.

Schureman, Paul. 1958. “Manual of Harmonic Analysis and Prediction of Tides. [Revised 1940 Edition Reprinted 1958 with Corrections, Reprinted 2001].” 317pp. https://doi.org/10.25607/OBP-155.

Smith, Stuart D. 1988. “Coefficients for Sea Surface Wind Stress, Heat Flux, and Wind Profiles as a Function of Wind Speed and Temperature.” *Journal of Geophysical Research* 93 (C12): 15467. https://doi.org/10.1029/JC093iC12p15467.

Soontiens, Nancy, and Jennifer Holden J. 2024. "A framework for evaluation and characterization of drift prediction in the marine environment." Can. Tech. Rep. Hydrogr. Ocean Sci. 383: ix + 45 p. https://waves-vagues.dfo-mpo.gc.ca/library-bibliotheque/41252287.pdf.

Sutherland, Graig, Nancy Soontiens, Fraser Davidson, Gregory C. Smith, Natacha Bernier, Hauke Blanken, Douglas Schillinger, et al. 2020. “Evaluating the Leeway Coefficient of Ocean Drifters Using Operational Marine Environmental Prediction Systems.” *Journal of Atmospheric and Oceanic Technology* 37 (11): 1943–54. https://doi.org/10.1175/JTECH-D-20-0013.1.

Woodworth, Philip L. 2019. “The Global Distribution of the M1 Ocean Tide.” *Ocean Science* 15 (2): 431–42. https://doi.org/10.5194/os-15-431-2019.

de Young, Brad, and Stephen Pond. 1988. “The Deepwater Exchange Cycle in Indian Arm, British Columbia.” *Estuarine, Coastal and Shelf Science* 26 (3): 285–308. https://doi.org/10.1016/0272-7714(88)90066-2.

Zhang, Minghong, William Perrie, and Zhenxia Long. 2019. “Springtime North Pacific Oscillation and Summer Sea Ice in the Beaufort Sea.” *Climate Dynamics* 53 (1–2): 671–86. https://doi.org/10.1007/s00382-019-04627-1.

11. TABLES

Table 1. Key model parameters for the SSS150 and VH20 NEMO configurations.

Parameter	Outer grid (SSS150)	Inner grid (VH20)
Grid dimensions, NX x NY x NZ	710 x 826 x 39	1239 x 439 x 28
Horizontal resolution, ΔX x ΔY	Approx. 129 x 98 m	Approx. 26 x 20 m
Vertical resolution	1 m surface, 26 m bottom	1 m surface, 24 m bottom
Baroclinic / barotropic time step	20 s / 1s	2 s / 0.3333 s
Open boundary update frequency	1 h (W, S), 30 min (E)	15 min
Open Boundary SSH offset	-12 cm (W, S), 0 cm (E)	0 cm
Tidal constituents source	Salish Sea 500 and inference	Directly from SSS150
Tidal constituents forced	M2, S2, N2, K1, O1, Q1, K2, P1, L2, 2N2, NU2, J1, M1, OO1, SO1	N/A
Equation of state	EOS-80	EOS-80
Free surface	Variable volume	Variable volume
Light penetration	Two band	Two band
Lateral boundary condition	Partial slip (shlat=0.5)	Partial slip (shlat=0.5)
Momentum advection	Vector form, 10 sub-steps for vertical advection	Vector form, 8 sub-steps for vertical advection
Momentum lateral diffusion	Horizontal Laplacian and Smagorinsky	Smagorinsky and Horizontal Laplacian and Horizontal Bilaplacian
Tracer advection	Total Variance Dissipation, 10 vertical advection sub-steps	Total Variance Dissipation, 8 vertical advection sub-steps
Tracer lateral diffusion	Iso-neutral Laplacian and Smagorinsky	Iso-neutral Laplacian and Smagorinsky
Vertical diffusion	k-ε (GLS)	k-ε (GLS)
Bottom friction	Quadratic, spatially varying	Log-layer

Table 2. Data summary for the Mission open boundary non-stationary NS_TIDE model.

Station	Data used	Lag	Fallback/Prediction	Ramp to fallback timescale
Steveston 07607	Diurnal tidal range	—	—	—
Steveston 07607	Non-tidal water level	0	Zero	5 days
Hope 08MF005	Water level	10.5 h	Weekly climatology computed over 1912-2019	30 days
Hope 08MF005	Discharge	10.5 h	Weekly climatology computed over 1912-2019	30 days
Mission 08MF024	Water level	—	Computed from the non-stationary tide model for Mission	5 days

Table 3. Freshwater discharge sources used for the SSS150 domain (full list) and the VH20 domain (first five entries).

Source	Realtime data	Climatology	Climatology mean (m^3/s)
Capilano River	Metro Vancouver	Computed from 2019-2021 data	11.7
Mosquito Creek	North Vancouver via KWL	Computed from 2019-2021 data	0.5
Lynn Creek	North Vancouver via KWL	Computed from 2019-2021 data	6.7
Seymour River	North Vancouver via KWL	Computed from 2019-2021 data	14.5
Gallant Creek	North Vancouver via KWL	Computed from 2019-2021 data	0.1
Squamish River	—	Climatological values from (Morrison, Foreman, and Masson 2012) as used in the Salish Sea 500 model	514.3
Buntzen Powerhouse 2	—	Mean yearly value from de Young and Pond (1988)	23.0
Indian River	—	Computed using data from historical data from station 08GA005; yearly mean is consistent with estimate of 12 m^3/s from de Young and Pond (1988)	11.8
Pitt River	—	Computed from historical data from station 08MH017	53.5

Table 4. Water level station data used for evaluation and offsets used to shift the water level to CGVD28.

Station name	Station ID	Data available	Offset (m)
Darrell Bay	07808	Water level	3.190
Point Atkinson	07795	Water level	3.062
Sandy Cove	07786	Water level	3.069
Kitsilano	07707	Water level	3.046
Ambleside	07780	Water level	3.054
Vancouver	07735	Water level	2.9965
Port Moody	07755	Water level	3.123
Indian Arm Head	07774	Water level	3.051
Gibsons	07820	Constituents	—
Squamish	07811	Constituents	—
Second Narrows	07745	Constituents	—

Table 5. M2 constituent comparison for active tide gauges for year 2020 (upper part) and historical tide gauges (lower part).

	Observed		Amplitude Error (m)				Phase Error (deg)				Tidal error (m)			
Station name	**Amplitude (m)**	**Phase (deg)**	**CIOPSW**	**SS500**	**SSS150**	**VH20**	**CIOPSW**	**SS500**	**SSS150**	**VH20**	**CIOPSW**	**SS500**	**SSS150**	**VH20**
Darrell Bay	0.933 ± 0.002	31.5 ± 0.1	+0.034	-0.005	-0.001	—	+5.0	+0.3	-0.2	—	0.064	0.005	0.003	—
Point Atkinson	0.916 ± 0.002	30.8 ± 0.1	+0.021	-0.003	-0.004	—	+5.4	+0.5	+0.2	—	0.064	0.006	0.003	—
Sandy Cove	0.919 ± 0.002	30.9 ± 0.1	+0.019	-0.004	-0.003	-0.003	+5.4	+0.3	+0.1	-0.3	0.063	0.005	0.002	0.004
Kitsilano	0.929 ± 0.002	30.9 ± 0.2	+0.010	-0.011	-0.007	-0.007	+5.0	+0.1	+0.0	-0.6	0.058	0.008	0.005	0.009
Ambleside	0.930 ± 0.002	31.6 ± 0.2	+0.007	-0.013	-0.007	-0.009	+4.6	-0.5	-0.8	-1.2	0.053	0.011	0.010	0.015
Vancouver	0.938 ± 0.002	36.2 ± 0.1	—	—	+0.002	-0.001	—	—	-0.4	+0.0	—	—	0.004	0.001
Port Moody	0.969 ± 0.003	46.6 ± 0.2	—	—	+0.014	+0.006	—	—	+0.2	+2.6	—	—	0.010	0.031
Indian Arm Head	0.972 ± 0.003	47.0 ± 0.1	—	—	+0.011	—	—	—	+0.7	—	—	—	0.012	—
Gibsons	0.948	30.1	+0.005	-0.027	-0.017	—	+6.5	+1.6	+1.0	—	0.076	0.026	0.017	—
Squamish	0.942	31.2	+0.025	-0.011	-0.003	—	+5.4	+0.6	-0.0	—	0.065	0.010	0.002	—
Second Narrows	0.958	40.0	—	—	+0.005	-0.005	—	—	-2.5	+0.3	—	—	0.030	0.005

Table 6. N2 constituent comparison for active tide gauges for year 2020 (upper part) and historical tide gauges (lower part).

	Observed		Amplitude Error (m)				Phase Error (deg)				Tidal error (m)			
Station name	**Amplitude (m)**	**Phase (deg)**	**CIOPSW**	**SS500**	**SSS150**	**VH20**	**CIOPSW**	**SS500**	**SSS150**	**VH20**	**CIOPSW**	**SS500**	**SSS150**	**VH20**
Darrell Bay	0.200 ± 0.002	4.0 ± 0.6	-0.001	-0.007	-0.002	—	+3.8	+0.9	-2.1	—	0.009	0.006	0.005	—
Point Atkinson	0.197 ± 0.002	3.3 ± 0.6	-0.004	-0.007	-0.003	—	+4.1	+1.1	-1.9	—	0.010	0.006	0.005	—
Sandy Cove	0.197 ± 0.002	3.4 ± 0.6	-0.004	-0.007	-0.003	-0.002	+4.0	+1.0	-2.0	-2.4	0.010	0.006	0.005	0.006
Kitsilano	0.199 ± 0.002	3.2 ± 0.8	-0.006	-0.009	-0.003	-0.003	+3.9	+0.9	-1.7	-2.3	0.010	0.006	0.004	0.006
Ambleside	0.200 ± 0.002	3.9 ± 0.7	-0.008	-0.010	-0.004	-0.004	+3.5	+0.5	-2.4	-2.8	0.010	0.007	0.007	0.008
Vancouver	0.198 ± 0.002	9.6 ± 0.5	—	—	-0.002	-0.002	—	—	-2.2	-1.7	—	—	0.005	0.004
Port Moody	0.200 ± 0.002	22.1 ± 0.8	—	—	+0.002	0.000	—	—	-1.0	+1.6	—	—	0.003	0.004
Indian Arm Head	0.200 ± 0.003	22.9 ± 0.8	—	—	+0.002	—	—	—	-0.9	—	—	—	0.002	—
Gibsons	0.199	358.4	-0.002	-0.006	+0.001	—	+9.5	+6.5	+3.3	—	0.023	0.016	0.008	—
Squamish	0.194	3.9	+0.003	-0.002	+0.004	—	+4.3	+1.4	-1.9	—	0.010	0.004	0.006	—
Second Narrows	0.199	14.0	—	—	0.000	-0.004	—	—	-4.6	-1.4	—	—	0.011	0.004

Table 7. S2 constituent comparison for active tide gauges for year 2020 (upper part) and historical tide gauges (lower part).

	Observed		Amplitude Error (m)				Phase Error (deg)				Tidal error (m)			
Station name	**Amplitude (m)**	**Phase (deg)**	**CIOPSW**	**SS500**	**SSS150**	**VH20**	**CIOPSW**	**SS500**	**SSS150**	**VH20**	**CIOPSW**	**SS500**	**SSS150**	**VH20**
Darrell Bay	0.240 ± 0.002	59.8 ± 0.5	+0.011	-0.004	-0.004	—	+6.8	+2.1	+1.0	—	0.022	0.007	0.004	—
Point Atkinson	0.236 ± 0.002	59.2 ± 0.6	+0.007	-0.004	-0.003	—	+7.2	+2.0	+1.2	—	0.022	0.006	0.004	—
Sandy Cove	0.236 ± 0.002	59.1 ± 0.5	+0.007	-0.004	-0.002	-0.002	+7.3	+2.1	+1.2	+0.7	0.022	0.007	0.004	0.003
Kitsilano	0.238 ± 0.003	58.9 ± 0.6	+0.005	-0.005	-0.004	-0.004	+7.1	+1.9	+1.1	+0.3	0.022	0.007	0.004	0.003
Ambleside	0.239 ± 0.002	60.0 ± 0.6	+0.004	-0.006	-0.004	-0.004	+6.3	+1.0	-0.2	-0.6	0.019	0.005	0.003	0.003
Vancouver	0.238 ± 0.002	66.0 ± 0.4	—	—	-0.002	-0.003	—	—	+0.6	+1.1	—	—	0.002	0.004
Port Moody	0.241 ± 0.003	79.6 ± 0.5	—	—	+0.003	+0.001	—	—	+1.9	+4.7	—	—	0.006	0.014
Indian Arm Head	0.241 ± 0.003	80.3 ± 0.7	—	—	+0.001	—	—	—	+2.3	—	—	—	0.007	—
Gibsons	0.238	59.1	+0.010	-0.004	-0.002	—	+7.5	+2.5	+1.4	—	0.024	0.008	0.004	—
Squamish	0.232	60.1	+0.018	+0.004	+0.006	—	+6.1	+1.6	+0.5	—	0.022	0.006	0.004	—
Second Narrows	0.236	70.5	—	—	+0.005	+0.001	—	—	-1.9	+2.0	—	—	0.007	0.006

Table 8. O1 constituent comparison for active tide gauges for year 2020 (upper part) and historical tide gauges (lower part).

	Observed		Amplitude Error (m)				Phase Error (deg)				Tidal error (m)			
Station name	**Amplitude (m)**	**Phase (deg)**	**CIOPSW**	**SS500**	**SSS150**	**VH20**	**CIOPSW**	**SS500**	**SSS150**	**VH20**	**CIOPSW**	**SS500**	**SSS150**	**VH20**
Darrell Bay	0.484 ± 0.006	264.0 ± 0.6	-0.018	+0.017	+0.020	—	+12.9	+2.4	-0.5	—	0.076	0.019	0.015	—
Point Atkinson	0.479 ± 0.005	263.6 ± 0.6	-0.014	+0.012	+0.014	—	+13.4	+2.5	-0.2	—	0.078	0.017	0.010	—
Sandy Cove	0.479 ± 0.006	264.0 ± 0.6	-0.014	+0.013	+0.015	+0.015	+13.0	+2.1	-0.6	-0.9	0.076	0.015	0.011	0.012
Kitsilano	0.482 ± 0.006	264.0 ± 0.6	-0.015	+0.010	+0.015	+0.015	+12.9	+2.2	-0.4	-0.9	0.076	0.015	0.011	0.012
Ambleside	0.480 ± 0.007	264.3 ± 0.6	-0.014	+0.012	+0.016	+0.015	+12.7	+1.9	-0.9	-1.2	0.075	0.014	0.013	0.013
Vancouver	0.475 ± 0.006	266.5 ± 0.6	—	—	+0.017	+0.016	—	—	-0.2	-0.1	—	—	0.012	0.011
Port Moody	0.476 ± 0.005	273.2 ± 0.6	—	—	+0.016	+0.016	—	—	-0.7	+0.6	—	—	0.012	0.012
Indian Arm Head	0.476 ± 0.005	273.4 ± 0.7	—	—	+0.019	—	—	—	-0.4	—	—	—	0.013	—
Gibsons	0.483	262.2	-0.022	+0.008	+0.010	—	+13.9	+2.7	-0.4	—	0.082	0.017	0.007	—
Squamish	0.493	264.3	-0.034	-0.002	-0.002	—	+13.1	+2.7	-0.1	—	0.081	0.016	0.002	—
Second Narrows	0.512	270.1	—	—	-0.011	-0.002	—	—	-1.5	+0.8	—	—	0.012	0.005

Table 9. K1 constituent comparison for active tide gauges for year 2020 (upper part) and historical tide gauges (lower part).

	Observed		Amplitude Error (m)				Phase Error (deg)				Tidal error (m)			
Station name	**Amplitude (m)**	**Phase**	**CIOPSW**	**SS500**	**SSS150**	**VH20**	**CIOPSW**	**SS500**	**SSS150**	**VH20**	**CIOPSW**	**SS500**	**SSS150**	**VH20**
Darrell Bay	0.871 ± 0.005	286.4 ± 0.4	-0.028	+0.011	+0.006	—	+11.8	+0.7	+0.1	—	0.126	0.011	0.004	—
Point Atkinson	0.860 ± 0.005	286.3 ± 0.3	-0.019	+0.007	+0.004	—	+11.9	+0.2	-0.1	—	0.125	0.006	0.003	—
Sandy Cove	0.861 ± 0.006	286.3 ± 0.4	-0.019	+0.006	+0.005	+0.004	+11.9	+0.2	-0.1	-0.4	0.125	0.005	0.004	0.005
Kitsilano	0.866 ± 0.006	286.2 ± 0.4	-0.021	+0.001	+0.002	+0.001	+11.9	+0.3	-0.1	-0.5	0.126	0.003	0.002	0.006
Ambleside	0.865 ± 0.006	286.6 ± 0.4	-0.022	+0.001	+0.002	+0.002	+11.6	-0.1	-0.6	-0.8	0.123	0.001	0.006	0.009
Vancouver	0.860 ± 0.005	289.2 ± 0.3	—	—	+0.006	+0.006	—	—	-0.3	-0.1	—	—	0.005	0.004
Port Moody	0.864 ± 0.005	295.6 ± 0.4	—	—	+0.009	+0.008	—	—	-0.2	+1.1	—	—	0.007	0.013
Indian Arm Head	0.866 ± 0.005	295.8 ± 0.3	—	—	+0.009	—	—	—	+0.0	—	—	—	0.006	—
Gibsons	0.872	285.2	-0.031	+0.002	-0.002	—	+12.7	+1.3	+0.6	—	0.136	0.014	0.006	—
Squamish	0.875	286.8	-0.029	+0.010	+0.007	—	+11.9	+0.8	+0.1	—	0.128	0.011	0.005	—
Second Narrows	0.893	292.1	—	—	-0.009	-0.005	—	—	-1.3	+0.6	—	—	0.016	0.007

Table 10. K2 constituent comparison for active tide gauges for year 2020 (upper part) and historical tide gauges (lower part).

	Observed		Amplitude Error (m)				Phase Error (deg)				Tidal error (m)			
Station name	**Amplitude (m)**	**Phase (deg)**	**CIOPSW**	**SS500**	**SSS150**	**VH20**	**CIOPSW**	**SS500**	**SSS150**	**VH20**	**CIOPSW**	**SS500**	**SSS150**	**VH20**
Darrell Bay	0.066 ± 0.002	62.6 ± 1.9	+0.008	+0.002	+0.001	—	+5.5	-6.0	+0.7	—	0.008	0.005	0.001	—
Point Atkinson	0.066 ± 0.002	60.9 ± 2.2	+0.006	+0.002	-0.002	—	+6.6	-4.5	+2.1	—	0.007	0.004	0.002	—
Sandy Cove	0.065 ± 0.002	61.6 ± 1.8	+0.006	+0.002	-0.001	-0.001	+6.0	-5.0	+1.7	+1.1	0.007	0.004	0.002	0.001
Kitsilano	0.065 ± 0.003	61.1 ± 2.5	+0.007	+0.002	-0.002	-0.001	+5.8	-4.6	+1.2	+1.2	0.007	0.004	0.001	0.001
Ambleside	0.066 ± 0.002	60.9 ± 2.0	+0.006	+0.001	-0.001	-0.001	+6.2	-4.0	+2.0	+1.4	0.007	0.003	0.002	0.002
Vancouver	0.067 ± 0.002	63.6 ± 1.4	—	—	0.000	-0.001	—	—	+0.1	+0.6	—	—	0.000	0.001
Port Moody	0.072 ± 0.002	65.1 ± 1.8	—	—	+0.001	0.000	—	—	-1.7	+0.4	—	—	0.002	0.000
Indian Arm Head	0.074 ± 0.003	64.4 ± 2.1	—	—	+0.001	—	—	—	-1.1	—	—	—	0.001	—
Gibsons	0.066	60.3	+0.005	+0.001	-0.001	—	+6.9	-4.2	+2.0	—	0.007	0.003	0.002	—
Squamish	0.063	67.0	+0.009	+0.006	+0.005	—	+0.5	-11.1	-4.7	—	0.007	0.010	0.005	—
Second Narrows	0.077	63.9	—	—	-0.004	-0.001	—	—	-1.2	+0.2	—	—	0.003	0.001

Table 11. P1 constituent comparison for active tide gauges for year 2020 (upper part) and historical tide gauges (lower part).

	Observed		Amplitude Error (m)				Phase Error (m)				Tidal error (m)			
Station name	**Amplitude (m)**	**Phase (deg)**	**CIOPSW**	**SS500**	**SSS150**	**VH20**	**CIOPSW**	**SS500**	**SSS150**	**VH20**	**CIOPSW**	**SS500**	**SSS150**	**VH20**
Darrell Bay	0.278 ± 0.005	285.1 ± 1.0	-0.021	+0.003	-0.007	—	+12.4	-1.3	-1.0	—	0.043	0.005	0.006	—
Point Atkinson	0.275 ± 0.005	285.6 ± 1.0	-0.019	+0.001	-0.008	—	+12.0	-1.7	-1.2	—	0.042	0.006	0.007	—
Sandy Cove	0.275 ± 0.006	285.3 ± 1.2	-0.020	+0.001	-0.008	-0.008	+12.3	-1.4	-1.0	-1.2	0.043	0.005	0.007	0.007
Kitsilano	0.277 ± 0.006	284.9 ± 1.2	-0.020	-0.002	-0.010	-0.010	+12.7	-1.2	-0.7	-1.1	0.044	0.004	0.007	0.008
Ambleside	0.277 ± 0.006	285.9 ± 1.4	-0.021	-0.002	-0.010	-0.010	+11.9	-2.1	-1.7	-1.9	0.042	0.007	0.009	0.010
Vancouver	0.273 ± 0.005	289.0 ± 1.1	—	—	-0.007	-0.008	—	—	-1.4	-1.1	—	—	0.007	0.007
Port Moody	0.274 ± 0.006	296.3 ± 1.2	—	—	-0.007	-0.007	—	—	-1.0	+0.2	—	—	0.006	0.005
Indian Arm Head	0.276 ± 0.006	296.0 ± 1.2	—	—	-0.007	—	—	—	-0.2	—	—	—	0.005	—
Gibsons	0.274	286.4	-0.021	0.000	-0.008	—	+11.0	-2.4	-2.2	—	0.039	0.008	0.009	—
Squamish	0.272	284.1	-0.020	+0.001	-0.012	—	+14.8	+1.4	+1.9	—	0.050	0.005	0.011	—
Second Narrows	0.281	292.5	—	—	-0.022	-0.021	—	—	-1.5	+0.6	—	—	0.016	0.015

Table 12. Q1 constituent comparison for active tide gauges for year 2020 (upper part) and historical tide gauges (lower part).

	Observed		Amplitude Error (m)				Phase Error (deg)				Tidal error (m)			
Station name	**Amplitude (m)**	**Phase (deg)**	**CIOPSW**	**SS500**	**SSS150**	**VH20**	**CIOPSW**	**SS500**	**SSS150**	**VH20**	**CIOPSW**	**SS500**	**SSS150**	**VH20**
Darrell Bay	0.076 ± 0.005	255.8 ± 3.7	-0.001	+0.005	+0.006	—	+17.1	+0.7	+0.1	—	0.016	0.003	0.004	—
Point Atkinson	0.076 ± 0.005	255.8 ± 3.8	-0.002	+0.002	+0.003	—	+17.2	+1.3	+1.2	—	0.016	0.002	0.003	—
Sandy Cove	0.077 ± 0.005	256.4 ± 3.9	-0.002	+0.002	+0.003	+0.003	+16.6	+0.7	+0.7	+0.2	0.016	0.001	0.002	0.002
Kitsilano	0.078 ± 0.006	255.5 ± 4.3	-0.003	+0.001	+0.003	+0.002	+17.5	+1.2	+1.1	+0.5	0.017	0.002	0.002	0.002
Ambleside	0.077 ± 0.007	256.3 ± 4.2	-0.003	+0.002	+0.003	+0.003	+16.8	+0.8	+0.4	+0.1	0.016	0.001	0.002	0.002
Vancouver	0.076 ± 0.006	260.6 ± 3.7	—	—	+0.004	+0.004	—	—	+0.9	+1.1	—	—	0.003	0.003
Port Moody	0.078 ± 0.006	269.6 ± 4.0	—	—	+0.004	+0.004	—	—	+1.1	+2.5	—	—	0.003	0.004
Indian Arm Head	0.078 ± 0.005	269.9 ± 4.1	—	—	+0.003	—	—	—	+1.5	—	—	—	0.003	—
Gibsons	0.079	256.7	+0.001	+0.007	+0.010	—	+14.5	-1.0	-1.0	—	0.014	0.005	0.007	—
Squamish	0.074	255.5	+0.005	+0.008	+0.008	—	+19.7	+7.0	+7.9	—	0.019	0.009	0.009	—
Second Narrows	0.092	263.3	—	—	-0.007	-0.005	—	—	+5.1	+7.4	—	—	0.007	0.009

Table 13. L2 constituent comparison for active tide gauges for year 2020 (upper part) and historical tide gauges (lower part).

	Observed		Amplitude Error (m)				Phase Error (deg)				Tidal error (m)			
Station name	**Amplitude (m)**	**Phase (deg)**	**CIOPSW**	**SS500**	**SSS150**	**VH20**	**CIOPSW**	**SS500**	**SSS150**	**VH20**	**CIOPSW**	**SS500**	**SSS150**	**VH20**
Darrell Bay	0.030 ± 0.003	61.0 ± 6.4	-0.012	-0.020	+0.006	—	+21.4	-24.9	-10.1	—	0.011	0.015	0.006	—
Point Atkinson	0.029 ± 0.002	61.1 ± 6.6	-0.013	-0.019	+0.004	—	+21.5	-30.7	-11.3	—	0.011	0.015	0.005	—
Sandy Cove	0.029 ± 0.003	60.7 ± 5.5	-0.013	-0.019	+0.005	+0.005	+21.9	-30.2	-10.6	-11.5	0.011	0.015	0.006	0.006
Kitsilano	0.031 ± 0.004	59.0 ± 7.0	-0.015	-0.020	+0.003	+0.003	+20.6	-34.5	-11.5	-12.2	0.012	0.016	0.005	0.005
Ambleside	0.032 ± 0.003	60.5 ± 5.8	-0.016	-0.021	+0.003	+0.003	+20.7	-31.0	-12.0	-12.3	0.013	0.017	0.005	0.005
Vancouver	0.034 ± 0.003	54.8 ± 4.7	—	—	+0.006	+0.006	—	—	-7.0	-8.4	—	—	0.006	0.006
Port Moody	0.041 ± 0.004	48.0 ± 4.2	—	—	+0.013	+0.013	—	—	-3.2	-2.5	—	—	0.009	0.009
Indian Arm Head	0.041 ± 0.004	46.6 ± 5.2	—	—	+0.013	—	—	—	-1.9	—	—	—	0.010	—
Gibsons	0.025	66.8	-0.013	-0.016	+0.009	—	+6.8	-53.1	-22.7	—	0.009	0.015	0.010	—
Squamish	0.027	70.9	-0.016	-0.018	+0.007	—	+12.6	-55.0	-24.1	—	0.012	0.016	0.010	—
Second Narrows	0.031	47.9	—	—	+0.008	+0.009	—	—	+0.1	-0.5	—	—	0.006	0.006

Table 14. J1 constituent comparison for active tide gauges for year 2020 (upper part) and historical tide gauges (lower part).

	Observed		Amplitude Error (m)				Phase Error (deg)				Tidal error (m)			
Station name	**Amplitude (m)**	**Phase (deg)**	**CIOPSW**	**SS500**	**SSS150**	**VH20**	**CIOPSW**	**SS500**	**SSS150**	**VH20**	**CIOPSW**	**SS500**	**SSS150**	**VH20**
Darrell Bay	0.047 ± 0.005	328.4 ± 6.5	-0.011	-0.032	-0.003	—	+131.6	+135.5	+1.4	—	0.054	0.041	0.002	—
Point Atkinson	0.047 ± 0.005	328.4 ± 6.3	-0.012	-0.032	-0.003	—	+132.1	+128.7	+1.0	—	0.054	0.041	0.002	—
Sandy Cove	0.048 ± 0.006	327.4 ± 6.3	-0.012	-0.033	-0.003	-0.003	+133.1	+129.0	+2.1	+2.0	0.054	0.041	0.002	0.002
Kitsilano	0.049 ± 0.005	327.9 ± 6.7	-0.013	-0.034	-0.003	-0.003	+132.9	+127.8	+2.3	+1.7	0.055	0.042	0.002	0.002
Ambleside	0.047 ± 0.006	328.8 ± 8.0	-0.011	-0.032	-0.002	-0.002	+131.9	+126.6	+1.1	+0.7	0.054	0.041	0.002	0.002
Vancouver	0.047 ± 0.005	336.1 ± 6.0	—	—	-0.002	-0.002	—	—	+0.5	+1.4	—	—	0.002	0.002
Port Moody	0.050 ± 0.006	350.2 ± 7.4	—	—	-0.002	-0.002	—	—	+3.5	+5.5	—	—	0.003	0.004
Indian Arm Head	0.052 ± 0.005	351.0 ± 6.5	—	—	-0.003	—	—	—	+3.5	—	—	—	0.003	—
Gibsons	0.054	324.2	-0.018	-0.039	-0.002	—	+127.5	+115.0	+5.9	—	0.057	0.043	0.004	—
Squamish	0.053	315.8	-0.013	-0.033	-0.010	—	+137.3	+130.5	+16.1	—	0.062	0.048	0.012	—
Second Narrows	0.060	345.1	—	—	-0.016	-0.016	—	—	-6.6	-2.4	—	—	0.012	0.011

Table 15. NO1 constituent comparison for active tide gauges for year 2020 (upper part) and historical tide gauges (lower part).

	Observed		Amplitude Error (m)				Phase Error (deg)				Tidal error (m)			
Station name	**Amplitude (m)**	**Phase (deg)**	**CIOPSW**	**SS500**	**SSS150**	**VH20**	**CIOPSW**	**SS500**	**SSS150**	**VH20**	**CIOPSW**	**SS500**	**SSS150**	**VH20**
Darrell Bay	0.039 ± 0.004	294.8 ± 5.6	-0.020	-0.029	+0.001	—	+85.1	+147.7	-25.0	—	0.030	0.034	0.012	—
Point Atkinson	0.037 ± 0.004	293.0 ± 5.3	-0.017	-0.026	+0.002	—	+87.6	+143.1	-22.2	—	0.029	0.033	0.010	—
Sandy Cove	0.038 ± 0.004	295.1 ± 6.0	-0.018	-0.027	+0.001	+0.001	+85.5	+140.2	-24.1	-24.5	0.029	0.033	0.011	0.012
Kitsilano	0.038 ± 0.004	295.7 ± 5.9	-0.018	-0.028	+0.002	+0.002	+84.5	+134.8	-23.8	-24.3	0.029	0.032	0.011	0.012
Ambleside	0.039 ± 0.004	295.3 ± 7.1	-0.019	-0.028	+0.001	+0.001	+85.0	+136.9	-23.2	-23.5	0.030	0.033	0.011	0.011
Vancouver	0.038 ± 0.004	298.7 ± 5.2	—	—	+0.002	+0.002	—	—	-22.6	-22.0	—	—	0.011	0.011
Port Moody	0.042 ± 0.004	308.6 ± 5.1	—	—	+0.001	+0.001	—	—	-22.0	-20.2	—	—	0.011	0.011
Indian Arm Head	0.042 ± 0.004	309.0 ± 5.0	—	—	+0.001	—	—	—	-21.6	—	—	—	0.011	—
Gibsons	0.023	301.3	+0.010	-0.007	+0.023	—	+64.8	+78.9	-18.0	—	0.022	0.018	0.017	—
Squamish	0.027	261.0	+0.059	+0.037	+0.058	—	+97.9	+93.4	+41.1	—	0.066	0.050	0.048	—
Second Narrows	0.048	301.5	—	—	+0.045	+0.049	—	—	+3.6	+7.1	—	—	0.032	0.035

Table 16. OO1 constituent comparison for active tide gauges for year 2020 (upper part) and historical tide gauges (lower part).

	Observed		Amplitude Error (m)				Phase Error (deg)				Tidal error (m)			
Station name	**Amplitude (m)**	**Phase (deg)**	**CIOPSW**	**SS500**	**SSS150**	**VH20**	**CIOPSW**	**SS500**	**SSS150**	**VH20**	**CIOPSW**	**SS500**	**SSS150**	**VH20**
Darrell Bay	0.034 ± 0.005	337.1 ± 7.2	-0.029	-0.033	+0.006	—	+59.7	+59.4	+9.4	—	0.023	0.024	0.006	—
Point Atkinson	0.035 ± 0.004	335.7 ± 7.3	-0.029	-0.034	+0.005	—	+64.0	+55.5	+8.9	—	0.023	0.024	0.006	—
Sandy Cove	0.034 ± 0.005	335.2 ± 7.0	-0.028	-0.033	+0.006	+0.006	+64.4	+67.0	+9.4	+9.2	0.023	0.024	0.006	0.006
Kitsilano	0.033 ± 0.005	335.5 ± 8.2	-0.028	-0.032	+0.007	+0.007	+63.2	+91.1	+9.5	+8.9	0.022	0.023	0.007	0.006
Ambleside	0.033 ± 0.005	336.3 ± 8.9	-0.027	-0.032	+0.007	+0.007	+62.5	+92.8	+8.5	+8.2	0.022	0.023	0.006	0.006
Vancouver	0.035 ± 0.004	341.1 ± 6.9	—	—	+0.006	+0.006	—	—	+6.9	+7.5	—	—	0.005	0.005
Port Moody	0.035 ± 0.005	348.9 ± 8.0	—	—	+0.007	+0.007	—	—	+7.3	+8.7	—	—	0.006	0.006
Indian Arm Head	0.035 ± 0.005	348.3 ± 7.2	—	—	+0.007	—	—	—	+8.2	—	—	—	0.006	—
Gibsons	0.039	331.2	-0.030	-0.034	+0.008	—	+62.7	+47.4	+11.1	—	0.025	0.025	0.008	—
Squamish	0.030	313.2	-0.013	-0.019	+0.030	—	+99.7	+89.2	+30.7	—	0.027	0.023	0.026	—
Second Narrows	0.037	333.8	—	—	+0.024	+0.025	—	—	+11.9	+13.1	—	—	0.018	0.019

Table 17. SO1 constituent comparison for active tide gauges for year 2020 (upper part) and historical tide gauges (lower part).

	Observed		Amplitude Error (m)				Phase Error (deg)				Tidal error (m)			
Station name	**Amplitude (m)**	**Phase (deg)**	**CIOPSW**	**SS500**	**SSS150**	**VH20**	**CIOPSW**	**SS500**	**SSS150**	**VH20**	**CIOPSW**	**SS500**	**SSS150**	**VH20**
Darrell Bay	0.028 ± 0.006	46.8 ± 10.5	+0.024	+0.001	-0.002	—	+59.5	+49.8	+5.5	—	0.032	0.017	0.002	—
Point Atkinson	0.028 ± 0.005	45.8 ± 11.3	+0.024	+0.002	-0.002	—	+60.6	+49.7	+6.4	—	0.032	0.017	0.002	—
Sandy Cove	0.027 ± 0.006	43.4 ± 10.9	+0.025	+0.003	-0.001	-0.001	+62.9	+52.0	+8.6	+7.8	0.033	0.018	0.003	0.003
Kitsilano	0.027 ± 0.006	43.1 ± 14.6	+0.025	+0.003	+0.001	0.000	+63.1	+51.7	+8.8	+8.8	0.033	0.018	0.003	0.003
Ambleside	0.027 ± 0.007	46.6 ± 13.5	+0.025	+0.003	0.000	0.000	+59.7	+48.5	+6.1	+5.7	0.032	0.017	0.002	0.002
Vancouver	0.032 ± 0.005	52.8 ± 9.8	—	—	-0.001	-0.001	—	—	+4.6	+5.0	—	—	0.002	0.002
Port Moody	0.043 ± 0.007	58.4 ± 7.8	—	—	0.000	+0.001	—	—	+4.7	+6.0	—	—	0.003	0.003
Indian Arm Head	0.045 ± 0.006	59.1 ± 6.5	—	—	-0.001	—	—	—	+4.4	—	—	—	0.003	—
Gibsons	0.027	40.2	+0.030	+0.008	+0.006	—	+68.4	+59.6	+19.0	—	0.038	0.022	0.008	—
Squamish	0.030	40.4	+0.009	-0.013	-0.016	—	+64.8	+51.1	-22.9	—	0.027	0.017	0.013	—
Second Narrows	0.041	47.7	—	—	-0.022	-0.019	—	—	-17.2	-12.8	—	—	0.016	0.014

Table 18. NU2 constituent comparison for active tide gauges for year 2020 (upper part) and historical tide gauges (lower part).

	Observed		Amplitude Error (m)				Phase Error (deg)				Tidal error (m)			
Station name	**Amplitude (m)**	**Phase (deg)**	**CIOPSW**	**SS500**	**SSS150**	**VH20**	**CIOPSW**	**SS500**	**SSS150**	**VH20**	**CIOPSW**	**SS500**	**SSS150**	**VH20**
Darrell Bay	0.040 ± 0.002	11.1 ± 3.1	-0.037	-0.038	+0.001	—	+53.7	+43.8	+3.2	—	0.027	0.027	0.002	—
Point Atkinson	0.039 ± 0.003	9.8 ± 2.9	-0.036	-0.037	0.000	—	+52.2	+53.5	+5.4	—	0.026	0.027	0.003	—
Sandy Cove	0.039 ± 0.002	10.3 ± 3.3	-0.036	-0.037	0.000	0.000	+51.4	+54.4	+5.5	+5.1	0.027	0.027	0.003	0.002
Kitsilano	0.039 ± 0.003	11.0 ± 3.9	-0.036	-0.035	+0.002	+0.002	+40.3	+44.7	+5.2	+4.8	0.026	0.026	0.003	0.003
Ambleside	0.039 ± 0.003	11.0 ± 3.6	-0.035	-0.035	+0.002	+0.002	+42.5	+47.2	+5.7	+5.2	0.026	0.026	0.003	0.003
Vancouver	0.040 ± 0.002	16.5 ± 2.7	—	—	+0.001	+0.001	—	—	+3.2	+3.9	—	—	0.002	0.002
Port Moody	0.041 ± 0.002	26.8 ± 3.4	—	—	+0.002	+0.002	—	—	+2.9	+5.1	—	—	0.002	0.003
Indian Arm Head	0.042 ± 0.003	24.6 ± 3.8	—	—	+0.001	—	—	—	+4.9	—	—	—	0.003	—
Gibsons	0.038	8.0	-0.036	-0.036	+0.003	—	+64.3	+23.2	+6.1	—	0.027	0.026	0.003	—
Squamish	0.040	10.7	-0.038	-0.040	0.000	—	+59.2	+0.1	+2.3	—	0.028	0.028	0.001	—
Second Narrows	0.040	19.5	—	—	+0.002	+0.002	—	—	+0.8	+3.1	—	—	0.002	0.002

Table 19. 2N2 constituent comparison for active tide gauges for year 2020 (upper part) and historical tide gauges (lower part).

	Observed		Amplitude Error				Phase Error				Tidal error			
Station name	**Amplitude**	**Phase**	**CIOPSW**	**SS500**	**SSS150**	**VH20**	**CIOPSW**	**SS500**	**SSS150**	**VH20**	**CIOPSW**	**SS500**	**SSS150**	**VH20**
Darrell Bay	0.018 ± 0.002	340.3 ± 7.0	-0.009	-0.006	-0.004	—	+123.4	+97.6	+32.0	—	0.017	0.017	0.007	—
Point Atkinson	0.019 ± 0.002	337.3 ± 5.8	-0.010	-0.006	-0.005	—	+124.7	+98.4	+37.3	—	0.018	0.017	0.008	—
Sandy Cove	0.018 ± 0.002	338.4 ± 6.8	-0.009	-0.005	-0.004	-0.004	+123.7	+97.9	+37.2	+36.0	0.017	0.016	0.008	0.007
Kitsilano	0.016 ± 0.003	340.8 ± 9.5	-0.007	-0.004	-0.003	-0.002	+120.1	+96.5	+35.8	+36.6	0.016	0.015	0.007	0.007
Ambleside	0.017 ± 0.002	338.6 ± 8.8	-0.008	-0.004	-0.003	-0.003	+122.9	+99.1	+38.9	+37.2	0.016	0.016	0.008	0.007
Vancouver	0.020 ± 0.002	343.8 ± 5.6	—	—	-0.004	-0.004	—	—	+29.8	+31.9	—	—	0.007	0.007
Port Moody	0.024 ± 0.002	352.9 ± 6.6	—	—	-0.003	-0.003	—	—	+20.6	+23.5	—	—	0.006	0.007
Indian Arm Head	0.025 ± 0.002	352.7 ± 5.6	—	—	-0.004	—	—	—	+22.0	—	—	—	0.007	—
Gibsons	0.032	316.3	-0.020	-0.021	-0.027	—	-159.7	+179.0	+26.1	—	0.031	0.030	0.020	—
Squamish	0.029	334.2	-0.022	-0.026	-0.018	—	-120.3	-110.6	-16.9	—	0.024	0.022	0.013	—
Second Narrows	0.020	357.6	—	—	-0.011	-0.012	—	—	-26.3	-19.2	—	—	0.009	0.009

Table 20. Tidal water level scores for year 2020.

	CRMSE (m)				γ^2				Pearson			
Station name	**CIOPSW**	**SS500**	**SSS150**	**VH20**	**CIOPSW**	**SS500**	**SSS150**	**VH20**	**CIOPSW**	**SS500**	**SSS150**	**VH20**
Darrell Bay	0.199	0.096	0.051	—	0.038	0.009	0.002	—	0.981	0.996	0.999	—
Point Atkinson	0.201	0.094	0.052	—	0.040	0.009	0.003	—	0.980	0.996	0.999	—
Sandy Cove	0.198	0.094	0.052	0.053	0.039	0.009	0.003	0.003	0.981	0.996	0.999	0.999
Kitsilano	0.199	0.094	0.053	0.054	0.038	0.009	0.003	0.003	0.981	0.996	0.999	0.999
Ambleside	0.194	0.094	0.054	0.056	0.036	0.008	0.003	0.003	0.982	0.996	0.999	0.998
Vancouver	—	—	0.053	0.052	—	—	0.003	0.003	—	—	0.999	0.999
Port Moody	—	—	0.056	0.065	—	—	0.003	0.004	—	—	0.999	0.998
Indian Arm Head	—	—	0.058	—	—	—	0.003	—	—	—	0.999	—

Table 21. Non-tidal water level scores for year 2020.

	CRMSE (m)				γ^2				Pearson			
Station name	**CIOPSW**	**SS500**	**SSS150**	**VH20**	**CIOPSW**	**SS500**	**SSS150**	**VH20**	**CIOPSW**	**SS500**	**SSS150**	**VH20**
Darrell Bay	0.052	0.050	0.049	—	0.150	0.140	0.136	—	0.926	0.934	0.936	—
Point Atkinson	0.044	0.040	0.042	—	0.112	0.094	0.100	—	0.944	0.954	0.952	—
Sandy Cove	0.043	0.040	0.041	0.041	0.115	0.100	0.104	0.106	0.943	0.951	0.950	0.949
Kitsilano	0.046	0.043	0.044	0.044	0.134	0.116	0.125	0.124	0.934	0.943	0.940	0.940
Ambleside	0.045	0.042	0.043	0.043	0.130	0.114	0.117	0.117	0.935	0.943	0.943	0.942
Vancouver	—	—	0.042	0.042	—	—	0.102	0.103	—	—	0.950	0.950
Port Moody	—	—	0.044	0.045	—	—	0.116	0.117	—	—	0.944	0.943
Indian Arm Head	—	—	0.070	—	—	—	0.202	—	—	—	0.893	—

Table 22. Total water level scores for year 2020.

	bias (m)				CRMSE (m)			
Station name	**CIOPSW**	**SS500**	**SSS150**	**VH20**	**CIOPSW**	**SS500**	**SSS150**	**VH20**
Darrell Bay	0.153	0.178	0.179	—	0.206	0.107	0.071	—
Point Atkinson	0.066	0.081	0.078	—	0.205	0.101	0.063	—
Sandy Cove	0.068	0.082	0.078	0.081	0.203	0.101	0.063	0.064
Kitsilano	0.018	0.033	0.032	0.034	0.203	0.102	0.067	0.068
Ambleside	0.027	0.043	0.039	0.042	0.199	0.102	0.067	0.069
Vancouver	—	—	0.021	0.024	—	—	0.064	0.063
Port Moody	—	—	0.046	0.049	—	—	0.069	0.078
Indian Arm Head	—	—	0.106	—	—	—	0.090	—
	γ^2				Pearson			
	CIOPSW	**SS500**	**SSS150**	**VH20**	**CIOPSW**	**SS500**	**SSS150**	**VH20**
Darrell Bay	0.040	0.011	0.005	—	0.980	0.995	0.998	—
Point Atkinson	0.040	0.010	0.004	—	0.980	0.995	0.998	—
Sandy Cove	0.040	0.010	0.004	0.004	0.980	0.995	0.998	0.998
Kitsilano	0.039	0.010	0.004	0.004	0.980	0.995	0.998	0.998
Ambleside	0.037	0.010	0.004	0.004	0.981	0.995	0.998	0.998

Station name	bias (m)				CRMSE (m)			
	CIOPSW	SS500	SSS150	VH20	CIOPSW	SS500	SSS150	VH20
Vancouver	—	—	0.004	0.004	—	—	0.998	0.998
Port Moody	—	—	0.004	0.006	—	—	0.998	0.997
Indian Arm Head	—	—	0.007	—	—	—	0.996	—

Table 23. Storms considered for storm surge analysis.

Storm Name	Peak Date
feb17	2017-02-05 00:00
mar17	2017-03-05 18:00
apr17	2017-04-12 12:00
feb19	2019-02-04 00:00
oct20	2020-10-12 00:00
feb21	2021-02-13 12:00
BCFloods	2021-11-15 00:00
dec21	2021-12-25 00:00

Table 24. Storm surge scores for each station, averaged over the number of storms indicated in column labelled N.

Station	N	CRMSE (m)				γ^2				Pearson			
		CIOPSW	SS500	SSS150	VH20	CIOPSW	SS500	SSS150	VH20	CIOPSW	SS500	SSS150	VH20
Darrell Bay	5	0.049	0.043	0.042	—	0.293	0.283	0.276	—	0.879	0.894	0.894	—
Point Atkinson	8	0.032	0.030	0.031	—	0.189	0.172	0.174	—	0.911	0.923	0.923	—
Sandy Cove	8	0.032	0.030	0.030	0.031	0.181	0.158	0.164	0.167	0.914	0.926	0.924	0.923
Kitsilano	7	0.034	0.031	0.030	0.031	0.173	0.146	0.144	0.150	0.929	0.934	0.934	0.932
Ambleside	5	0.034	0.032	0.033	0.033	0.160	0.131	0.141	0.144	0.919	0.936	0.933	0.931
Vancouver	8	—	—	0.029	0.029	—	—	0.143	0.143	—	—	0.933	0.933
Port Moody	5	—	—	0.033	0.033	—	—	0.131	0.130	—	—	0.935	0.936
Indian Arm Head	5	—	—	0.037	—	—	—	0.142	—	—	—	0.930	—

Table 25. Periods used to analyze the Second Narrows HADCP data.

period	start	end	length (days)
year2018a	2018-03-13	2018-09-16	187
year2019a	2019-08-12	2019-12-21	131
year2020a	2020-01-07	2020-06-04	149
year2020b	2020-06-13	2021-05-01	322
year2021b	2021-07-20	2022-01-01	165

Table 26. Total, non-tidal and tidal scores for five periods for the Second Narrows HADCP alongshore current.

	period	mean (m/s)	bias (m/s)			CRMSE (m/s)			γ^2			Pearson		
			SSS150	VH20	Cons.	SSS150	VH20	Cons.	SSS150	VH20	Cons.	SSS150	VH20	Cons.
Total	year2018a	-0.129	-0.001	0.015	-0.075	0.244	0.270	0.316	0.045	0.055	0.075	0.980	0.979	0.981
	year2019a	-0.139	0.004	0.022	-0.046	0.213	0.163	0.208	0.031	0.018	0.030	0.993	0.992	0.990
	year2020a	-0.144	0.007	0.031	-0.044	0.257	0.164	0.205	0.041	0.017	0.026	0.993	0.992	0.991
	year2020b	-0.137	0.005	0.021	-0.050	0.245	0.192	0.229	0.040	0.025	0.035	0.989	0.988	0.988
	year2021b	-0.137	0.006	0.025	-0.042	0.253	0.188	0.211	0.042	0.023	0.029	0.990	0.989	0.988
Non tidal	year2018a	—	—	—	—	0.189	0.193	—	0.827	0.858	—	0.423	0.427	—
	year2019a	—	—	—	—	0.113	0.112	—	0.262	0.261	—	0.869	0.862	—
	year2020a	—	—	—	—	0.121	0.120	—	0.273	0.270	—	0.859	0.857	—
	year2020b	—	—	—	—	0.146	0.147	—	0.699	0.705	—	0.550	0.569	—
	year2021b	—	—	—	—	0.148	0.145	—	0.327	0.316	—	0.830	0.828	—
Tidal	year2018a	—	—	—	—	0.154	0.189	0.257	0.019	0.028	0.051	0.993	0.992	0.994
	year2019a	—	—	—	—	0.181	0.118	0.235	0.023	0.010	0.039	0.997	0.996	0.988
	year2020a	—	—	—	—	0.227	0.111	0.230	0.033	0.008	0.034	0.997	0.996	0.989
	year2020b	—	—	—	—	0.197	0.124	0.154	0.026	0.010	0.016	0.997	0.995	0.997
	year2021b	—	—	—	—	0.204	0.118	0.234	0.029	0.010	0.037	0.997	0.995	0.986

Table 27. Tidal constituents analyzed over five periods for the Second Narrows HADCP alongshore current.

Const.	period	Observed		Ampl. Error (m/s)		Phase Error (deg)		Tidal Error (m/s)	
		Ampl.	Phase	SSS150	VH20	SSS150	VH20	SSS150	VH20
M2	year2018a	1.321	319.3	-0.102	+0.151	-2.7	-3.4	0.083	0.122
	year2019a	1.421	319.5	-0.182	+0.061	-2.4	-3.3	0.134	0.073
	year2020a	1.470	319.1	-0.239	-0.009	-2.0	-2.9	0.173	0.053
	year2020b	1.427	319.0	-0.194	+0.054	-1.9	-2.6	0.140	0.061
	year2021b	1.448	319.6	-0.208	+0.045	-2.7	-3.5	0.154	0.072
N2	year2018a	0.255	297.0	+0.006	+0.047	-3.4	-4.8	0.012	0.037
	year2019a	0.311	291.2	-0.045	-0.004	-3.2	-4.0	0.034	0.016
	year2020a	0.329	295.9	-0.055	-0.018	-3.7	-3.6	0.041	0.019
	year2020b	0.300	297.3	-0.043	-0.008	-6.1	-7.4	0.037	0.028
	year2021b	0.295	300.8	-0.035	+0.001	-5.4	-6.8	0.031	0.025
S2	year2018a	0.338	352.8	-0.009	+0.031	-0.4	-1.3	0.007	0.022
	year2019a	0.398	346.0	-0.054	-0.004	+3.1	+0.8	0.041	0.005
	year2020a	0.414	354.7	-0.064	-0.023	-2.1	-3.1	0.046	0.022
	year2020b	0.379	350.0	-0.051	-0.011	+1.9	+0.8	0.037	0.009
	year2021b	0.398	348.4	-0.066	-0.020	+2.9	+1.5	0.049	0.016
O1	year2018a	0.321	195.5	-0.031	+0.031	+1.9	-3.9	0.023	0.027
	year2019a	0.332	192.9	-0.046	+0.018	+1.5	-4.0	0.033	0.021
	year2020a	0.355	191.4	-0.062	-0.002	+2.2	-3.1	0.044	0.013
	year2020b	0.349	194.5	-0.052	+0.005	-1.6	-7.4	0.037	0.032
	year2021b	0.345	193.2	-0.064	-0.002	-0.3	-6.7	0.045	0.028
K1	year2018a	0.623	210.9	-0.052	+0.053	-1.2	-2.6	0.038	0.043
	year2019a	0.613	205.4	-0.089	+0.002	-0.2	-1.8	0.063	0.014
	year2020a	0.650	210.7	-0.114	-0.020	-0.3	-2.3	0.081	0.023
	year2020b	0.669	210.3	-0.104	-0.001	-0.8	-2.5	0.074	0.021
	year2021b	0.654	208.3	-0.105	-0.002	-0.6	-2.2	0.074	0.018
P1	year2018a	0.203	226.2	-0.037	0.000	-16.3	-17.9	0.045	0.045
	year2020b	0.211	213.8	-0.043	-0.010	-2.6	-5.1	0.031	0.015
Q1	year2018a	0.054	197.5	+0.001	+0.007	+5.2	-2.3	0.004	0.005
	year2019a	0.063	182.6	-0.007	-0.003	+7.4	-3.3	0.007	0.003
	year2020a	0.064	198.1	-0.011	-0.005	+5.4	-3.5	0.009	0.005
	year2020b	0.066	189.6	-0.008	-0.001	+8.6	-2.5	0.008	0.002
	year2021b	0.068	193.6	-0.008	+0.001	+6.7	-3.5	0.008	0.003
K2	year2018a	0.082	359.8	-0.004	+0.012	-16.5	-22.7	0.016	0.026
	year2020b	0.090	346.8	-0.010	+0.010	-3.1	-6.3	0.008	0.010

Table 28. Total current scores for two ADCP deployments subset to four depths.

Station	Depth (m)	bias u (m/s)		bias v (m/s)		RMSE (m/s)		γ^2		vector correlation magnitude		vector correlation angle (deg)	
		SSS150	VH20	SSS150	VH20	SSS150	VH20	SSS150	VH20	SSS150	VH20	SSS150	VH20
BUW02	24.9	0.29	0.25	0.01	0.01	0.49	0.46	0.55	0.51	0.72	0.70	20.0	3.5
	29.9	0.26	0.22	0.02	0.03	0.45	0.42	0.57	0.53	0.72	0.69	20.1	6.2
	34.9	0.18	0.15	0.04	0.03	0.43	0.39	0.66	0.58	0.67	0.66	17.9	8.0
	39.9	0.08	0.05	0.05	0.05	0.40	0.37	0.73	0.61	0.61	0.64	19.3	10.4
BIIP	10.0	0.00	0.00	0.02	0.00	0.24	0.23	0.44	0.38	0.80	0.80	9.6	-0.8
	15.0	0.05	0.04	-0.01	-0.03	0.23	0.21	0.42	0.33	0.82	0.83	9.5	1.2
	25.0	0.01	0.01	-0.02	0.00	0.19	0.19	0.23	0.23	0.88	0.88	-2.4	2.9
	35.0	-0.18	-0.09	0.03	0.03	0.36	0.22	0.72	0.29	0.83	0.86	-40.7	-3.5

Table 29. Non-tidal current scores for two ADCP deployments subset to four depths.

Station	Depth (m)	RMSE (m/s)		γ^2		vector correlation magnitude		vector correlation angle (deg)	
		SSS150	VH20	SSS150	VH20	SSS150	VH20	SSS150	VH20
BUW02	24.9	0.36	0.33	1.41	1.53	0.09	0.08	3.2	-10.2
	29.9	0.31	0.29	1.19	1.50	0.19	0.20	12.1	0.7
	34.9	0.24	0.25	1.02	1.50	0.22	0.24	14.0	-0.5
	39.9	0.20	0.21	0.99	1.29	0.20	0.26	16.4	1.1
BIIP	10.0	0.22	0.22	1.08	1.07	0.25	0.33	29.6	-0.3
	15.0	0.20	0.20	1.10	1.08	0.19	0.31	25.0	4.8
	25.0	0.16	0.16	1.08	1.06	0.27	0.33	-1.0	5.6
	35.0	0.25	0.19	0.96	0.91	0.24	0.34	-31.5	3.8

Table 30. Tidal current scores for two ADCP deployments subset to four depths.

Station	Depth (m)	RMSE (m/s)		γ^2	
		SSS150	VH20	SSS150	VH20
BUW02	24.9	0.34	0.32	0.45	0.39
	29.9	0.33	0.30	0.49	0.41
	34.9	0.35	0.30	0.61	0.43
	39.9	0.35	0.29	0.68	0.47
BIUP	10.0	0.10	0.05	0.12	0.03
	15.0	0.12	0.06	0.16	0.04
	25.0	0.09	0.09	0.07	0.06
	35.0	0.26	0.11	0.65	0.12

Table 31. Sea surface temperature scores for English Bay (buoy 46304).

Station name	score	CIOPSW	SS500	SSS150
English Bay (46304)	bias (deg C)	-0.59	-0.52	-0.68
	CRMSE (deg C)	1.60	1.05	0.98
	γ^2	0.13	0.06	0.05
	Pearson	0.95	0.98	0.98

Table 32. Moored CTD scores for Burrard Inlet Instrument Platform for temperature and salinity over two deployments.

Station name	score	Temperature		Salinity	
		SSS150	VH20	SSS150	VH20
BIIP 2019-03	bias	0.32	0.29	-0.36	0.08
	CRMSE	0.34	0.29	0.33	0.29
	γ^2	0.09	0.06	0.62	0.50
	Pearson	0.98	0.98	0.72	0.73
BIIP 2020-10	bias	0.16	0.17	-0.20	0.27
	CRMSE	0.31	0.27	0.38	0.36
	γ^2	0.07	0.05	0.65	0.61
	Pearson	0.99	0.98	0.68	0.66

Table 33. Number of CTD casts per region.

Region	Number of casts
Howe Sound	381
English Bay	196
Vancouver Harbour	181
Vancouver Harbour East	64
Port Moody	14
Indian Arm	112

Table 34. Molcard and separation distance scores for the drift evaluation.

Hour	Molcard Skill		Separation Distance (km)	
	SSS150	VH20	SSS150	VH20
1	0.22	0.20	0.74	0.73
2	0.21	0.22	1.59	1.46
3	0.21	0.24	2.20	1.95
4	0.20	0.23	2.95	2.50
5	0.19	0.24	3.53	2.91

12. FIGURES

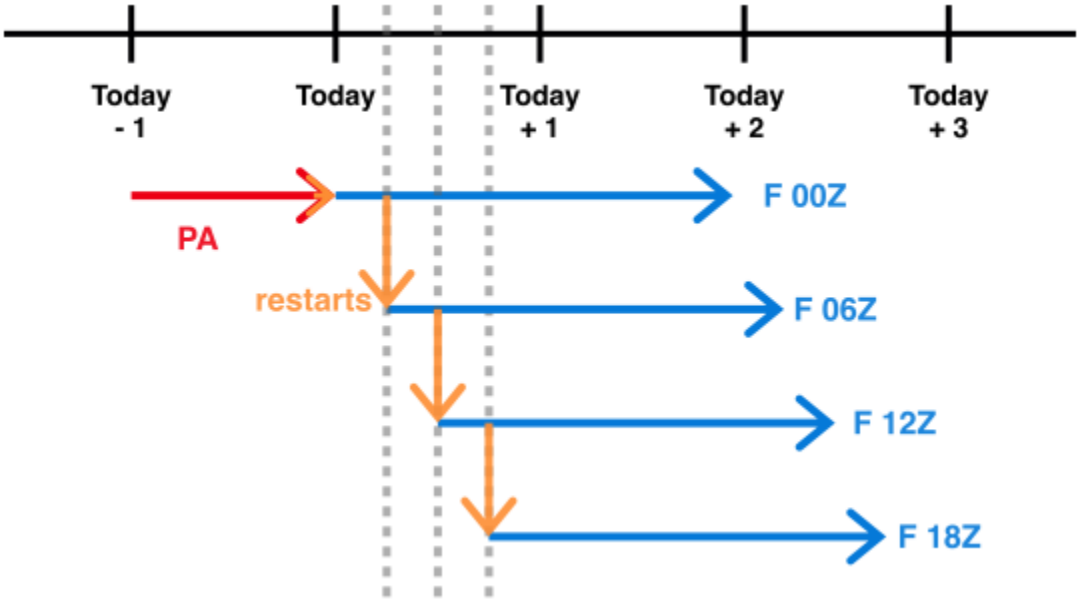

Figure 1. Schematic of one timestamp's set of pseudo-analysis (PA, in red) and forecast (in blue) runs. Grey dashed lines are spaced six hours apart, and orange arrows indicate where a restart file is generated and used to launch the subsequent step. The PA for today+1 will start with the same restart used to start today's 00Z forecast, and the pattern will repeat.

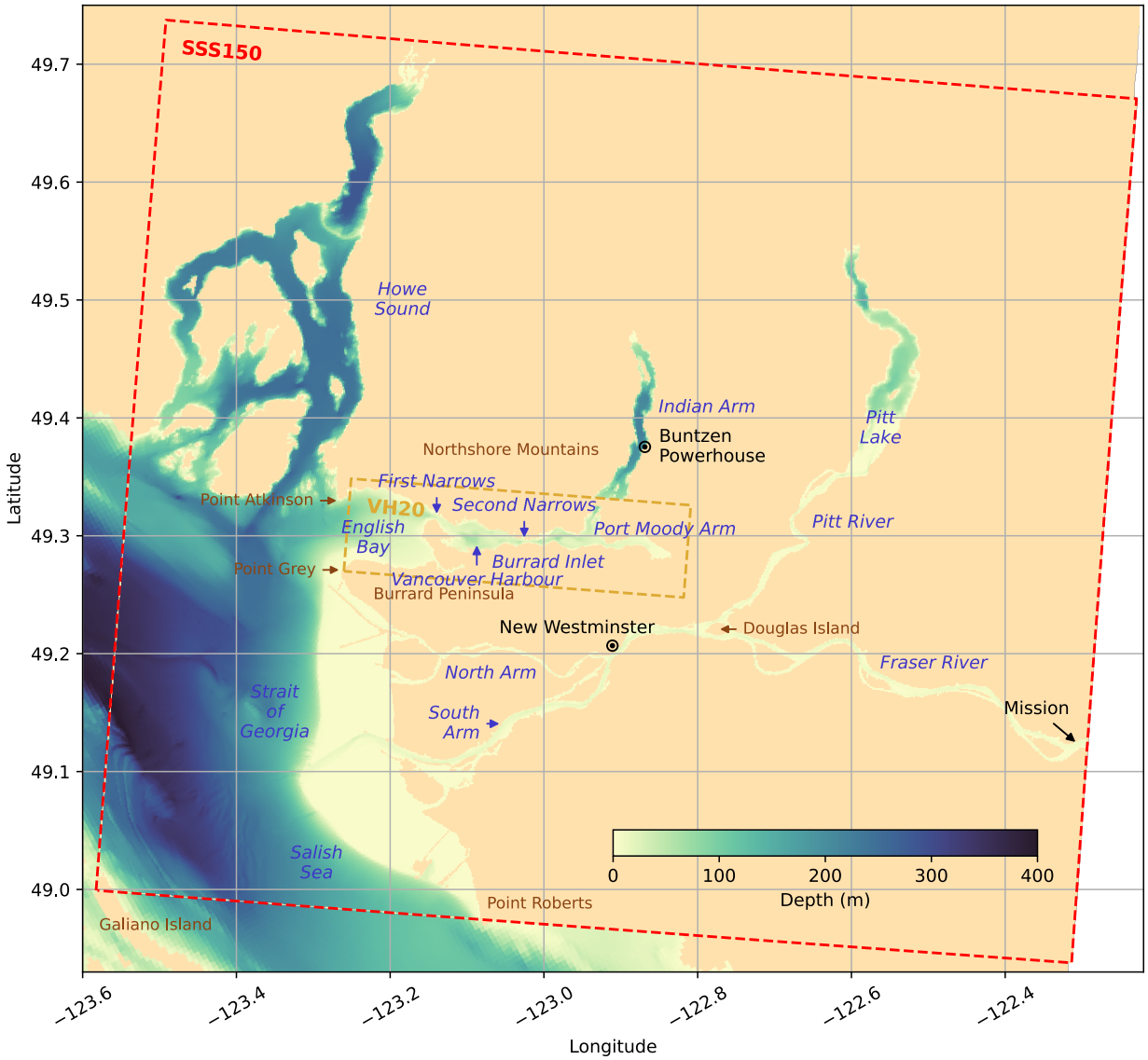

Figure 2. Model domain showing the outer SSS150 grid (red dashed line) and inner VH20 grid (dark yellow dashed line).

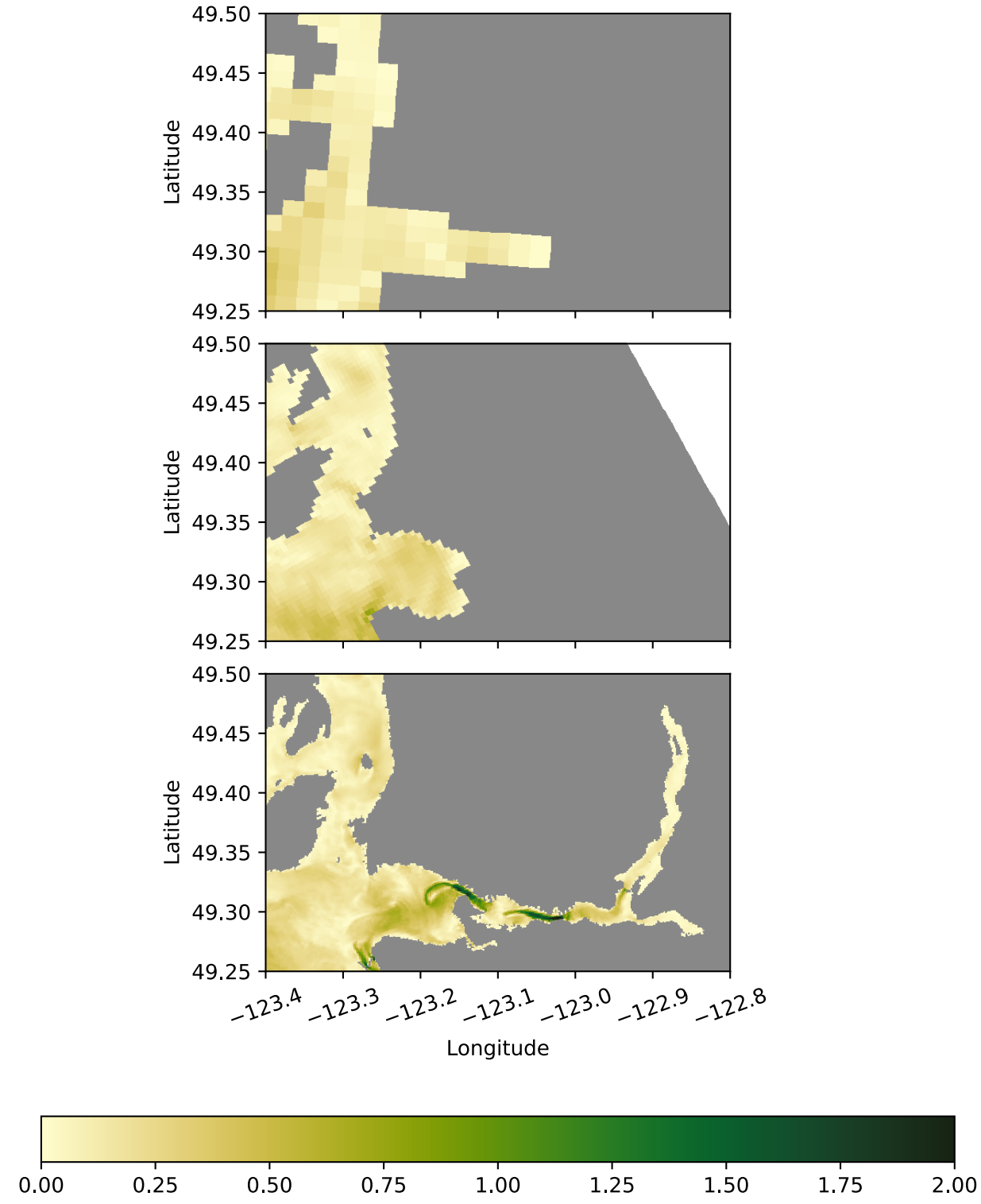

Figure 3. Surface speed (m/s) for CIOPS-W, SS500 and SSS150 for Burrard Inlet.

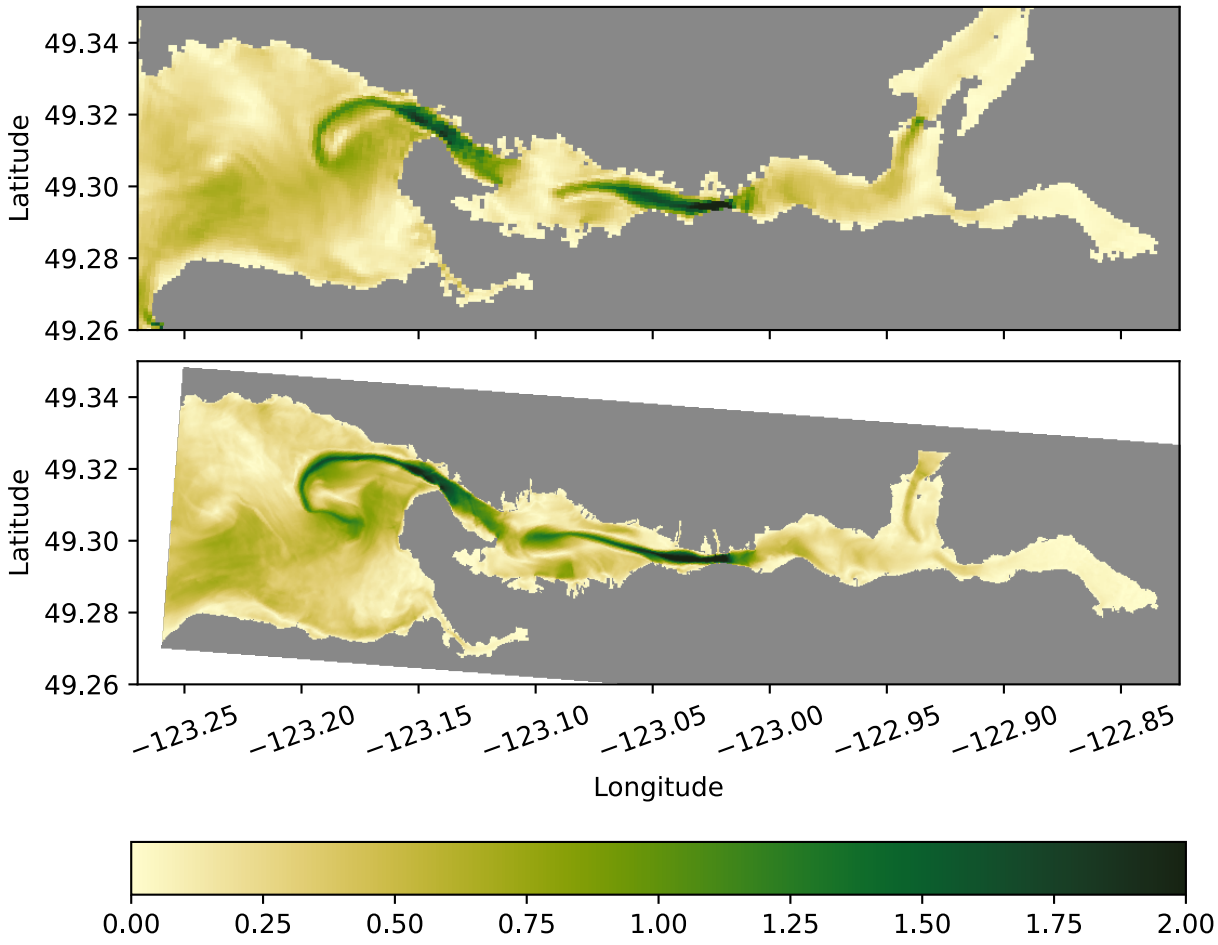

Figure 4. Surface speed (m/s) for SSS150 and VH20 for Vancouver Harbour.

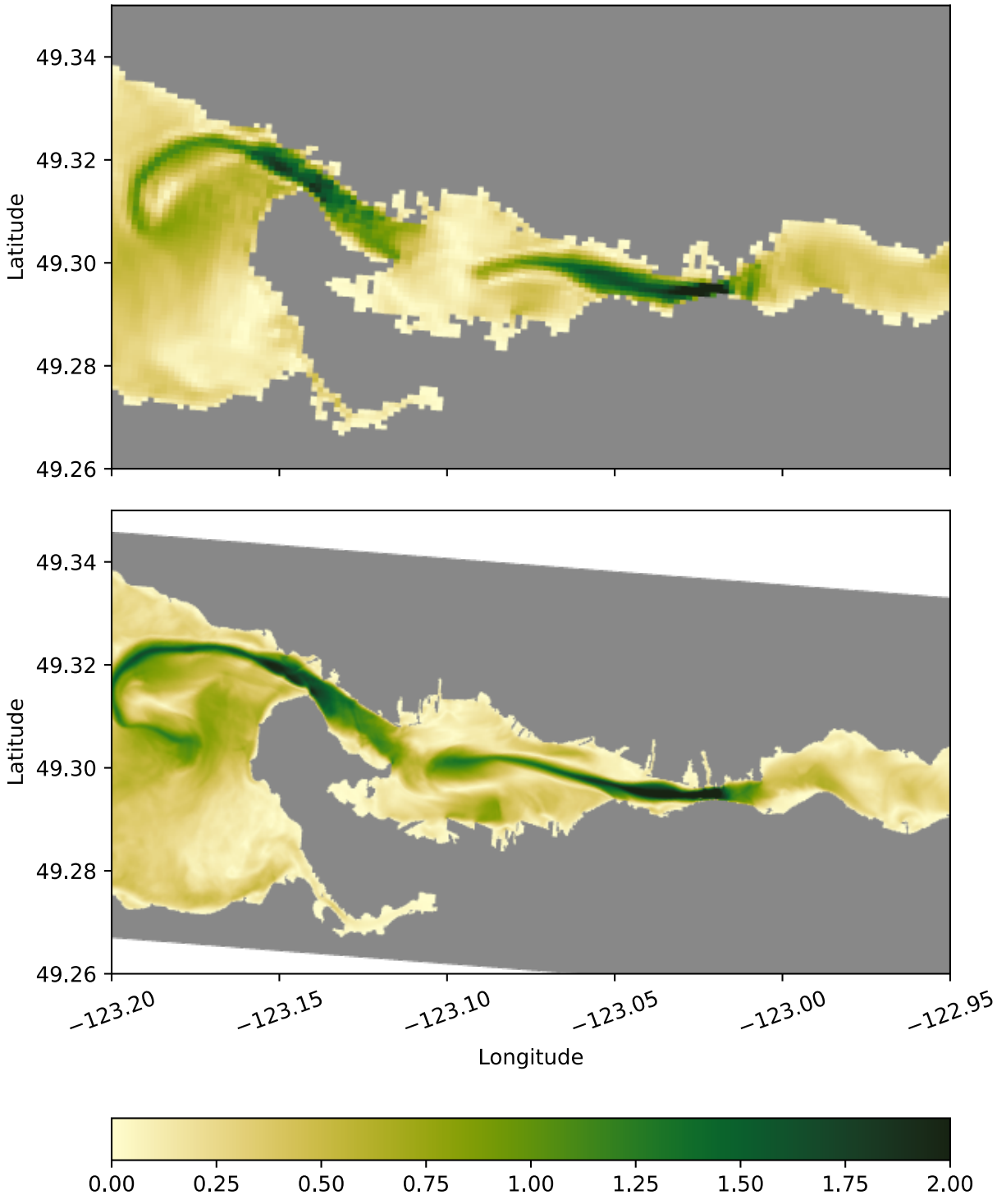

Figure 5. Surface speed (m/s) for SSS150 and VH20 for Vancouver Harbour (zoom over First and Second Narrows).

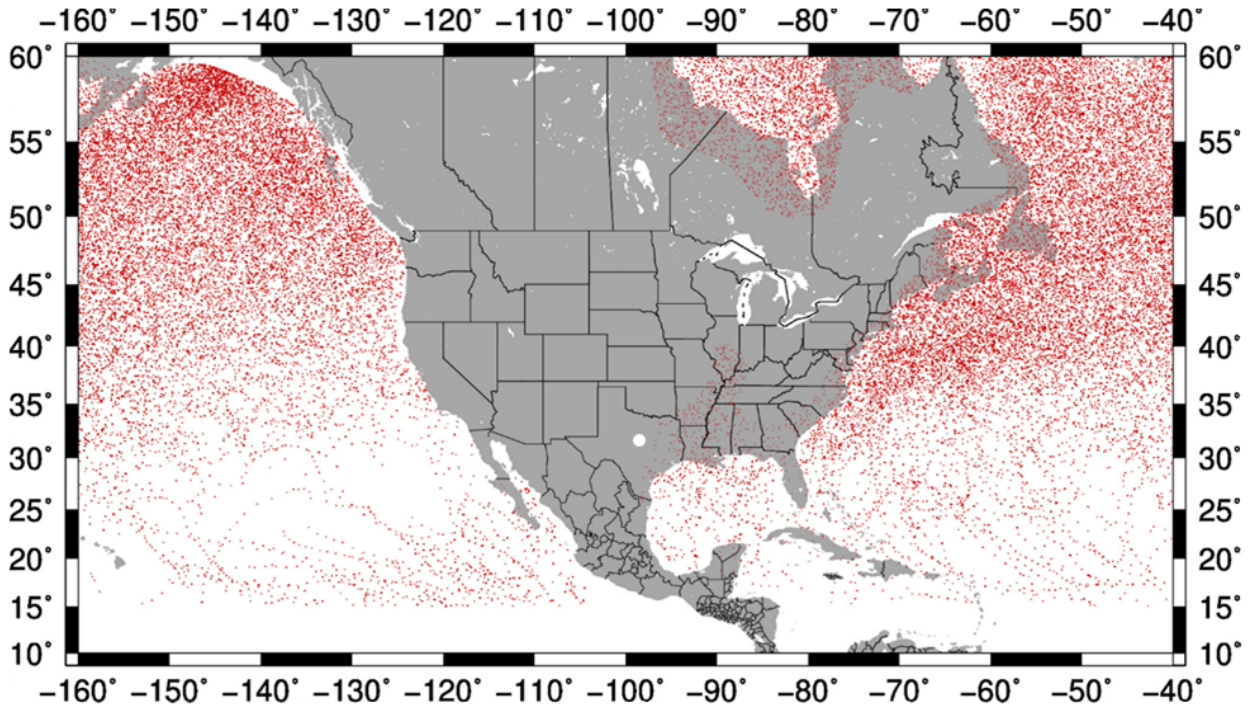

Figure 6. Cyclone locations every six hours from 2010-2021.

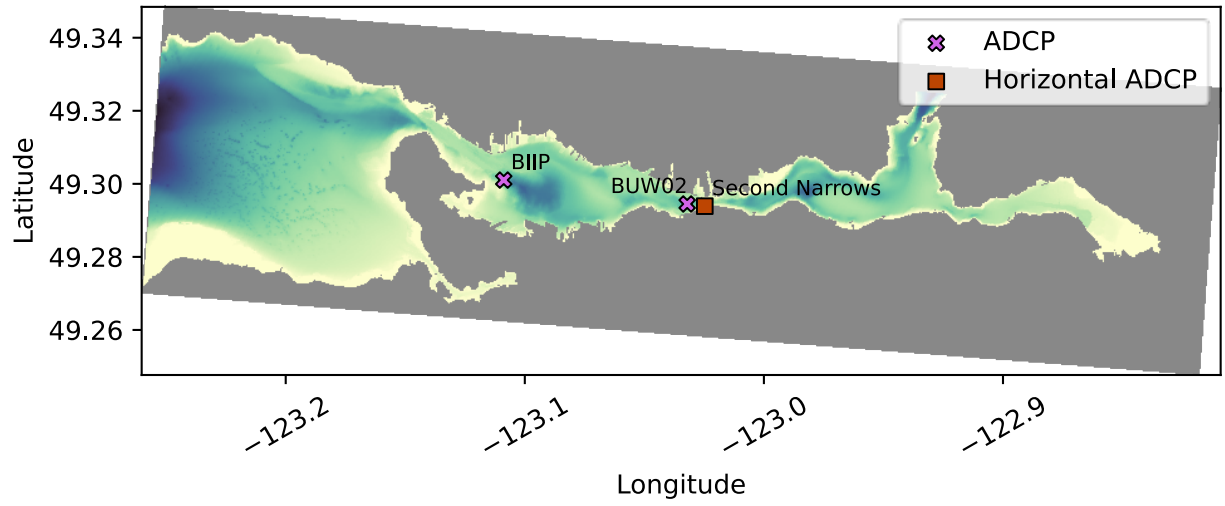

Figure 7. Locations of two ADCPs and one HADCP used in the evaluation.

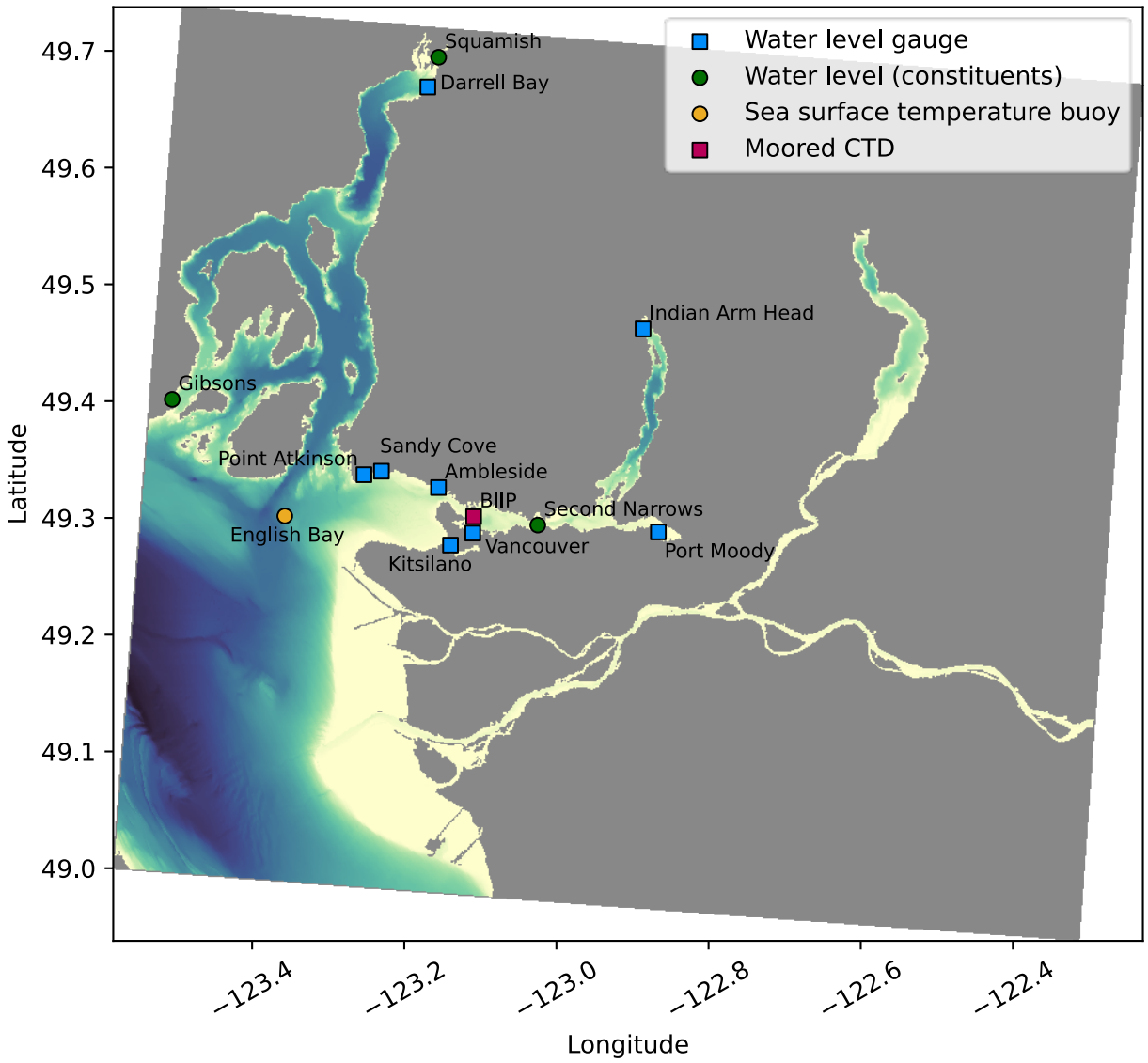

Figure 8. Locations of eight water level gauges, three water level constituent records, one sea-surface temperature buoy and one moored CTD used for this evaluation.

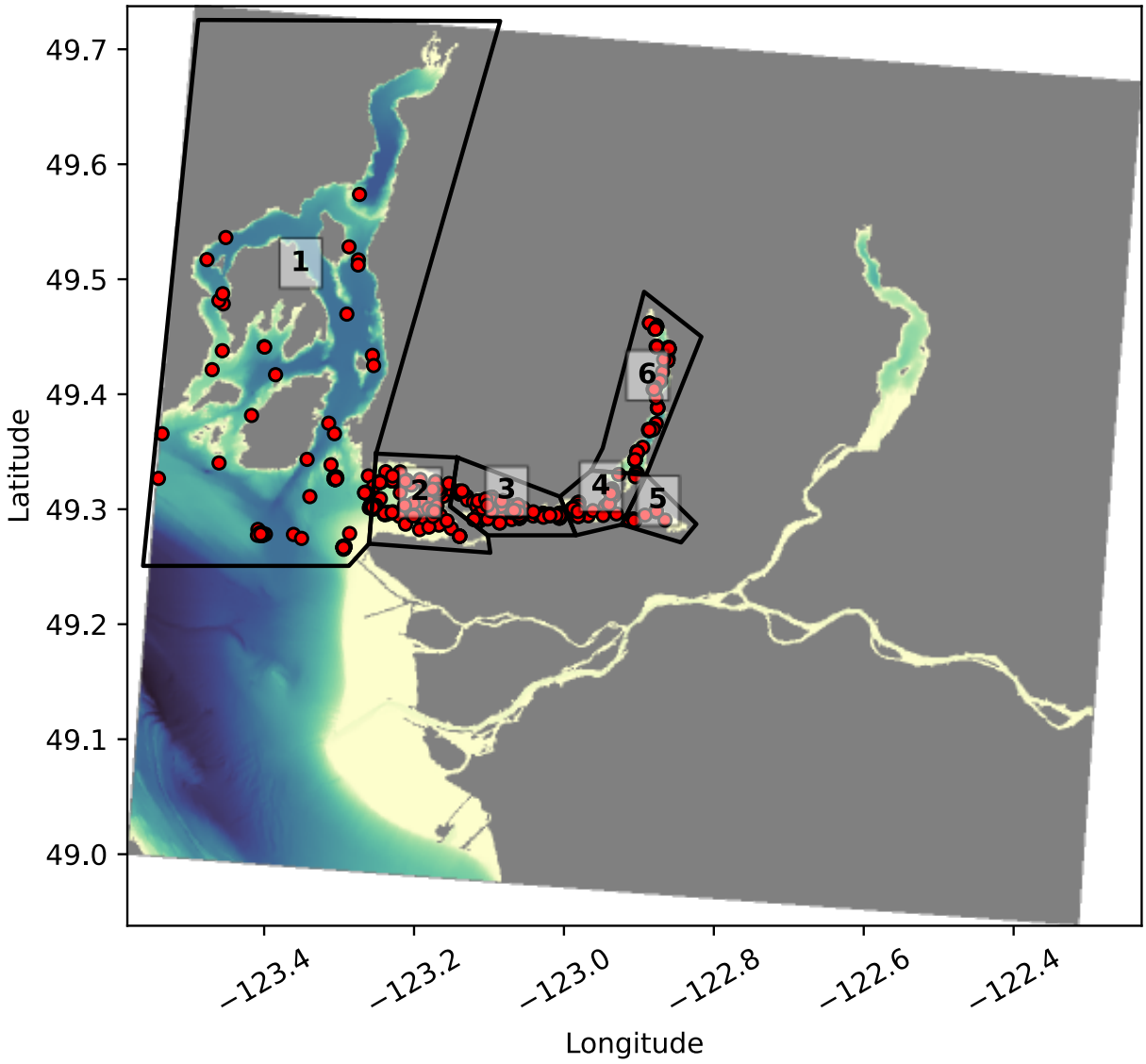

Figure 9. Subregions used for CTD profile analysis: (1) Howe Sound, (2) English Bay, (3) Vancouver Harbour, (4) Vancouver Harbour East, (5) Port Moody and (6) Indian Arm.

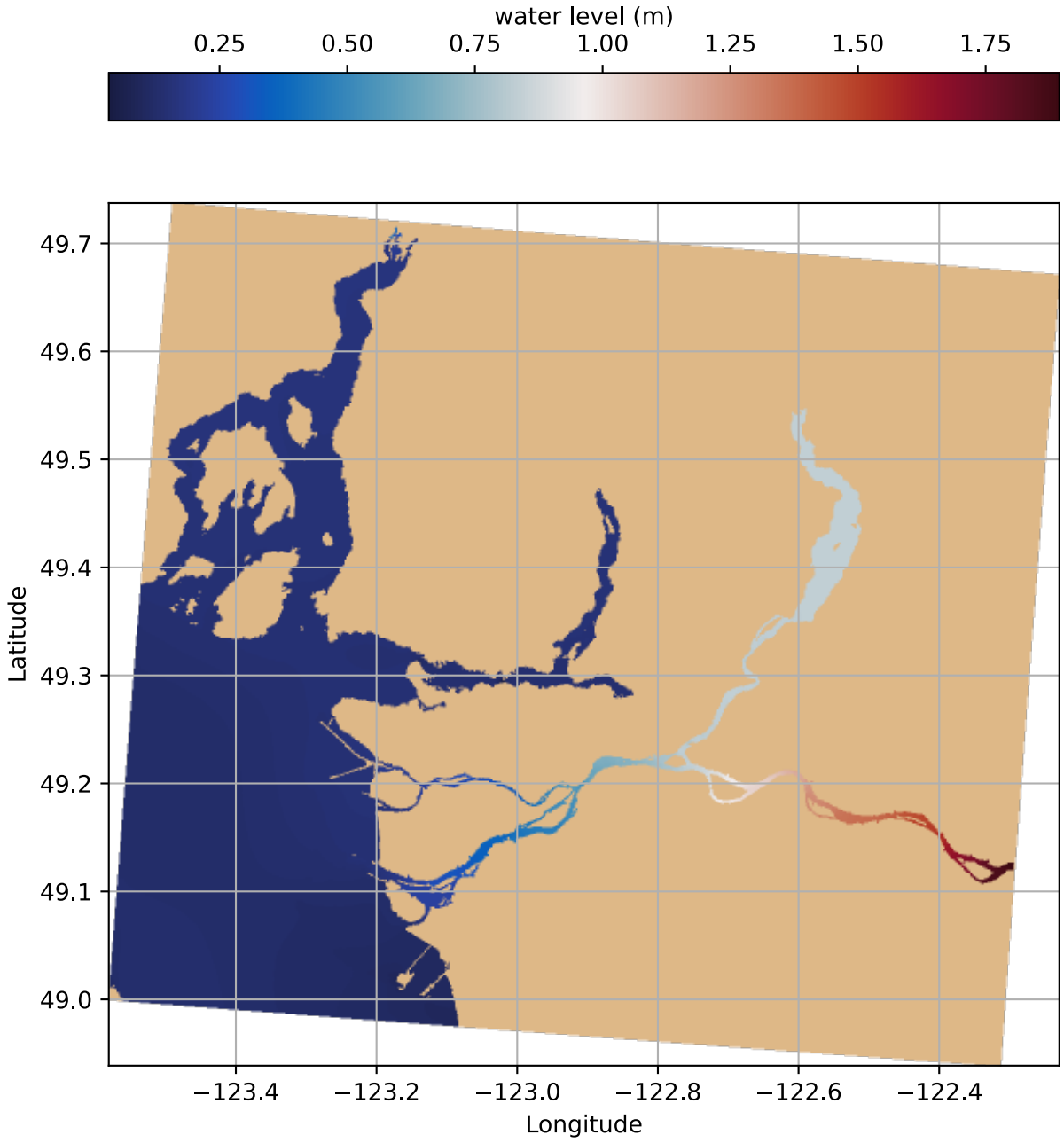

Figure 10. Mean water level for the outer domain SSS150 computed over the five-year hindcast period 2017-2021.

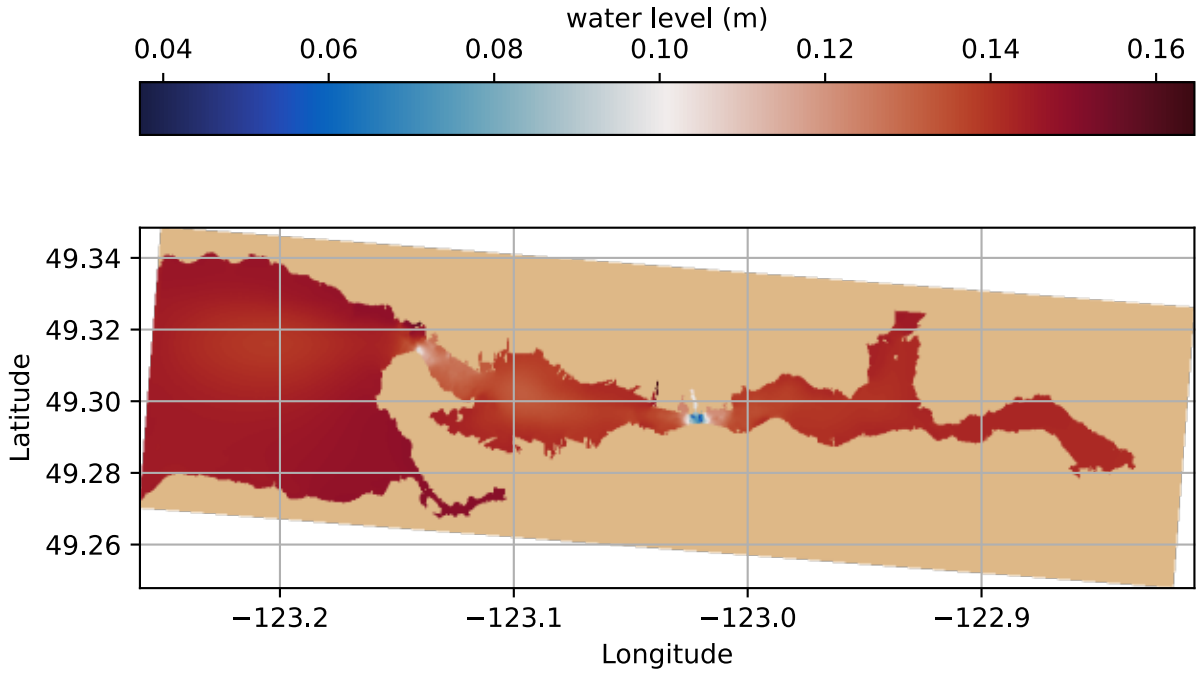

Figure 11. Mean water level for the inner domain VH20 computed over the five-year hindcast period 2017-2021.

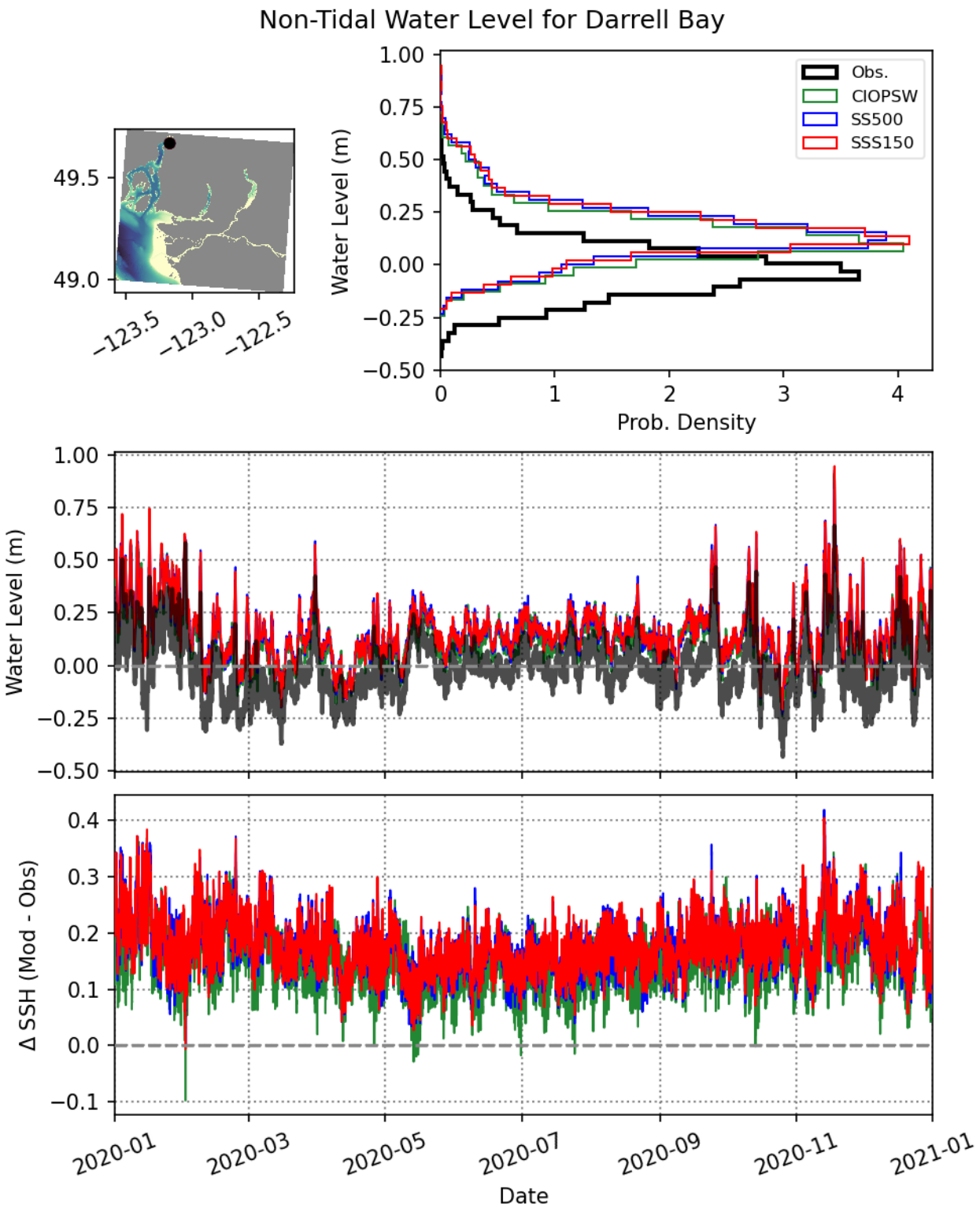

Figure 12. Non-tidal water level comparison for Darrell Bay for year 2020.

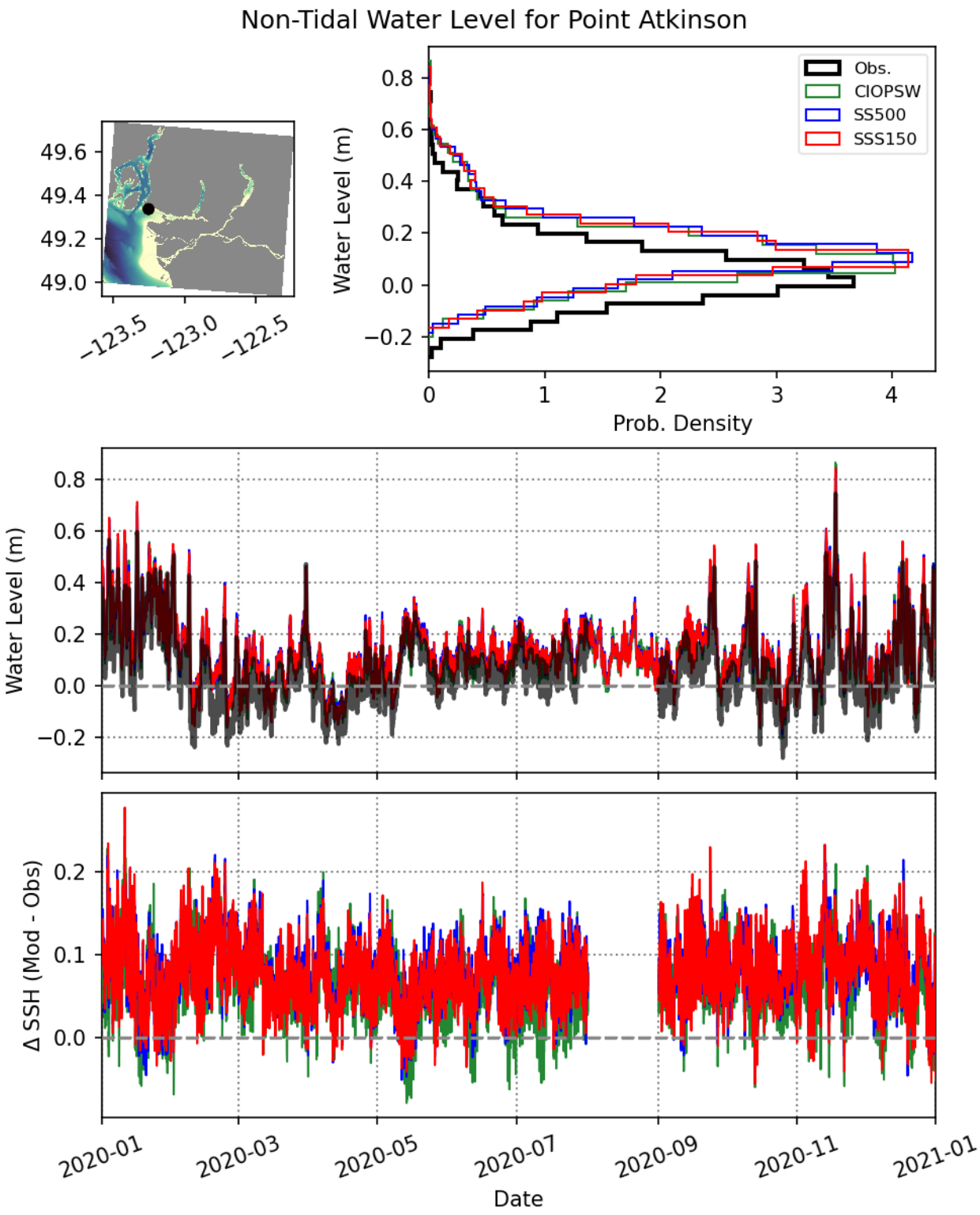

Figure 13. Non-tidal water level comparison for Point Atkinson for year 2020.

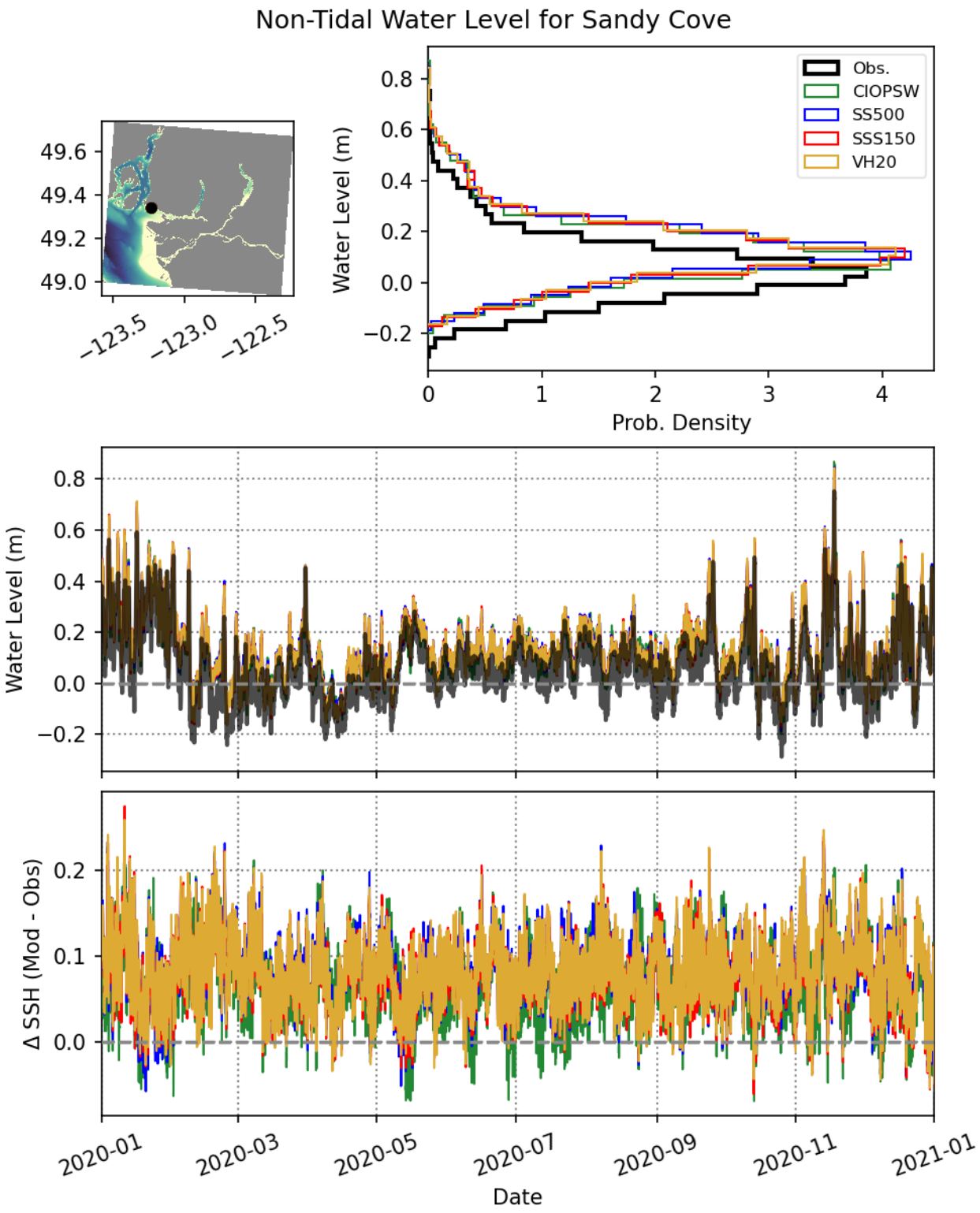

Figure 14. Non-tidal water level comparison for Sandy Cove for year 2020.

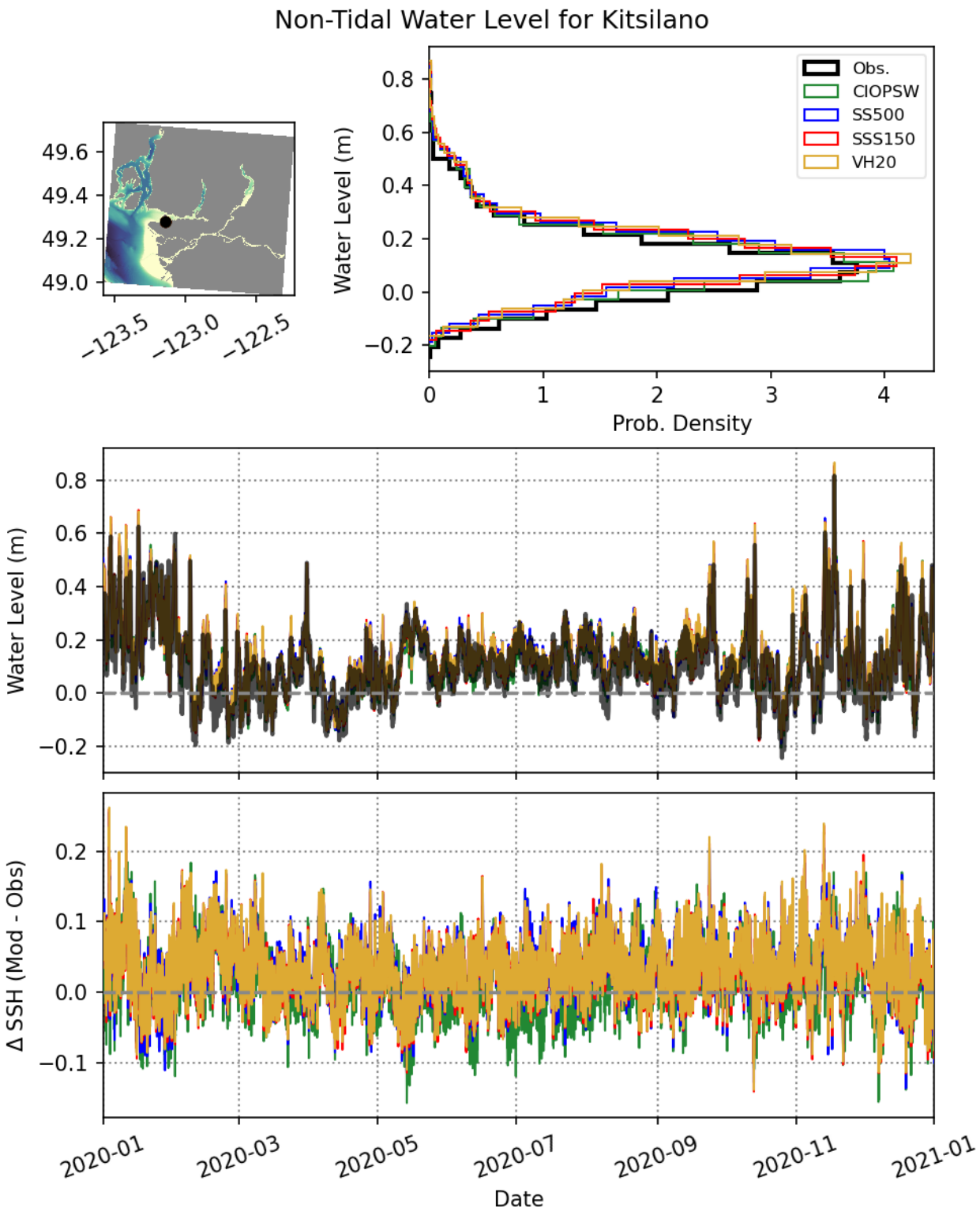

Figure 15. Non-tidal water level comparison for Kitsilano for year 2020.

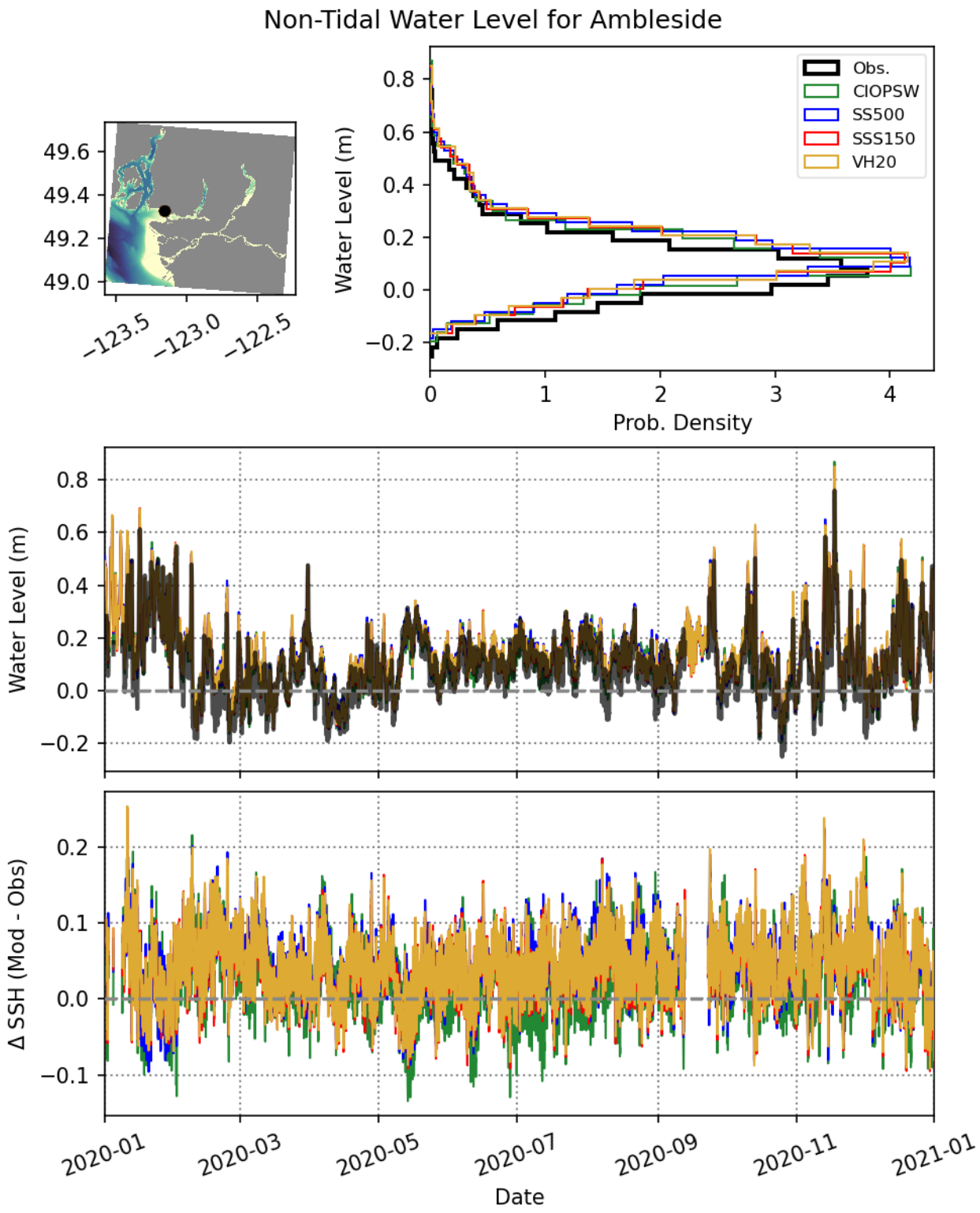

Figure 16. Non-tidal water level comparison for Ambleside for year 2020.

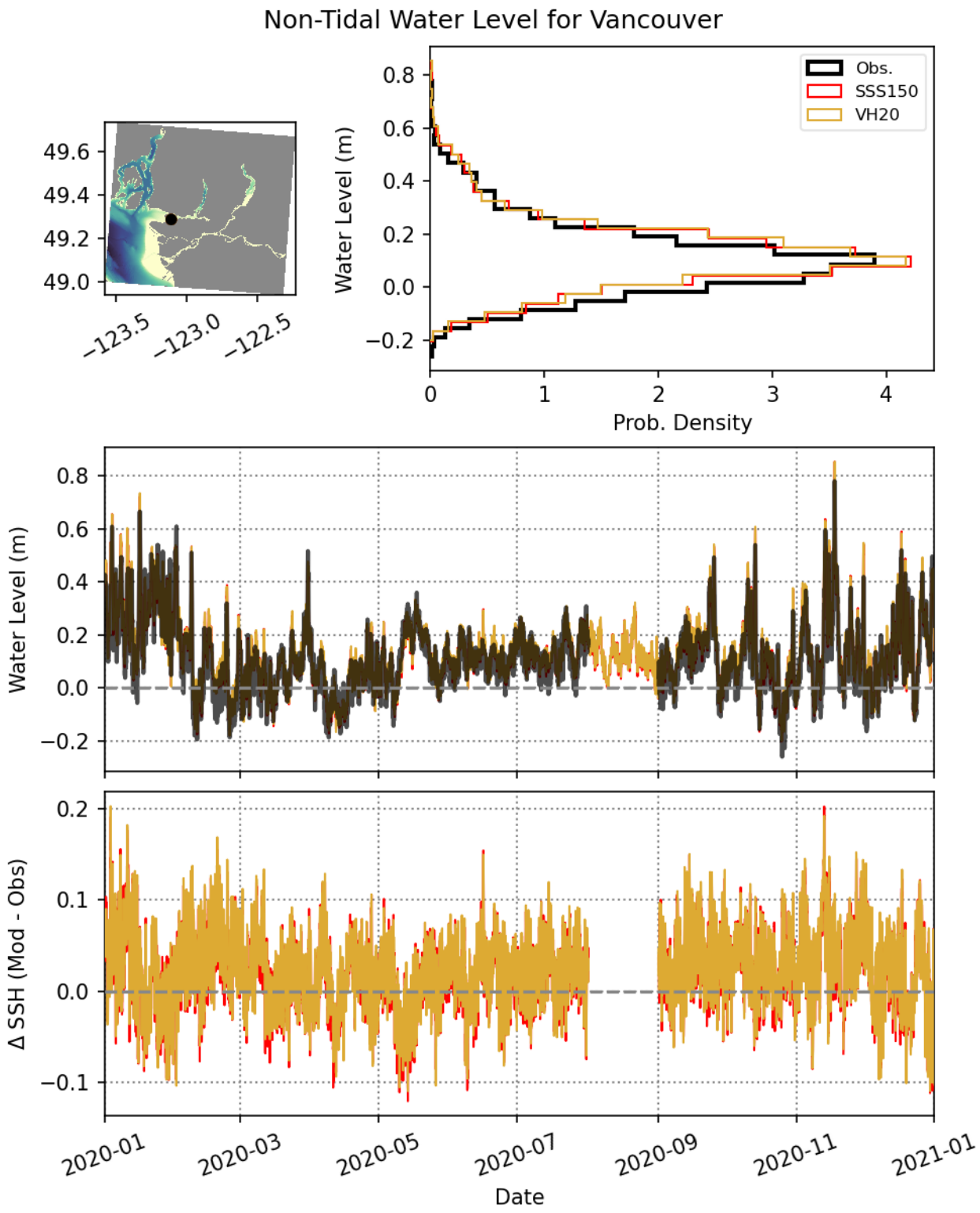

Figure 17. Non-tidal water level comparison for Vancouver for year 2020.

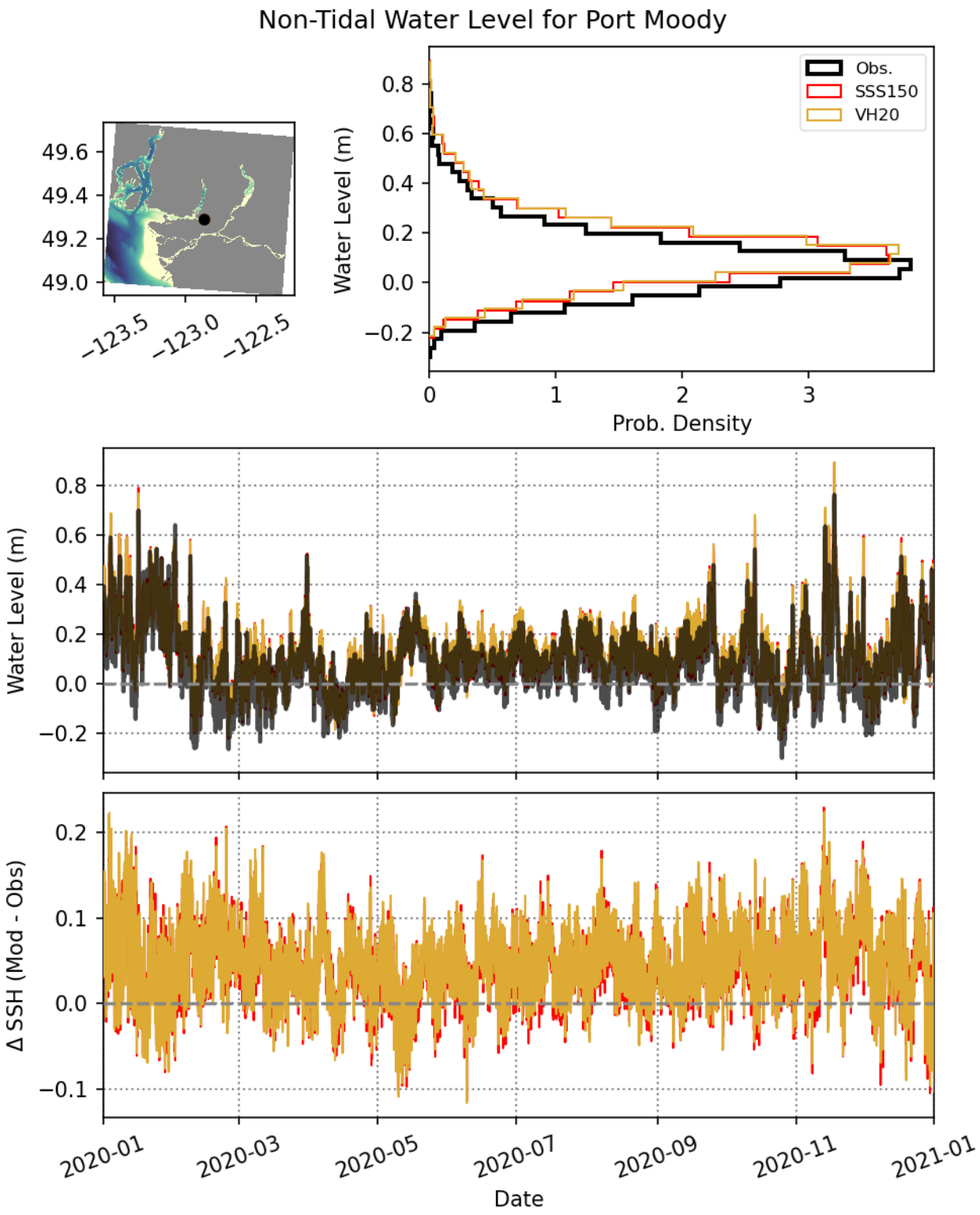

Figure 18. Non-tidal water level comparison for Port Moody for year 2020.

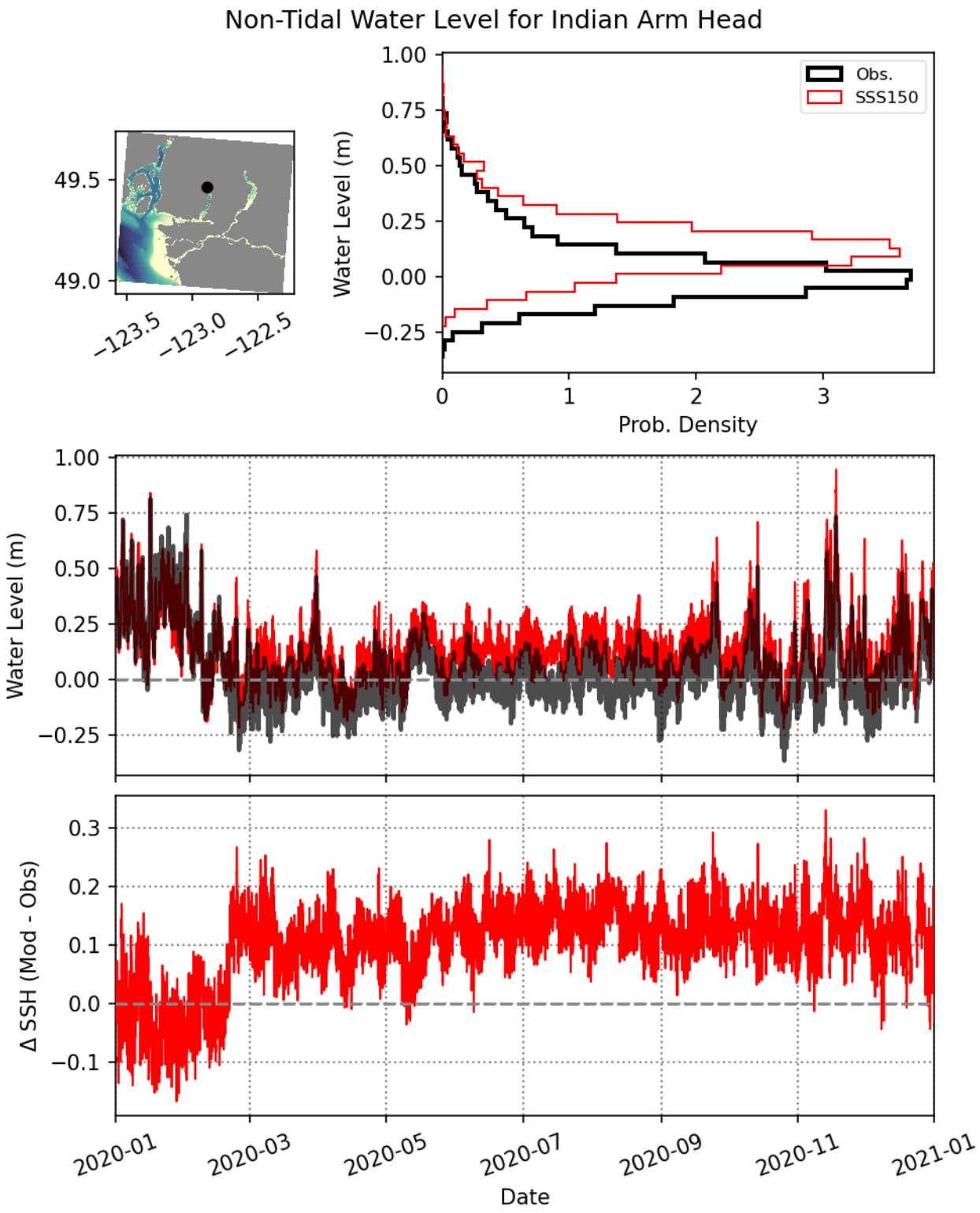

Figure 19. Non-tidal water level comparison for Indian Arm Head for year 2020.

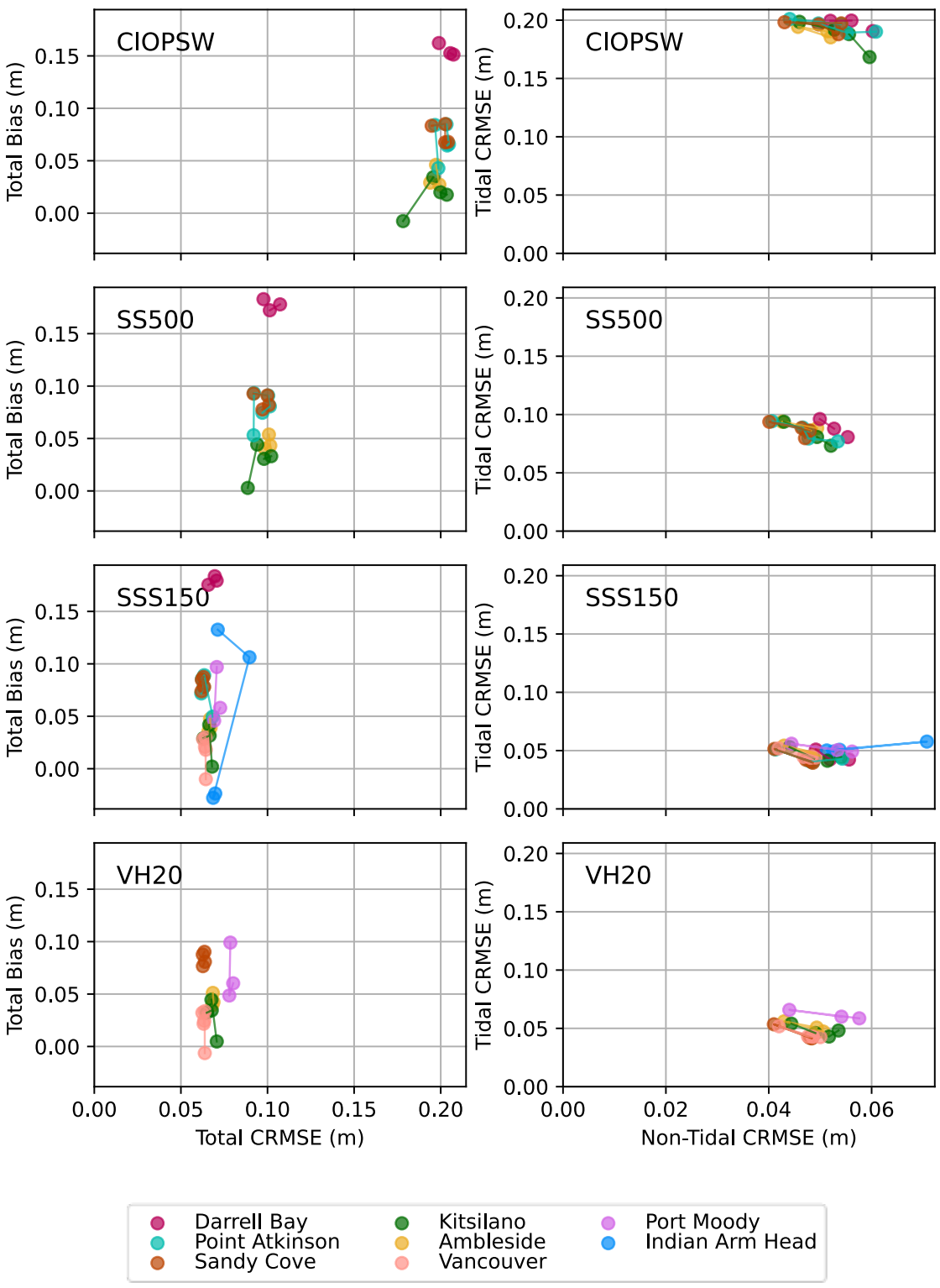

Figure 20. Water level score stability summary for each model under assessment (rows), where the left panels show total water level bias and CRMSE, where the right panels show tidal and non-tidal CRMSE, where each water level station is shown in a different colour, and where each marker represents a different year.

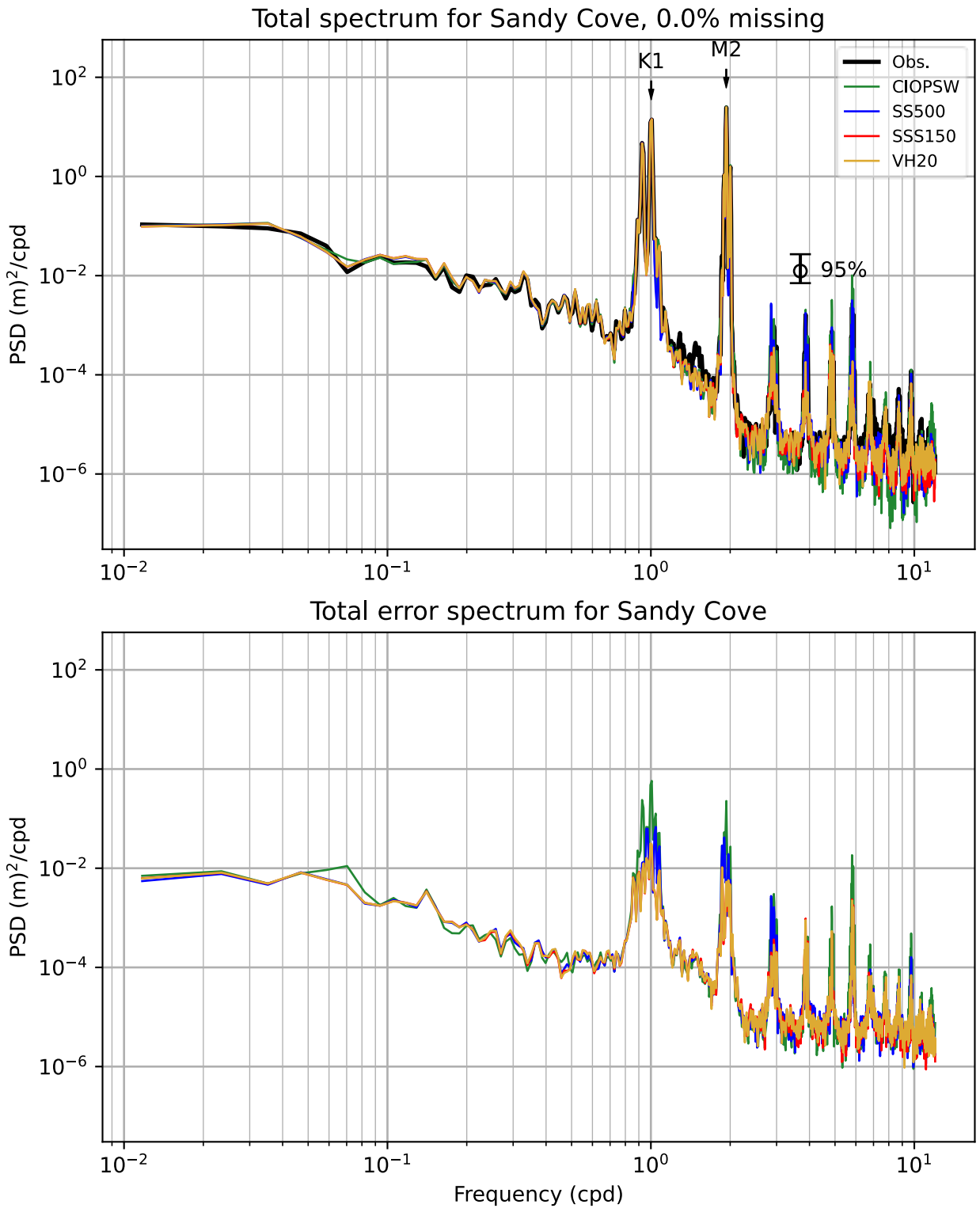

Figure 21. Total water level spectra (top) and error spectra (bottom) for Sandy Cove station, year 2018.

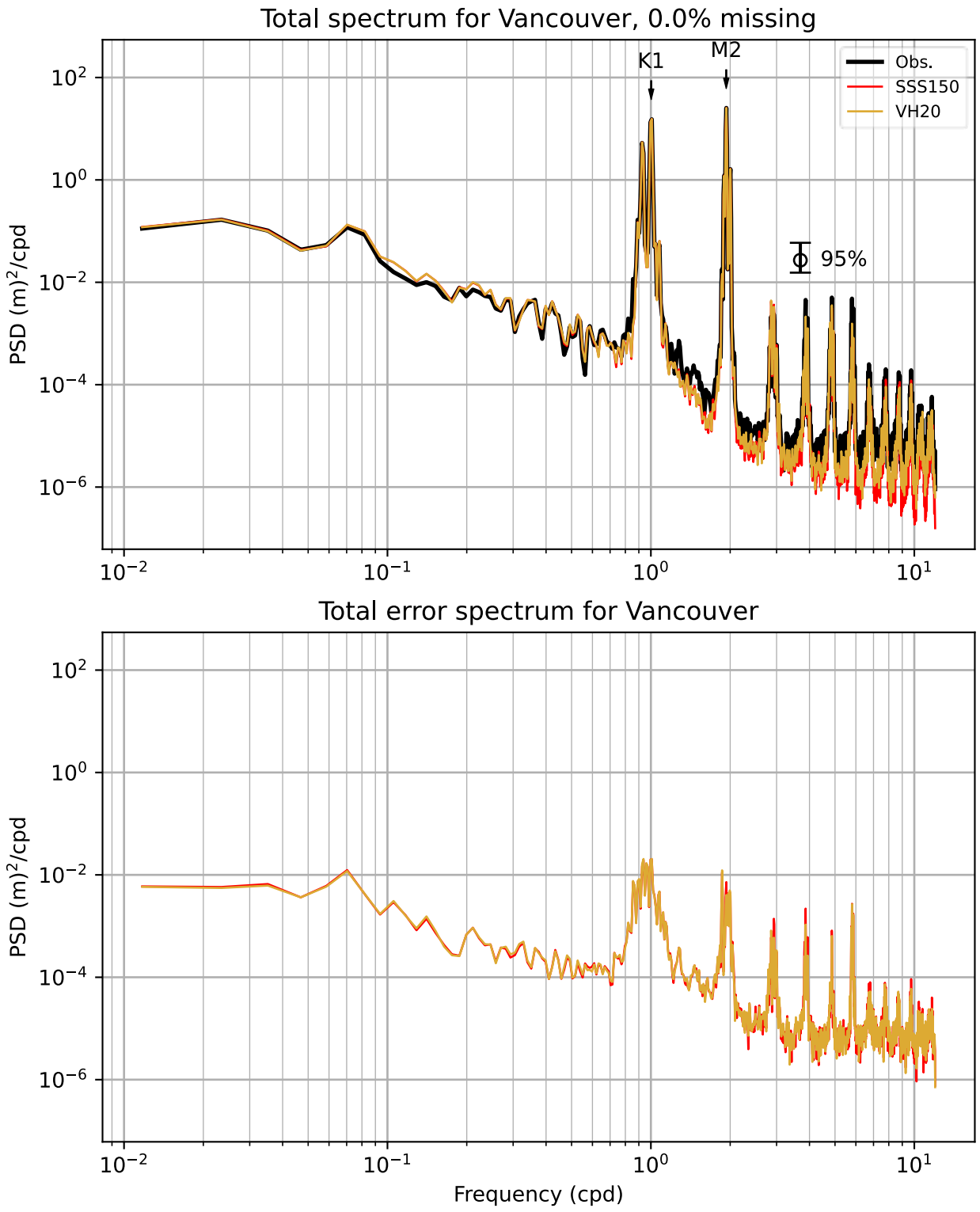

Figure 22. Total water level spectra (top) and error spectra (bottom) for Vancouver Harbour station, year 2019.

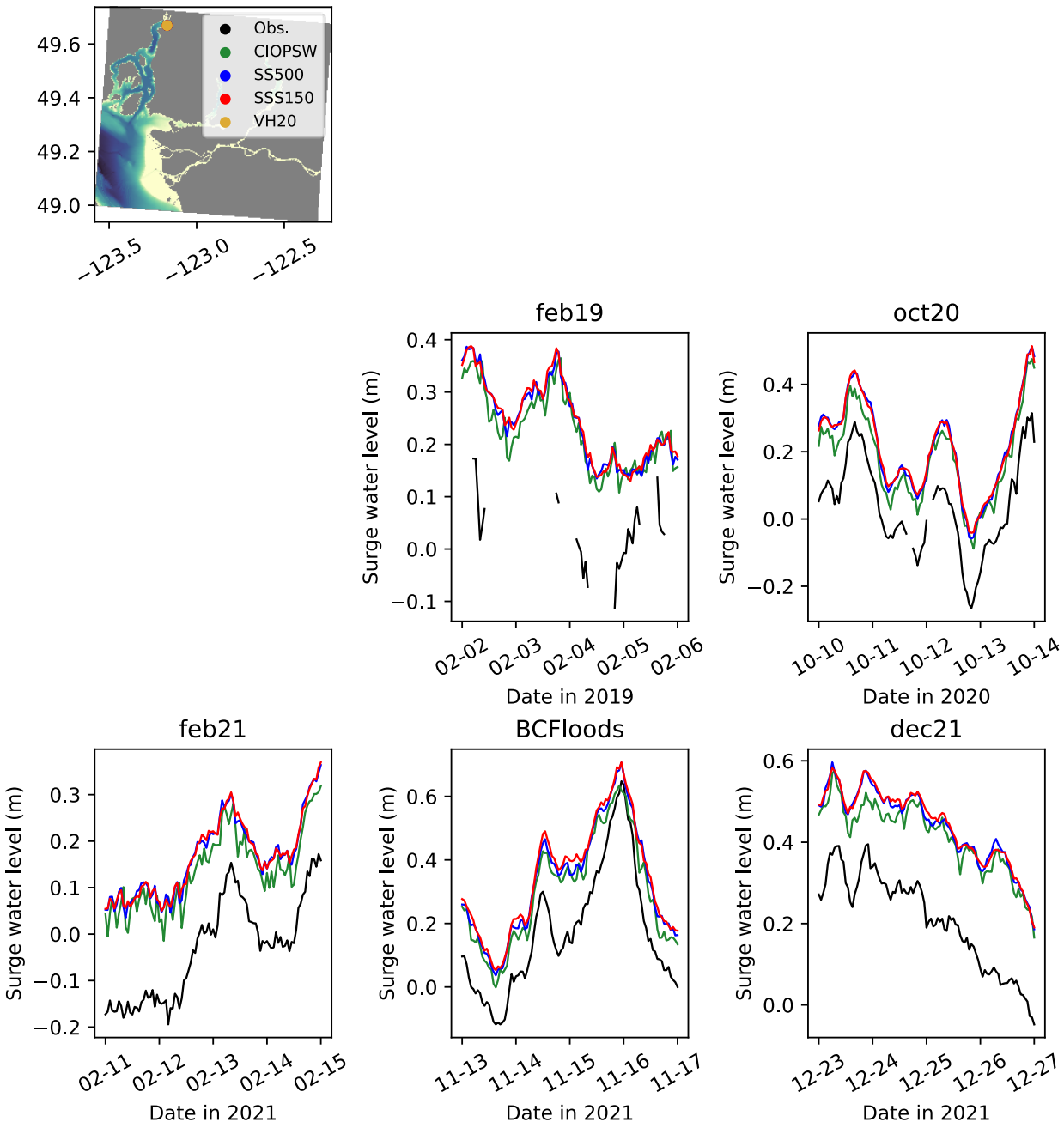

Figure 23. Storm surge analysis for Darrell Bay water level station.

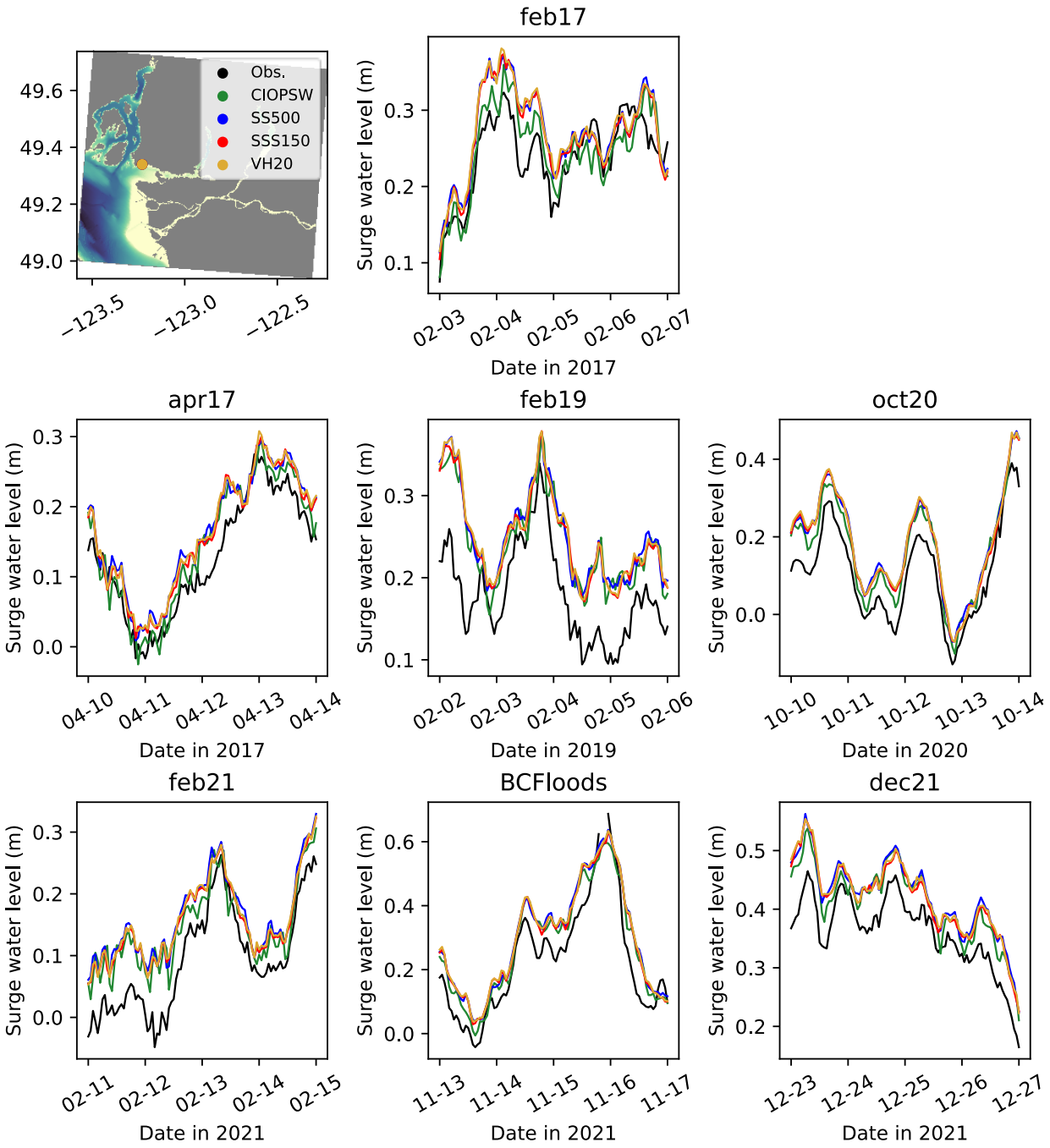

Figure 24. Storm surge analysis for Sandy Cove water level station.

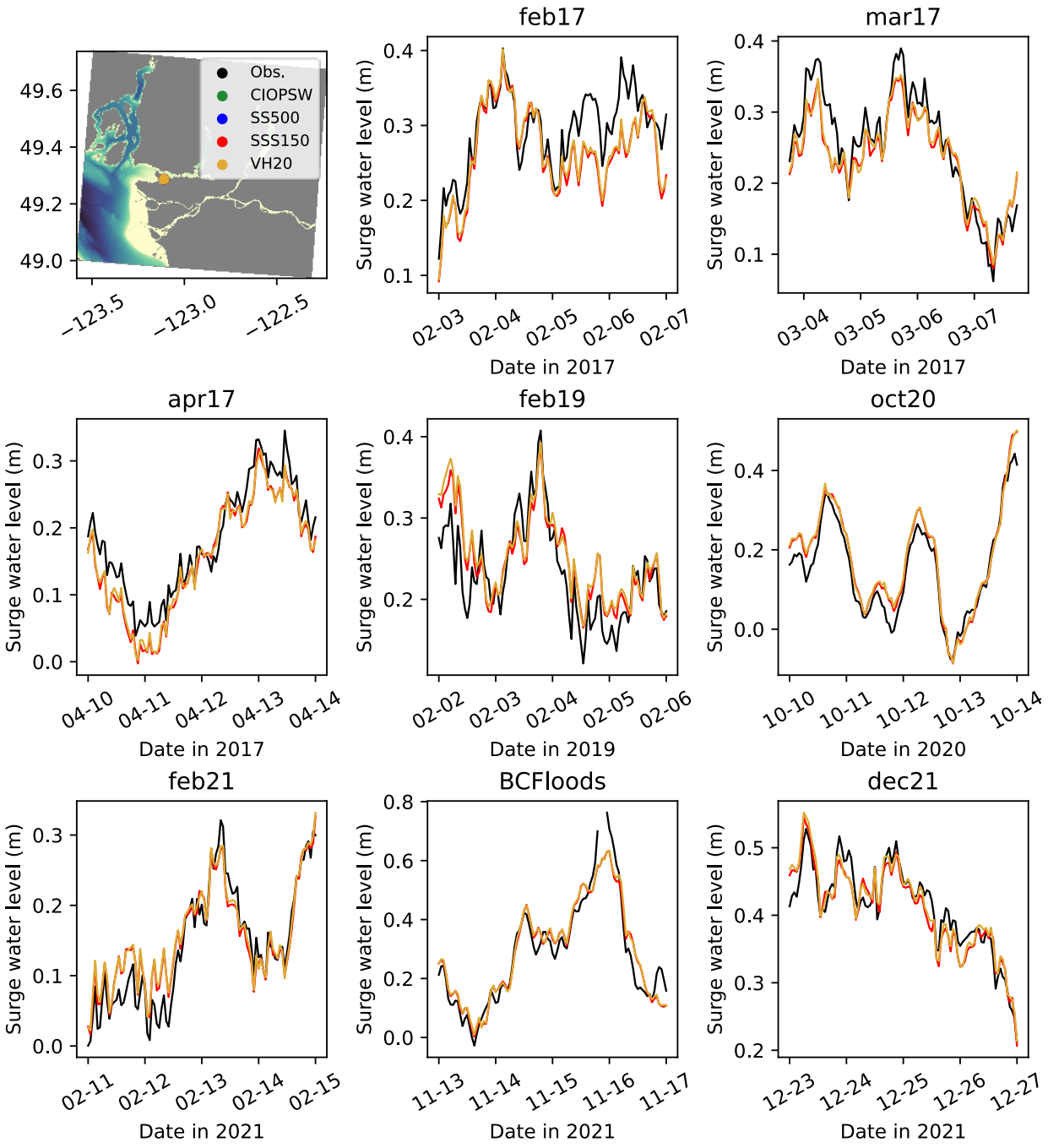

Figure 25. Storm surge analysis for Vancouver Harbour water level station.

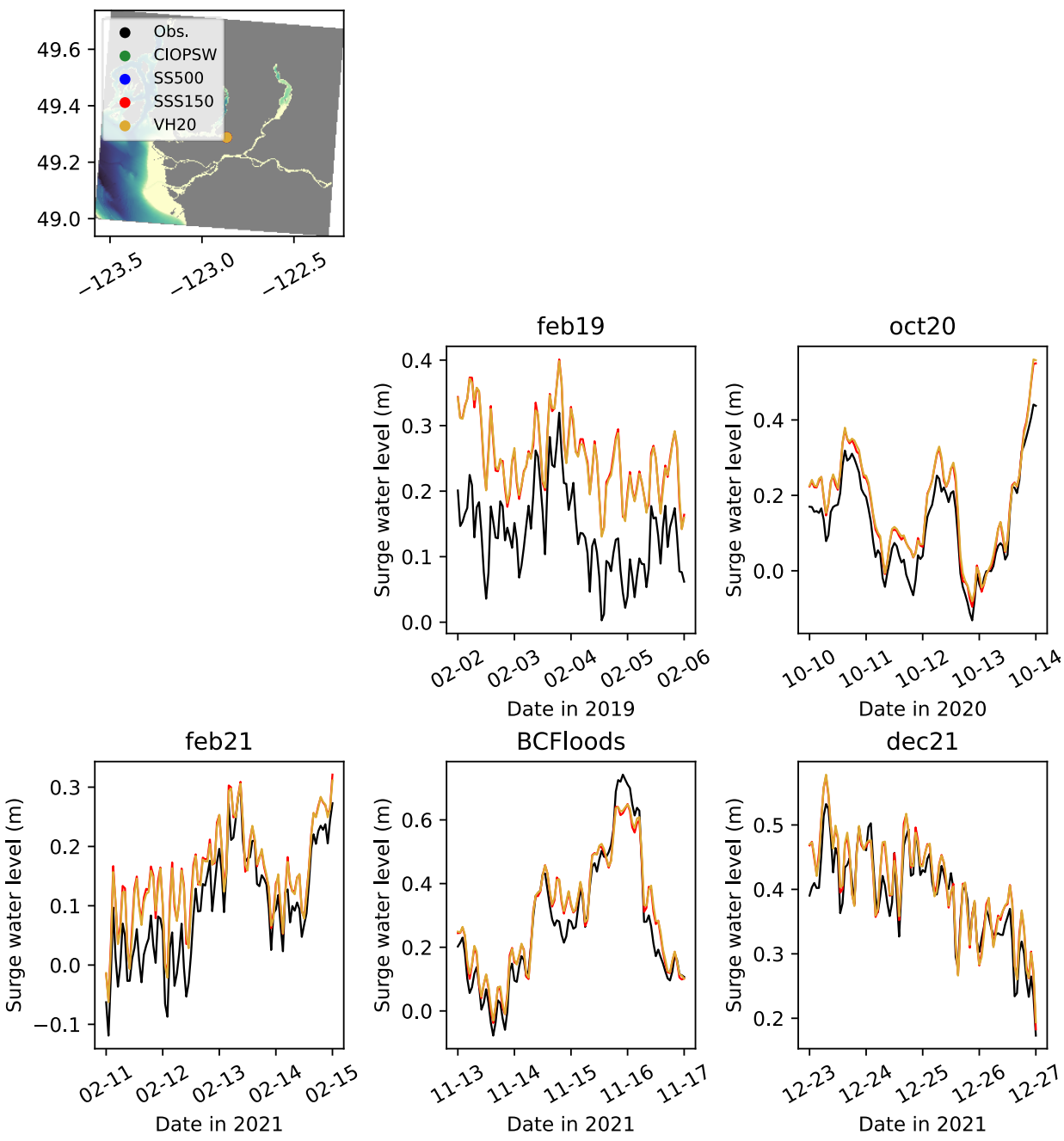

Figure 26. Storm surge analysis for Port Moody water level station.

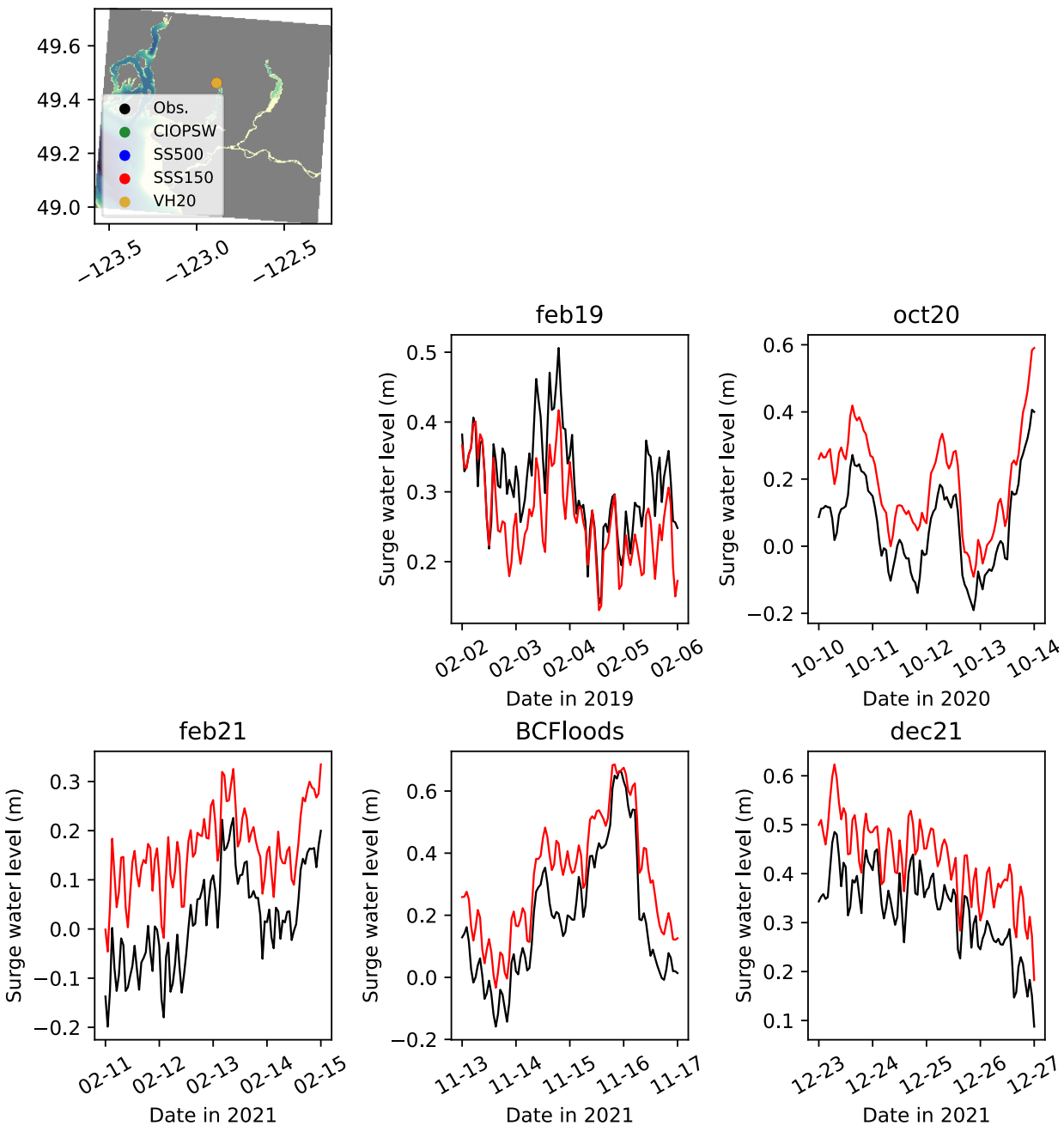

Figure 27. Storm surge analysis for Indian Arm water level station.

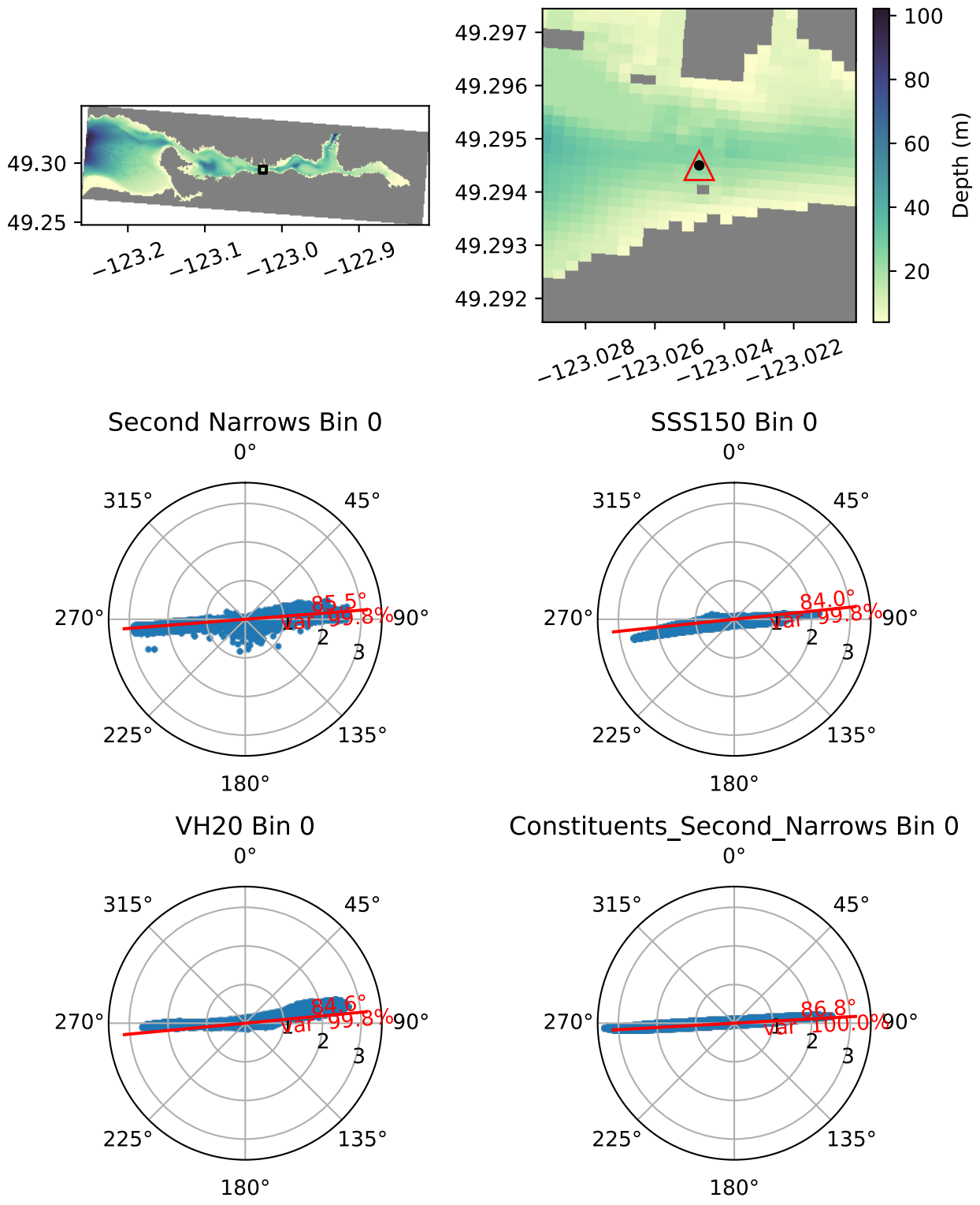

Figure 28. Observation location and scatterplots with principal axes of variance for the horizontal ADCP at Second Narrows. Circular grid lines indicate velocity in m/s. Date range shown here is 2020-06-13 through 2021-05-01 (322 days).

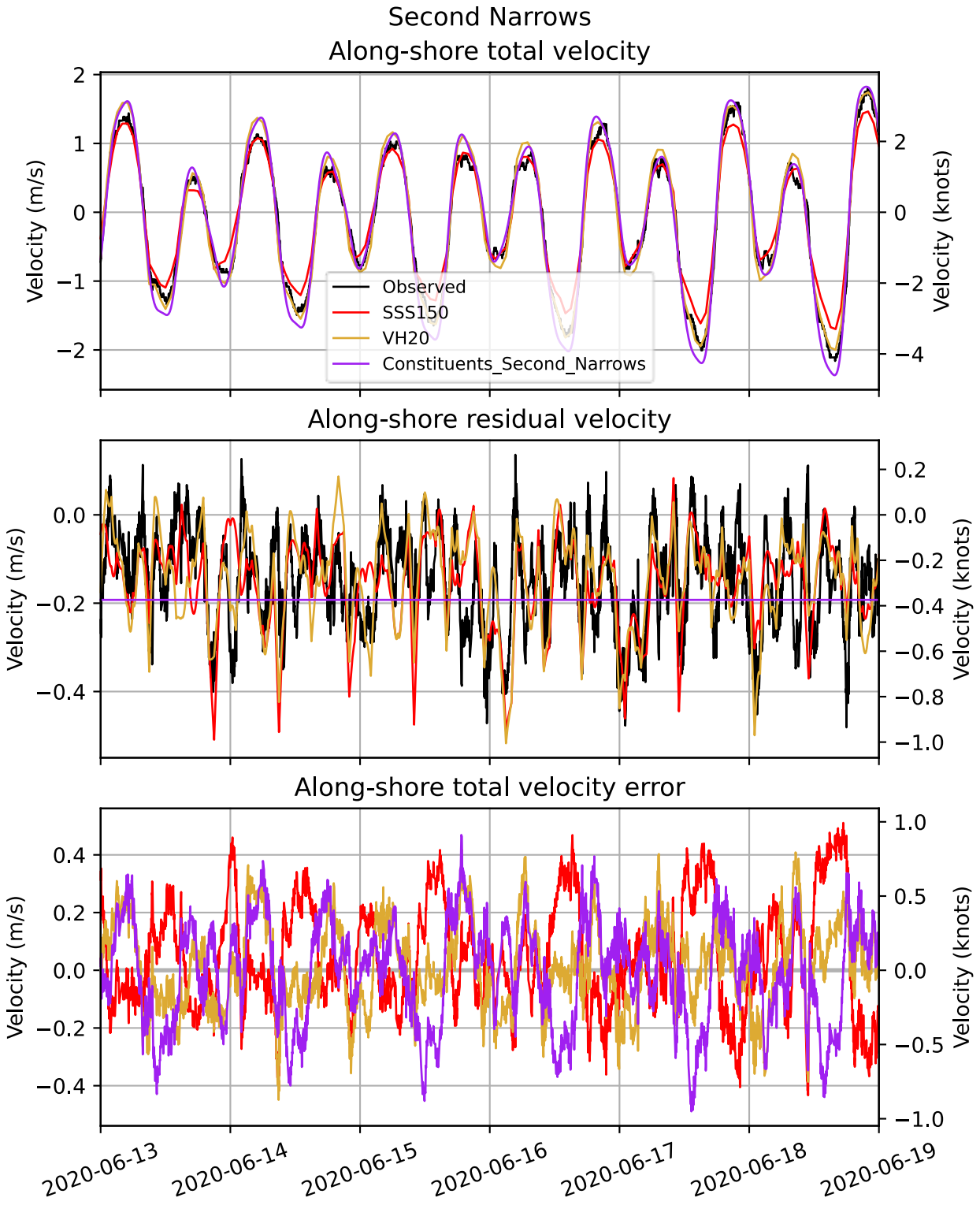

Figure 29. Sample period in June 2020 comparing model and data for the Second Narrows HADCP alongshore velocity, showing (top) total velocity, (middle) non-tidal velocity, and (bottom) total velocity error.

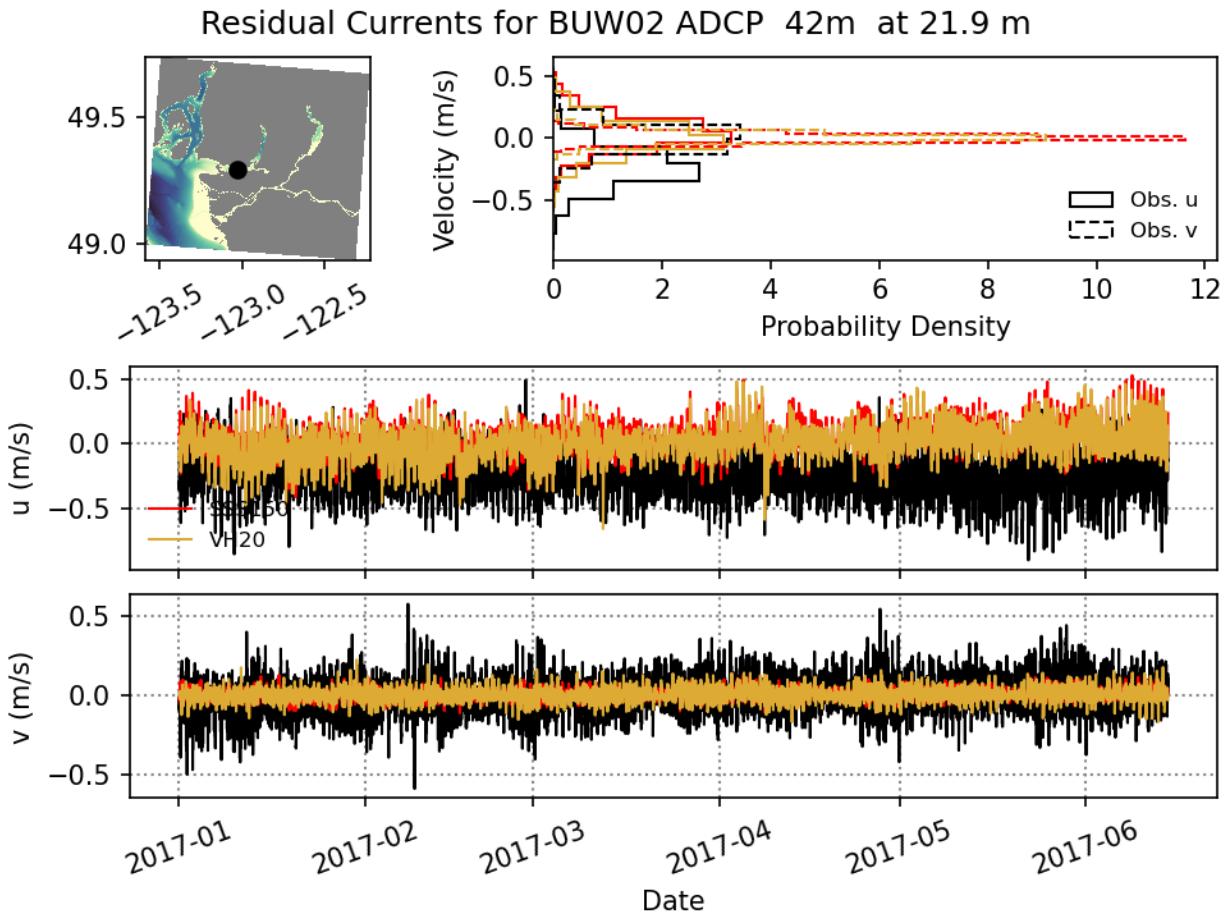

Figure 30. Residual currents at ADCP station BUW02 at 21.9 m depth.

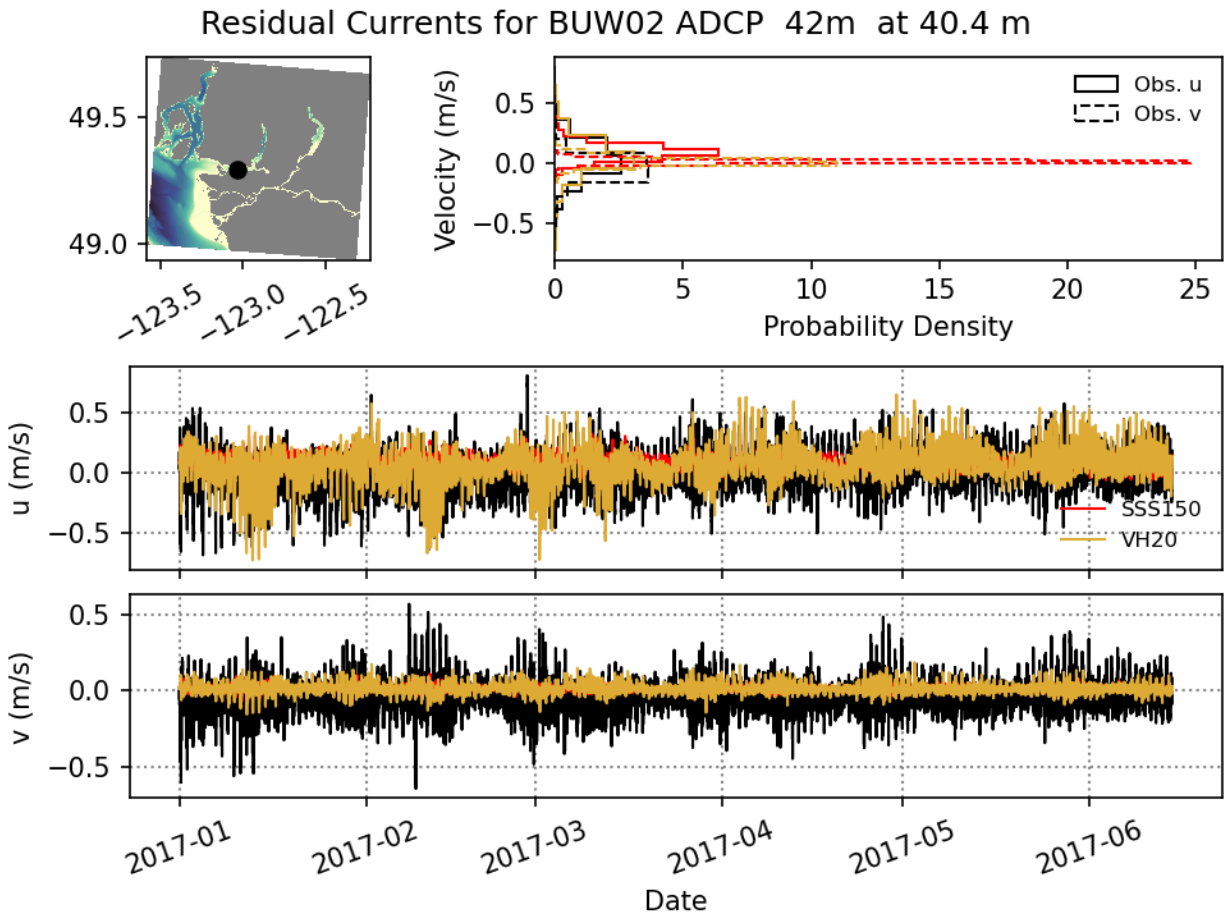

Figure 31. Residual currents at ADCP station BUW02 at 40.4 m depth.

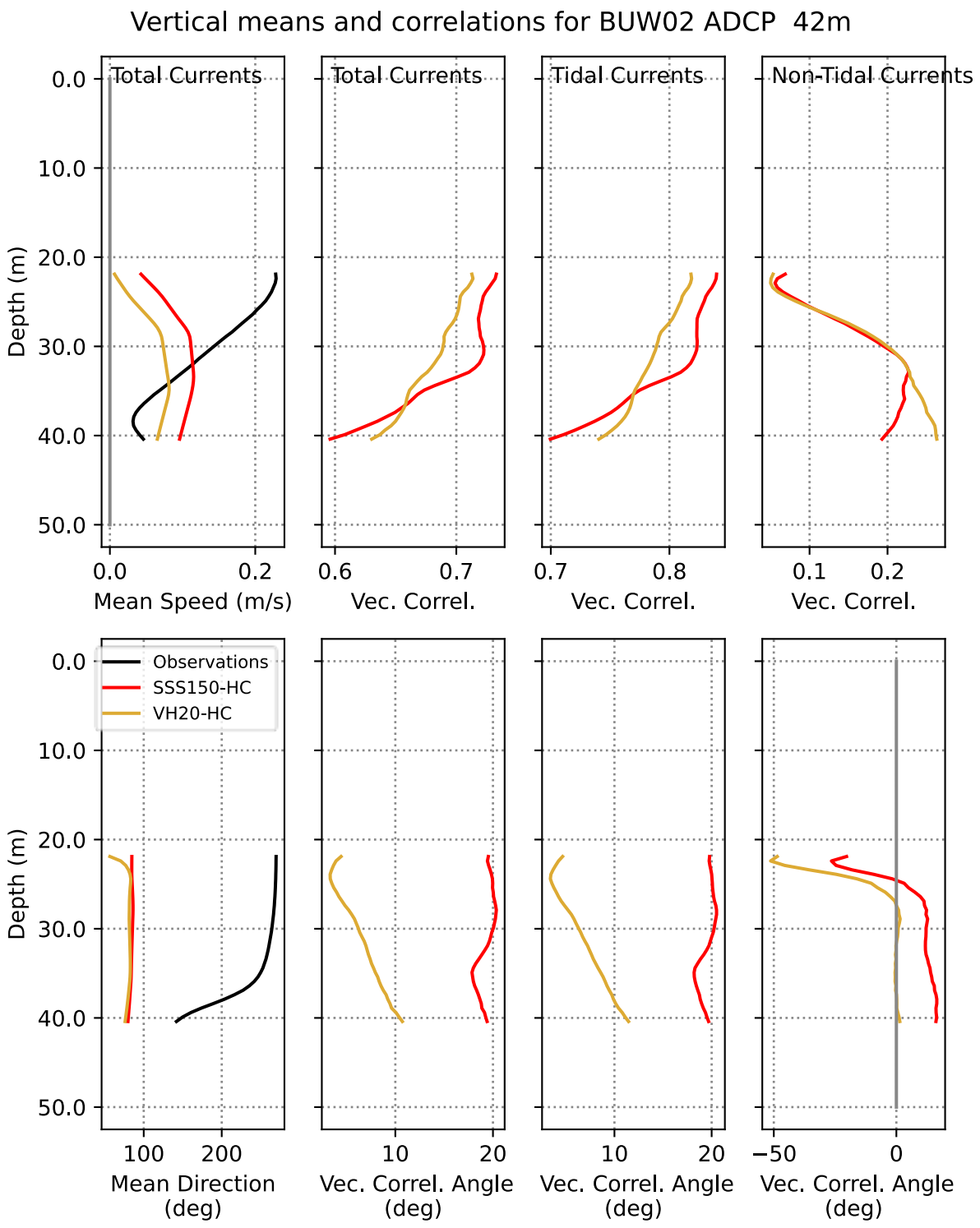

Figure 32. Mean currents (first column) and vector correlations for total (second column), tidal (third column) and non-tidal (fourth column) velocities for BUW02 ADCP deployment. Mean direction is measured clockwise from north.

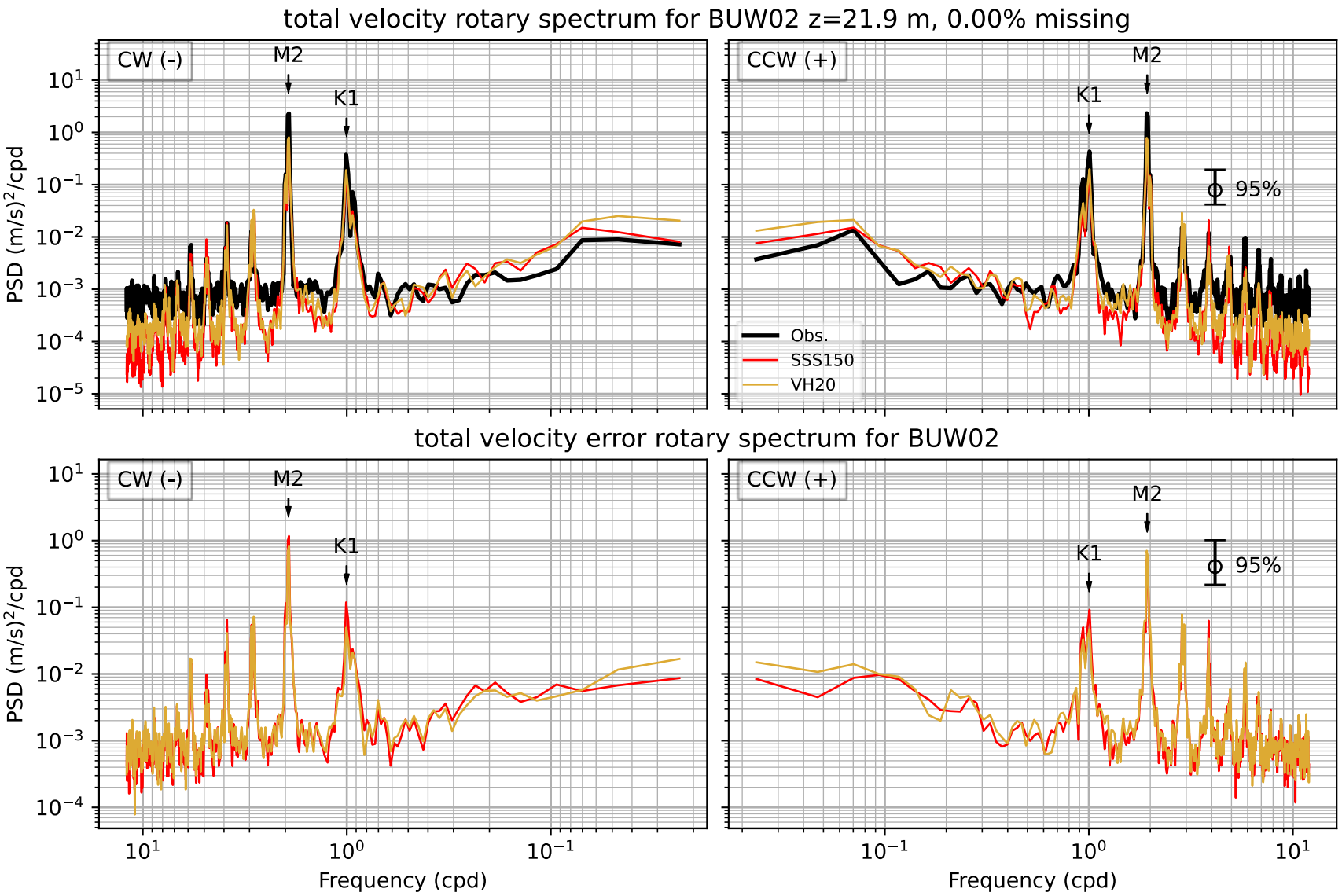

Figure 33. Rotary spectra for total velocity from BUW02 ADCP station at depth 21.9 m.

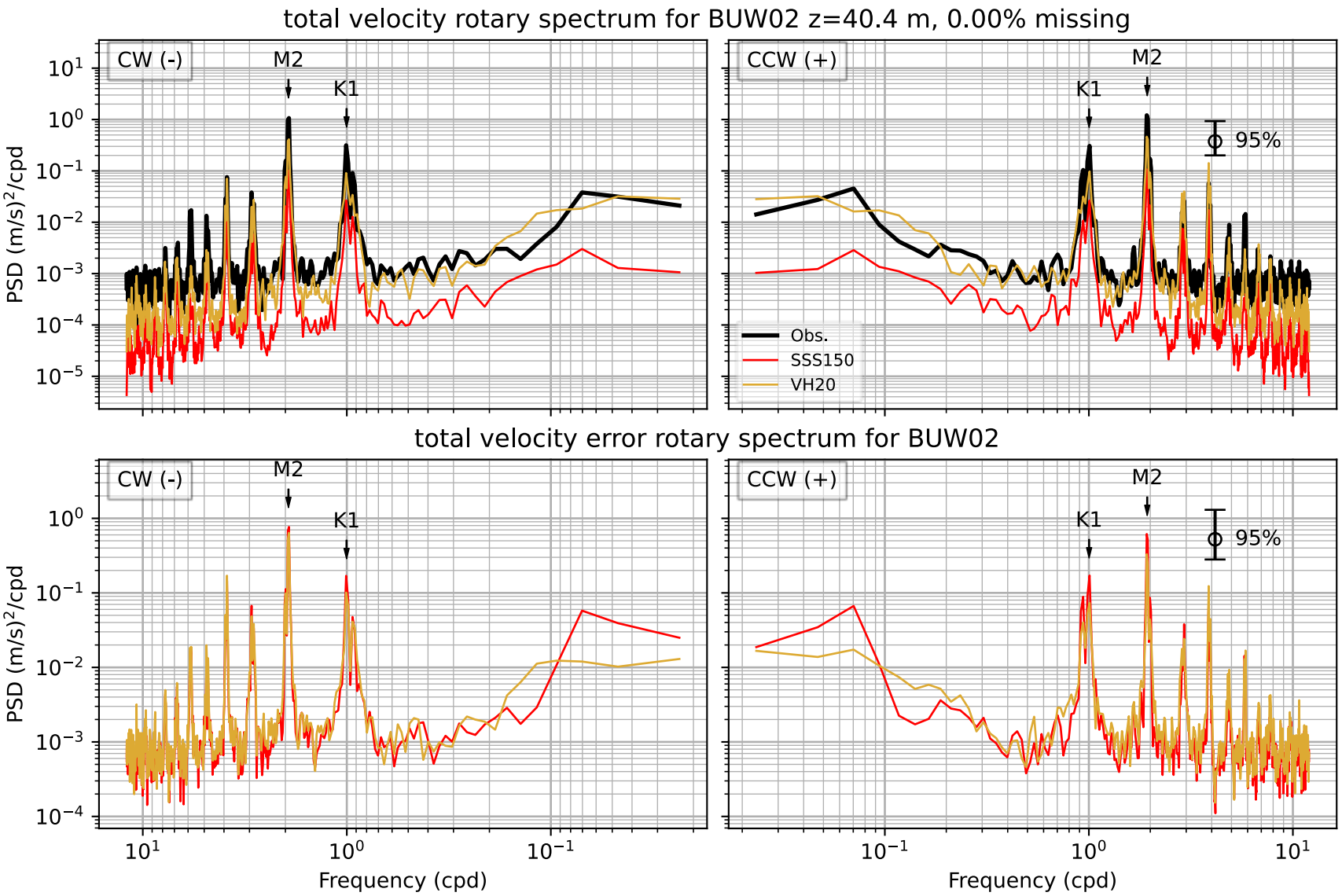

Figure 34. Rotary spectra for total velocity from BUW02 ADCP station at depth 40.4 m.

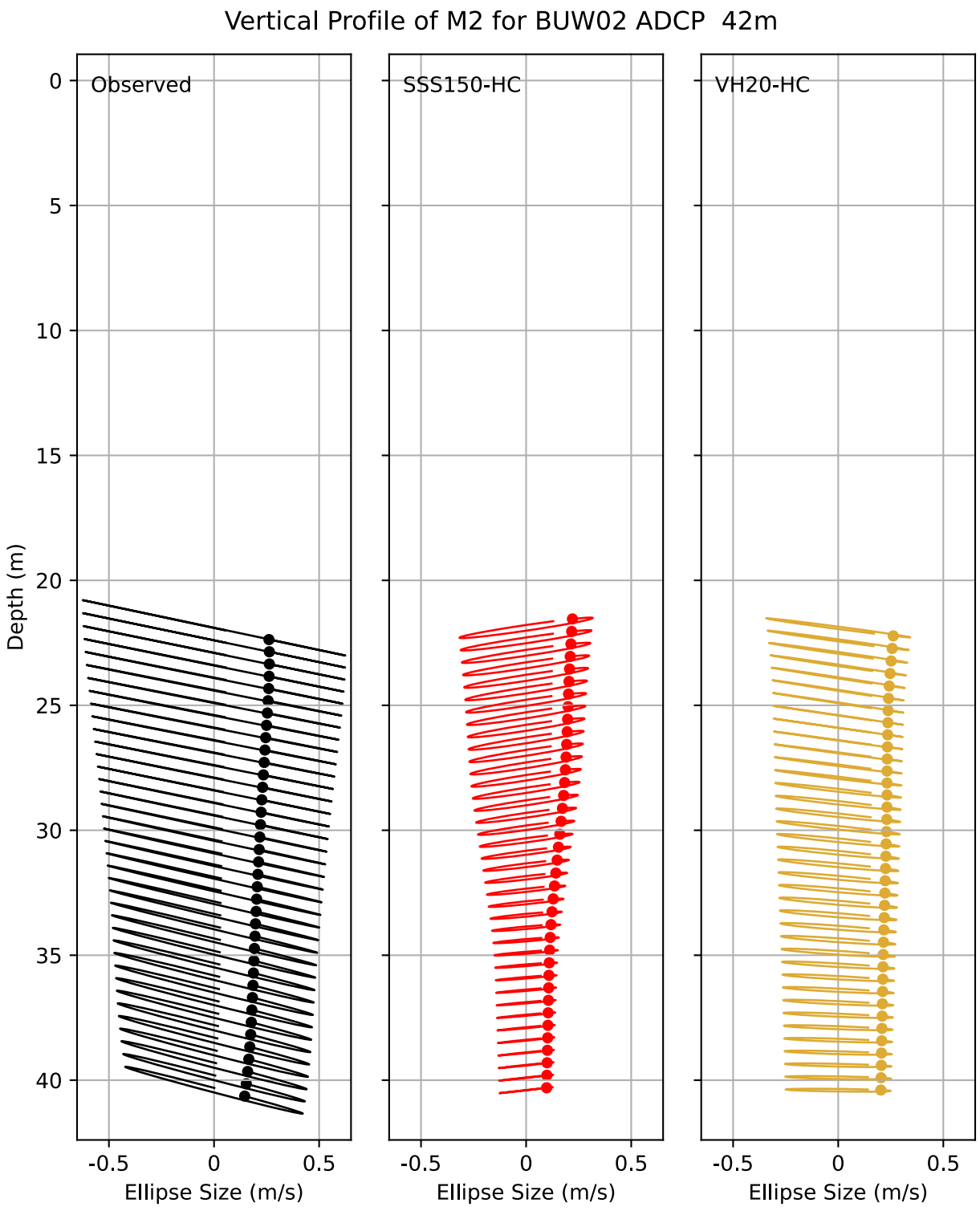

Figure 35. Current ellipses for M2 from the BUW02 ADCP.

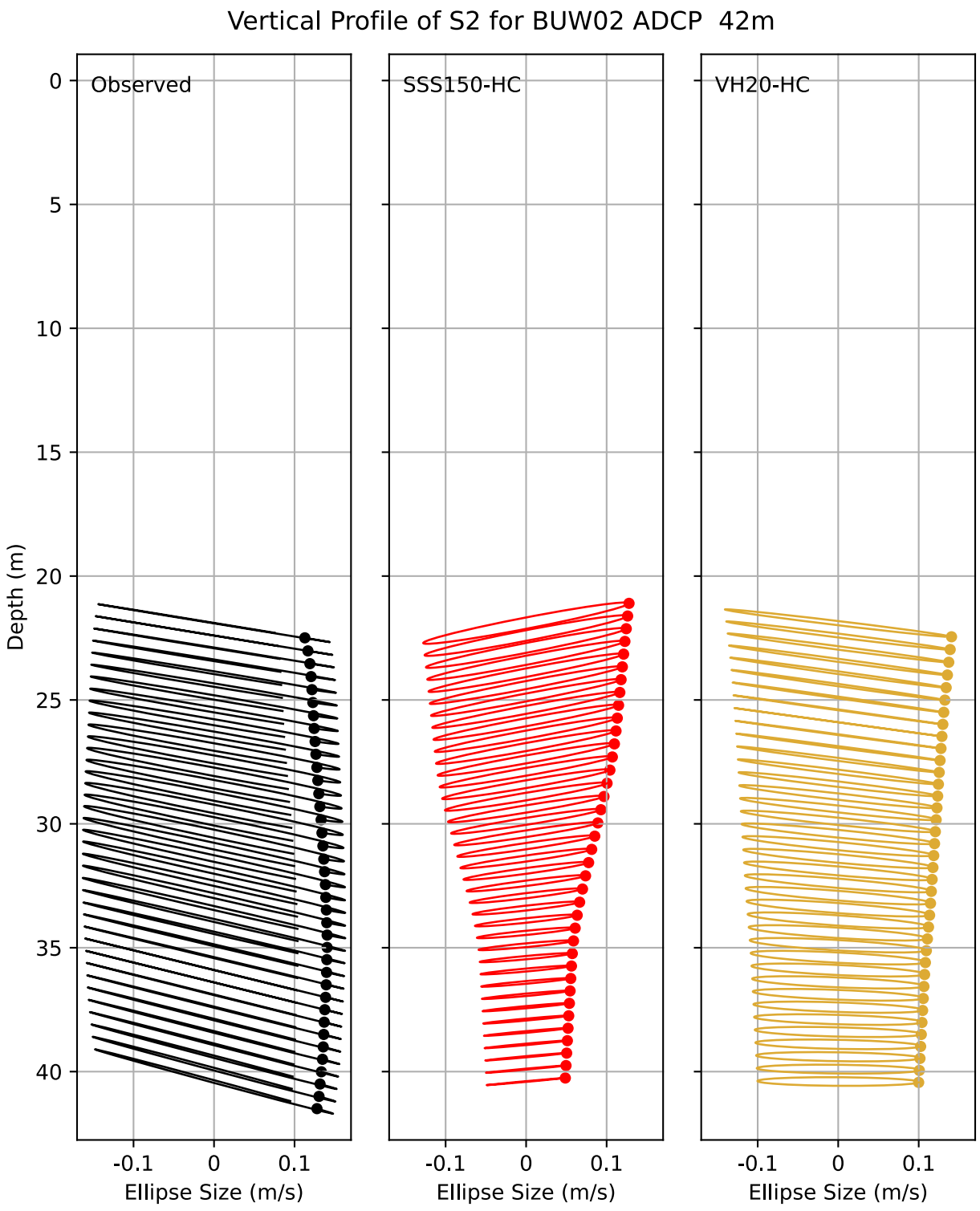

Figure 36. Current ellipses for S2 from the BUW02 ADCP.

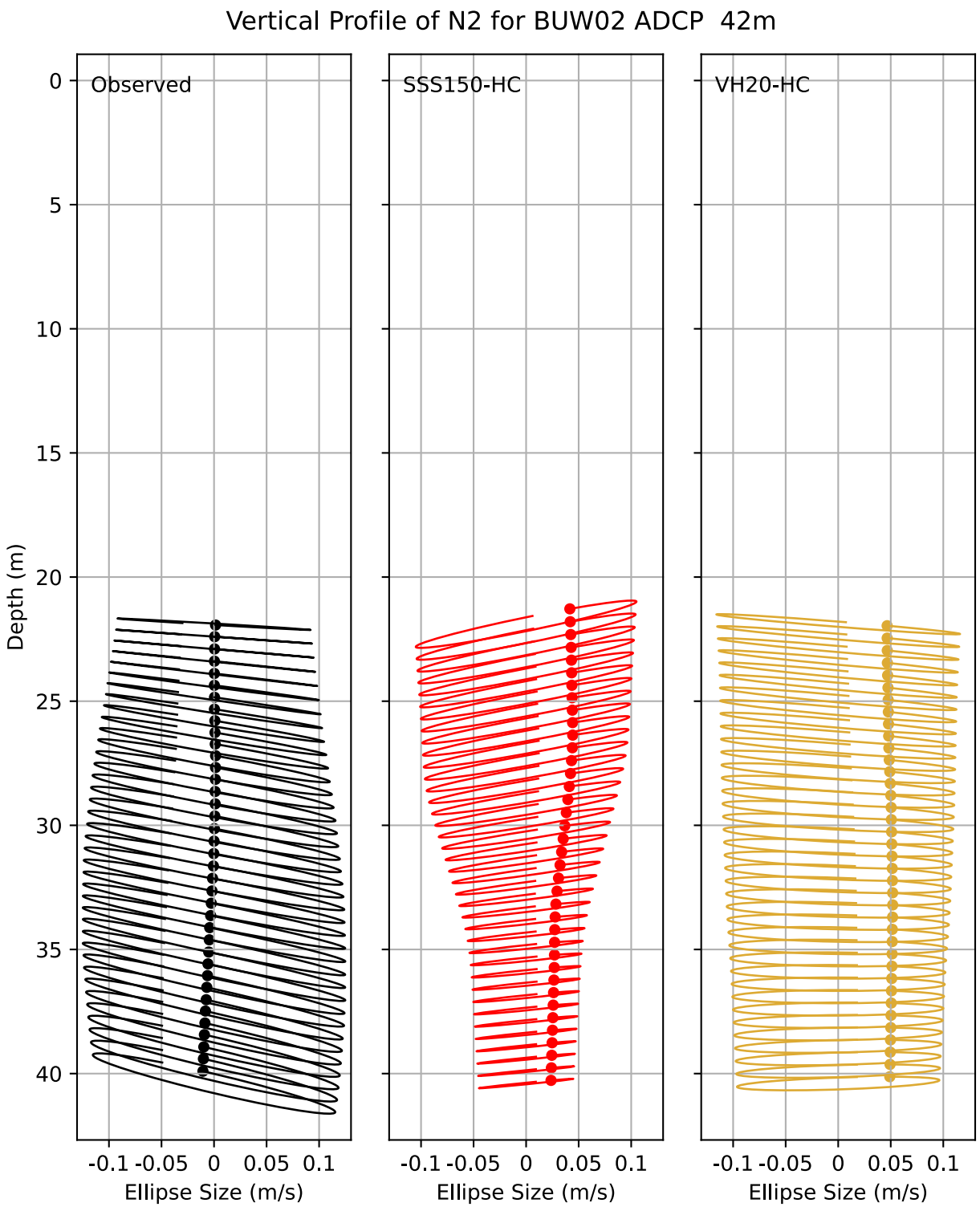

Figure 37. Current ellipses for N2 from the BUW02 ADCP.

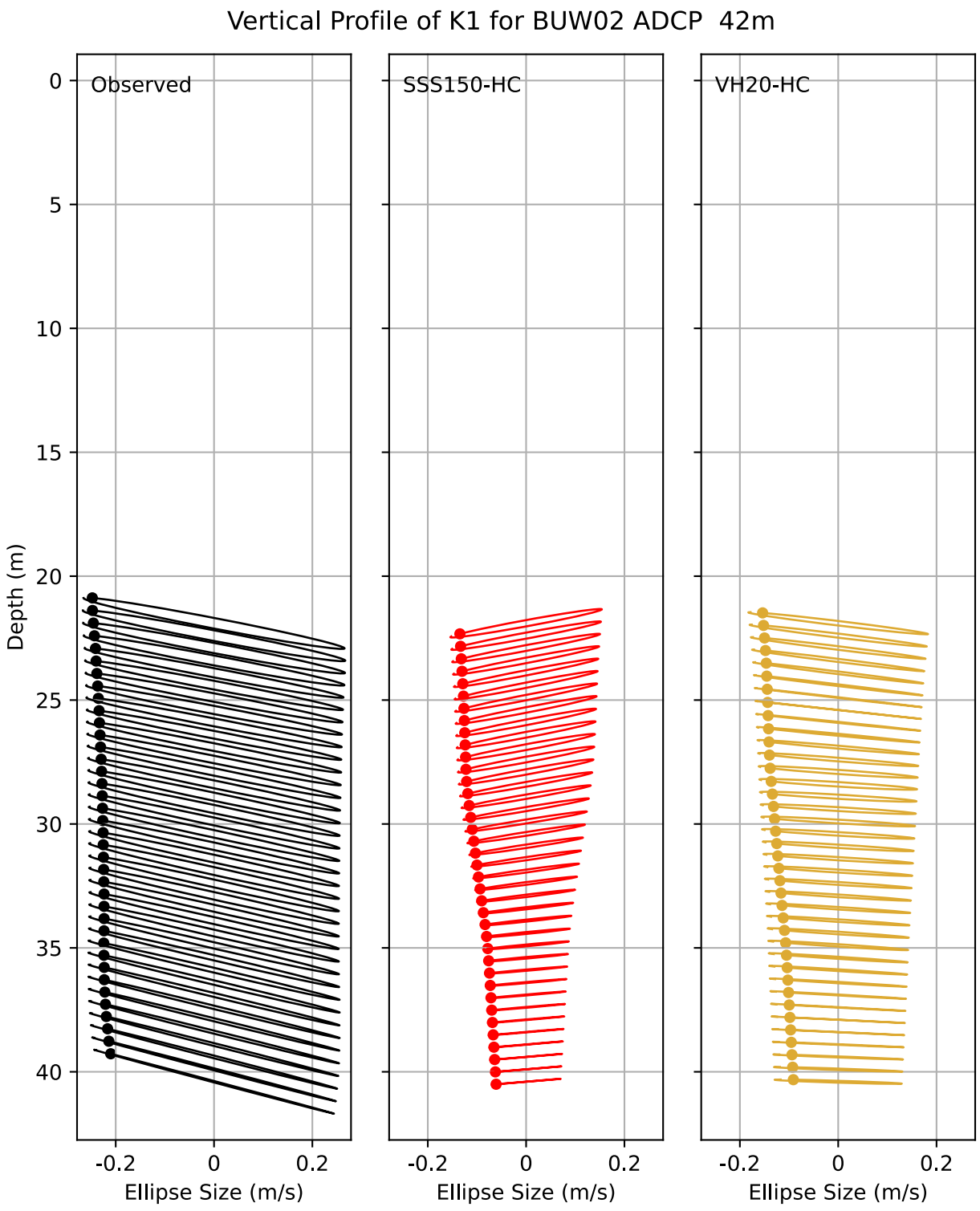

Figure 38. Current ellipses for K1 from the BUW02 ADCP.

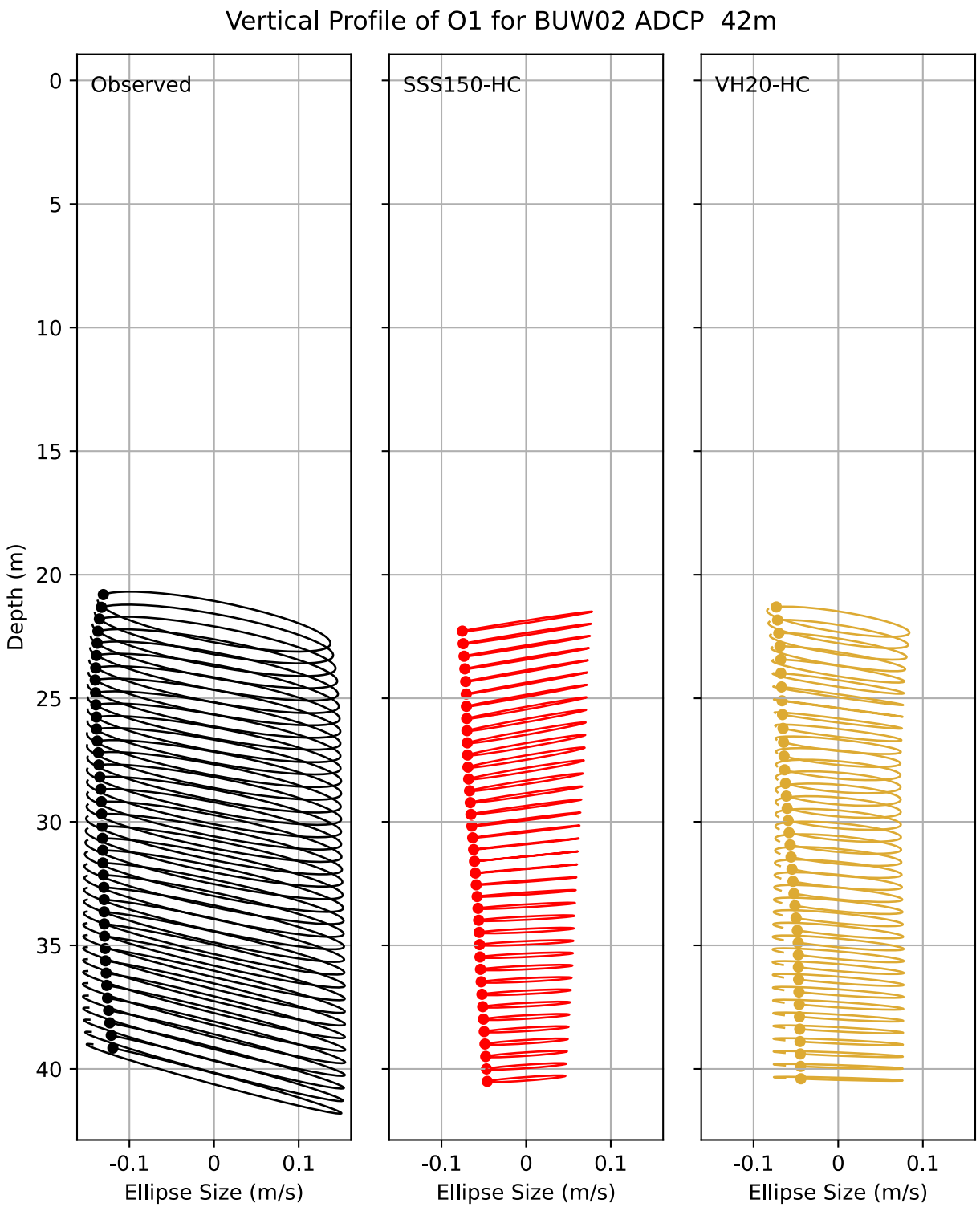

Figure 39. Current ellipses for O1 from the BUW02 ADCP.

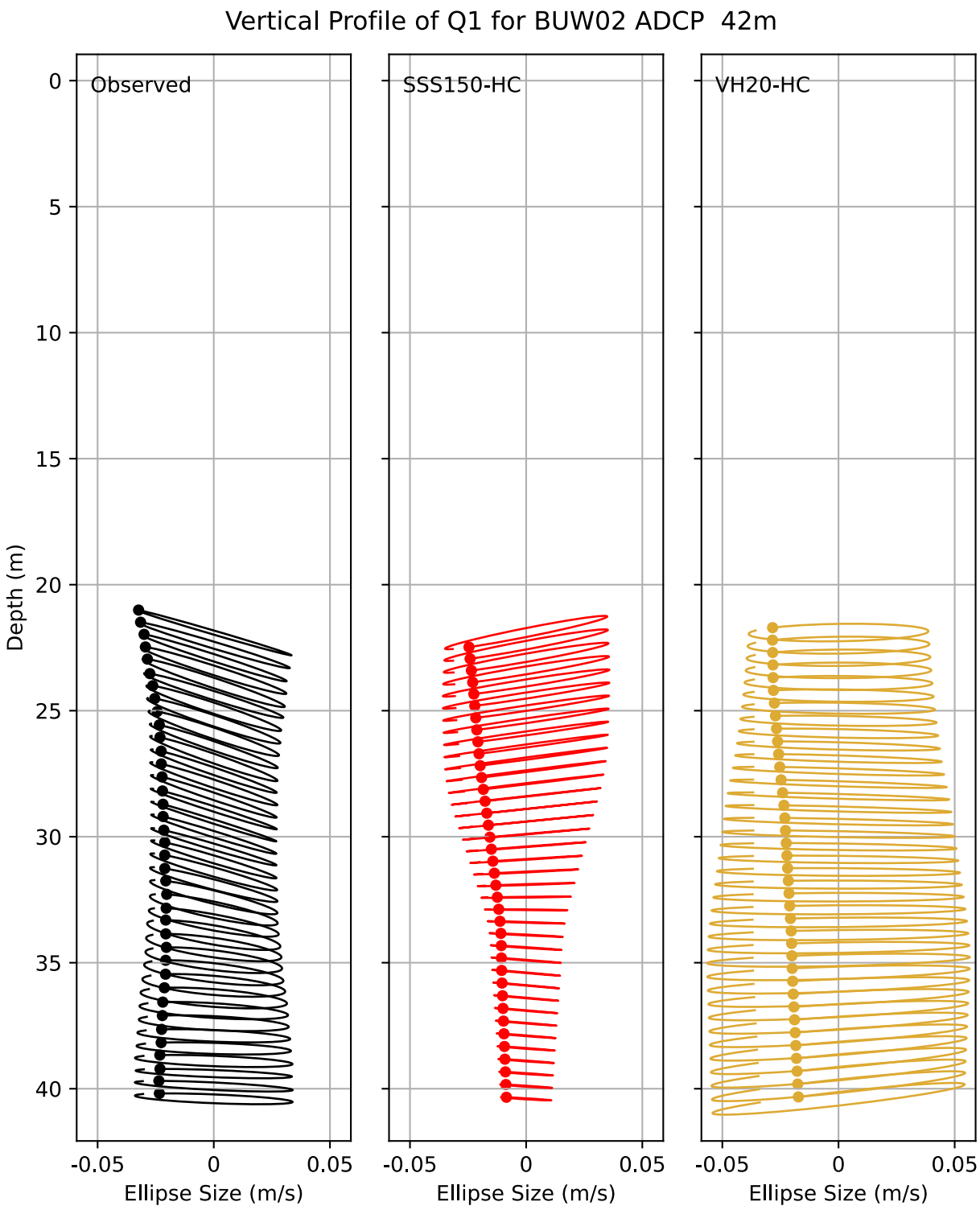

Figure 40. Current ellipses for Q1 from the BUW02 ADCP.

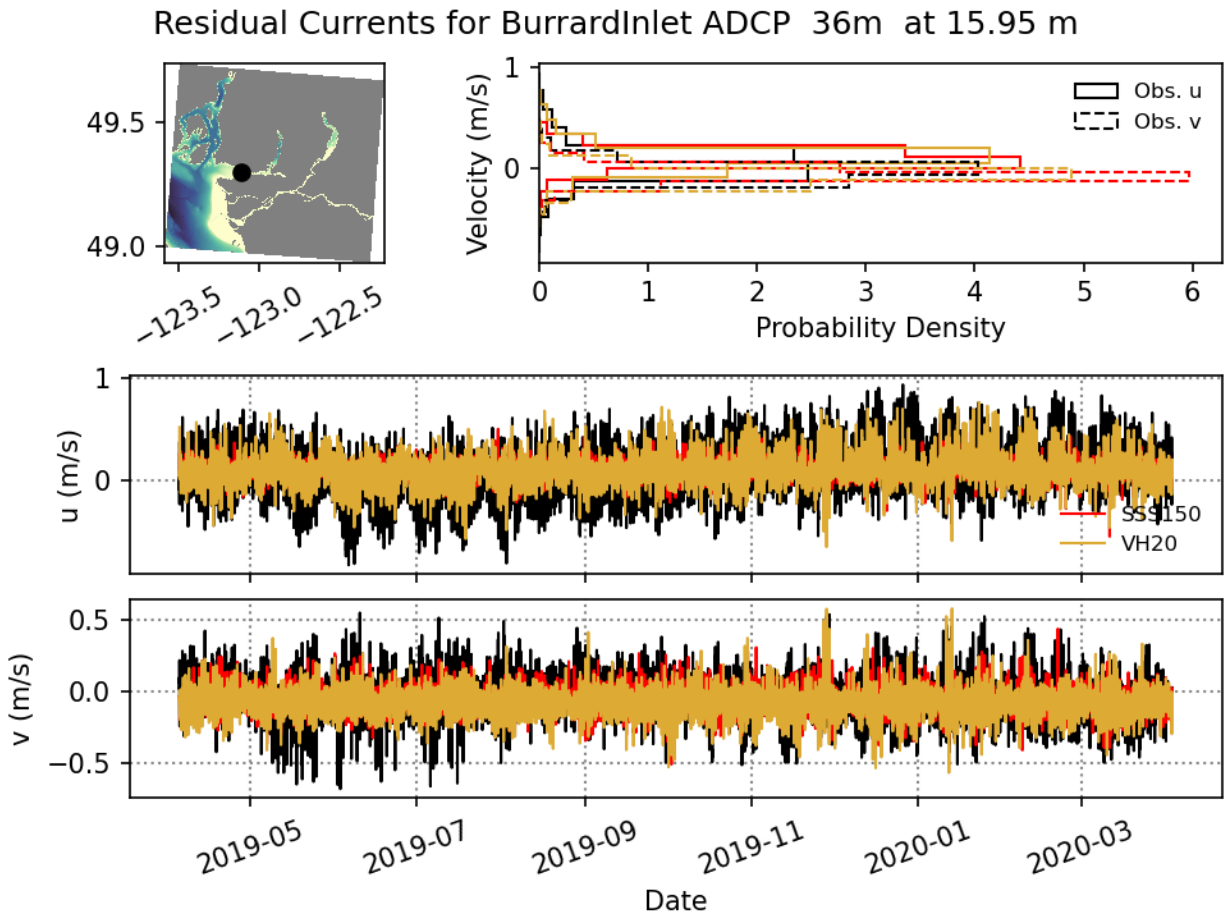

Figure 41. Residual currents at ADCP station BIIP at 15.95 m depth.

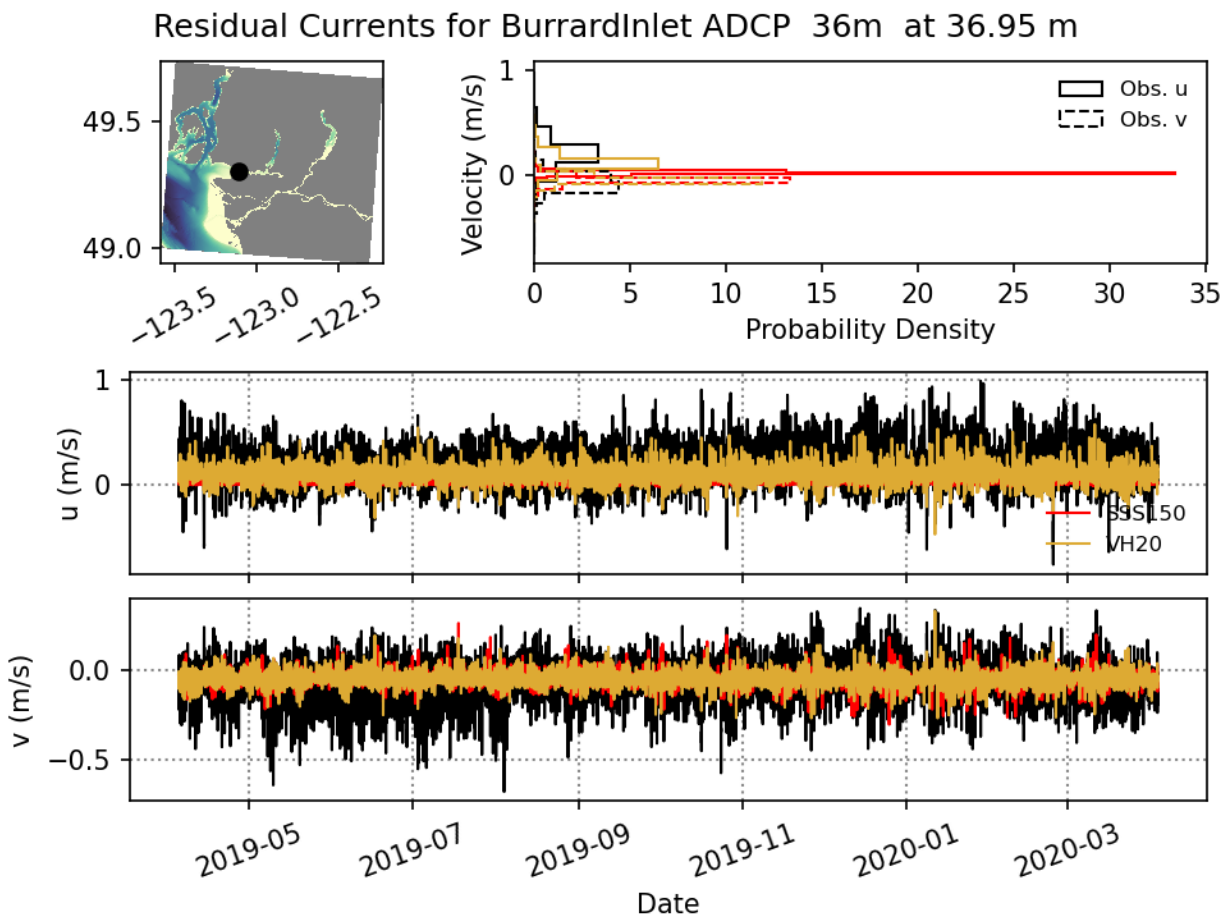

Figure 42. Residual currents at ADCP station BIIP at 36.95 m depth.

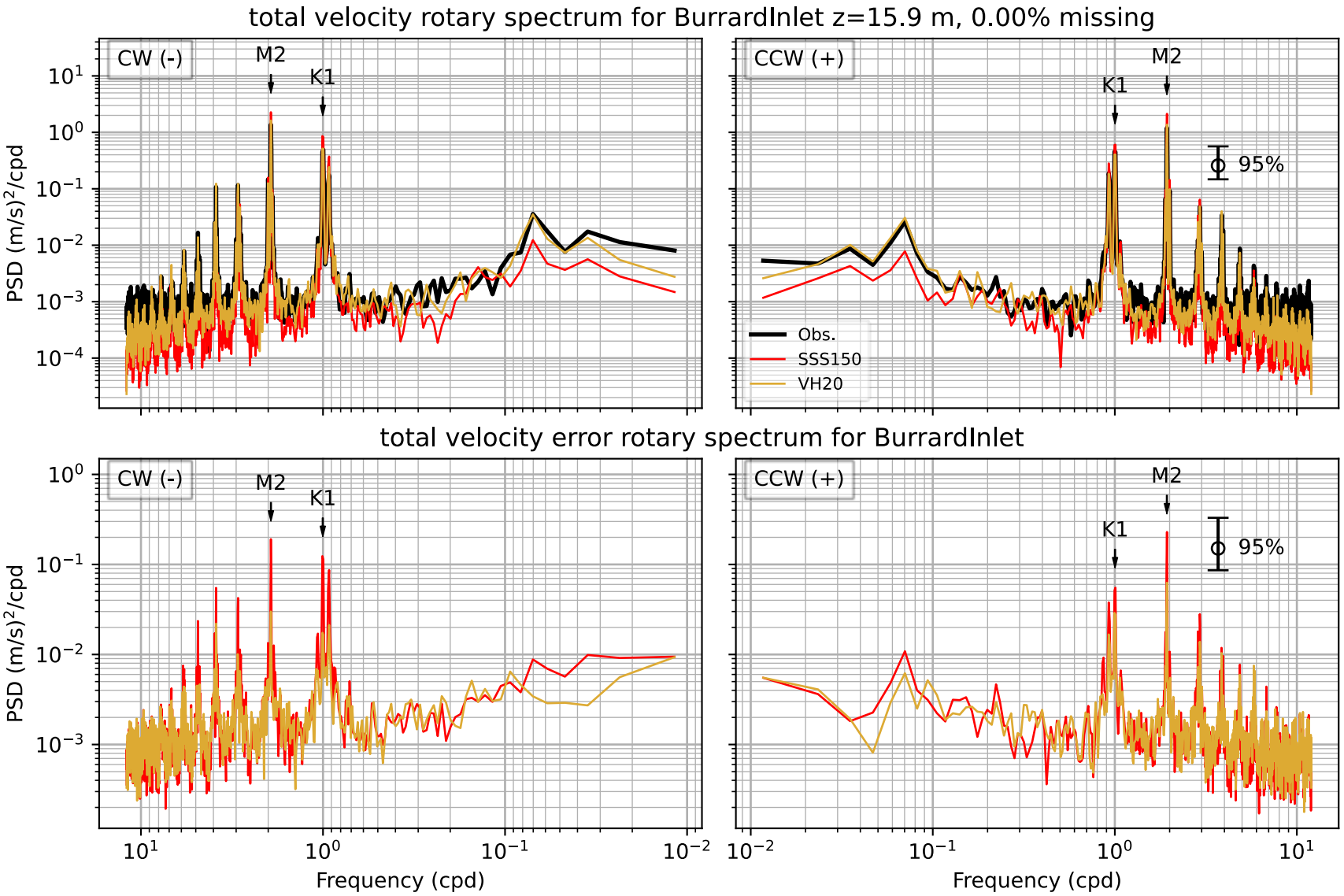

Figure 43. Rotary spectra for total velocity from Burrard Inlet ADCP station at depth 15.9 m.

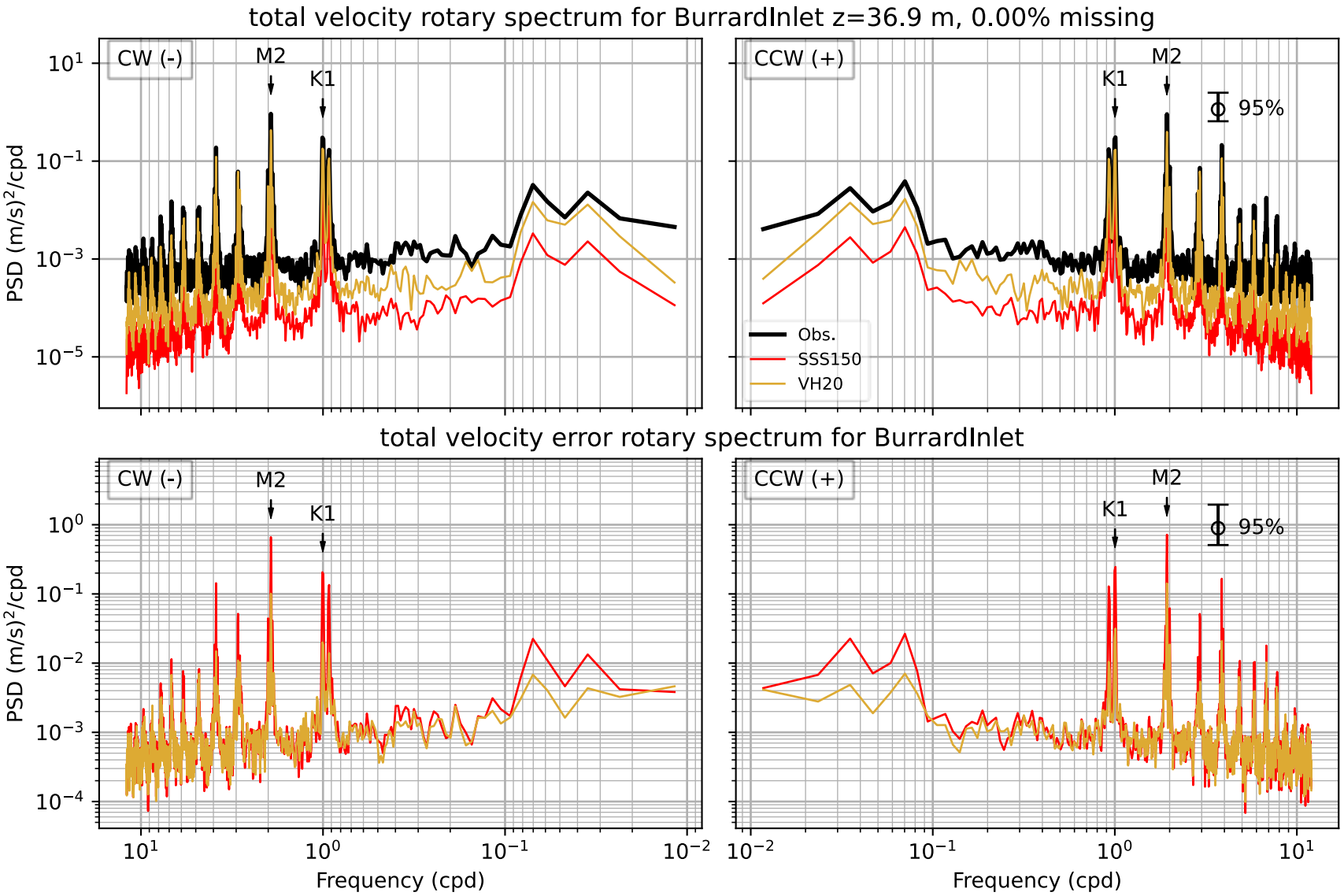

Figure 44. Rotary spectra for total velocity from Burrard Inlet ADCP station at near bottom depth 36.9 m.

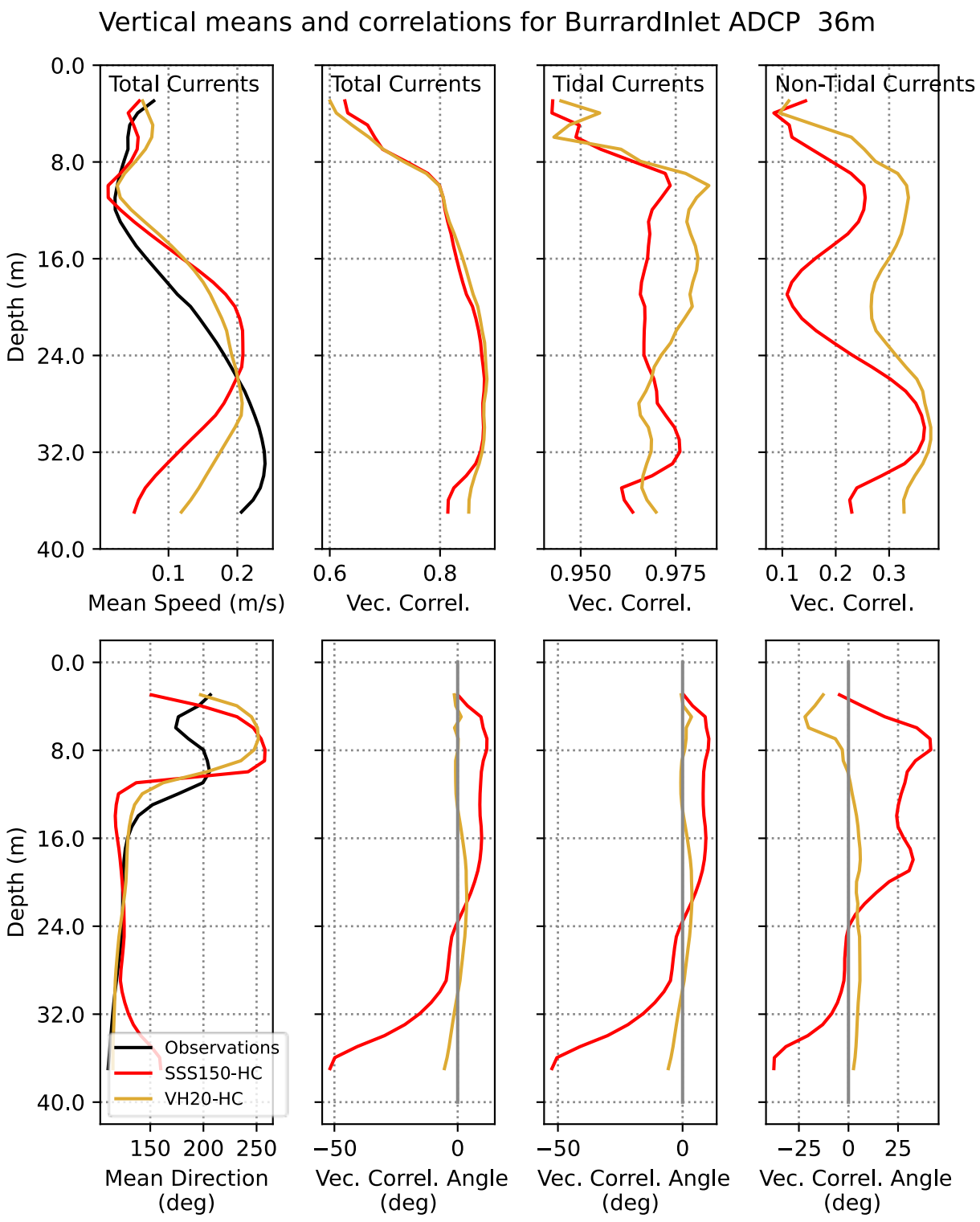

Figure 45. Mean currents (first column) and vector correlations for total (second column), tidal (third column) and non-tidal (fourth column) velocities for Burrard Inlet ADCP deployment.

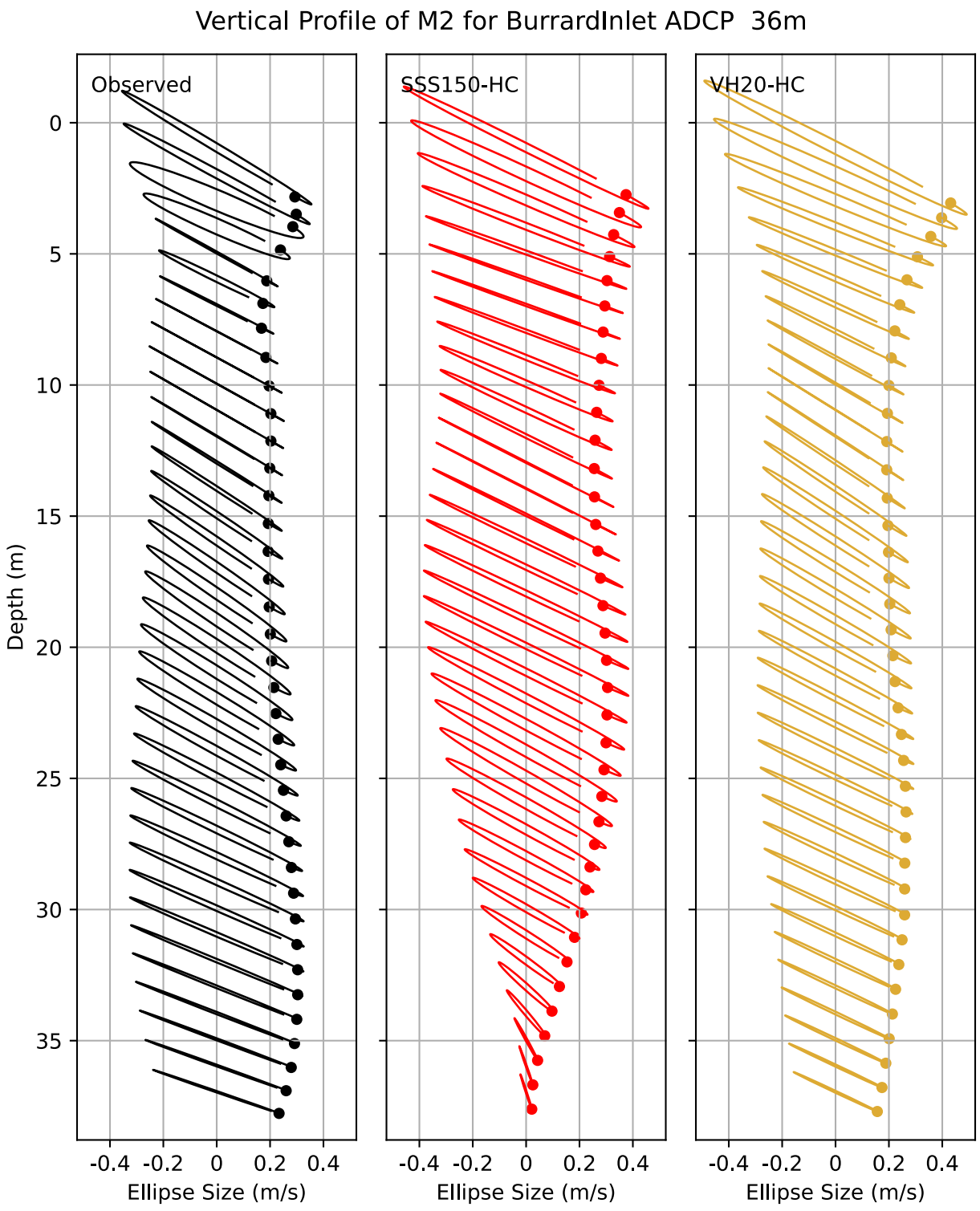

Figure 46. Current ellipses for M2 from the Burrard Inlet ADCP.

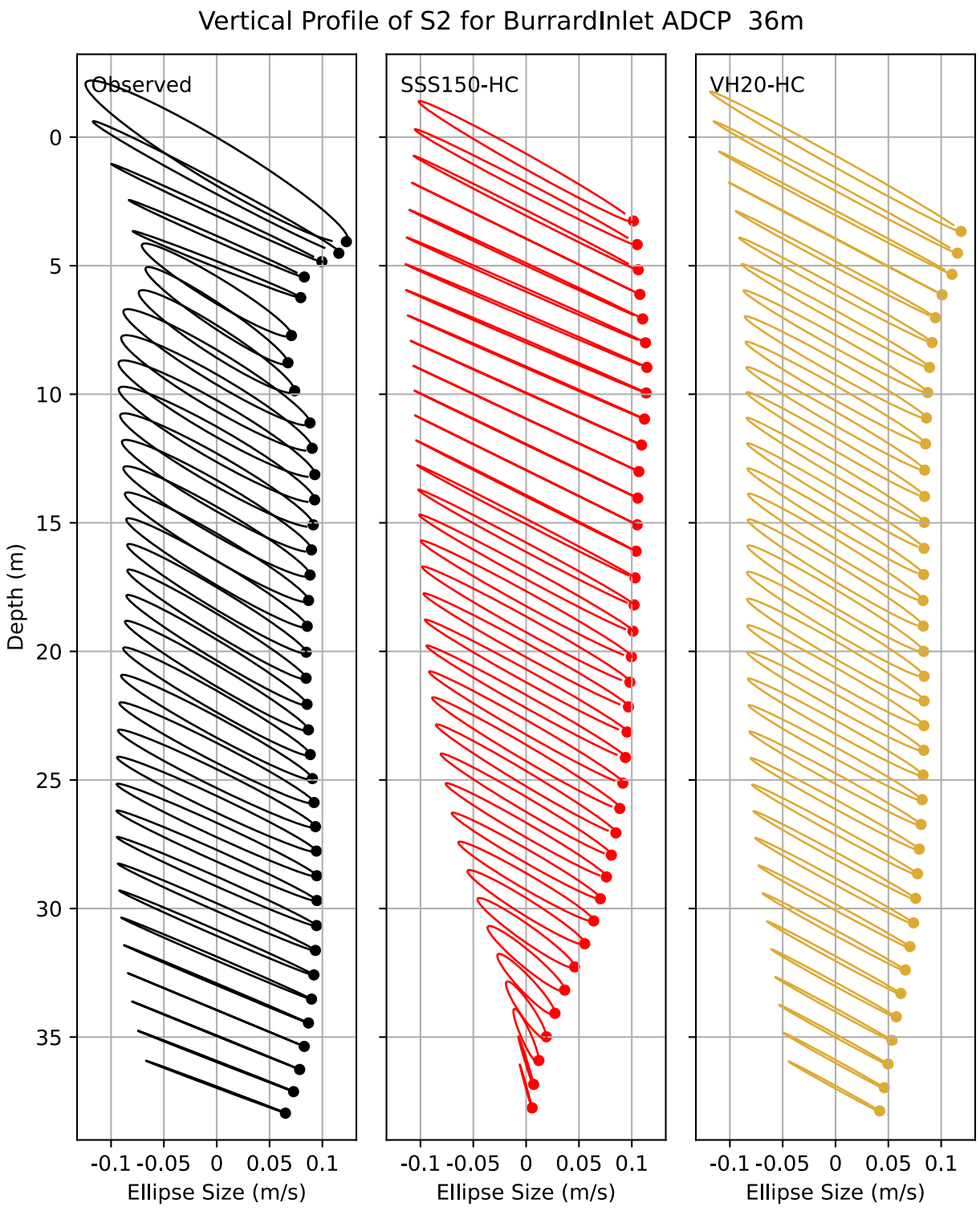

Figure 47. Current ellipses for S2 from the Burrard Inlet ADCP.

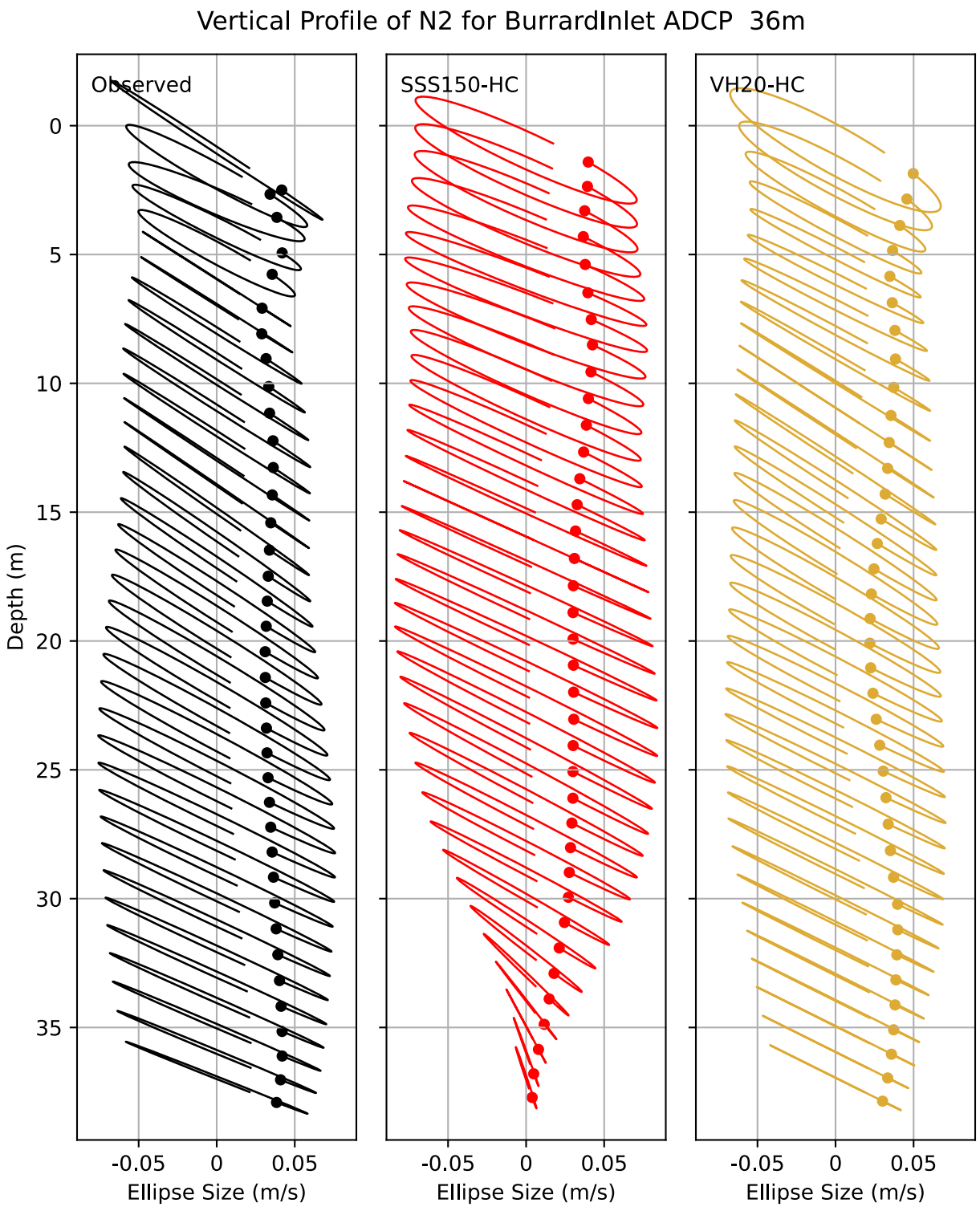

Figure 48. Current ellipses for N2 from the Burrard Inlet ADCP.

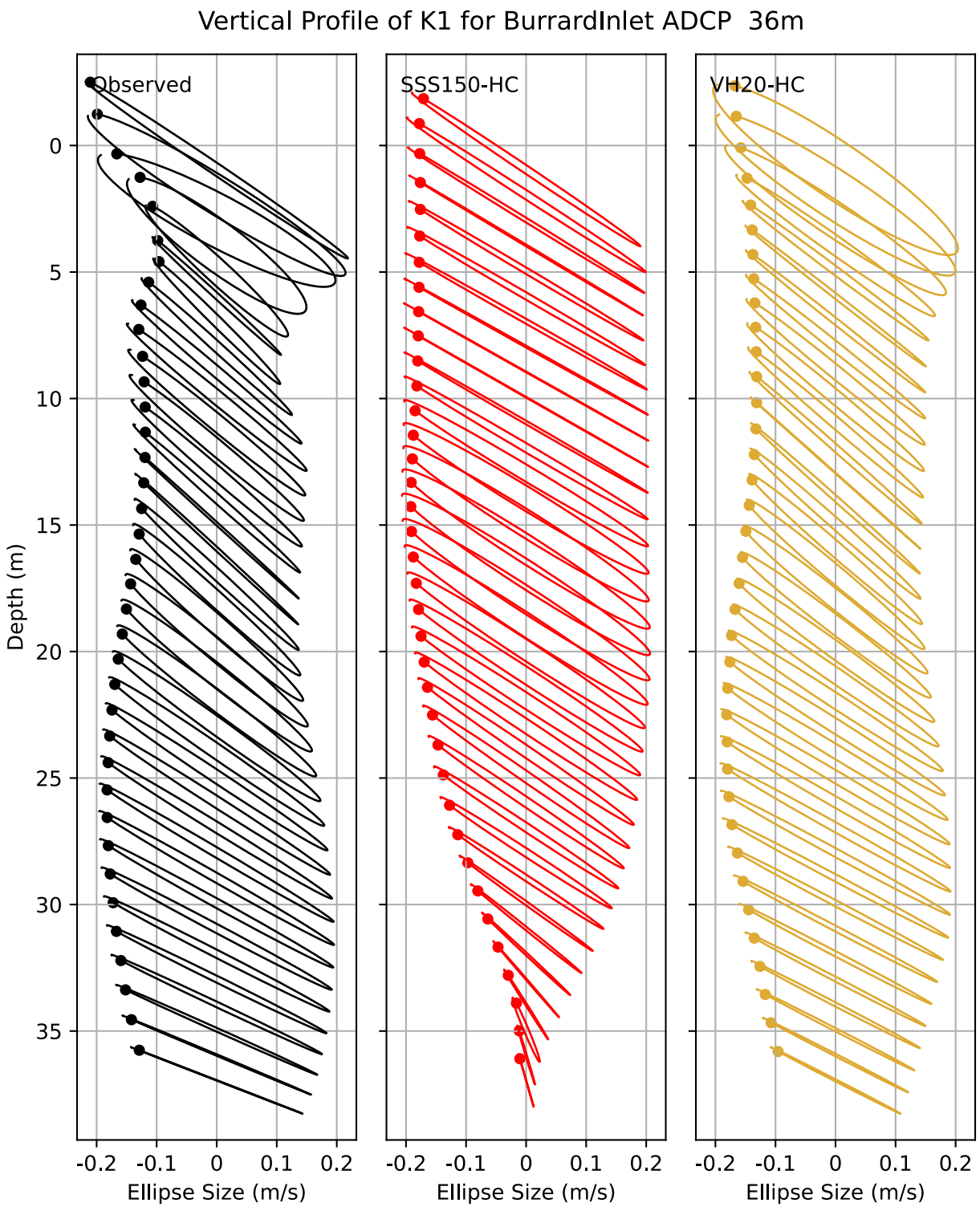

Figure 49. Current ellipses for K1 from the Burrard Inlet ADCP.

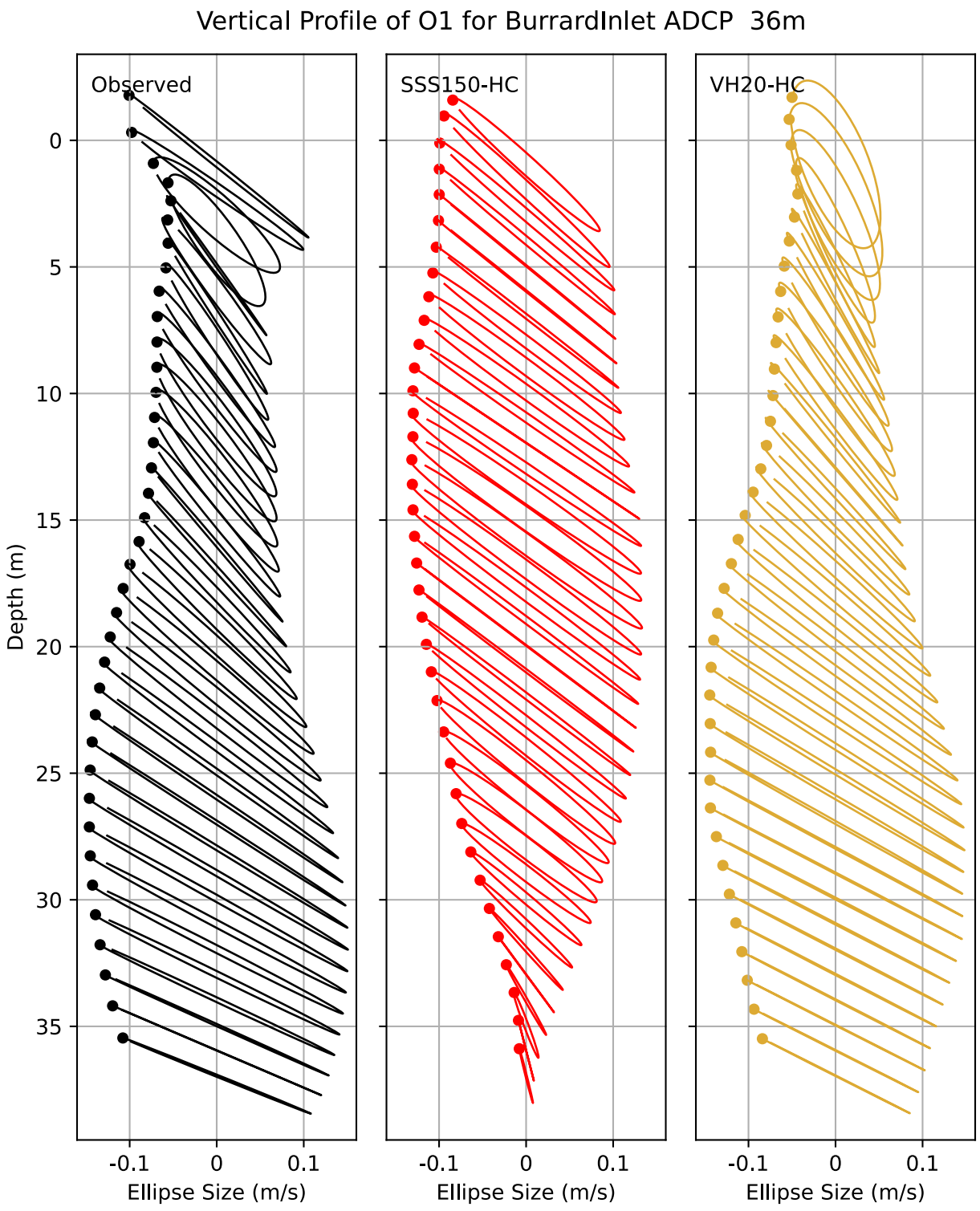

Figure 50. Current ellipses for O1 from the Burrard Inlet ADCP.

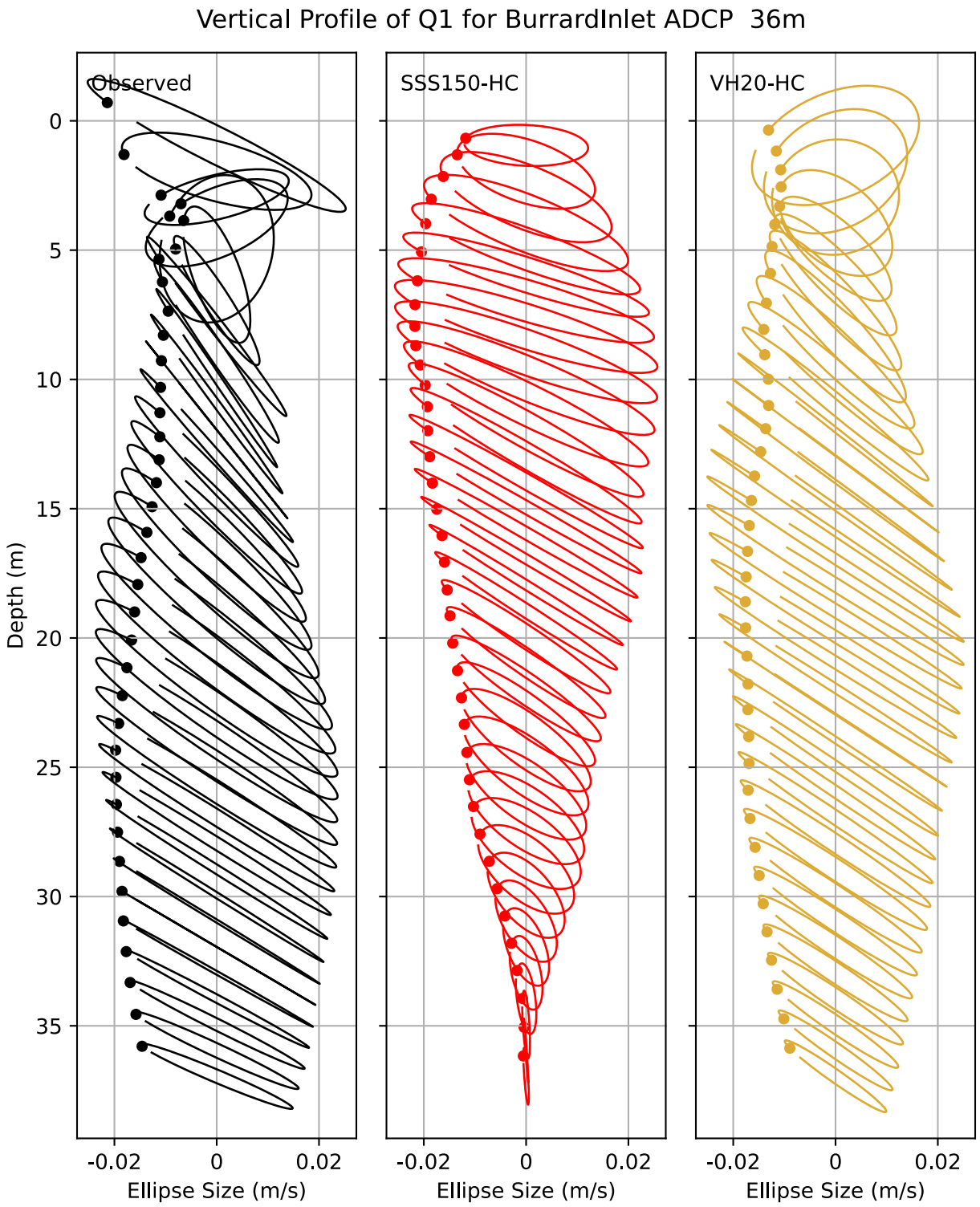

Figure 51. Current ellipses for Q1 from the Burrard Inlet ADCP.

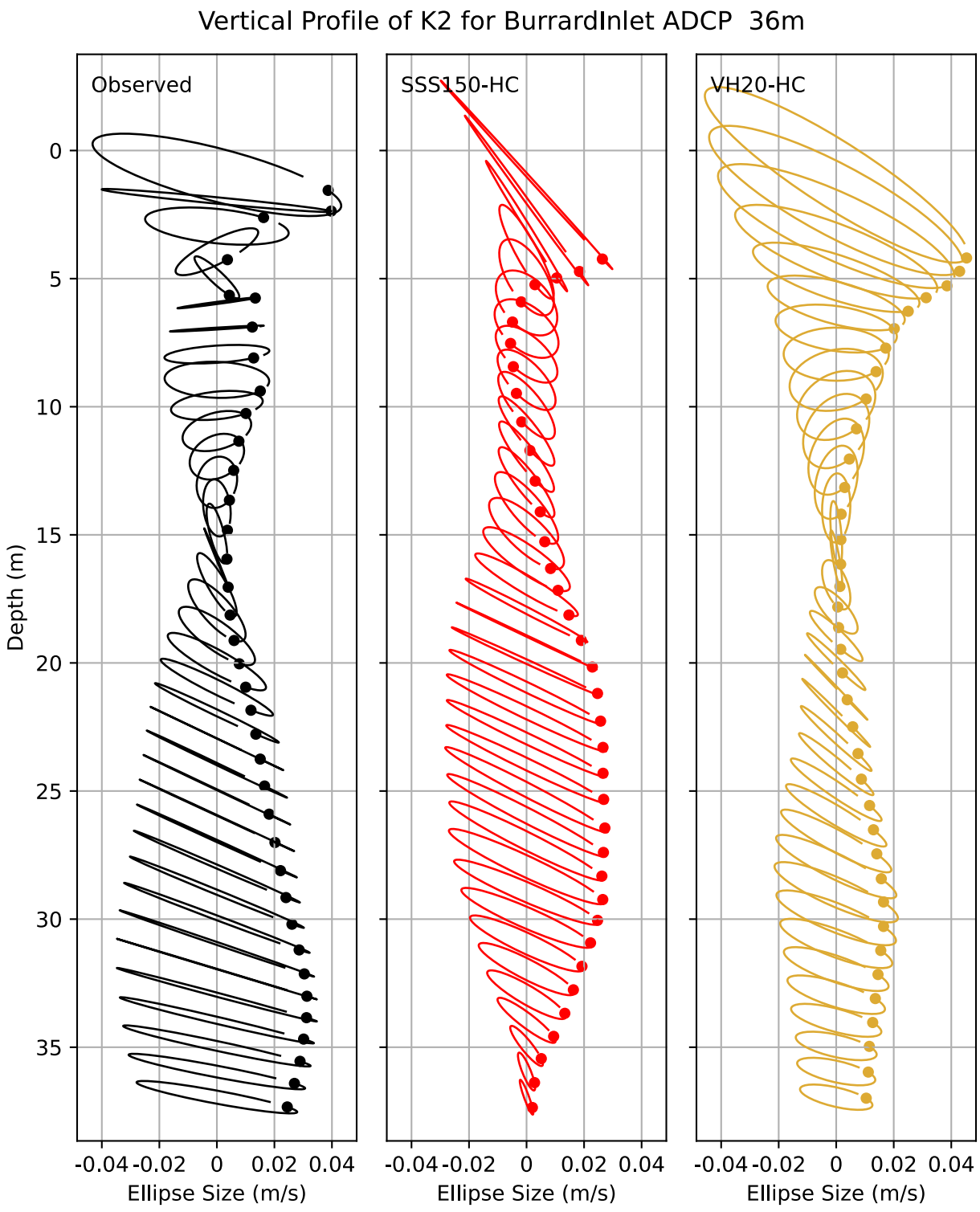

Figure 52. Current ellipses for K2 from the Burrard Inlet ADCP.

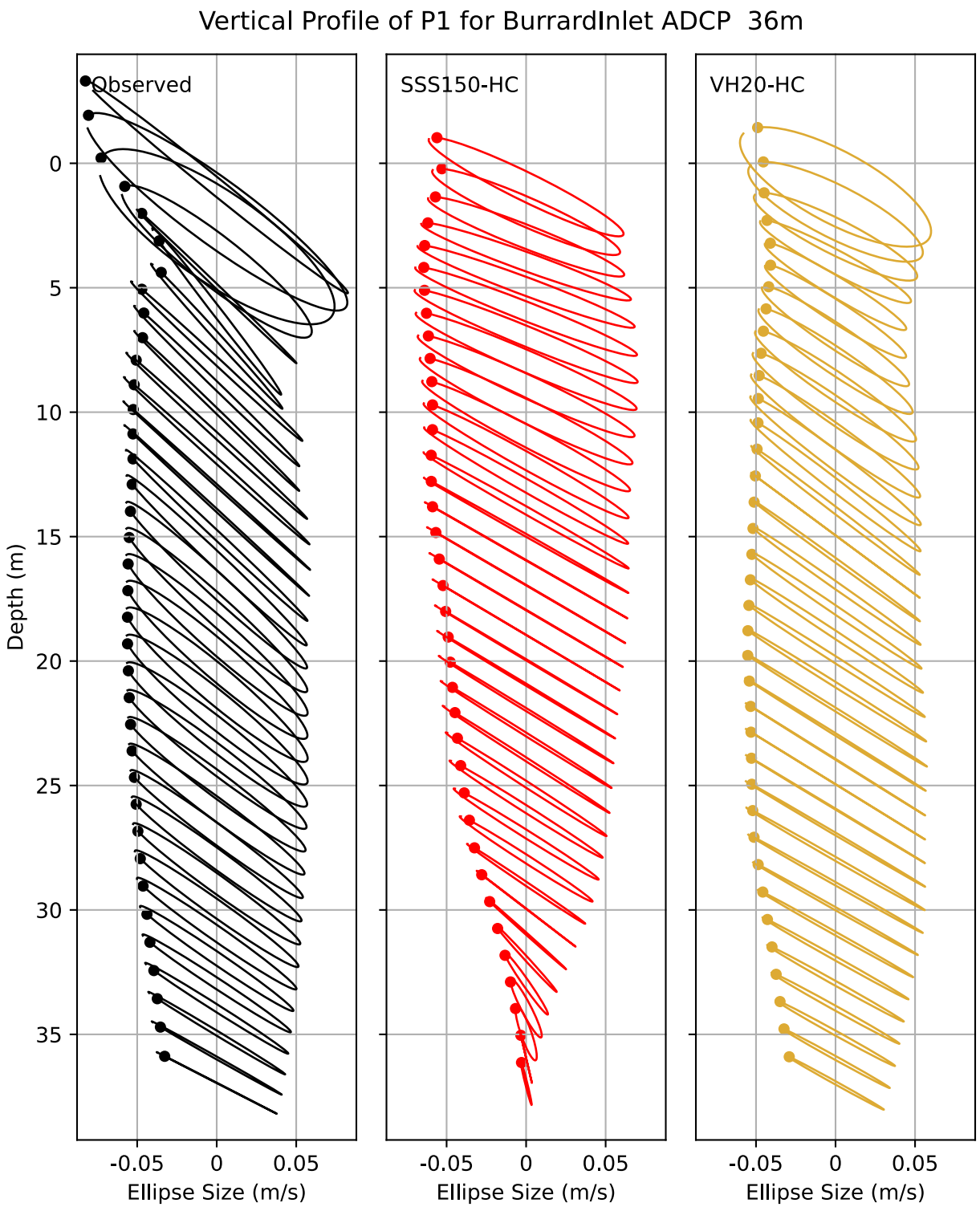

Figure 53. Current ellipses for P1 from the Burrard Inlet ADCP.

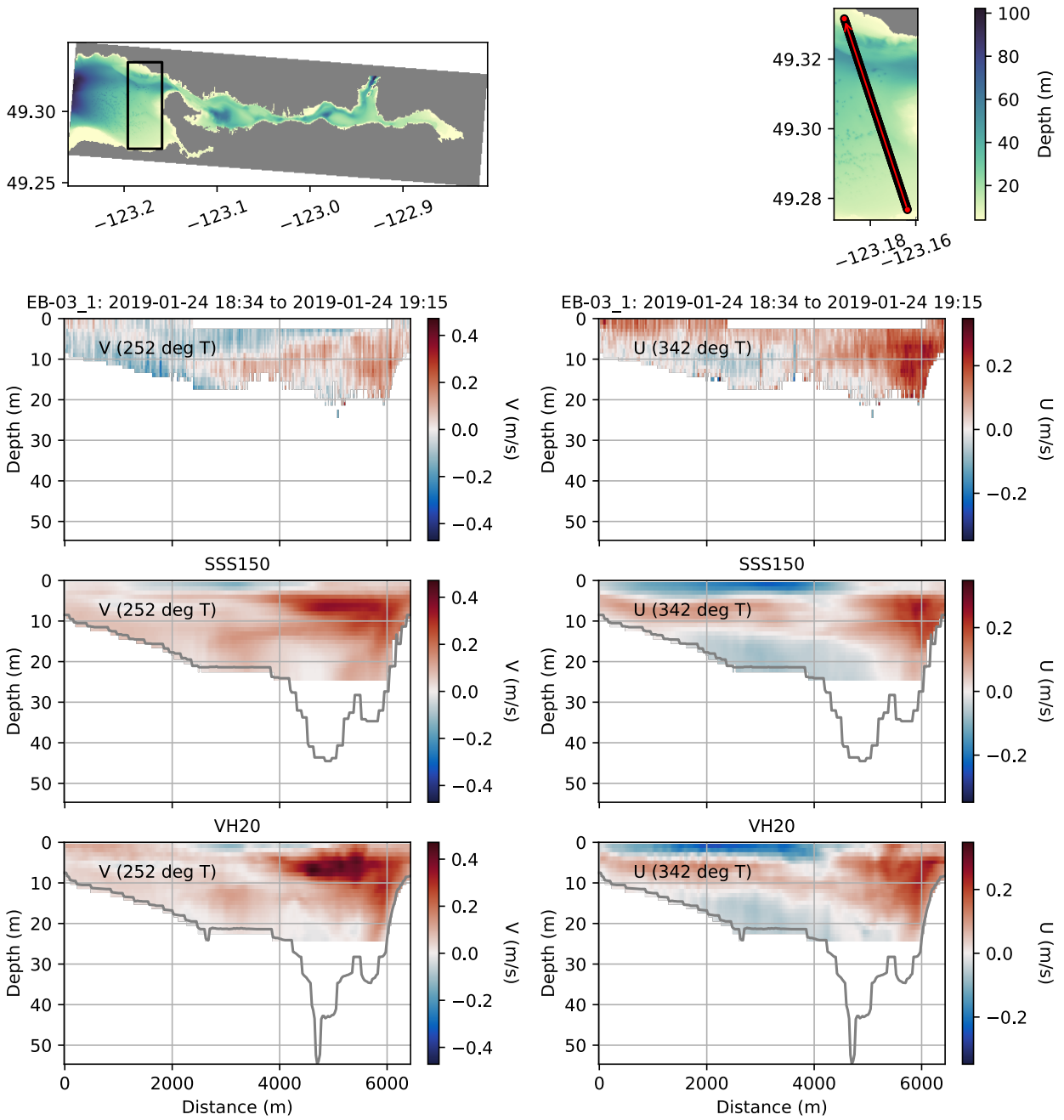

Figure 54. Observed and model current velocity components: Cross-transect (left panels) and along-transect (right panels) for an ADCP transect (EB-03_1) taken near First Narrows in English Bay. Positive direction is indicated in true degrees (deg T) in each panel. Transect location is shown in the upper panels. The black line in the upper right panel shows the transect and the red arrow indicates the direction of the transect.

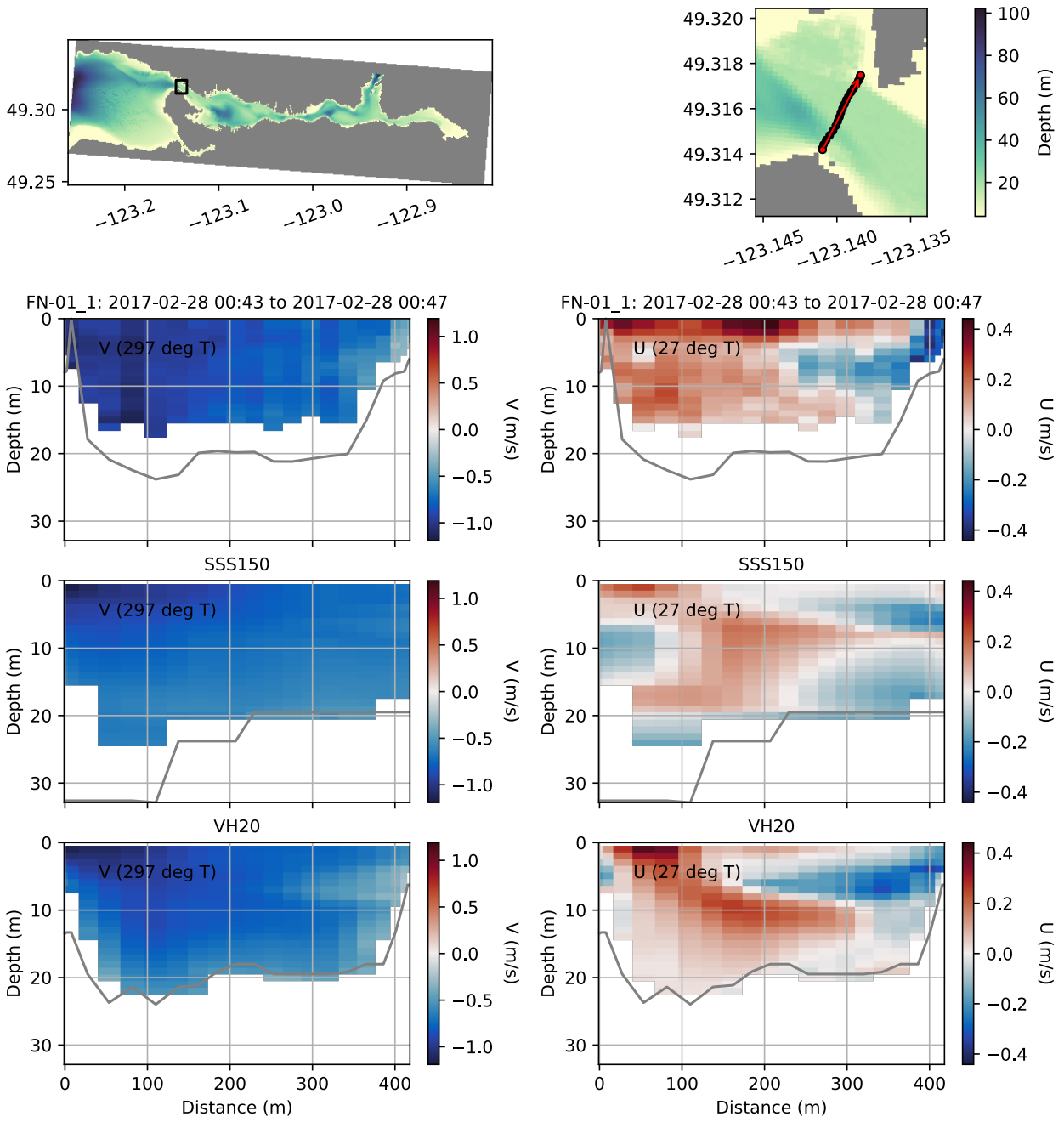

Figure 55. Same as Figure 54, but for an ADCP transect (FN-01_1) taken across First Narrows.

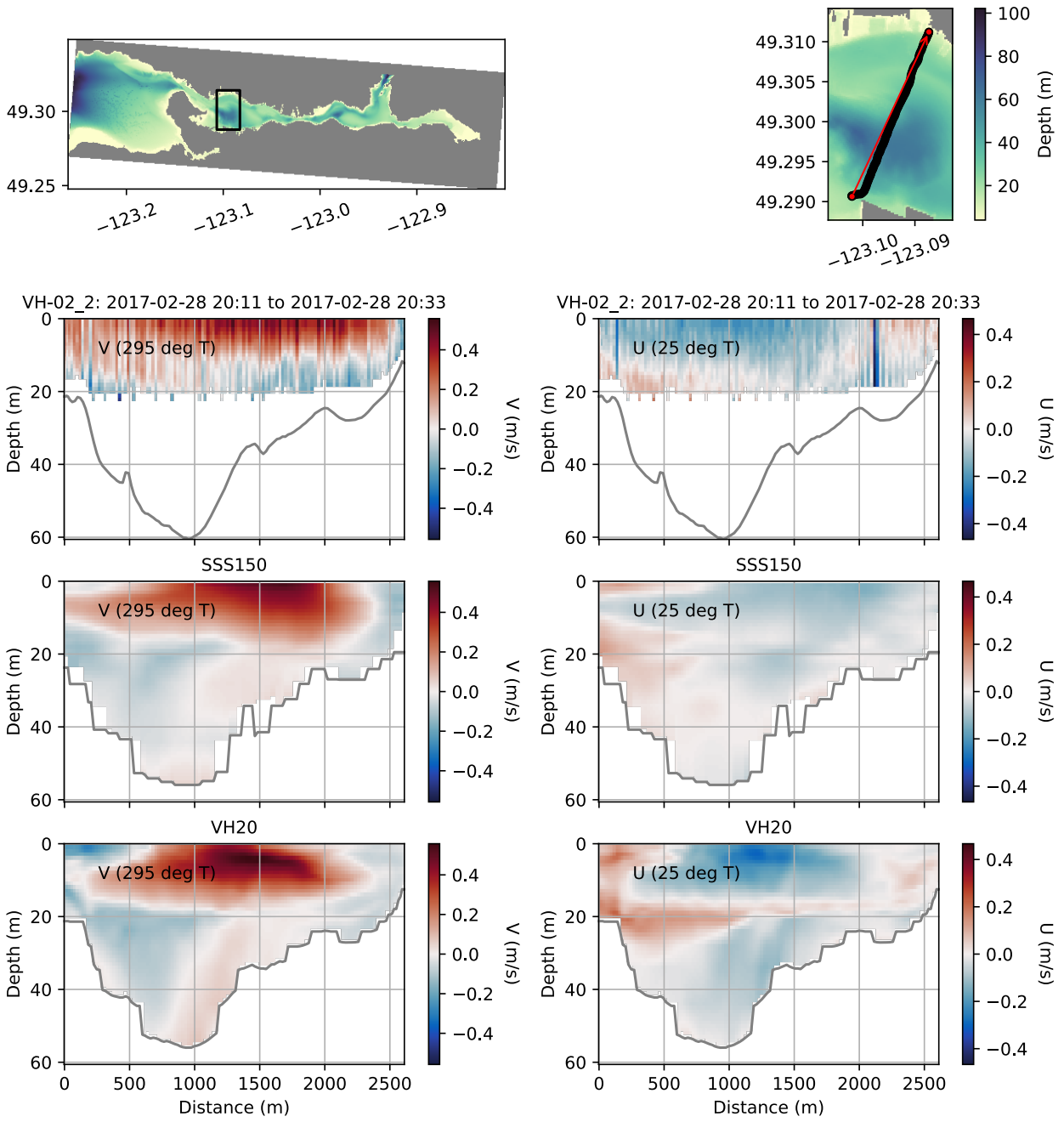

Figure 56. Same as Figure 54, but for an ADCP transect (VH-02_2) taken across Vancouver Harbour.

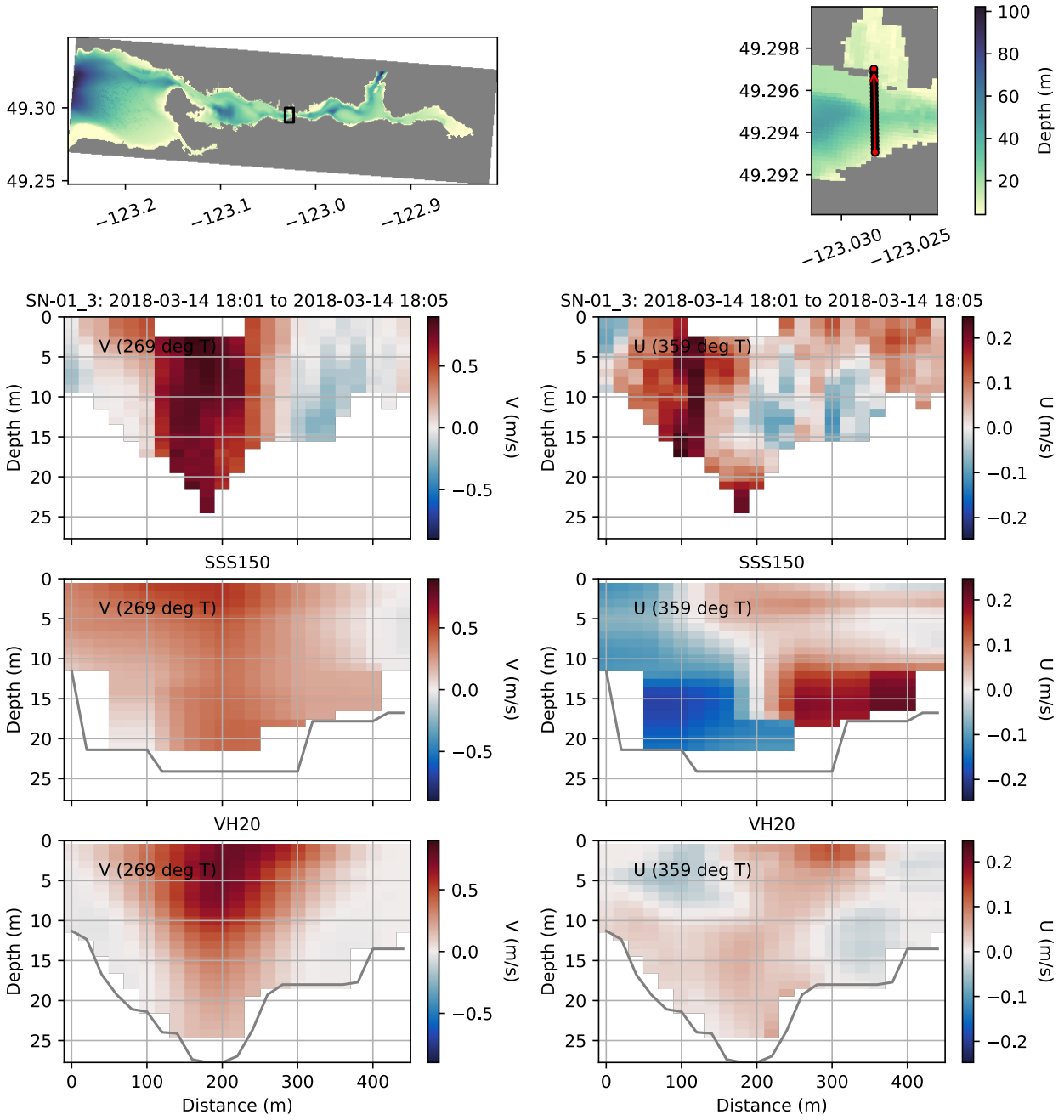

Figure 57. Same as Figure 54, but for an ADCP transect (SN-01_3) taken near Second Narrows.

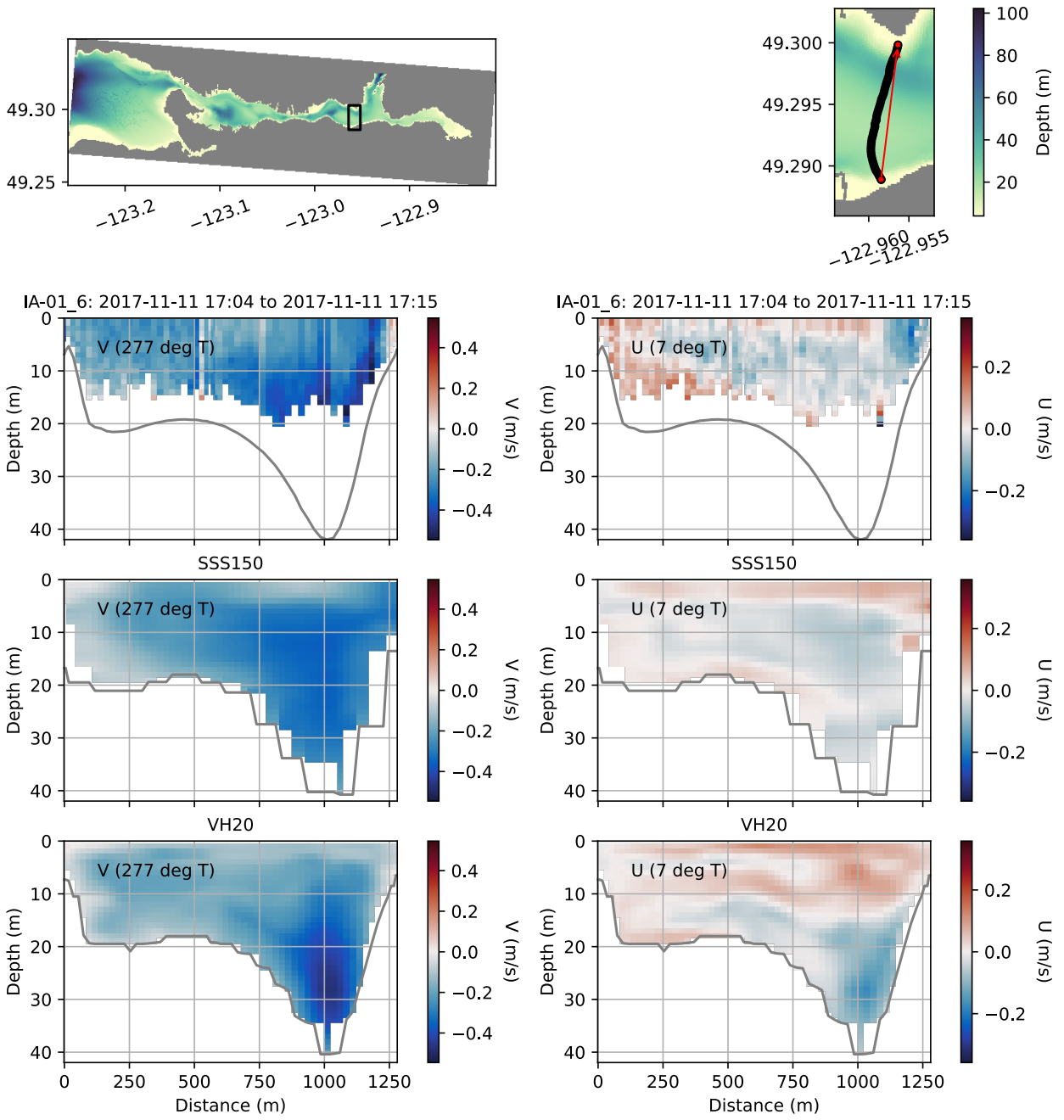

Figure 58. Same as Figure 54, but for an ADCP transect (IA-01_6) taken east of Second Narrows.

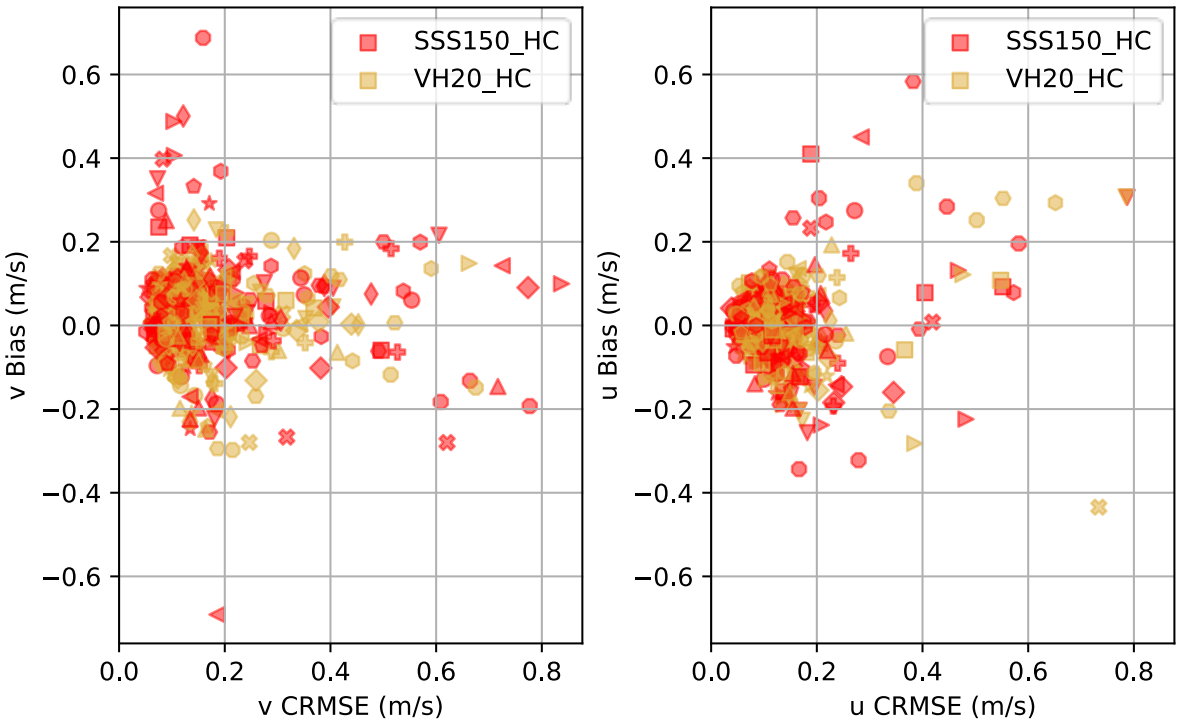

Figure 59. Scatter plot of mean bias and CRMSE for each transect for the normal to transect velocity (left) and the along transect velocity (right). Each marker represents one transect (marker shapes repeat due to a limited number of shapes) and color denotes the model.

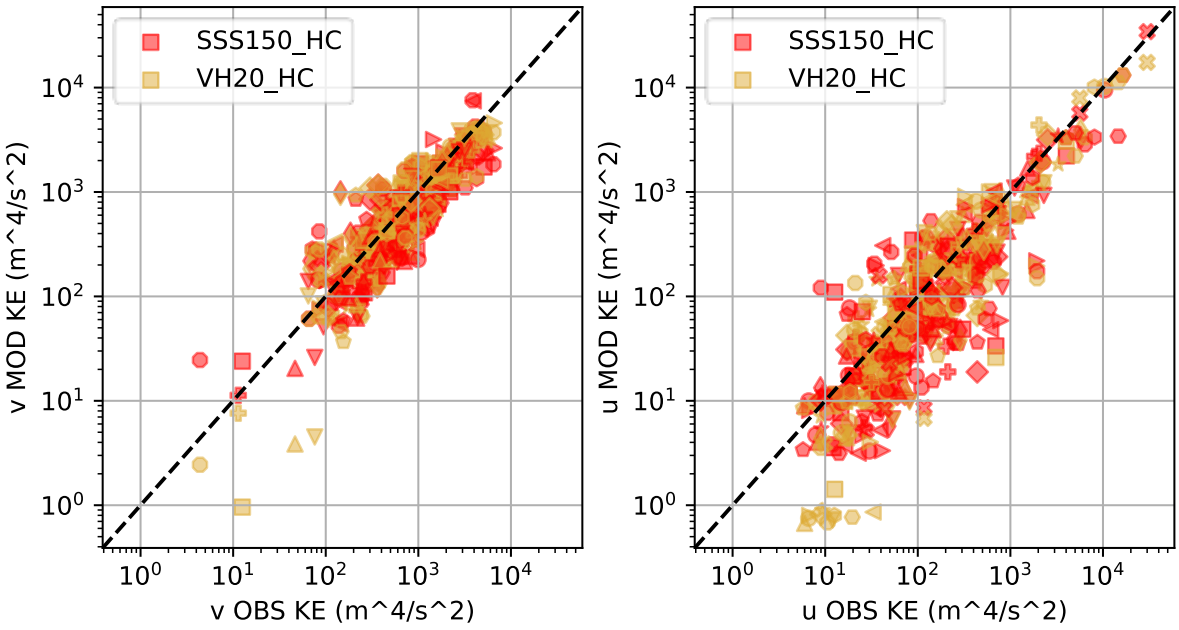

Figure 60. Kinetic energy (per unit density, per unit distance) comparison for (left) normal to transect velocity component and (right) along transect velocity component. Each marker represents one transect (marker shapes repeat due to a limited number of shapes) and color denotes the model.

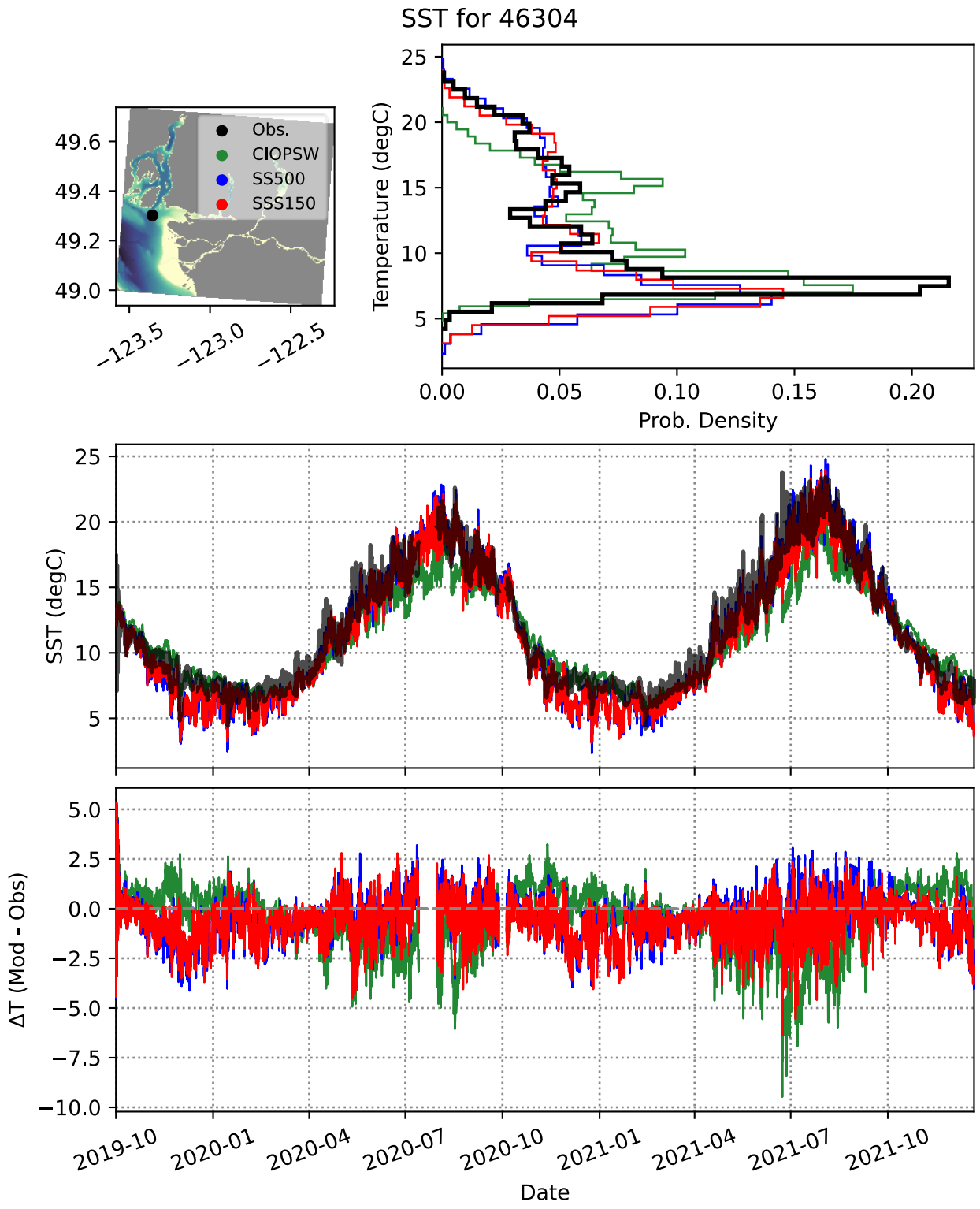

Figure 61. Sea surface temperature at the entrance to English Bay (buoy 46304).

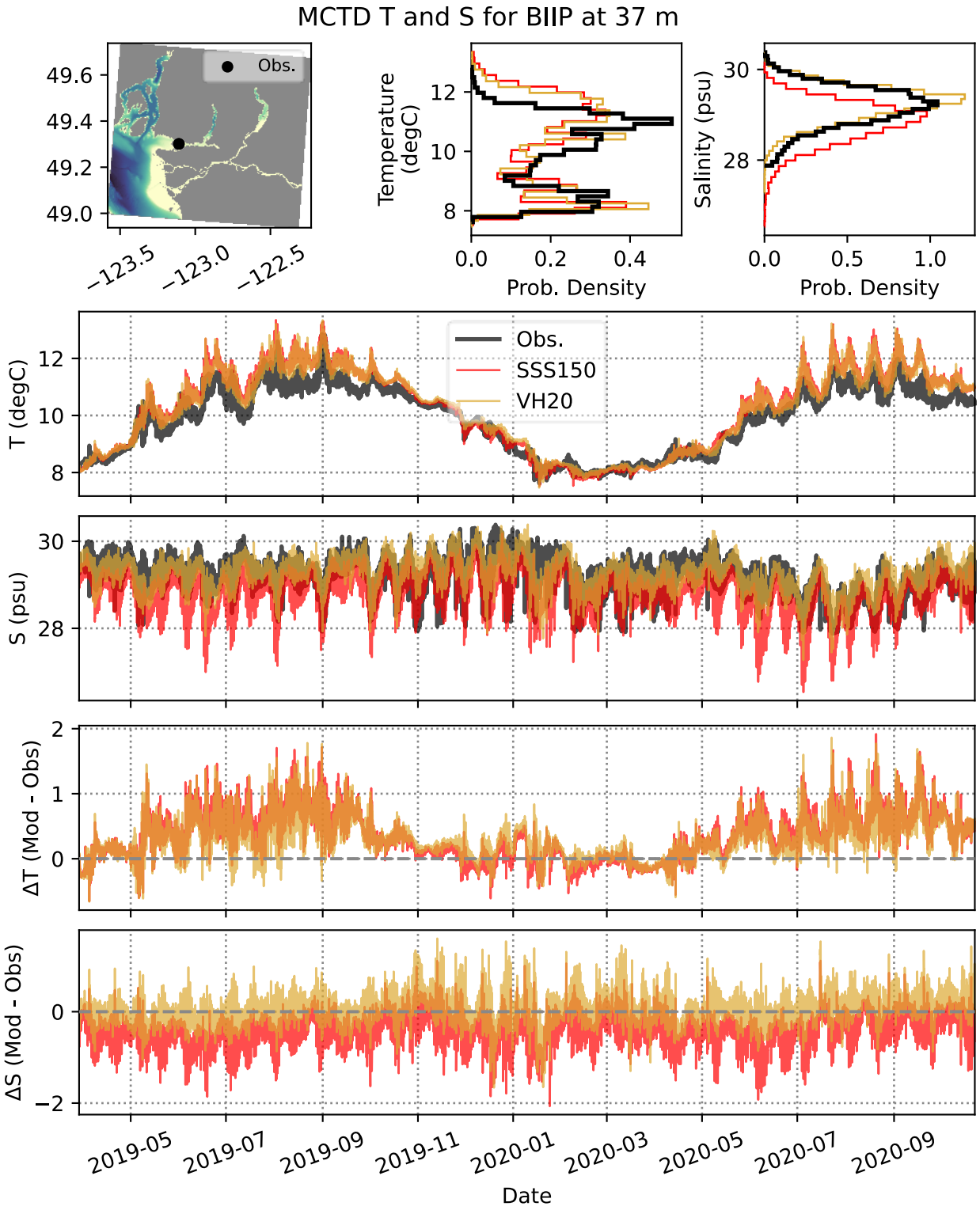

Figure 62. Moored CTD comparison from the Burrard Inlet Instrument Platform (2019-03 deployment) at 37 m depth.

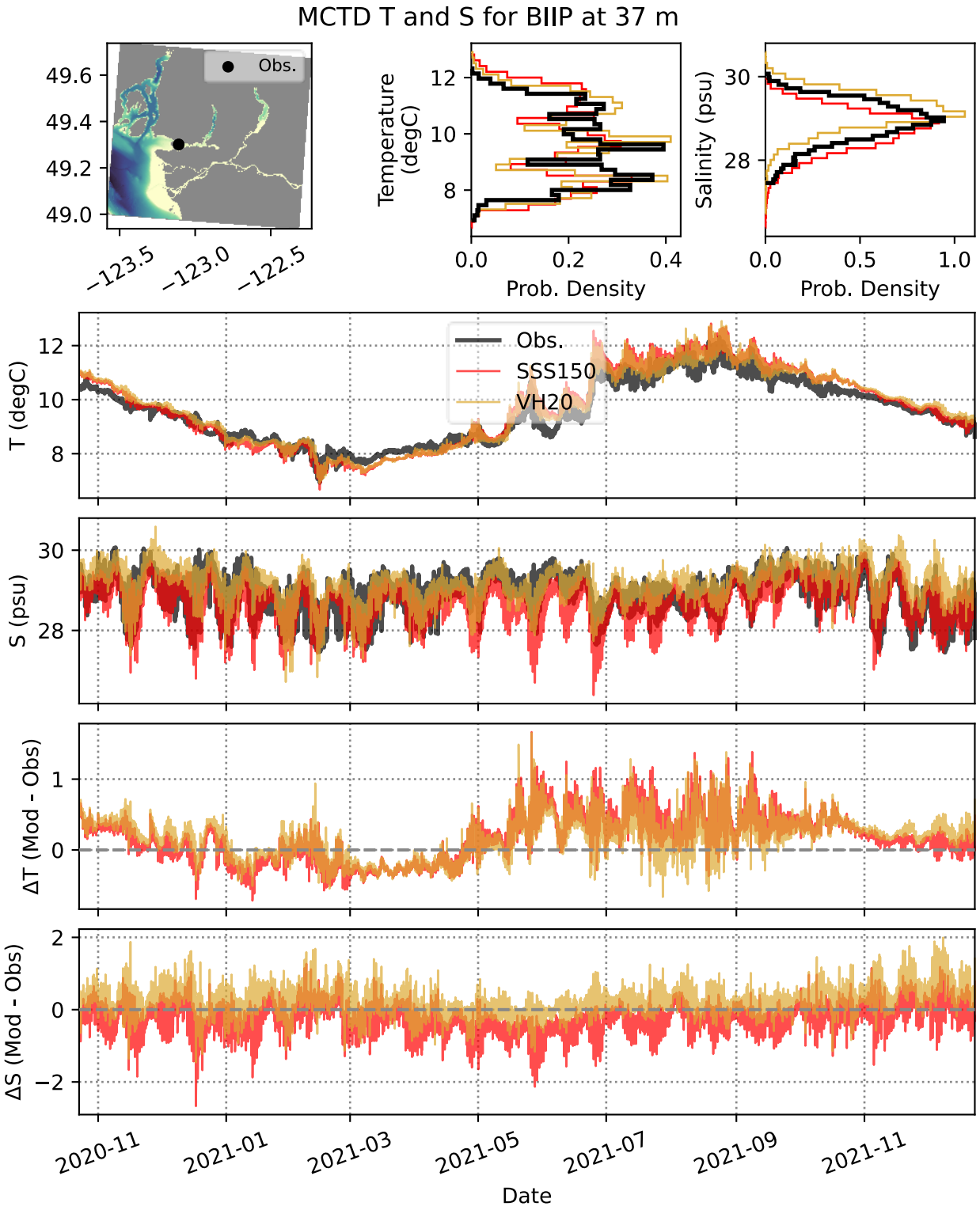

Figure 63. Moored CTD comparison from the Burrard Inlet Instrument Platform (2020-10 deployment) at 37 m depth.

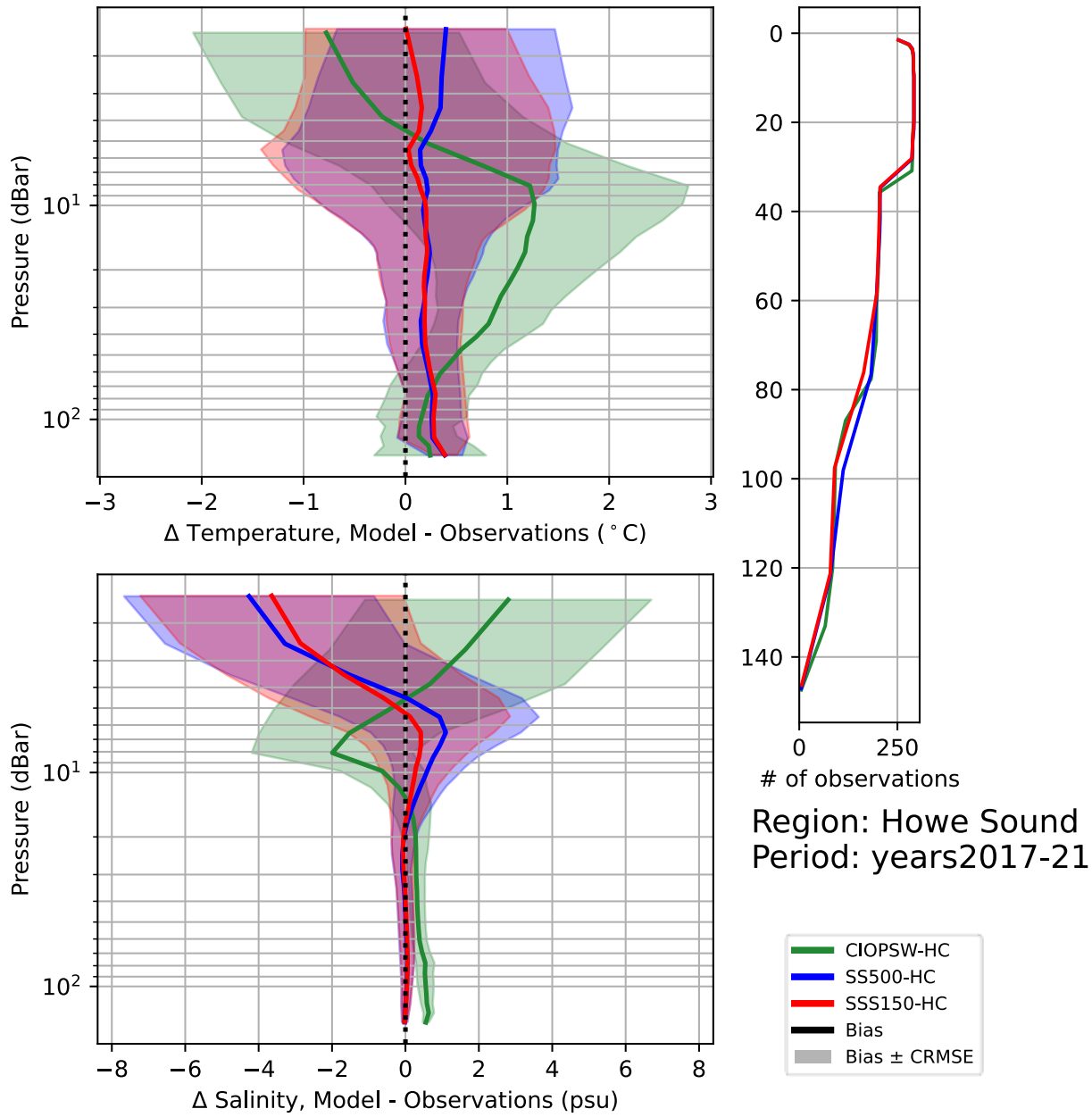

Figure 64. CTD comparison for region Howe Sound.

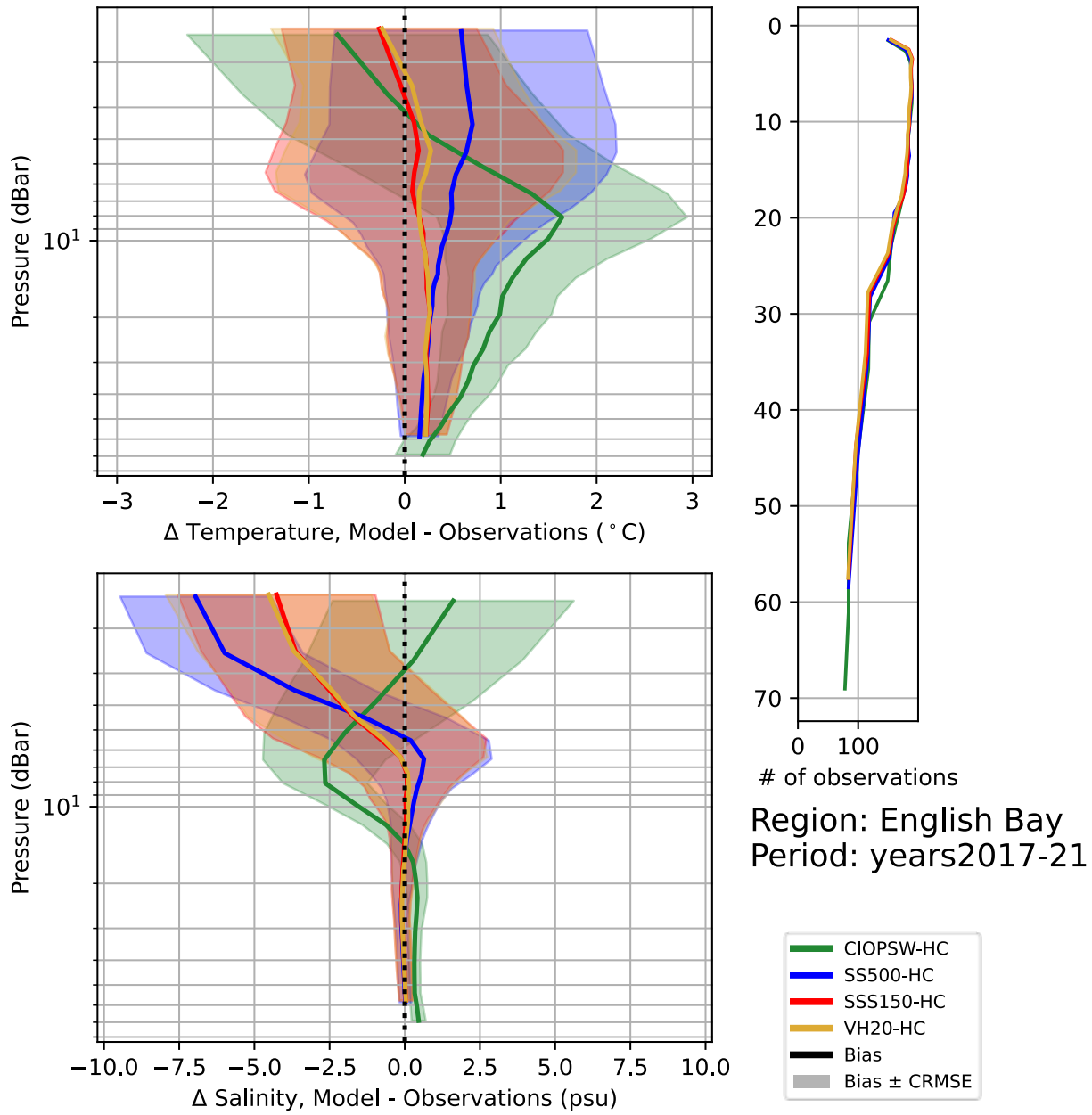

Figure 65. CTD comparison for region English Bay.

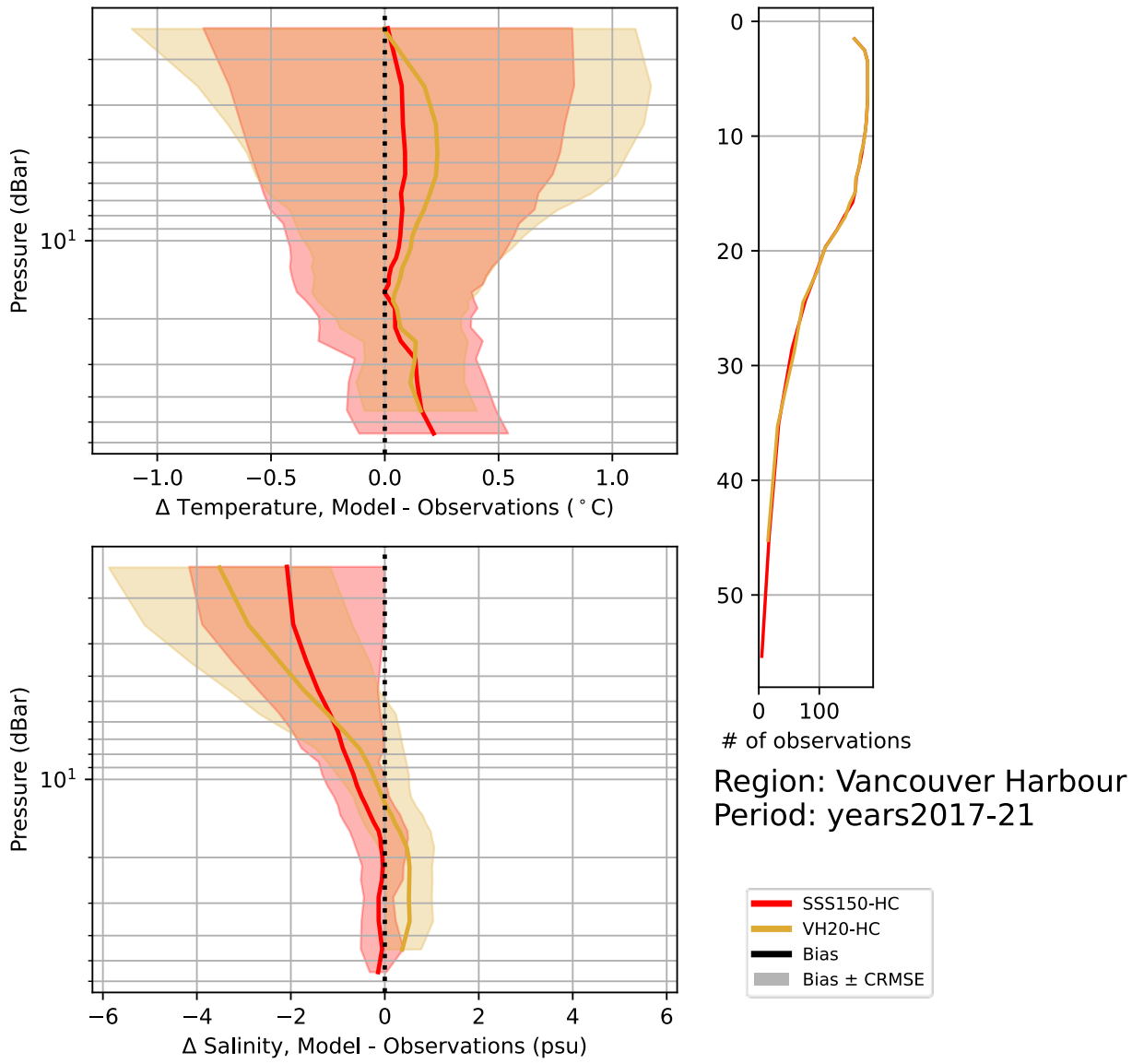

Figure 66. CTD comparison for region Vancouver Harbour.

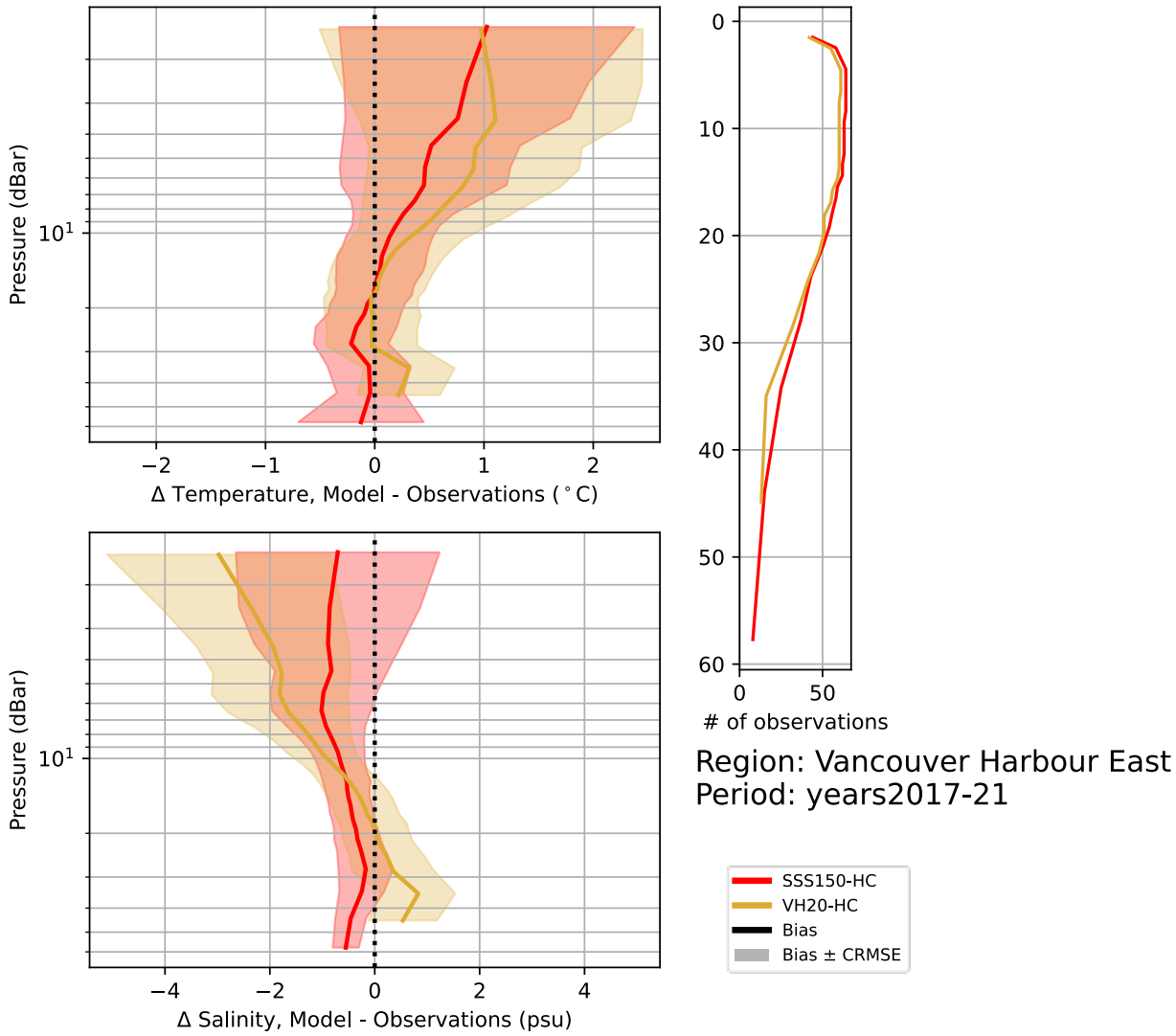

Figure 67. CTD comparison for region Vancouver Harbour East.

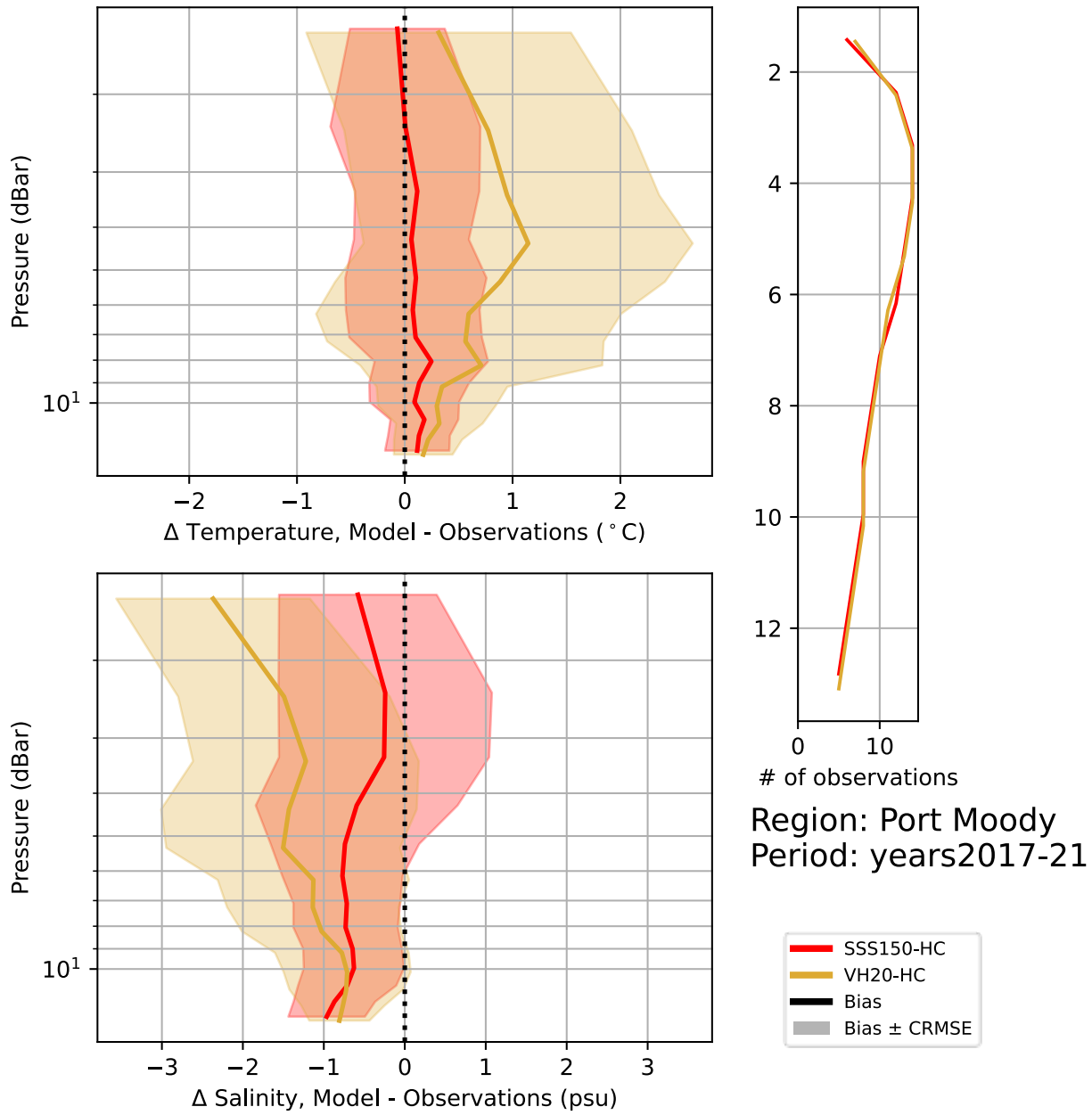

Figure 68. CTD comparison for region Port Moody.

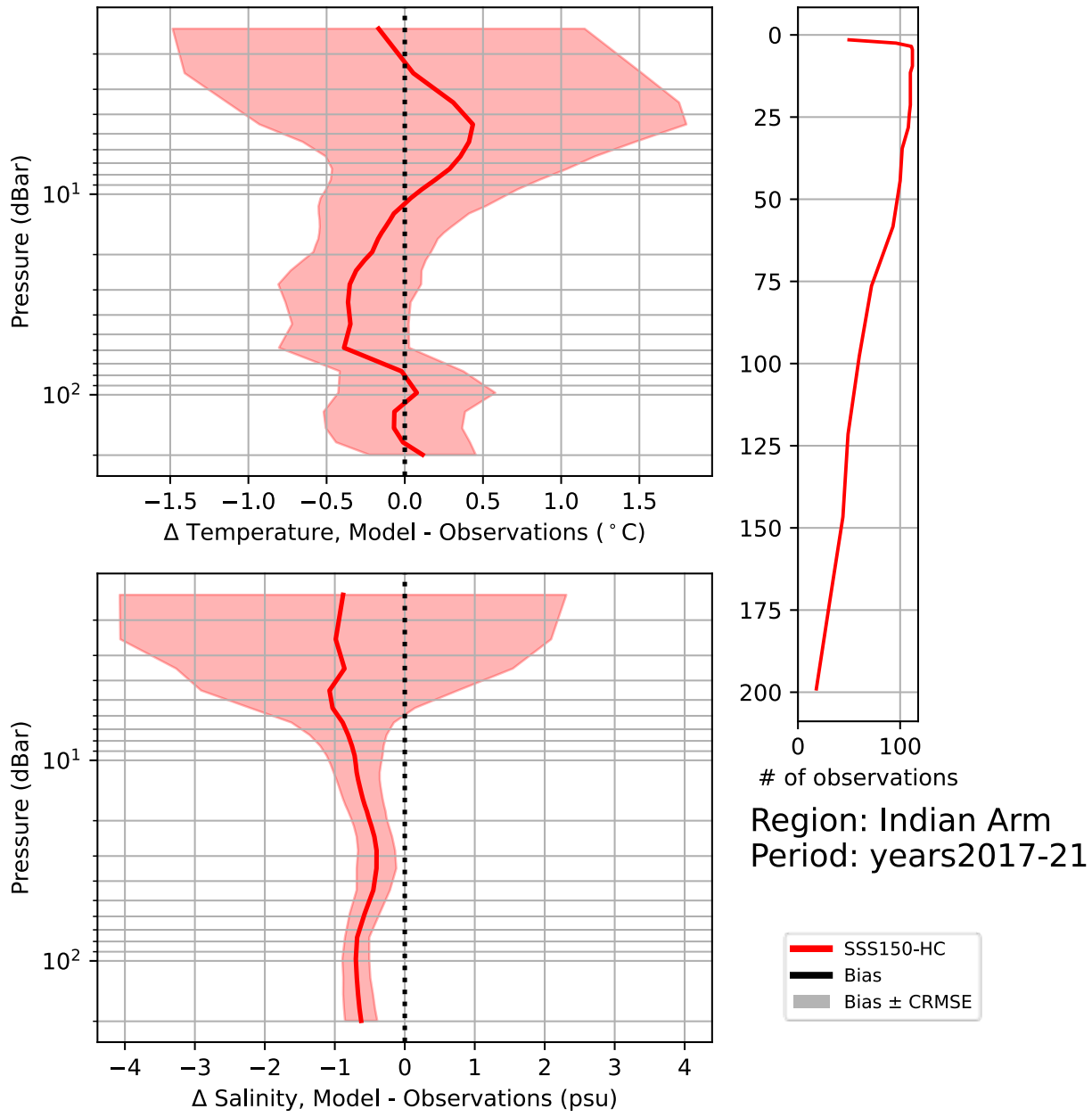

Figure 69. CTD comparison for region Indian Arm.

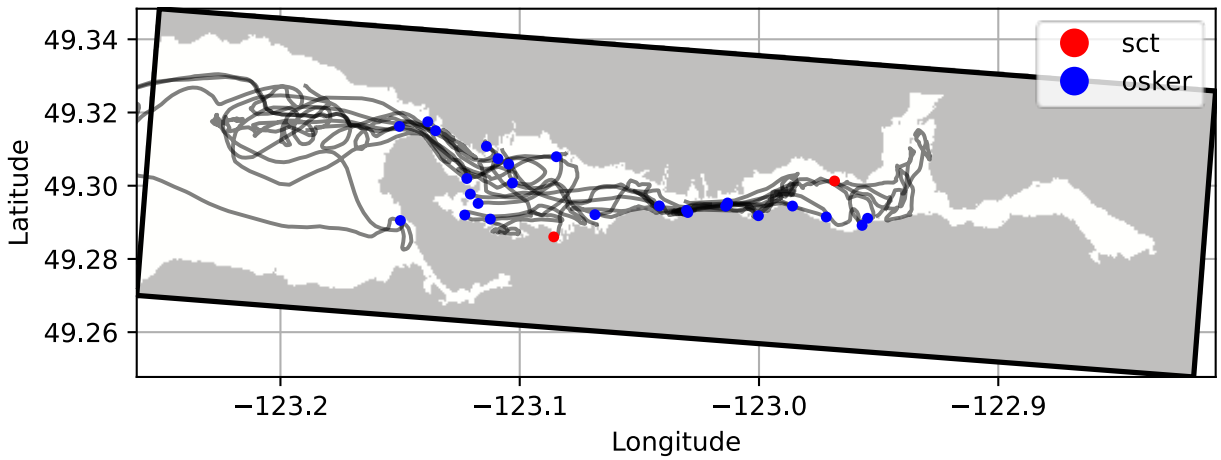

Figure 70. Drift tracks for the two drifter types (OSKER and SCT) used for the drift evaluation.

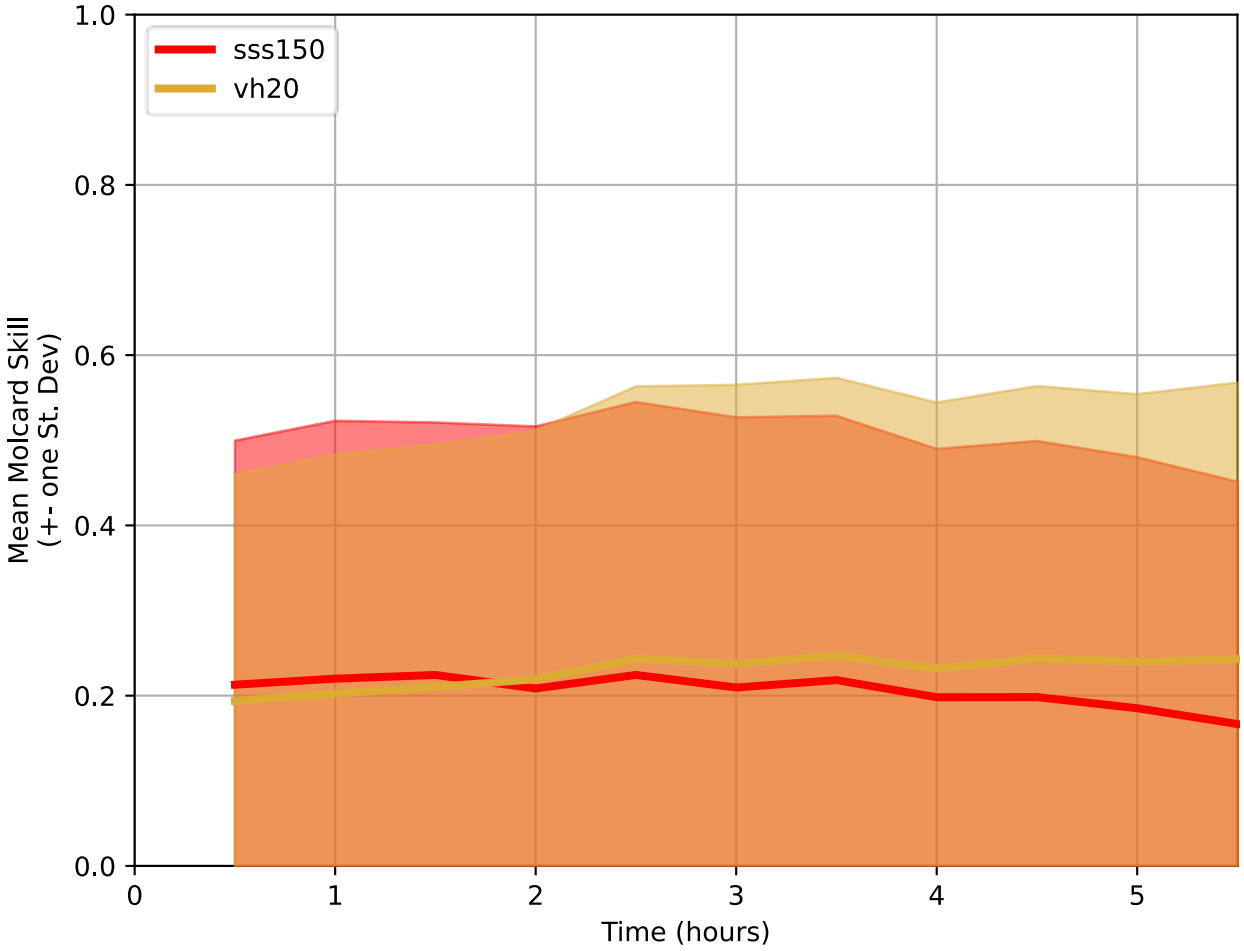

Figure 71. Molcard score as a function of time from the drift experiment. Shaded region shows ± one standard deviation.

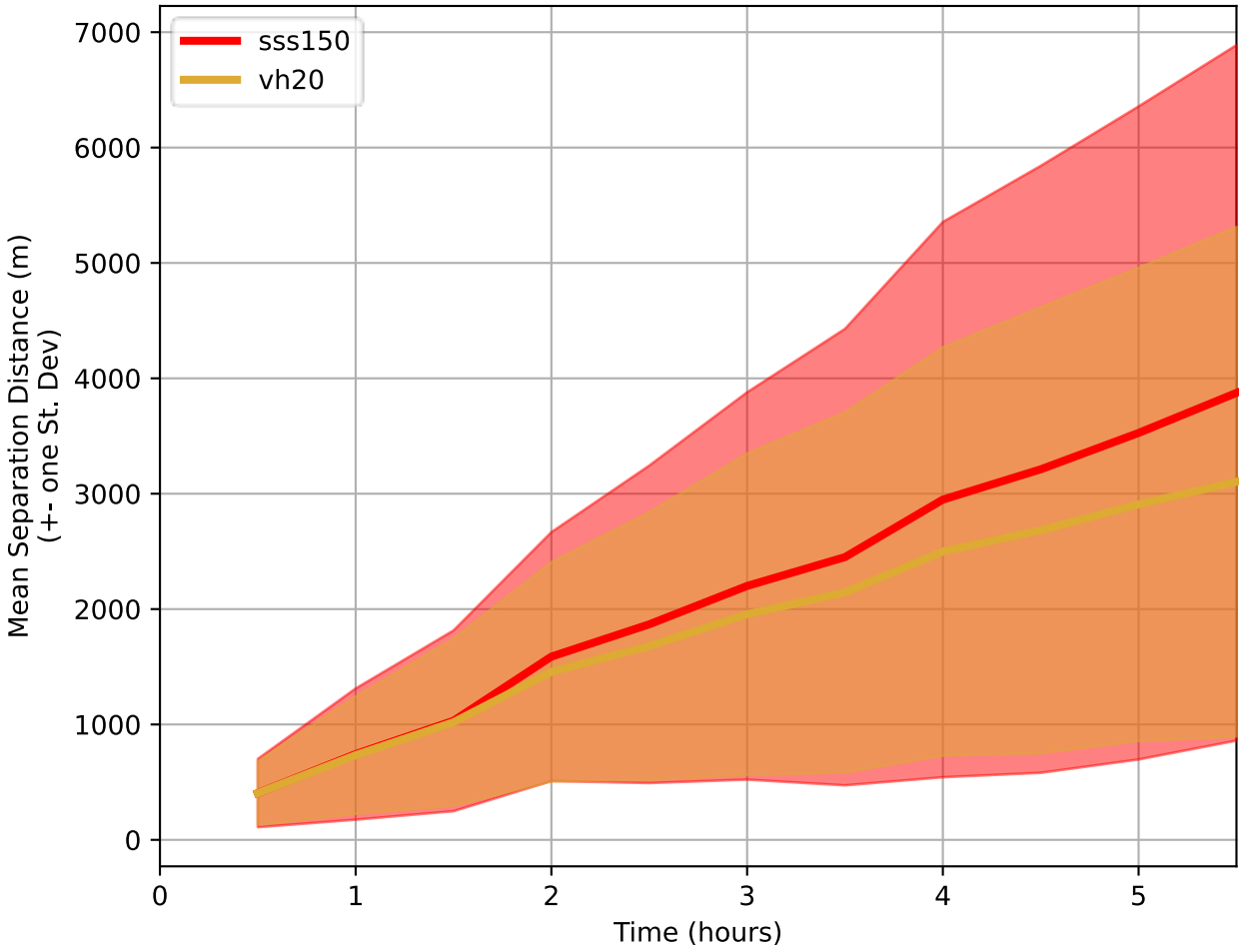

Figure 72. Separation distance as a function of time from the drift experiment. Shaded region shows ± one standard deviation.

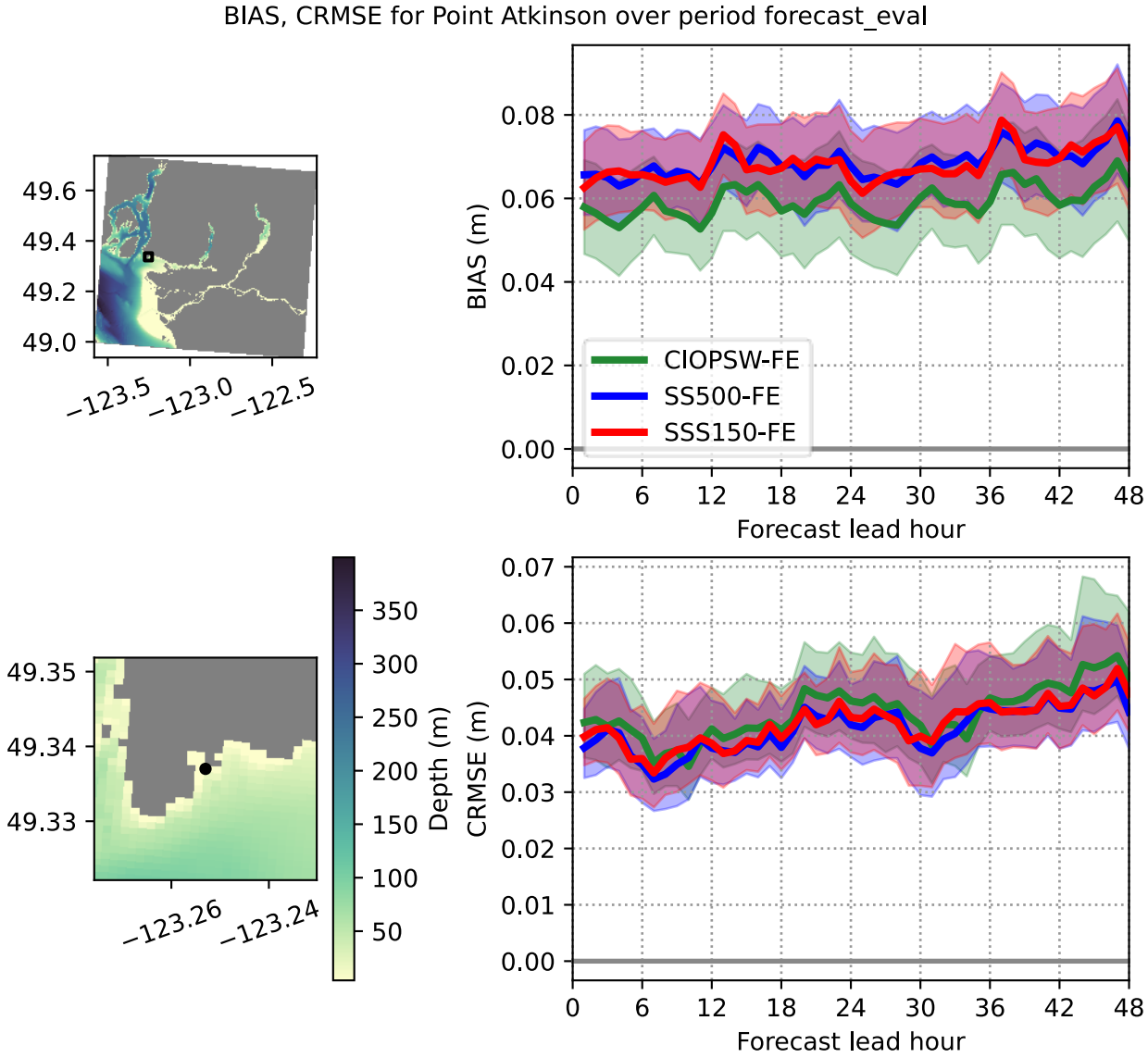

Figure 73. Forecast evaluation for non-tidal water level at Point Atkinson.

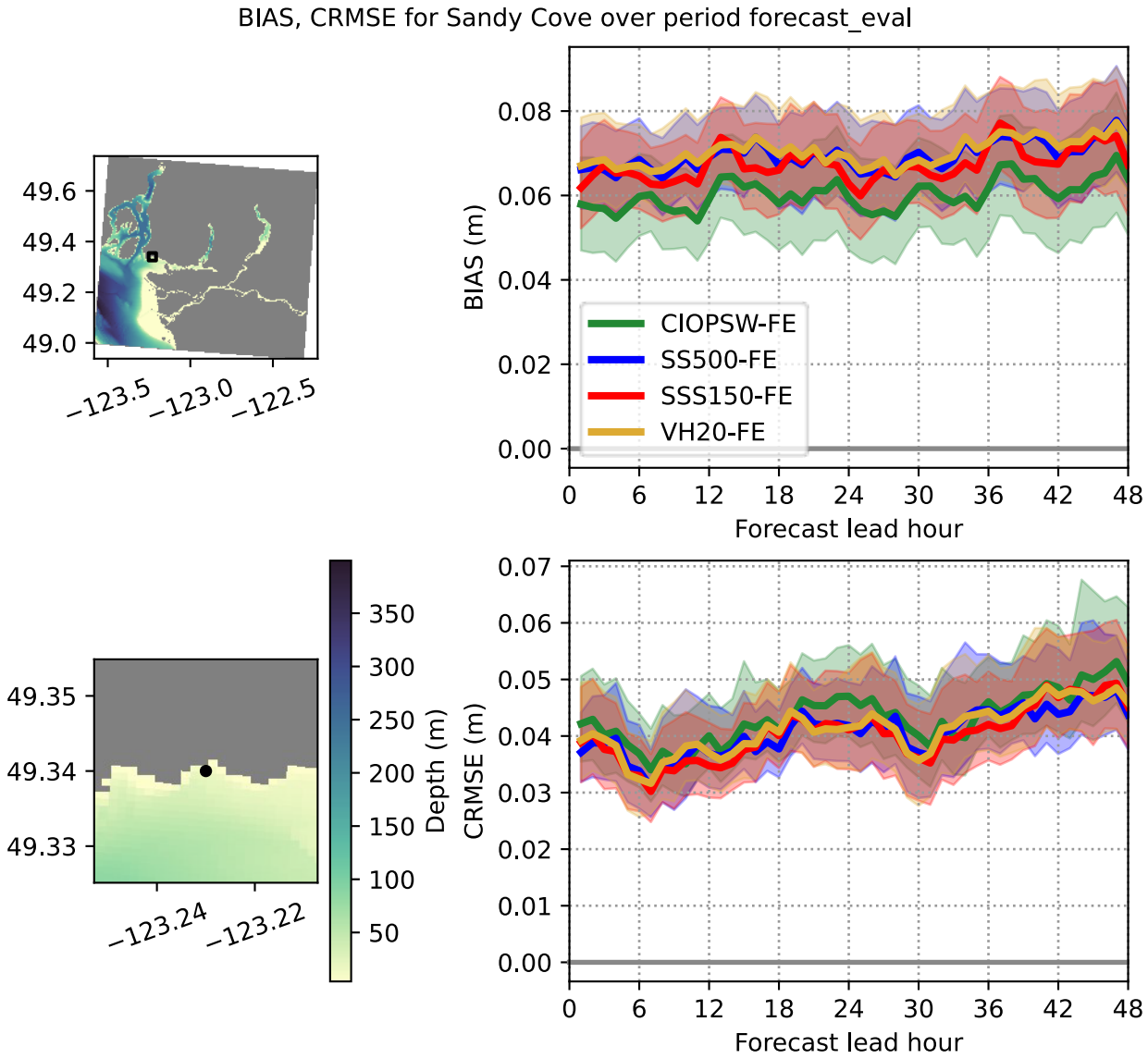

Figure 74. Forecast evaluation for non-tidal water level at Sandy Cove.

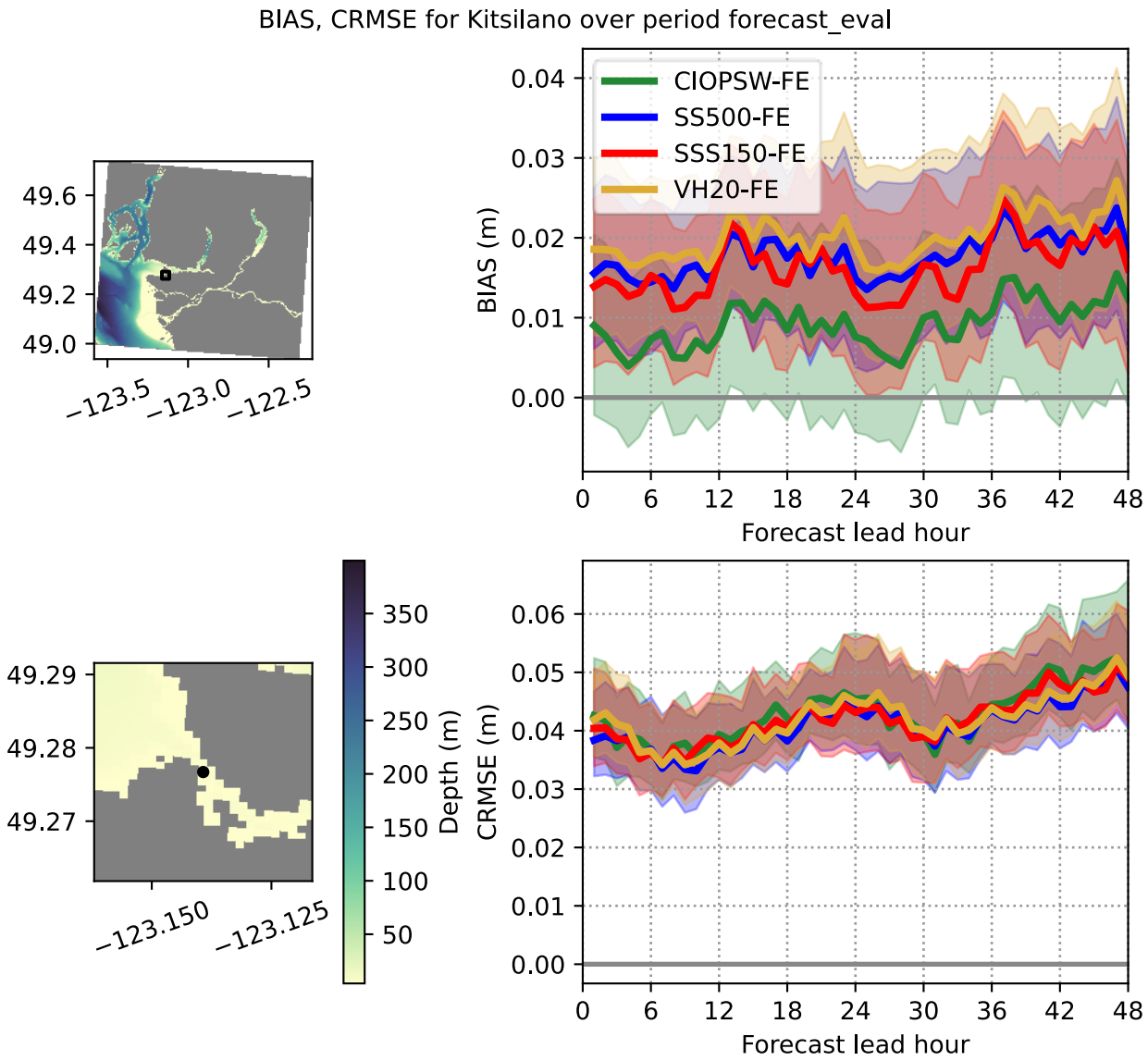

Figure 75. Forecast evaluation for non-tidal water level at Kitsilano.

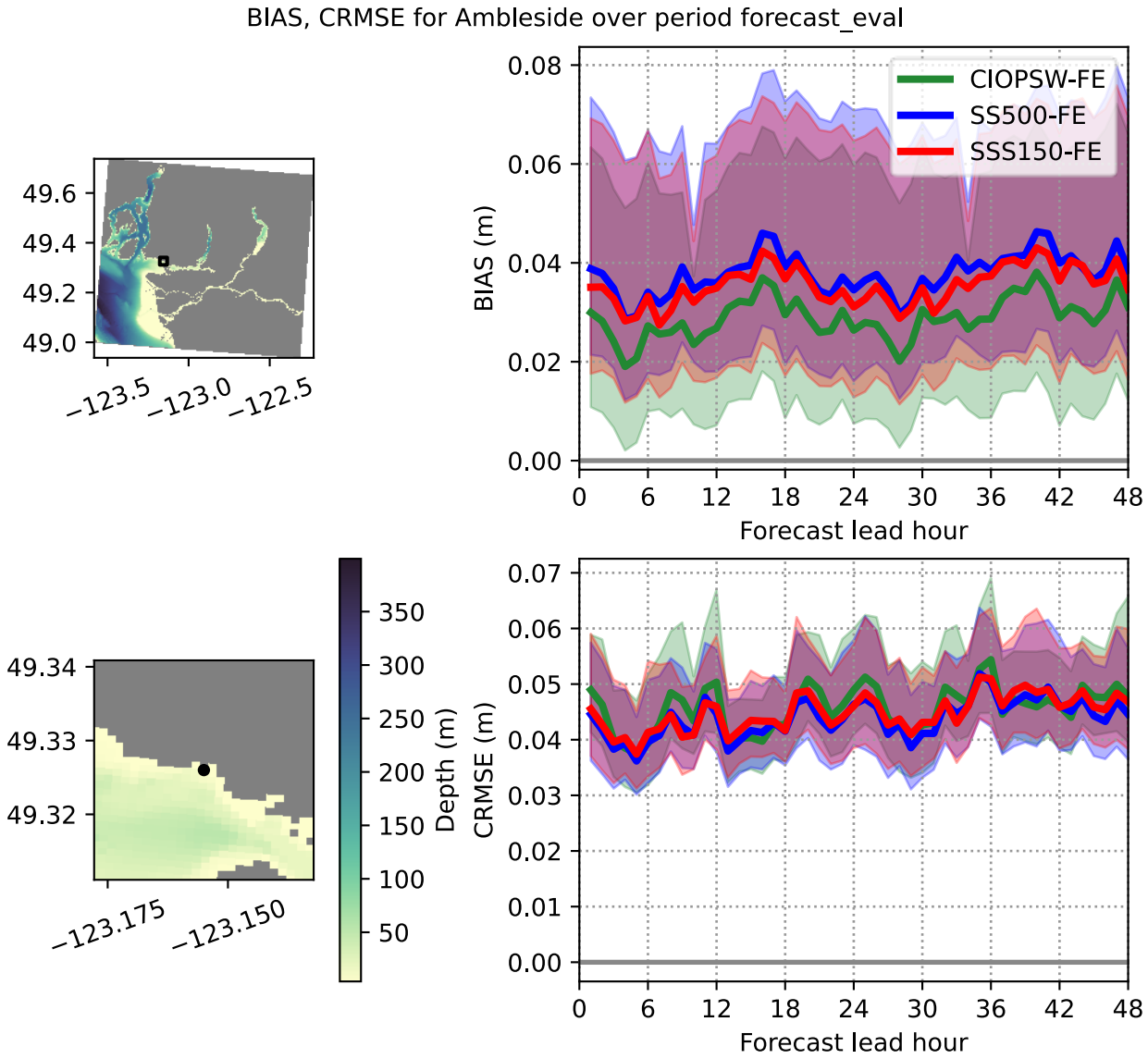

Figure 76. Forecast evaluation for non-tidal water level at Ambleside.

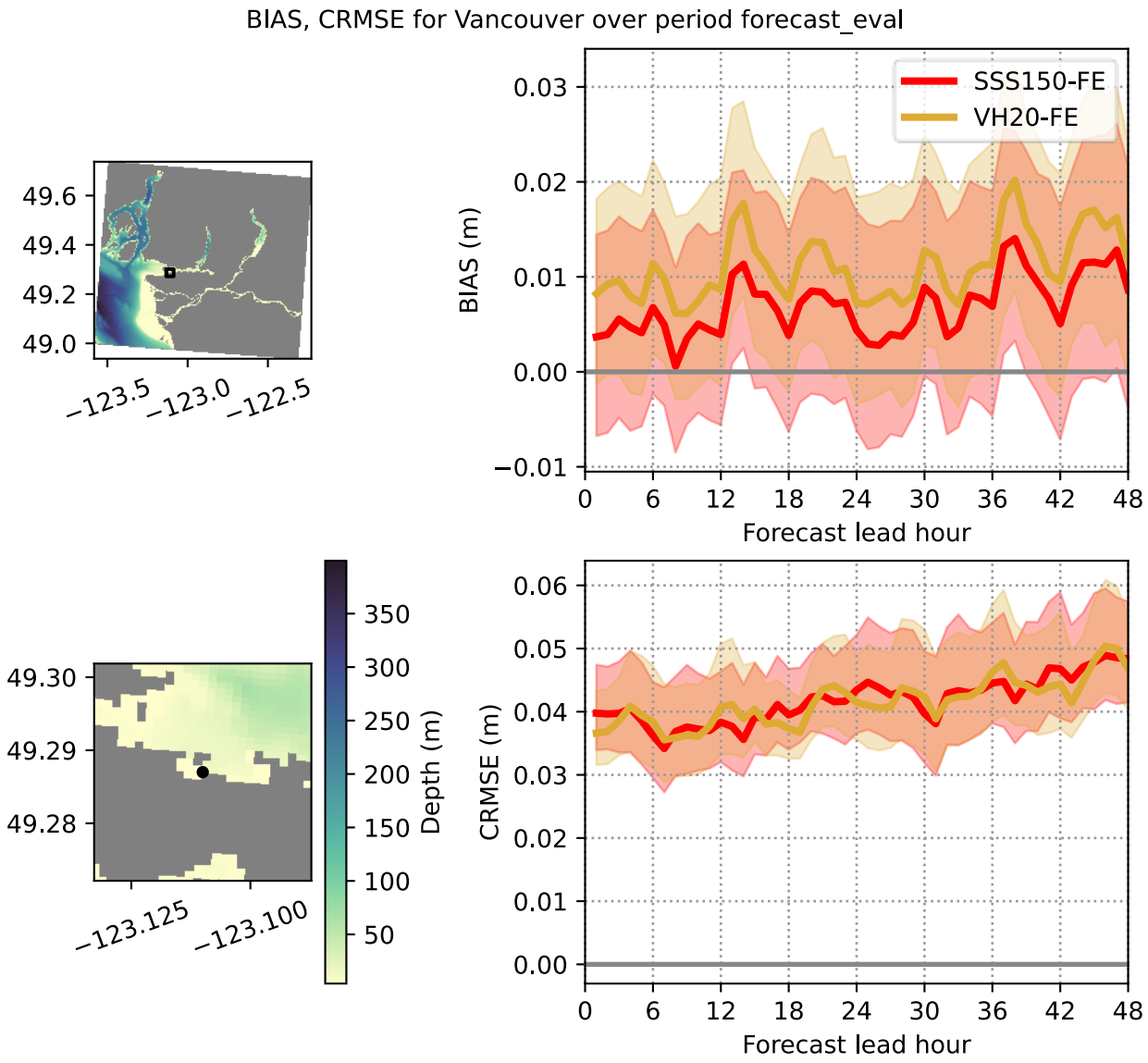

Figure 77. Forecast evaluation for non-tidal water level at Vancouver Harbour.

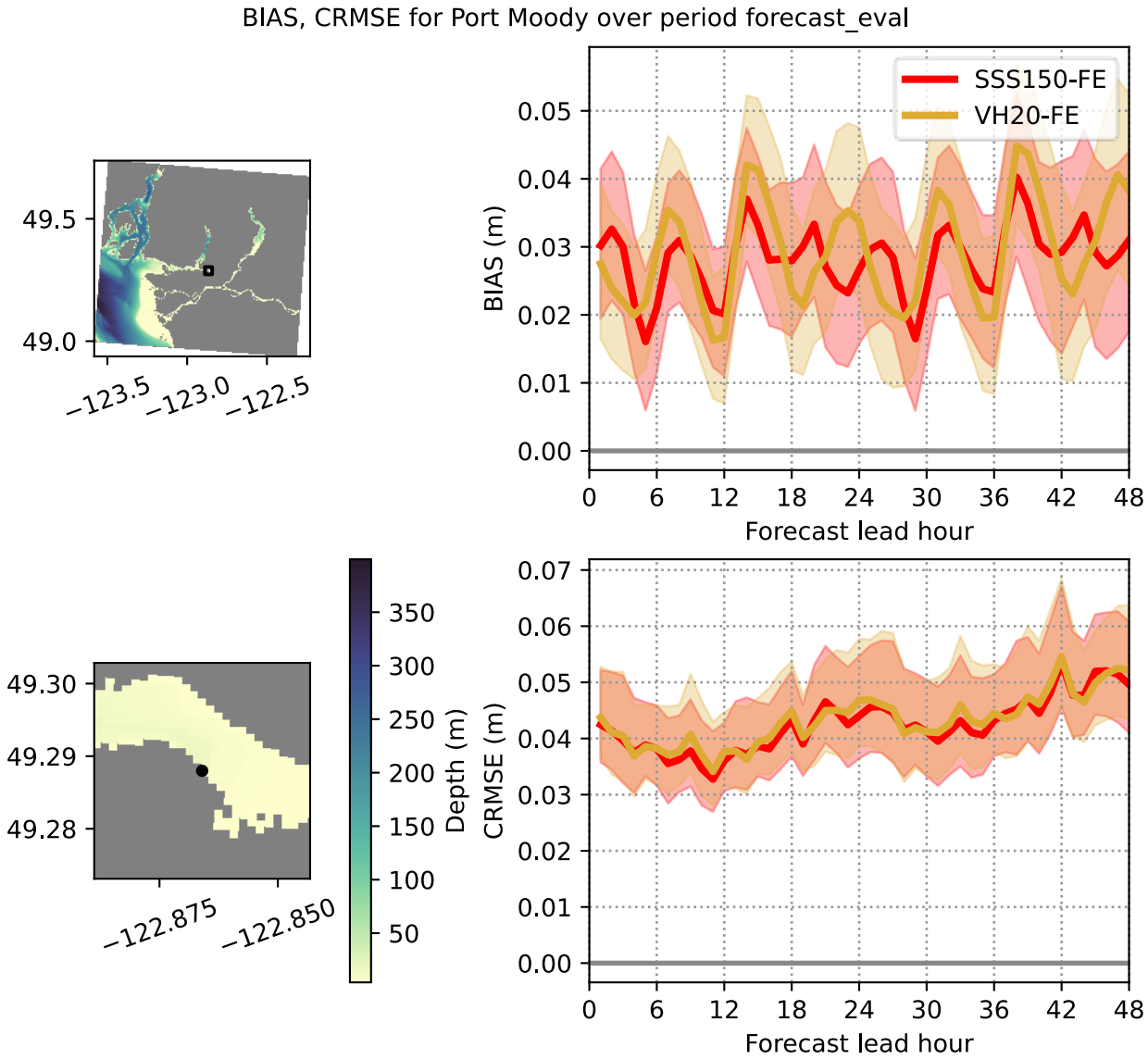

Figure 78. Forecast evaluation for non-tidal water level at Port Moody.

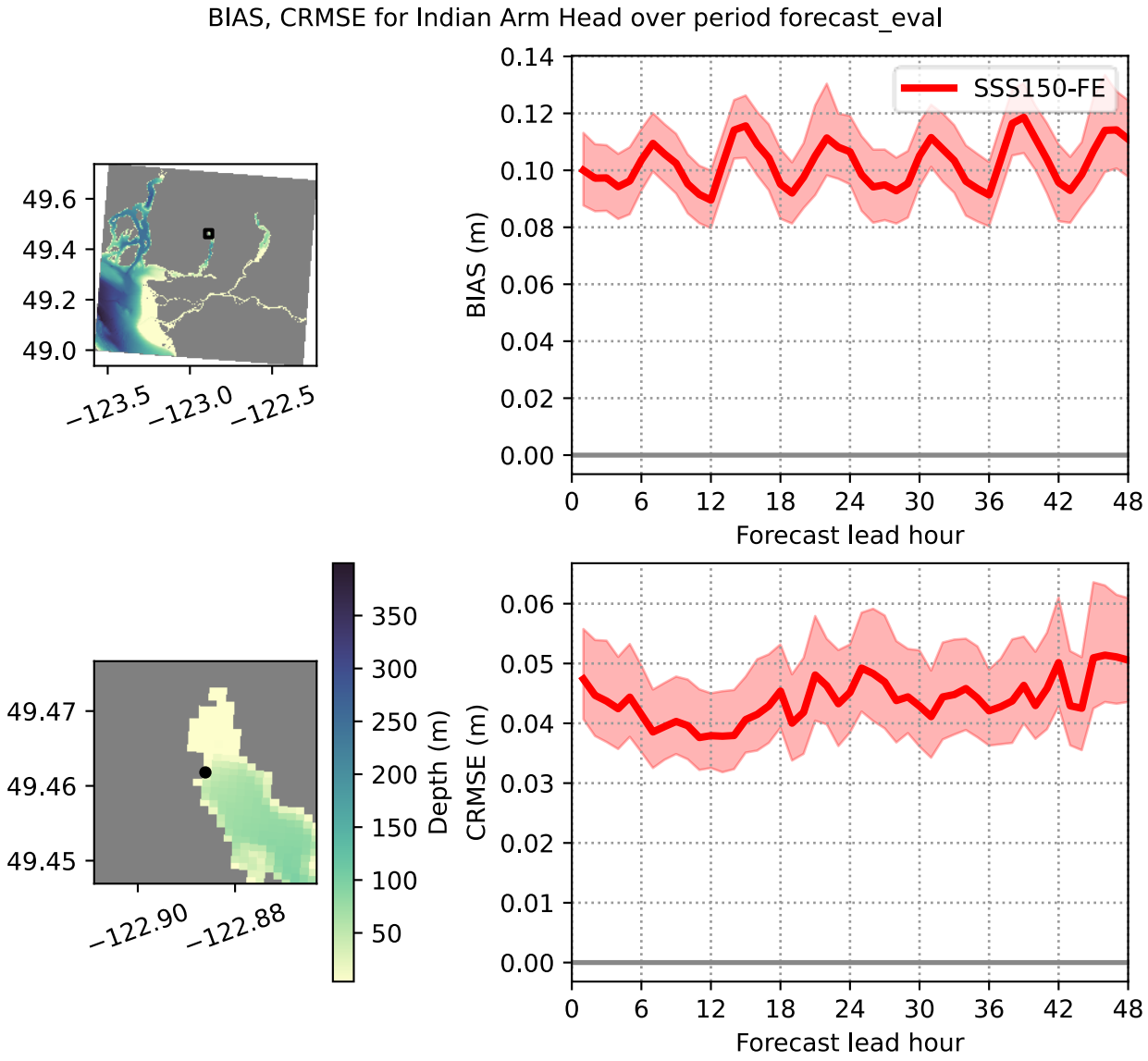

Figure 79. Forecast evaluation for non-tidal water level at Indian Arm Head.

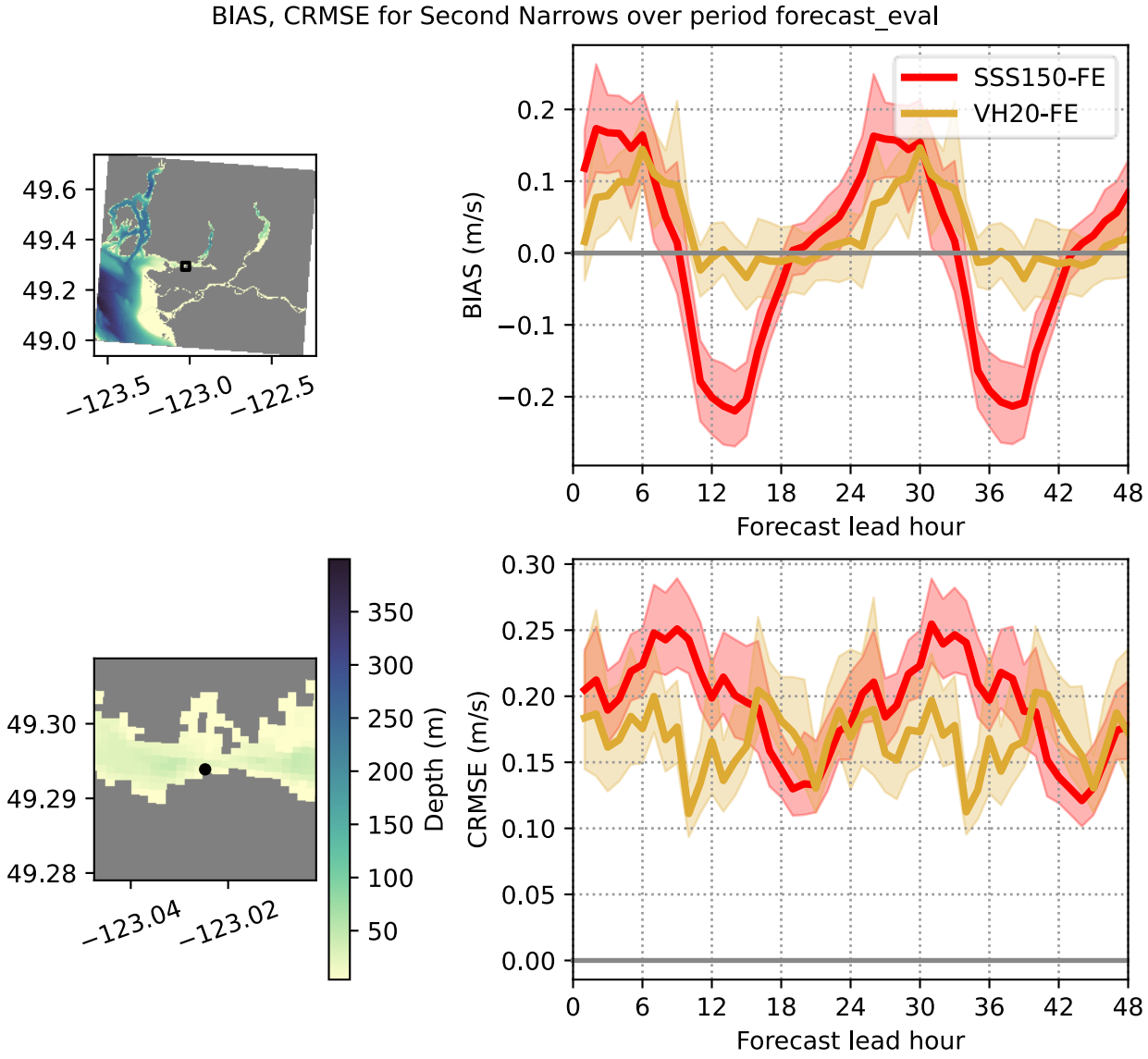

Figure 80. Forecast evaluation for alongshore currents at the Second Narrows HADCP in Vancouver Harbour.

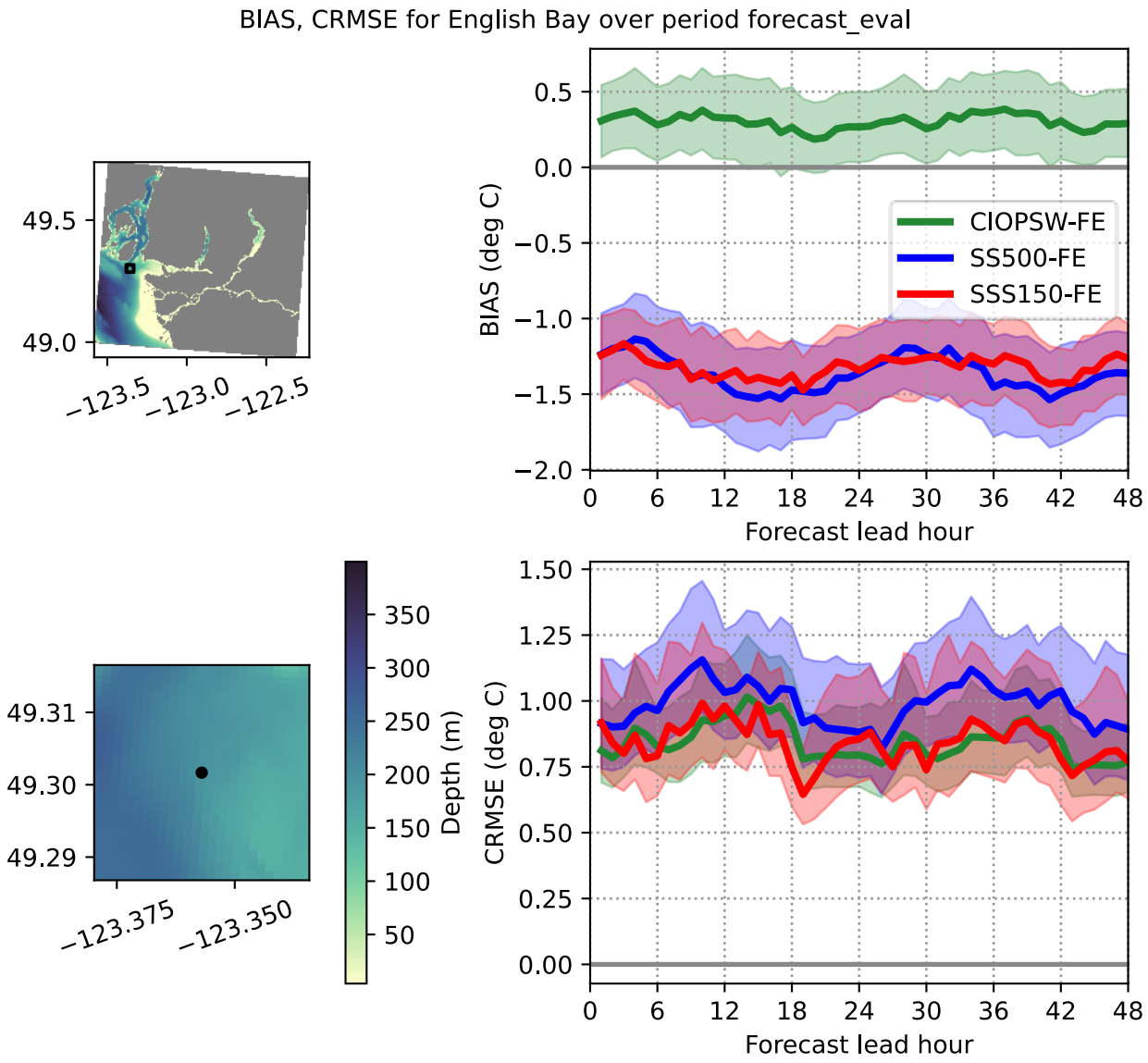

Figure 81. Forecast evaluation for sea-surface temperature at the entrance to English Bay (ECCC buoy 46304).